62

The Effect of Non-biological Particulates on Microbial Cell Disruption in a Slurry Bioreactor

by
Nicola Jeanne Scholtz
BSc. (Chem. Eng.) UCT

Thesis Presented for the Degree of
DOCTOR OF PHILOSOPHY
in the Department of Chemical Engineering
UNIVERSITY OF CAPE TOWN

February 1998

62

The Effect of Non-biological Particulates on Microbial Cell Disruption in a Slurry Bioreactor

by
Nicola Jeanne Scholtz
BSc. (Chem. Eng.) UCT

Thesis Presented for the Degree of
DOCTOR OF PHILOSOPHY
in the Department of Chemical Engineering
UNIVERSITY OF CAPE TOWN

February 1998

Dedicated to my parents
and TGB

Abstract

Cell damage from hydrodynamic stress is an important consideration in biological systems since it can result in the growth and function of the cell becoming impaired (Toma *et al.* 1991, Lilly *et al.* 1992). In the extreme case of cell damage, cell disruption occurs. This dissertation presents the results of an investigation into the disruption of stationary-phase microbial cells in a stirred tank reactor when agitated in the presence of biologically inert solid particles in the absence of aeration. Applications of biological processes, where cells and solid particles are used, include bead mills, minerals bioprocessing, soil bioremediation and immobilised biocatalysts. An understanding of the rate, extent and mechanisms of cell disruption in these systems will facilitate the design of bioreactors to minimise or maximise microbial cell disruption, depending on the application.

The primary objectives were to quantify and model the effect of incompletely and completely suspended solids on the kinetics of cell disruption, as a function of the solids concentration, agitation intensity and impeller flow pattern. *Saccharomyces cerevisiae* was used as model micro-organism and silica as the solid particles. Modelling the cell disruption enabled its prediction as a function of the operating parameters and further allowed the cell disruption mechanisms to be elucidated. A final objective was to quantify the solids suspension as a function of the operating parameters.

A 3 liter stirred tank reactor was used for all disruption experiments, with agitation produced by an overhead motor equipped with either a 6-bladed Rushton turbine or a 6-bladed pitched-blade turbine, pumping downwards. Disruption of the *Saccharomyces cerevisiae* was measured in terms of the soluble protein release into the supernatant, using the method of Lowry *et al.* (1951). The experimental apparatus was designed to allow measurement of the global power input into the system.

Solids suspension was quantified for both impeller types in terms of the critical impeller speed, defined as the speed at which the transition from the incompletely to the completely suspended solids regimes occurs. The effect of an increase in suspended solid concentration on the cell disruption at a constant particle momentum was investigated by varying the solids concentration between 5% and 40% (v/v) at a constant impeller speed of 750 rpm (impeller tip speed of 2.91 ms^{-1}), which exceeds the critical impeller speed at 40% solids. The Rushton turbine was used for these disruption experiments. The effect of incompletely and completely suspended solid particles on the cell disruption was investigated as a function of the particle momentum using the Rushton turbine at either 10% or 20% solids (v/v), and the pitched-blade turbine at 20% solids (v/v). At each of these conditions, the impeller speed was varied between 200 and 900 rpm

(impeller tip speeds of 0.77 to 3.49 m s^{-1}), which straddles the respective critical impeller speeds at 10% and 20% solids (v/v).

Critical impeller speeds for the Rushton turbine were measured at 5%, 10%, 15%, 20% and 40% solids (v/v) by visual observation and from the maxima in the power number (N_P) as a function of the impeller Reynolds number (N_{RE}). Measurements of the critical impeller speed for the Rushton turbine using these two methods agreed to within 9%. The critical impeller speed for the pitched-blade turbine at 20% solids (v/v) was also measured by visual observation and from a N_P-N_{RE} curve. It was found that only visual observation was suitable with the pitched-blade turbine since no maximum was apparent in the N_P-N_{RE} curve. This can be explained in terms of the flow pattern of this impeller. A mathematical relationship, expressing the measured critical impeller speeds as a function of the operating parameters, was determined. This relationship was used in the modelling of the cell disruption.

Negligible cell disruption occurs in the stirred tank reactor in the absence of solid particles, suggesting that cell disruption in the slurry reactor is essentially caused by interaction between the cells and solid particles. First order kinetics describe this disruption, allowing it to be quantified in terms of a maximum extent and a rate. In the presence of solid particles, a constant maximum extent of cell breakage was observed at equilibrium conditions for both the Rushton and pitched-blade turbines at all the hydrodynamic conditions investigated, indicating that the maximum extent of cell disruption is independent of the level of solids suspension. At a constant impeller speed of 750 rpm above the critical impeller speed, the first order disruption rate constant (k) exhibits a power law dependence on the solids volume fraction. However, at a fixed solids loading, the functional dependence of k on the impeller speed differs in relation to the critical impeller speed for both the Rushton and pitched-blade turbines. A power law dependence was observed in the incompletely suspended solids regime owing to the increase in volume fraction of suspended solids with impeller speed. At speeds above the critical impeller speed, k exhibits a linear dependence on the impeller speed. Here, the volume fraction of suspended solids is constant and only the effect of increasing agitation intensity on cell disruption is observed.

Comparison of the cell disruption resulting from agitation with the Rushton turbine and the pitched-blade turbine showed that, for a given impeller speed, the rate of cell disruption is less for the pitched-blade turbine owing to the lower power input of this impeller. However, for a given power input above the critical impeller speed, the same cell disruption rate results, independently of the flow pattern type.

Existing cell damage and disruption models were applied to the cell disruption observed in the slurry reactor on agitation with the Rushton turbine. Since these models describe the cell disruption data poorly, several new models were developed. Mechanistic and predictive models were developed for the Rushton turbine system at speeds above the critical impeller speed. These models describe the first order disruption rate constants in terms of the total solids volume fraction and the power input to the system per unit volume. The work suggests that cell disruption in the completely suspended solids regime occurs primarily in the impeller region as a result of solid-cell-solid collisions, solid-cell collisions and solid-cell-reactor collisions. The effect of cell-eddy interactions is negligible. The new mechanistic and predictive models were validated by applying them to the cell disruption from the pitched-blade turbine in the slurry reactor, and to cell damage in animal cell-microcarrier systems (Croughan *et al.* 1988 1989, Croughan and Wang 1989). The new models describe the first order disruption rate constants of the pitched-blade turbine, indicating that the same mechanism of cell disruption applies when using the Rushton and pitched-blade turbines in the completely suspended solids regime. However, these models need to be modified for application to the animal cell-microcarrier system to account for cell-eddy interactions as a source of cell damage as well as cell damage from both inert solids and microcarrier particles.

In modelling the cell disruption at speeds below the critical impeller speed, the slurry reactor was considered to consist of two regions: an upper region in which the solids are completely suspended and cells are disrupted by collisions between the cells and one or more solid particles; and a lower region where the solids are not suspended and the cells are disrupted by the grinding action of adjacent solid particles. A predictive model was developed for the incompletely suspended solids regime, which describes the first order disruption rate constants, for both the Rushton and pitched-blade turbines, as a function of the total solids volume fraction, the volume fraction of suspended solids and the power input per unit volume. Cell disruption was also successfully modelled for the bead mill system (Mogren *et al.* 1974, Rehacek and Schaefer 1977, Schutte *et al.* 1986) where all the solid particles are unsuspended and cell disruption is achieved by the combined action of collisions and grinding between stream layers of solid particles of different velocity (Kula and Schutte 1987). The constants obtained in the mechanistic model describing the cell disruption in bead mills were compared to the corresponding constants in the cell disruption model for the slurry reactor, thus adding to the fundamental understanding of cell disruption in particulate systems.

Acknowledgments

I would like to express my sincere thanks to the following people:

Dr S.T.L. Harrison, my Ph.D. supervisor, for her input, guidance and encouragement throughout this project. I am particularly grateful for the opportunity to present my work at the Bioreactor and Bioprocess Fluid Dynamics Conference in Edinburgh (July 1997).

Dr A.B. Pandit of the University of Bombay for his invaluable input in the development of the models presented in this work.

AECI Research and Development Department, Modderfontein, South Africa and the FRD for their financial support of this project.

Anchor Yeast (Cape Town, South Africa) for the supply of *Saccharomyces cerevisiae* used in this work.

Thando Moutlana for her assistance with the disruption experiments performed with the pitched-blade turbine.

Staff of the electronic and main workshops in the Chemical Engineering Department: Mr E.W. Randall, Mr G. de la Cruz, Mr P. Dobias, Mr J. Macke and Mr J. Daniels, for building and maintaining much of the equipment used.

The Bio Group in the department for their willing assistance, whenever necessary, and their friendship and support throughout the past few years.

Last, but not least, TGB, my parents and family for their enormous support and interest in my studies.

Table of Contents:

List of Figures

List of Tables

Nomenclature

B	=	Baffle width (m)
B	=	Mass of solids in suspension per mass of liquid, given as a percent (%) (Equations 5.1, 5.2, 5.7, 5.8, 5.9)
C	=	Impeller clearance above the vessel base (m)
C_i	=	Concentration of inert solid particles (kg m^{-3})
C_M	=	Microcarrier concentration (kg m^{-3})
C_p	=	Protein content of one cell (mg protein / cell)
c	=	Cell dry weight concentration (kg m^{-3})
c_D	=	Drag coefficient associated with the impeller (Equation 7.40)
c_D	=	Soluble protein concentration of a diluted, disrupted sample (kg m^{-3}) (Equations D.2, D.3, D.4, D.5)
c_U	=	Soluble protein concentration of an undiluted, disrupted sample (kg m^{-3})
D	=	Impeller diameter (m)
d_p	=	Particle diameter (m)
E	=	Energy input per unit volume (J m^{-3})
$E(k)$	=	One-dimensional energy distribution function for turbulent eddies
E_x	=	Cell volume fraction
F	=	Factor used by Hetherington *et al.* (1971) to account for the volume fraction of the aqueous phase in the disrupted sample (Equation D.1)
F	=	Number of interactions between microcarriers per unit time and volume (m^{-3} hr^{-1}) (Equation 7.28)
F	=	Force acting on fluid adjacent to the impeller in the stirred tank (N) (Equation 7.40)
H	=	Height of liquid in vessel (m)
H_u	=	Length of impeller hub (m)
h	=	Solid boundary height above the mid-plane of the impeller (m)
j	=	Number of CSTRs in series
k	=	Wavenumber of turbulent eddy (m^{-1}) (Equations 7.33, 7.34)
k	=	First order disruption rate constant = k_{total} (s^{-1})
$k_{collision}$	=	First order disruption rate constant, accounting for collisions between the cells and suspended solid particles (s^{-1})

k_{grind} = First order disruption rate constant, accounting for the grinding of the cells by adjacent unsuspended solid particles (s^{-1})

k_la = Oxygen mass transfer rate (s^{-1})

L = Distance from tip of torque arm to center of torque table (m)(Equation 3.1)

L = Length of impeller blade (m)

m = Mass reading on load cell (kg) (Equation 3.1)

m = Mass of solid particle (kg) (Equations 7.24, 7.26, 7.35)

N = Impeller speed (rps or rpm, units stated in equation)

N = Number of intact cells at time, t (Equations 6.1, 6.2, 6.4, 6.5, 6.6)

N_{JS} = Critical impeller speed (rpm)

N_p = Power number = $P / (\rho N^3 D^5)$, where N is in rps

N_{RE} = Impeller Reynolds number = $N D^2 \rho / \mu$, where N is in rps

n = Number of impellers

n_b = Number of impeller blades

P = Power (W)

P_{osm} = Osmotic pressure of suspending medium (bar)

Q = Biosuspension flow rate ($m^3 s^{-1}$)

q = Cell death rate (hr^{-1})

R = Soluble protein released at time, t (mg protein / g cell)

R_i = Maximum soluble protein released under the specified operating conditions (mg protein / g cell)

R_M = Maximum soluble protein available for disruption (mg protein / g cell)

s = Dimensionless constant in Equation 5.1 which is a function of the type of stirrer, T/C and T/D

T = Tank diameter (m)

t_c = Average circulation time of fluid in vessel (s)

V = Volume (m^3)

v = Velocity of Kolmogorov microscale = $(\varepsilon \nu)^{0.25}$ ($m s^{-1}$)

v = Impeller tip speed ($m s^{-1}$) (Equation 7.40)

v_{av} = Average velocity of the medium over the impeller blade ($m s^{-1}$)

v_G = Superficial gas velocity ($m s^{-1}$)

v_{rel} = Relative velocity of colliding solid particles ($m s^{-1}$)

W = Width of impeller blade (m)

X_{min} = Value of x-intercept in Weibull function (Equation 8.8)

X_{span} = Parameter that determines the width of the Weibull function (Equation 8.8)

Greek letters:

ρ = Fluid density (kg m^{-3})

$\Delta\rho$ = Density difference between solid and liquid phases (kg m^{-3})

μ = Fluid dynamic viscosity (Pa s)

μ = Intrinsic cell growth rate (hr^{-1}) (Equation 7.30)

η = Length of Kolmogorov microscale = $(\nu^3/\varepsilon)^{0.25}$ (m)

ν = Liquid kinematic viscosity (m^2 /s)

τ = Mean residence time (s) (Equation 8.5)

τ = Shear stress (Pa) (Equations 7.21, 7.22)

σ = Quality of solids distribution

φ = Relative quality of solids distribution

γ = Shear rate (s^{-1})

ε = Turbulent power dissipation rate per mass of liquid (W / kg)

Φ = Volume of suspended solids / V_T

Φ_i = Volume of inert solid particles / V_T

Φ_M = Volume of microcarriers / V_T

Φ_T = Total solids volume / V_T

Φ_U = Volume of unsuspended solids / V_T

Subscripts:

l = Liquid

o = Initial

sl = Slurry

so = Suspending medium

s, p = Solid particles

T = Total

x = Cells

Glossary

Bead Mill: An industrial cell disruption device in which the cell suspension is mixed in a chamber at high rotational speeds in the presence of a high volume fraction of solid particles.

Cell Damage: Refers to the altered response of cells on exposure to stresses. This may be manifest as a change in the cells' morphology, ability to grow and reproduce, metabolic rate and/or metabolic pathway.

Cell Lysis/Disruption: Refers to the rupture of the cell envelope.

Coefficient of Variance: Standard deviation of values divided by their mean. The coefficient of variance was used in this study as a relative measure of the accuracy of the models in predicting the measured values.

Complete Solids Suspension: None of the solid particles rest on the vessel base for more than 1 or 2 seconds.

Critical Impeller Speed: The impeller speed at which the solids do not remain on the vessel base for more than 1 or 2 seconds.

Extent of Cell Disruption: Ratio of the soluble protein release (R) in the slurry reactor at time, t, to the maximum soluble protein released under the operating conditions (R_i).

First Order Disruption Rate Constant: Kinetic parameter, k, in first order disruption expression, which indicates the rate of cell disruption.

Incomplete Solids Suspension: Refers to the solid particles being unsuspended or partially suspended.

Least Squares Analysis: Method by which the models in this work were fitted to the experimental data. The method minimises the error between the predicted and experimental values.

Mass Transfer-type Model: Model of the form: $k = A\,(P/V)^{b}\Phi^{c}$, used to describe the first order disruption rate constant (k) as a function of the power input per unit volume (P/V) and the solids volume fraction (Φ).

Maximum Extent of Cell Disruption: Ratio of the maximum soluble protein release at the operating conditions in the slurry reactor (R_i) to the maximum available soluble protein for release (R_M).

Microcarrier: Solid particle used as a support for animal cell cultures.

Parity Chart: Graph comparing measured values to those predicted by a model.

Slurry Reactor: Stirred tank reactor where solid particles are agitated in the presence of a liquid.

Solids Volume Fraction: Volume fraction of solid particles, which excludes the interstitial volume fraction.

Abbreviations:

CV: Coefficient of variance
DT: 6-bladed Rushton turbine.
ICS: Impeller Collision Severity
PTD: 6-bladed Pitched-blade turbine, with the pumping action downwards.
SD: Standard deviation
TCS: Turbulent Collision Severity

Chapter 1: Introduction

The cultivation of micro-organisms in the presence of solid particles has a number of important applications in industry: minerals bioprocessing, soil bioremediation and immobilised biocatalysts. The fundamental differences between these processes are the function of the solid particles and the location of the micro-organisms. Solid particles are used in minerals bioprocessing and soil bioremediation as the energy source for cell growth. In processes where immobilised biocatalysts are used, the solid particles provide the support surfaces for the attached growth of the cells. Hence micro-organisms in these slurry systems may be either attached to the solid particles or remain freely suspended in the slurry. In some systems, such as minerals bio-oxidation, both attached and freely suspended micro-organisms are found.

The interaction between the microbial phase and the particulate phase may be provided in packed beds, trickle beds or heap processes. However, the design of active systems in which controlled conditions are maintained and adequate oxygen supply for aerobic processes provided is receiving increased attention. Hence an understanding of physical and biological processes in agitated, aerated slurry bioreactors is necessary. Good mixing conditions are required in the bioreactors to ensure that there is adequate mass transfer of oxygen and nutrients to the micro-organisms (Croughan *et al.* 1989). However, excessive agitation can result in cell damage from fluid mechanical forces (Toma *et al.* 1991, Lilly *et al.* 1992). Interactions between the cells and solid particles (Croughan *et al.* 1988) and bubble rupture at the free gas-liquid interface (Kunas and Papoutsakis 1990, Michaels *et al.* 1996) have also been shown to be damaging to the cells.

Studies of *Penicillium chrysogenum*, *Brevibacterium flavum*, *Trichoderma reesei*, *Saccharomyces cerevisiae* and hybridoma cells, in the absence of particulates, indicate that microbial cell damage as a consequence of hydrodynamic stress can lead to changes in the cell metabolic rate, morphology, and metabolic pathway (Kunas and Papoutsakis 1990, Smith *et al.* 1990, Toma *et al.* 1991). These responses result in reduced productivity of the biological process. In the extreme case of cell damage, cell disruption occurs. Selection of the optimum operating conditions in minerals bioprocessing, soil bioremediation and immobilised biocatalyst processes therefore requires a compromise between the operating conditions that favour mass transfer and minimise the hydrodynamic damage to the cells. Although correlations have been developed to describe mass transfer in slurry reactors (Oguz *et al.* 1987), equivalent expressions have not been developed to describe cell damage and disruption. Cell disruption is further required in downstream processing, for example bead mills, in the recovery of intracellular products (Harrison 1991). There is thus a need to quantify and model the microbial cell damage and disruption in systems where cells and solids are

present, and to understand the mechanisms of the damage and disruption. This would facilitate the design of bioreactors in which microbial cell damage and disruption could be either maximised or minimised, depending on the application.

This dissertation presents the results of an investigation into the disruption of freely suspended micro-organisms agitated in a stirred tank reactor in the presence of biologically inert solid particles and in the absence of aeration. *Saccharomyces cerevisiae* (Baker's yeast) was chosen as the model micro-organism because it is a relatively well understood biological system for which analytical techniques to quantify the cell damage and disruption have been well established. In addition, *Saccharomyces cerevisiae* was available in reproducible batches as Baker's yeast cream from Anchor Yeast (Cape Town, South Africa). Silica was used as the particulate phase because it is biologically inert and is not susceptible to attrition in the stirred tank.

The work presented in this thesis is an extension of a study performed by Pearce (1993), in which the effect of particle size, shape and density, solids concentration, biomass concentration and agitation intensity on the disruption of *Saccharomyces cerevisiae* and a mixed culture of *thiobacilli* were investigated. A 1 liter stirred tank reactor was used in the investigation of Pearce (1993). A review of Pearce's work and that of other workers in this area revealed that although the effect of completely suspended solid particles on cell damage and disruption is relatively well understood, little work has been conducted to investigate the effect of incompletely suspended solid particles on micro-organisms. An understanding of the effect of incompletely and completely suspended solid particles on cell disruption would facilitate the selection of the optimum operating conditions for systems where cells are processed in the presence of particulates. One of the primary objectives of this study was thus to quantify the disruption of the *Saccharomyces cerevisiae* in the regimes of incompletely and completely suspended solid particles, as a function of the agitation intensity, solids concentration and impeller flow pattern. Radial flow was achieved by using a Rushton turbine whereas predominantly axial flow was achieved by using a pitched-blade turbine, with the pumping action downwards. To define the regimes of incomplete and complete solids suspension, the solids suspension in the slurry reactor needed to be quantified. This was a further objective in this work. A final objective was to assess the applicability of existing cell damage and disruption models to the cell disruption observed in the slurry reactor. If these models were inapplicable, the aim was to develop a model which described the cell disruption in terms of the operating parameters, and which allowed the mechanisms of cell disruption to be elucidated. This model would require validation by applying it to the cell damage and disruption observed in other slurry systems.

To place the study into context, industrially important systems, where microbial cells are processed in the presence of particulates, are reviewed in Chapter 2. In addition, research performed to date on the effect of incompletely and completely suspended solids on cell disruption is reviewed in this chapter.

A 3 liter stirred tank reactor of standard geometry was used to investigate the disruption of the *Saccharomyces cerevisiae* in the presence of the silica particles. Details of the experimental apparatus, the experimental protocol and the analytical techniques, used to assess the cell disruption, are presented in Chapter 3. The study was primarily concerned with cell disruption in the Rushton turbine system. Limited experiments were performed with the pitched-blade turbine to assess the applicability of the model, developed to describe cell disruption, to other reactor geometries.

The properties of the yeast and silica model system are discussed in Chapter 4. Experimental data characterising the physical properties of the system are presented. The structure of the cell wall of *Saccharomyces cerevisiae* is reviewed as it provides the physical strength to the cell. Hence a more complete understanding to the disruption of the yeast can be obtained.

In Chapter 5, the degree of solids suspension and the various methods of its quantification are reviewed. Measurements of the critical impeller speed, used to define the transition between the regimes of incomplete and complete solids suspension, are then presented for the Rushton and pitched-blade turbines. These are validated by comparison to literature values. A model of these critical impeller speeds, in terms of the solids loading, is presented. This relationship is required for the modelling of the cell disruption data (Chapter 8).

In this study, cell disruption in the slurry reactor was measured in terms of soluble protein release. Use of a kinetic expression to model the profile of soluble protein release as a function of time, allowed the cell disruption to be quantifed in terms of a rate and a maximum extent. The kinetic expression used to model the disruption of the *Saccharomyces cerevisiae* and the calculation of the kinetic parameters are described in Chapter 6. The results from the cell disruption experiments, performed using the Rushton turbine and the pitched-blade turbine at a range of solids loadings and agitation intensities, are also presented in this chapter and compared to literature results.

In the development of a model to describe the cell disruption in the slurry reactor, the cases of complete and incomplete solids suspension were considered separately. Modelling of the cell disruption for each of these cases is discussed in Chapters 7 and 8 respectively. In modelling the cell disruption in the regimes of

incomplete and complete solids suspension, the existing cell damage and disruption models were reviewed and were then applied to the cell disruption data from the Rushton turbine system. The inapplicability of many of these models motivated the development of new models. The mechanistic and predictive models developed in this work are presented in Chapters 7 and 8. These are validated by application to the data reported here and to other systems where cells and solid particles are used. In Chapter 9, the conclusions drawn from the study are presented and recommendations are made of areas in which further work may yield fruitful results on cell damage and disruption in particulate systems.

Chapter 2: Slurry Bioreactors - The Effect of Completely and Incompletely Suspended Solids on Cell Damage and Disruption

2.1 Review of Slurry Systems of Industrial Importance

Minerals bioprocessing, soil bioremediation, immobilised cell systems and bead mills are examples of processes of industrial significance that utilise micro-organisms and particulates. In this section, the basic features of these processes and the characteristics of the micro-organisms and particulates are reviewed. In Table 2.1, the characteristics of these slurry systems are listed and compared to the characteristics of the *Saccharomyces cerevisiae*-silica system used in this study.

2.1.1 Minerals Bioprocessing

Minerals bio-oxidation involves the use of a mixed population *of Thiobacillus ferrooxidans*, *Thiobacillus thiooxidans* and *Leptospirillum ferrooxidans* for the oxidation of iron and sulphur-containing ores. The oxidation of the iron and sulphur in the ores by the bacteria breaks down the ore matrix, thus permitting the dissolution of metal ions and making precious metal residues more amenable to subsequent processing (Gormely and Branion 1989). Bacterial oxidation has been applied to dump and heap leaching of base metals (Brierley 1978, Rossi 1990) and is being used increasingly in the treatment of gold-containing refractory ores in both vat and heap processes (van Aswegen 1993, Brierley *et al.* 1995).

In industry, active processes, in which the operating conditions are controlled, are preferred for the cultivation of the *Thiobacillus*-type bacteria (van Aswegen 1993). Growth of the *thiobacilli* in stirred tank reactors and air lift reactors allows the optimum temperature range of 30 to 45 °C (Pinches *et al.* 1991) and the optimum pH range of 1.2 to 1.8 (van Aswegen 1993) to be maintained throughout the bioreactor. Use of active processes further allows the high oxygen demand of the *thiobacilli* to be met. The oxygen demand of the micro-organisms is dependent on the sulphide content of the mineral, the solids particle size and the reactor solids concentration (Bailey 1993). Bailey (1993) reports an oxygen demand of 44.1 kg O^2 m^{-3} d^{-1} for a pyrite concentrate (28% S) at a solids concentration of 4.6% (v/v) (21.3% (w/v)). A final advantage of stirred tank reactors in minerals bioprocessing is that nutrient limitation to the cells can be avoided by using a sufficiently high agitation intensity (Rossi 1990). The scale of industrial processes, which utilise stirred

tank reactors in the bioprocessing of refractory gold ores, is reported to vary from 20 tpd at Vaal Reefs (South Africa) (Bailey 1993) to 960 tpd at Ashanti (Ghana) (Dew 1997).

Thiobacillus-type bacteria are reliant on the iron and/or sulphur in the ore as their energy source and use carbon dioxide as their main source of carbon (Schlegel 1988). The unicellular, gram-negative *Thiobacillus ferrooxidans* and *Thiobacillus thiooxidans* cells have an average diameter of 0.4-0.8 μm and an average length of 0.9-2.0 μm. *Leptospirillum ferrooxidans*, however, exhibits extensive morphological variability, ranging from a helix with 2-5 spires to a curved rod, 0.9-1.1 μm in length and 0.2-0.4 μm in diameter. The cell wall structure of this bacteria is similar to that of the other gram-negative bacteria (Rossi 1990). The greater proportion of the bacteria attach themselves directly to the mineral surface (Brierley 1978, Bailey 1993). Bio-oxidation of the mineral occurs via a two-step mechanism: the mineral is leached chemically by ferric iron, which is regenerated by the bacteria from the ferrous form (Boon *et al.* 1995).

The ore used for bacterial oxidation ranges from run-of-mine ore to high-sulphur flotation concentrates (Pinches *et al.* 1991). Barrett *et al.* (1993) have reported that gold occurs in minerals such as arsenopyrite, pyrite, pyrrhotite and chalcopyrite. The size of the particles used in minerals bio-oxidation generally appears to be 65 to 95% passing 75 μm (Gormely and Branion 1989, Pinches *et al.* 1991, Bailey 1993). Selection of the optimum solids concentration depends on the sulphide content of the ore (Pinches *et al.* 1991, Bailey 1993). Using a run-of-mine ore (1.2% S), Bailey (1993) found that the bio-oxidation rate was proportional to the solids concentration up to 21% solids (v/v) (60% (w/v)), the maximum solids concentration investigated. However, solids concentrations less than 5% (v/v) (20% (w/v)) are optimal when using high sulphide concentrates (28-33% S) (Torma *et al.* 1970, Hansford and Bailey 1993). Densities of three ores used in bioleaching have been reported by Bailey (1993): a density of 2801 kg m^{-3} for a Vaal Reefs run-of-mine concentrate, a density of 4592 kg m^{-3} for a Vaal Reefs pyrite flotation concentrate and a density of 4386 kg m^{-3} for a Prieska pyrite flotation concentrate.

2.1.2 Soil Bioremediation

Contaminated soils have a negative impact on the environment by impairing ground and surface water. Bioremediation of such soils involves the controlled use of micro-organisms to break down hazardous organic chemicals in the soil. The micro-organisms aerobically degrade the organic pollutants to biomass, carbon dioxide and water. Anaerobic degradation of the organic pollutants yields biomass, methane and water (Kleijntjens *et al.* 1992, Pearce *et al.* 1995). Soil bioremediation offers a comparably inexpensive yet efficient method of removing toxic chemicals from contaminated soils without destroying the soil

ecosystem. It can be used exclusively or in tandem with other physical and chemical soil remediation strategies, such as soil washing and soil vapour extraction.

A survey of the nature and extent of contaminated sites in South Africa was conducted by Pearce *et al.* (1995). Their survey showed that 51% of these sites were industry-related, and that contamination of the soil from petroleum products was most prevalent. Other organic pollutants identified in their survey were solvents, pesticides and herbicides, and wood-treating chemicals.

Degradation of these organic pollutants in soils by micro-organisms is broadly classified as being either *in-situ* or *ex-situ*. *In-situ* bioremediation involves the treatment of the contaminated soil on-site. Techniques used to enhance *in-situ* bioremediation include the injection of a synthetic surfactant or solvent into the contaminated zone to promote the release of hydrophobic contaminants and thus increase their bioavailability to the micro-organisms (Hoeppel *et al.* 1991), the use of a plough or rotovator to achieve oxygen penetration into the soil, and the addition of phosphorous and nitrogen to the soil to stimulate the micro-organisms in the degradation of organic contaminants (Bradford and Krishnamoorthy 1991). *In-situ* bioremediation is advantageous in that it is simple to implement and is cost-effective. Disadvantages of this method of bioremediation are that it is highly dependent on the permeability of the soil, and that the operating conditions are difficult to control.

Ex-situ bioremediation involves the excavation of the contaminated soil and its subsequent treatment with micro-organisms to reduce the contaminant concentrations to acceptable levels. Closer control over the operating parameters can thus be exercised. This allows the optimum environmental conditions to be created for the biodegradation of the organic pollutants so that more rapid degradation of the contaminants can be achieved. An understanding of the biological processes in slurry bioreactors is thus required for the further improvement of these processes. *Ex-situ* bioremediation has been performed in lined biocells provided with an aeration system (Pearce *et al.* 1995). Stirred tank reactors have also been used (Ryan *et al.* 1991, Stegmann *et al.* 1994). Here, the contaminated soil is treated as an aqueous slurry. Kleijntjens *et al.* (1992) investigated the use of a continuous, three phase suspension reactor to treat polluted soils at solids concentrations of 12.3% to 16.4% (v/v). Their 4.0 m^3 suspension reactor had a tapered bottom and was agitated by air, injected with the slurry at the bottom of the reactor. The air flow rate was adjusted so that the coarse, non-polluted soil fraction (700 to 4000 μm) was fluidised at the bottom of the reactor, and the small particles (1 to 700 μm), to which more than 90% of the organic pollutants were adsorbed, were suspended in the bulk of the vessel.

The micro-organisms used in soil bioremediation are the indigenous fungi and bacterial populations in the soil. Genetically engineered or specially adapted micro-organisms, which degrade target pollutants, may also be introduced to the contaminated soil. Pearce *et al.* (1995) report that 10^7 to 10^8 micro-organisms (colony forming units) should be used per gram of soil. A pH of 6 to 8, and a temperature of 15°C to 35°C are optimal for the metabolic activity of the micro-organisms. Moisture is essential for microbial growth, movement through the soil and the solubilisation of the organic contaminants to increase their bioavailability (Providenti *et al.* 1993). Aerobic degradation of the organic pollutants is preferred to anaerobic bioremediation since it is more rapid. However, anaerobic bioremediation is advantageous for the treatment of highly chlorinated compounds which are resistant to aerobic biodegradation (Pearce *et al.* 1995).

2.1.3 Immobilised Cell Systems

Cell immobilisation, *i.e* the attachment of cells to solid particles, provides various benefits. Cell immobilisation increases the number of cells per reactor volume (Tyagi *et al.* 1992). It allows the continuous production of secondary metabolites at dilution rates exceeding the maximum specific growth rates of the cells. Immobilisation further facilitates removal of the biological phase in downstream processing and gives rise to better oxygen transfer, on use of filamentous fungi, owing to a decrease in broth viscosity compared to traditional fermentations (Rosvear *et al.* 1987, Webb and Dervakos 1996). Cell immobilisation is also used to stabilise genetically engineered cells (Shu and Yang 1996) and anchorage-dependent cells (Croughan and Wang 1989).

Cell immobilisation can be classified as being either active or passive. Active immobilisation involves the attachment of the cells to the solid particles by chemical or physical means. Passive immobilisation occurs when films or flocs of cells form naturally on, around or within solid surfaces or particles (Black *et al.* 1984).

An important example of active immobilisation is the chemical bonding of *Saccharomyces cerevisiae* cells to solid support particles for the production of ethanol (Bandyopadhyay and Ghose 1982). Three methods are used in forming the chemical bond between the yeast cell and the support particle:

- Immobilisation of *Saccharomyces cerevisiae* by a chelation/ metal link process onto a porous inorganic support (Dias *et al.* 1982, Cabral *et al.* 1986, Kennedy and Cabral 1990).
- Formation of a covalent bond between the cells and glass beads, which have been dip-coated in gelatin and cross-linked with glutaraldehyde (Doran and Bailey 1986).

- Formation of a covalent bond between the yeast cells and silica beads, which have been pretreated with a silane and glutaraldehyde (Navarro and Durand 1977, Bandyopadhyay and Ghose 1982).

The porous inorganic supports used by these workers included controlled pore titanium, silica, silica gel, Spherosil XOB015 (porous silica) and pumice stone. The diameters of the particles ranged from 100 to 4000 μm. Each of these immobilisation methods results in the attachment of yeast cells via a strong covalent bond to the surface of the support to form, at most, a monolayer of cells. Doran and Bailey (1986) found that immobilised cells accounted for between 83 and 93% of the total cell number in the packed bed column reactor. The remaining cells were freely suspended in the medium.

Examples of passive immobilisation include waste water treatment, the growth of micro-organisms on biomass support particles, the immobilisation of *Saccharomyces cerevisiae* for the production of recombinant proteins, and the growth of animal cell cultures on microcarrier beads. In the activated-sludge process in waste water treatment, the suspended solid material is oxidised by micro-organisms which attach themselves to the particulates. A mixed population of cells, including *Zoogloea ramigera*, is used which agglomerate into flocs. These flocs, called activated sludge, have a high affinity for suspended organic matter which ranges in diameter from 1 to 100 μm. The main component of the activated-sludge process is a continuous flow aerated bioreactor, linked to a sedimentation tank where the liquid is clarified (Bailey and Ollis 1986).

Biomass support particles (BSPs) are essentially an open network of matrix support material with a high porosity of 0.80 to 0.97. They are typically constructed of stainless steel knitted mesh or reticulated polyester foam (Black *et al.* 1984). The diameter of the stainless steel spheres and the length of the polyester foam cubes, used by Black *et al.* (1984), were 6000 μm. Their respective densities, when filled with *Saccharomyces cerevisiae*, were 7700 and 1100 kg m^{-3}. Cells become entrapped within the lattice structure of the BSPs and then adhere to them. The interior of the BSP is characterised by an environment of low shear and it can thus retain the weakly adsorbed cells. Any cells which grow beyond the protected environment of the BSP are continuously removed by the abrasive forces of liquid shear and interparticle and particle-wall collisions that exist in stirred tank reactors and fluidised bed reactors (Atkinson *et al.* 1979, Black *et al.* 1984). Biomass support particles have been employed successfully in the passive immobilisation of cells for the treatment of sewage and industrial wastewater (Atkinson *et al.* 1981, Walker and Austin 1981). Black *et al.* (1984) found that BSPs could also be used for the passive immobilisation of *Saccharomyces cerevisiae* cells for the production of ethanol.

Saccharomyces cerevisiae has been used as the host organism for the production of several recombinant proteins (Heslot and Gaillardin 1991). It has been found that improved plasmid stability and productivity can be obtained with cell immobilisation (Kanayama *et al.* 1988). Shu and Yang (1996) passively immobilised *Saccharomyces cerevisiae* onto porous glass beads by adsorption for the continuous production of recombinant murine granulocyte-macrophage colony-stimulating factor (MuGM-CSF). A fluidised bed bioreactor was used at a dilution rate of 0.03 hr^{-1} and at particle concentrations ranging from 5% to 33% (v/v). The porous glass beads had an average diameter of 1000 μm, a porosity of 60% and a density of 2070 kg m^{-3}. Scanning electron micrographs showed that the yeast cells were immobilised by attachment to the external as well as the internal pore surfaces of the glass beads. As the particle loading increased from 5% to 33%, the concentration of immobilised cells increased from 4.88 to 28.68 g/l, and the concentration of freely suspended cells decreased from 11.28 to 6.63 g/l. The biomass loading per particle decreased from 0.160 to 0.098 g/g as particle loading increased. This was attributed to nutrient limitation at high solids concentrations.

Animal cells undergo passive immobilisation on microcarriers and are used on a large scale in agitated vessels for the production of biochemicals such as hormones, interferons, enzymes and antibodies (Croughan *et al.* 1987). As a result of the relatively large size (10 to 15 μm) of these anchorage-dependent cells (Kunas and Papoutsakis 1990) and their lack of a protective cell wall, animal cells are particularly susceptible to cell damage. Extensive research has been conducted into the damage of animal cells in spinner vessels at the laboratory scale (Croughan *et al.* 1987, 1988, 1989; Cherry and Papoutsakis 1988, Croughan and Wang 1989, Lakhotia and Papoutsakis 1992). Cytodex 1 and Cytodex 3 beads were the most frequently used microcarriers in this research. The hydrated average bead diameter and density of Cytodex 1 microcarriers were reported by Croughan *et al.* (1988) as 178 μm and 1030 kg m^{-3} respectively. The solids volume fraction used in these studies was always less than 0.03.

2.1.4 Bead Mills

The products in biological processes are often intracellular with the result that the cells need to be disrupted for the product recovery (Bailey and Ollis 1986). Bead mills provide an efficient mechanical method of disrupting micro-organisms by agitation of the cell suspension at high impeller tip speeds (5 to 20 m s^{-1}) in the presence of a high volume fraction of inert solid particles (44-47%). Disruption of the microbial cells is achieved by collisions and by grinding between stream layers of solid particles of different velocity (Engler 1985, Harrison 1991). The mill consists of a horizontally or vertically oriented chamber with a motor driven central shaft. A number of agitator discs or pins, attached to the shaft either centrically or eccentrically, accelerate the solid particles (beads) used as grinding elements. The beads are retained in the

chamber by sieve plates or by a coaxial ring slot which is integrated into the bearing housing. The micro-organism suspension is passed through the bead mill, usually in a continuous fashion. An efficient cooling jacket is required since most of the energy is dissipated as heat. Commercially available bead mills range from 0.6 to 200 liters in volume. Further scale-up is limited by the heat removal required (Mogren *et al.* 1974, Chisti and Moo-Young 1986, Kula and Schutte 1987).

The efficiency of bead milling is dependent on many variables, among which the most important are agitator speed, the residence time in the mill, the concentration of the cells, the size and concentration of the beads, the bead density, temperature, the design of the stirrer and the geometry of the grinding chamber (Harrison 1991). Bead mills have been used successfully to disrupt the yeasts *Saccharomyces cerevisiae*, *Saccharomyces carlsbergensis*, *Candida utilis* and *Candida boidinii*, and the bacteria *Lactobacillus confusus*, *Escherichia coli*, *Bacillus sphaericus*, *Brevibacterium ammoniagenes* and *Bacillus subtilis* (Rehacek 1971, Mogren *et al.* 1974, Schutte *et al.* 1983). Hedenskog and Ebbinghaus (1972) report the use of bead mills for the disruption of the algae *Scenedesmus obliquus* and *Spirulina platensis*, for intracellular protein release. Complete disruption of the fungus *Aspergillus niger* has also been achieved (Rehacek 1971). The size of the micro-organisms disrupted in bead mills therefore ranges between 1 and 10 μm (Kula and Schutte 1987). An optimum wet weight concentration of 40 to 50% (w/v) has been reported by Kula and Schutte (1987) for the disruption of yeast cells in bead mills. Since the micro-organisms are temperature sensitive with protein denaturation or deactivation occurring at elevated temperatures, the recommended temperature range for bead mills is 5 to 15 °C (Kula and Schutte 1987).

Glass beads are most commonly used as the grinding elements in bead mills since they are relatively cheap and available in a range of sizes. The density of the glass beads ranges between 2500 to 2900 kg m^{-3}. Other grinding elements that have been used include zirconium oxide beads (density of 5400 kg m^{-3}) and ceramic beads made partially from zirconium oxide (density of 3800 kg m^{-3}) (Kula and Schutte 1987). The optimal size of the grinding elements is determined by the size of the micro-organisms and the location of the desired enzyme in the cell. Experimental findings have established that yeasts are more efficiently disrupted using beads with diameters in the range of 500 to 850 μm whilst bacterial disruption is favoured by using beads smaller than 500 μm in diameter (Marffy and Kula 1974, Kula and Schutte 1987). Larger beads are more efficient in solubilising enzymes in the periplasmic space than those found in the cytoplasm (Schutte *et al.* 1983). Selection of a solids concentration is restricted to below 47% (v/v) since heating of the cell homogenate and the power consumption increase markedly beyond this point (Schutte *et al.* 1983).

2.1.5 Concluding Remarks

This study concerns an investigation into the disruption of freely suspended *Saccharomyces cerevisiae* in a slurry reactor. The motivation behind choosing *Saccharomyces cerevisiae* and silica as the model system in this work was detailed in Chapter 1. From Table 2.1, which compares the characteristics of systems utilising particulates and micro-organisms, it can be seen that the conditions used in this work simulate most closely the disruption of freely suspended bacteria in the minerals bio-oxidation system, the disruption of freely suspended bacteria in the suspension reactor used by Kleijntjens *et al.* (1992) for soil bioremediation, the disruption of freely suspended *Saccharomyces cerevisiae* used in the system of Shu and Yang (1996) for the production of recombinant protein, and the disruption of freely suspended *Saccharomyces cerevisiae* in bead mills.

2.2 The Effect of Completely and Incompletely Suspended Solids on Cell Damage and Disruption -A Review

In this section, literature concerning the effect of completely and incompletely suspended solids on cell damage and disruption is reviewed. This includes work performed in the minerals bio-oxidation system and the animal cell-microcarrier system. Completely suspended solids were used in these systems to achieve good mass transfer of nutrients and oxygen to, and products away from the attached cells. Any decrease in the cell growth upon agitation could thus be attributed to hydrodynamic forces or momentum transfer alone. Completely suspended solid particles were further used in the minerals bioprocessing system to ensure a uniform flow of solids through the train of stirred tank reactors (Gormely and Branion 1989). The work of Pearce (1993), where the effect of completely and incompletely suspended solids on the disruption of freely suspended *Saccharomyces cerevisiae* was investigated using a slurry bioreactor, is also reviewed.

Table 2.1 Comparison of slurry systems reviewed in Section 2.1 and the *Saccharomyces cerevisiae*-silica system used in this study

Cell-Solid System	Micro-organism		Location of Cell	Solid Particle				Reactor Type
	Type	Diameter (μm)		Type	Diameter (μm)	Density (kg m^{-3})	Solids Loading	
This Study	*Saccharomyces cerevisiae*	5.4	Freely suspended	Silica	600-850	2664	10%, 20% (v/v)	Stirred tank
Minerals Bioprocessing	*Thiobacillus ferrooxidans*, *Thiobacillus thiooxidans*, *Leptospirillum ferrooxidans*	0.4-0.8 μm by 0.9-2.0 μm	Attached (greater proportion) and freely suspended	Iron and sulphur-containing ores (eg. arsenopyrite, pyrite, pyrrhotite, chalcopyrite)	generally 65 to 95% passing 75 μm	2800-4400	5-20% (v/v)	Stirred tank, air lift reactor
Soil bioremediation	Mixed population of indigenous/genetically engineered/adapted bacteria and fungi	1 (bacteria)	Freely suspended	Soil (range of ores including sand and clay)	generally 1-4000	2100-2500		Landfarming Slurry reactor
							12.3-16.4% (v/v)	Air-agitated suspension reactor
Bead Mills	Yeasts, Bacteria, Fungi and Algae	1-10	Freely suspended	Glass, ceramic or zirconium oxide beads	400-1500	2500-5400	44-47% (v/v)	Chamber with agitator discs or pins on shaft
Immobilised Cell Systems								
1.Active Immobilisation	*Saccharomyces cerevisiae*	5	Attached	Glass beads, controlled pore titanium, silica, silica gel, Spherosil XOB 015, pumice stone	100-4000			Packed bed reactor

Table 2.1 Continued

Cell-Solid System	Micro-organism		Location of Cell	Solid Particle				Reactor Type
	Type	Diameter (μm)		Type	Diameter (μm)	Density (kg m^{-3})	Solids Loading	
Immobilised Cell Systems								
2.Passive Immobilisation								
Activated-sludge Process	Mixed population; most common bacterium is *Zoogloea ramigera*	Formation of flocs	Attached	Organic material	1-100			Aerobic reactor linked to a sedimentation tank with recycle
BSPs	Mixed population used in treatment of sewage and industrial wastewater, *Saccharomyces cerevisiae*	Formation of flocs	Attached	Stainless steel knitted mesh	6000	7700		Stirred tank, fluidised bed
		5		Reticulated polyester foam	1000	1100		
Production of Recombinant Proteins	*Saccharomyces cerevisiae*	5	Attached and freely suspended	Porous glass beads	1000	2070	5-33% (v/v)	Fluidised bed
Animal cell-Microcarrier System	eg. FS-4 cells, bovine embryonic kidney cells, hybridoma cells	10-15	Attached	Microcarriers eg. Cytodex 1, Cytodex 3	180	1030	0.02-3.06% (v/v)	Spinner vessel at laboratory scale

2.2.1 Minerals Bioprocessing

The effect of completely suspended solids on the *thiobacilli* used in the minerals bioleaching system has been investigated in terms of variation in the agitation intensity, impeller flow pattern and the solids concentration. During the bio-oxidation of high sulphide content material at high solids concentrations, the oxygen demand of the bacteria is high, necessitating the use of high agitation rates to improve mass transfer (Bailey 1993). There is a dearth of information in the bio-oxidation literature regarding the effect of agitation intensity on cell damage. This highlights the need for a rigorous investigation into the effect of agitation intensity on the free and attached bacteria. One of the few studies performed is that of Hackl *et al.* (1989), who found, during their pilot plant testwork, that a tip speed of 5.3 m s^{-1} was detrimental to the leach rates of *thiobacilli*. However, when the tip speed of the Rushton turbine was reduced to 3.3 m s^{-1}, the bioleach rates started to increase and, within 4 days, returned to normal. At the laboratory scale (1 liter), Pearce (1993) found that agitation of *thiobacilli* with a 6-bladed Rushton turbine at 630 rpm (impeller tip speed of 2.6 m s^{-1}) in the presence of 10% (w/v) pyrite completely inhibited the growth of the cells. However, agitation of the cells at 350 rpm (impeller tip speed of 1.4 m s^{-1}) was not detrimental to them. The use of high agitation intensities, during the initial stages of growth of *thiobacilli*, also hinders their attachment to the surfaces of mineral particles with the result that their growth and bioleach rates are inhibited (Gormely and Branion 1989, Hackl *et al.* 1989). The reduced attachment of *Thiobacillus ferrooxidans* at conditions of high shear was illustrated by Cook (1964), using stationary and shaken flasks. Inhibition of cell growth was only observed in the shaken flasks and was overcome when the flasks were left for 3 days prior to shaking.

Hackl *et al.* (1989) investigated the effect of the impeller flow pattern on the damage to a mixed culture of *Thiobacillus ferrooxidans*, *Thiobacillus thiooxidans* and *Leptospirillum ferroxidans*, at an impeller tip speed of 5.3 m s^{-1}, which was above the critical impeller speed. Agitation of the suspension with a Rushton turbine resulted in an immediate 14% reduction in the bioleach rate. However, agitation of the suspension with a 45 degree pitched-blade turbine resulted in normal leach rates. This indicated that at a constant impeller speed of 5.3 m s^{-1}, the cells were more damaged by agitation with the Rushton turbine. These findings are supported by the study of Pearce (1993), in which an axial flow impeller and a Rushton turbine were used to agitate *thiobacilli* in a stirred tank in the presence of 10% (w/v) pyrite. Agitation with the Rushton turbine at an impeller tip speed of 2.6 m s^{-1}, completely inhibited the cell growth (lag > 20 days) whereas cell growth was observed after a lag time of 11 days on agitation with the axial flow impeller at 2.6 m s^{-1}. This is explained by the fact that at a given impeller speed, the power input per unit volume is higher for the radial flow pattern of the Rushton turbine than for the predominantly axial flow pattern of the pitched-blade turbine. In addition to the higher power consumption of the Rushton turbine, these impellers

generate more shear. The effect of impeller flow pattern on the cell damage was determined by Hackl *et al.* (1989) and Pearce (1993) at a single impeller speed in their respective studies. To draw meaningful conclusions regarding the effect of impeller flow pattern on cell damage, a range of impeller speeds should be used for the axial and radial flow impellers.

The effect of solids concentration on the performance of the bacteria in bioleaching has been investigated using completely suspended systems. Beyer *et al.* (1986) determined the batch oxidation rates of *Thiobacillus ferrooxidans* in an airlift reactor at 2%, 10% and 20% (w/v) concentrations of coal (3.3% S). The rate of oxidation of pyrite was observed to increase from 58 to 338 mg pyritic sulphur per liter per day as the solids concentration increased from 2 to 10%. However, at 20% solids this rate was reduced to 128 mg pyritic sulphur per liter per day. Measurement of the number of viable cells showed that the cell concentration was four orders of magnitude less for the 20% solids concentration than for the 10% solids concentration. This was attributed to the greater shear to which the cells were exposed at 20% solids.

Torma *et al.* (1970) investigated the effect of increased solids concentration (0 to 27% (w/v)) on the oxidation of zinc from a zinc sulphide concentrate (33% S) using *Thiobacillus ferrooxidans*. The zinc extraction rate was found to be directly proportional to the solids concentration for solids concentrations below 14% (w/v). Between 14 and 20% solids, the extraction rate was independent of the solids concentration and above 20% solids, the rate decreased. The researchers postulated that the decrease in oxidation rate arose from the interference of the solids with the mass transfer of oxygen or carbon dioxide to the micro-organisms. This postulation is supported by Bailey (1993), following investigation of the bio-oxidation of two high grade pyrite concentrates (> 28% S) using a fluidised bed reactor. A solids concentration range of 20 to 45% (w/v) was employed and a mixed culture of *Thiobacillus ferrooxidans*, *Thiobacillus thiooxidans* and *Leptospirillum ferroxidans* used. Bailey (1993) found that the bio-oxidation rate at high solids concentrations was affected by the oxygen availability in the reactor. While oxygen or carbon dioxide availability may limit the bio-oxidation rate of the micro-organisms at high solids concentrations, the influence of mechanical stress has not been rigorously discounted.

2.2.2 Animal Cell-microcarrier System

The effect of completely suspended solids on the damage to anchorage-dependent animal cells immobilised on microcarriers in spinner vessels has been rigorously investigated (Croughan *et al.* 1987, 1988, 1989; Cherry and Papoutsakis 1988, Croughan and Wang 1989, Lakhotia and Papoutsakis 1992). These studies considered the effect of agitation intensity and solids concentration on the cell damage. Table 2.2

Table 2.2 **Systems used in investigation of the damage to immobilised animal cells.**
Impeller speeds employed are greater than the critical impeller speed.

Conditions employed	Solids concentration (% v/v)	Agitation intensity		Cell type and Microcarrier type	Volume of spinner vessel (ml)	Researcher
		Agitation rate (rpm)	Impeller tip speed ($m\ s^{-1}$)			
Fixed, low solids concentration, Varying agitation intensity	0.02	35-220 60-230	0.10-0.61 0.17-0.64	FS-4 cells, Cytodex 1 microcarriers	125 500	Croughan *et al.* (1989)
	0.3	60-220	0.12-0.44	FS-4 cells, Cytodex 1 microcarriers	100	Croughan *et al.* (1987)
Fixed, moderate/high solids concentration, Varying agitation intensity	0.5	75-150	0.16-0.43	Bovine embryonic kidney cells, Cytodex 3 microcarriers	2000*	Cherry and Papoutsakis (1988)
	0.5	45-160	0.10-0.35	Bovine embryonic kidney cells, Cytodex 3 microcarriers	100	Lakhotia and Papoutsakis (1992)
	0.5 1.5	35-150 35-150	0.10-0.42 0.14-0.61	FS-4 cells, Cytodex 1 microcarriers	125 500	Croughan and Wang (1989)
Fixed, low agitation intensity, Varying solids concentration	$\Phi_M = 0.1^{\Psi}$ $\Phi_I = 0\text{-}2.8^{\Psi}$	35	0.10	FS-4 cells, Cytodex 1 microcarriers, Sephadex G-50 beads as inert solid particles	125	Croughan *et al.* (1988)
Fixed, high agitation intensity, Varying solids concentration	$\Phi_M = 0.1^{\Psi}$ $\Phi_I = 0\text{-}2.9^{\Psi}$	150	0.42	FS-4 cells, Cytodex 1 microcarriers, Sephadex G-50 beads as inert solid particles	125	Croughan *et al.* (1988)

*Round-bottom tissue culture reactor.

Ψ Φ_M refers to the volume fraction of microcarriers, Φ_I refers to the volume fraction of inert solid particles.

summarises the types of cells and microcarriers as well as the ranges of agitation intensity and solids concentration used by the various workers. Damage to the animal cells in these systems was quantified in terms of changes in the attached, viable cell concentration.

The studies showed that at low to moderate levels of agitation, the apparent growth rate of the animal cells was not affected by fluid mechanical forces. Croughan *et al.* (1989) found that no cell death occurred when FS-4 cells, immobilised on microcarriers present at a solids loading of 0.02% (v/v), were agitated at 60 rpm (impeller tip speed of 0.17 m s^{-1}) in 500 ml spinner vessels. Lakhotia and Papoutsakis (1992) obtained similar results for the growth of bovine embryonic kidney cells, immobilised on 0.5% (v/v) microcarriers. The apparent specific growth rates of these cells were found to be independent of agitation rates below 90 rpm (impeller tip speed of 0.20 m s^{-1}). However, the apparent growth rates of the cells were reduced at high levels of agitation. This reduction in the apparent growth rates occurred even at very low microcarrier concentrations, as shown by the study of Croughan *et al.* (1989). These workers found that at the low microcarrier concentration of 0.02% (v/v), the apparent growth rates of FS-4 cells decreased from 0.016 hr^{-1} to -0.005 hr^{-1} as the agitation intensity was increased from 35 to 220 rpm (impeller tip speeds of 0.10 to 0.61 m s^{-1} respectively).

The apparent or measured growth rate of cells is defined as the difference between their intrinsic growth rate and their death rate. A reduction in the apparent growth rate of the animal cells in overagitated microcarrier cultures could thus be attributed to a reduction in their intrinsic growth rate (growth inhibition), an increase in their death rate or a combination of these. Croughan and Wang (1989) investigated this by considering the damage to FS-4 cells attached to 1.5% (v/v) microcarriers at agitation intensities of 35 and 150 rpm. No cell damage or removal was observed for the culture at 35 rpm, whereas the culture at 150 rpm exhibited a 15% decrease in attached cell concentration. The intact FS-4 cells, detached from the microcarriers, were found to lyse and disintegrate over a period of 1 to 2 days. Cell fragments observed in the culture fluid at 150 rpm thus originated from either lysis of detached FS-4 cells in the culture fluid, or disruption of attached cells. The DNA release into the culture fluid was measured for the experiments run at 35 rpm and 150 rpm to quantify the concentration of whole and lysed cells in suspension. Comparison of this data with mechanistic models showed that the reduction in the apparent growth rate of the cells at 150 rpm was due entirely to the irreversible and random removal of the cells from the microcarriers. The intrinsic growth rate of the cells at 150 rpm was the same as that at 35 rpm, and was thus unaffected by hydrodynamic forces.

Hydrodynamic death and removal of immobilised animal cells, at high agitation rates above the critical impeller speed, can be reduced by increasing the fluid viscosity through dextran supplementation. Lakhotia

and Papoutsakis (1992) used dextran to alter the medium viscosity between 1.0 and 2.6 cp. They found that the protective effect of viscosity on the apparent growth rate of bovine embryonic kidney cells was amplified as the agitation intensity was increased from 120 to 160 rpm (impeller tip speeds of 0.26 to 0.35 m s^{-1} respectively). However, increasing the medium viscosity had no effect on the apparent growth rate of the cells when an impeller speed below 90 rpm (impeller tip speed of 0.20 m s^{-1}) was used. This is supported by the observations of Croughan *et al.* (1989).

Croughan *et al.* (1988) investigated the effect of solids concentration on the damage to immobilised FS-4 cells at agitation intensities of 35 rpm and 150 rpm (above the critical impeller speed). A constant attached cell concentration was used in these experiments by fixing the microcarrier concentration at 0.1% (v/v). The effect of solids concentration on the microcarrier cultures was established by using solid particles of the same size and density as the microcarriers but which were chemically inert and incapable of supporting cell growth and attachment. Sephadex G-50 beads were found to fulfill these requirements and were used at concentrations of 0 to 2.9% (v/v). It was found that at 35 rpm, increasing the inert solids concentration to 2.9% had no effect on the apparent growth rate of the FS-4 cells. However, an increase in the inert solids concentration had a detrimental effect on the cells at 150 rpm. In the absence of inert microcarriers, the culture at 150 rpm grew to 45% of the maximum cell concentration in the control culture at 35 rpm. As inert microcarriers were added, the apparent growth of the cells progressively decreased to 8% of the maximum cell concentration of the control on addition of 2.9% inert solids. The addition of inert solids to the microcarrier cultures at 150 rpm also reduced the attachment of the cells to the microcarriers during the initial stages of the experiments. At 2.9% (v/v) inert solids, it was found that only 54% of the inoculum attached to the microcarriers as viable cells.

The effect of *microcarrier* concentration on the growth of FS-4 cells was also investigated by Croughan *et al.* (1988) at 35 rpm. In varying the microcarrier concentration, both the solids concentration and attached cell concentration were varied. The FS-4 cells were grown at microcarrier concentrations of 0.005 to 1.456% (v/v) and the medium was supplemented by either 5% or 10% fetal calf serum. Examination of the apparent growth rates of the cells as a function of the microcarrier concentrations, showed that the growth rates decreased above 0.019% solids and 0.015% solids when using 5% serum and 10% serum respectively. This finding contrasts with the observation that no cell damage occurred when the inert solids concentration was increased to 2.9% at an impeller speed of 35 rpm. Further investigations into the growth of FS-4 cells in T-flasks as a function of cell concentration, showed that the decreased performance of the high density microcarrier cultures was due to the presence of growth inhibitors at the high cell concentrations.

where N_{JS} is the critical impeller speed (rpm), ν_l is the liquid kinematic viscosity ($m^2\ s^{-1}$), d_p is the solid particle diameter (m), $\Delta\rho$ is the density difference between solid and liquid phases (kg m^{-3}), ρ is the density of the liquid phase (kg m^{-3}), B is the mass of suspended solids per mass of liquid (%), and D is the impeller diameter (m). Pearce (1993) found that the first order disruption rate constant and the maximum extent of cell disruption increased rapidly over the particle size range of 114 to 300 μm. However, as the particle diameter was increased beyond 300 μm, the first order disruption rate constant approached a constant value of $5 \times 10^{-4}\ s^{-1}$. The maximum extent of disruption increased gradually to a maximum value of 96% at a particle size of 1245 μm. This motivated the use of particles of diameter 600 to 850 μm in this work. The results of Pearce (1993) show that the disruption kinetic parameters are not sensitive to particle size in this range.

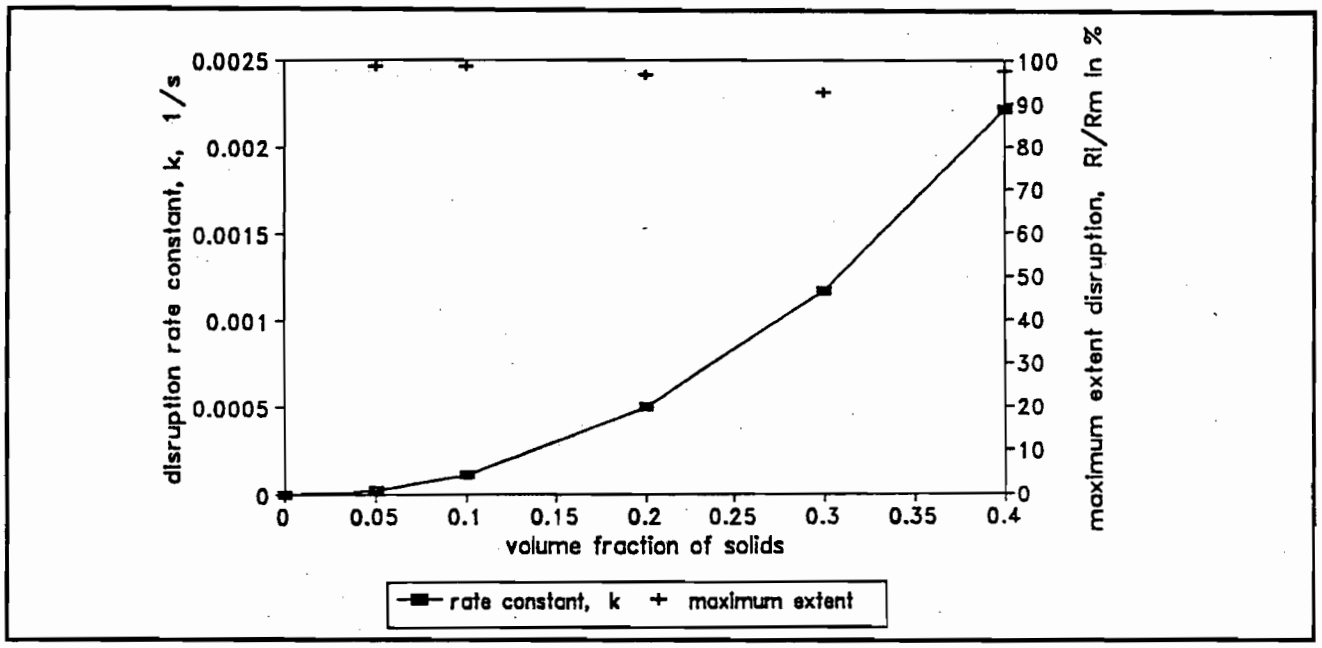

Figure 2.1. **Effect of solids volume fraction on the disruption kinetic parameters of *Saccharomyces cerevisiae* on agitation with a Rushton turbine (Pearce 1993).**
Impeller speed of 772 rpm, silica particles with geometric mean particle diameter of 1245 μm, cell dry weight concentration of 50 to 60 kg m^{-3}.

The effect of particle density on cell disruption over the range of 1600 to 4500 kg m^{-3} was investigated by Pearce (1993) by using activated carbon, silica and chromite as the solid phase in the slurry reactor. In this range, particle density was found to have negligible effect on the rate and extent of cell disruption at a solids concentration of 20% (v/v) and an agitation intensity of 772 rpm (impeller tip speed of 2.18 m s^{-1}). While the activated carbon and silica suspensions are well suspended at this impeller speed (N_{JS} in range 311-542

rpm, Equation 5.7), the chromite is not fully suspended (N_{JS} of 805 rpm, Equation 5.7). At a 0.20 solids volume fraction and an impeller speed of 772 rpm, a 20% decrease in the rate constant and a 19% increase in the maximum extent of disruption were observed on use of jagged silica particles with respect to smooth silica particles (Pearce 1993). Pearce (1993) further found that an increase in the biomass concentration from 20 to 130 kg m^{-3} resulted in a 36% decrease in the first order disruption rate constants. Increasing the biomass concentration over this range increases the viscosity of the yeast suspensions by 166% (Vand 1948). The findings of Pearce (1993) are thus in agreement with the observations in animal cell-microcarrier cultures that viscosity has a protective effect in reducing cell damage and disruption from hydrodynamic stress (Croughan *et al.* 1989, Lakhotia and Papoutsakis 1992) (Section 2.2.2).

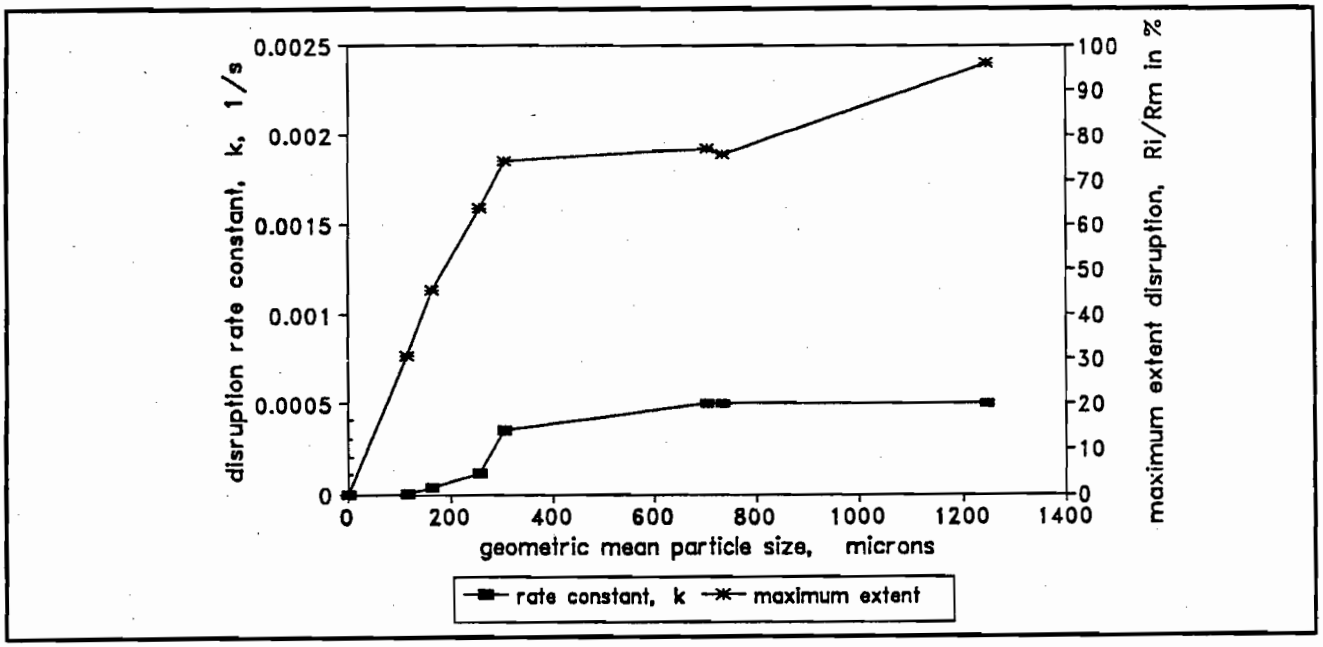

Figure 2.2. **Effect of particle size on the disruption kinetic parameters of *Saccharomyces cerevisiae* on agitation with a Rushton turbine (Pearce 1993).**
Silica particles, impeller speed of 772 rpm, solids volume fraction of 0.20, cell dry weight concentration of 50 to 60 kg m^{-3}.

The results from the cell disruption experiments performed over the agitation intensity range of 150 to 1090 rpm (impeller tip speeds of 0.42 to 3.08 m s^{-1}) are shown in Figure 2.3. In these experiments, Pearce (1993) used a solids volume fraction of 20%, silica particles with a geometric mean diameter of 1245 μm and a biomass concentration of 50 to 60 kg m^{-3}. At these conditions, the critical impeller speed is 685 rpm (Equation 5.7). These experiments thus show the effect of incompletely suspended solids on cell disruption at impeller speeds below 685 rpm, and the effect of completely suspended solids on cell disruption at

impeller speeds above 685 rpm. Figure 2.3 shows that the first order disruption rate constants (k) exhibit a power law dependency on the impeller speed (N) below 600 rpm. This power law relationship is described by Equation 2.2 with a correlation coefficient of 0.953 (Pearce 1993).

$$k = 1.278 \times 10^{-9} N^{1.906} \qquad \textbf{Equation 2.2}$$

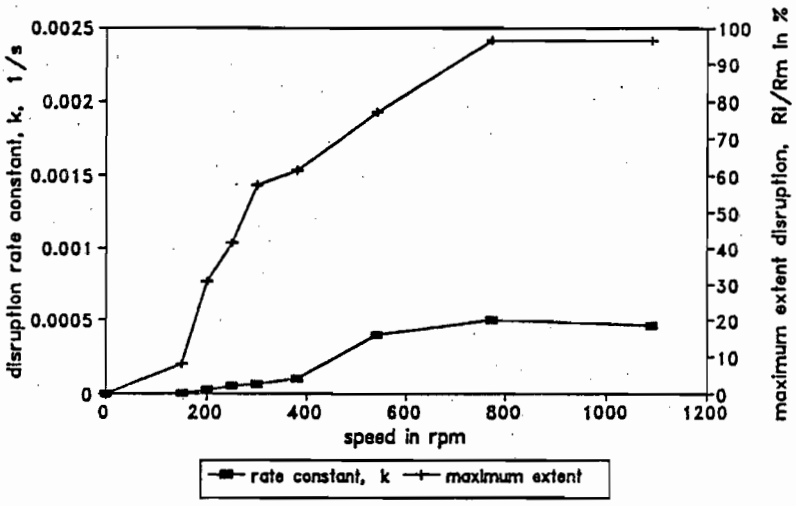

Figure 2.3. **Effect of agitation intensity on the disruption kinetic parameters of *Saccharomyces cerevisiae* on agitation with a Rushton turbine (Pearce 1993).**
Solids volume fraction of 0.20, silica particles with geometric mean particle diameter of 1245 μm, cell dry weight concentration of 50 to 60 kg m^{-3}.

Above 600 rpm, the disruption rate constant approaches a constant value. There is clearly a change in the dependency of k on the impeller speed in the vicinity of the critical impeller speed. Figure 2.2 also shows that the maximum extent of disruption (R_i/R_M) increases with impeller speed and reaches a maximum above 600 rpm. This indicates that incremental breakage of the cells occurs at equilibrium conditions below 600 rpm. Pearce (1993) suggested that this incremental breakage could be attributed to the reduced collision frequency and collision force of the incompletely suspended solids with the cells. The results of Pearce (1993) therefore suggest that the dependence of the disruption kinetic parameters on impeller speed is different in the regimes of incomplete and complete solids suspension. This requires further investigation.

To understand the increase in the maximum extent of disruption with impeller speed below an agitation intensity of 600 rpm, Pearce (1993) investigated the relative contribution of cell wall damage and cell membrane damage. The release of the wall-associated enzyme, invertase, and cytoplasmic proteins was

compared as a function of the impeller speed. A first order rate equation was used to describe the kinetics of invertase release. In Figure 2.4, the ratio of the rate of invertase release, k_{Rw}, and the rate of total soluble protein release, k, are shown as a function of the impeller speed. The results show that the rate constant of invertase release is three times greater than the rate constant of overall protein release at an impeller speed of 115 rpm but that above an impeller speed of 350 rpm, the two rate constants are effectively equal. Hence at low values of agitation intensity, the yeast is damaged principally at the cell wall. At impeller speeds exceeding 350 rpm, rupture of the cell membrane results in the release of cytoplasmic proteins as well as wall-associated proteins.

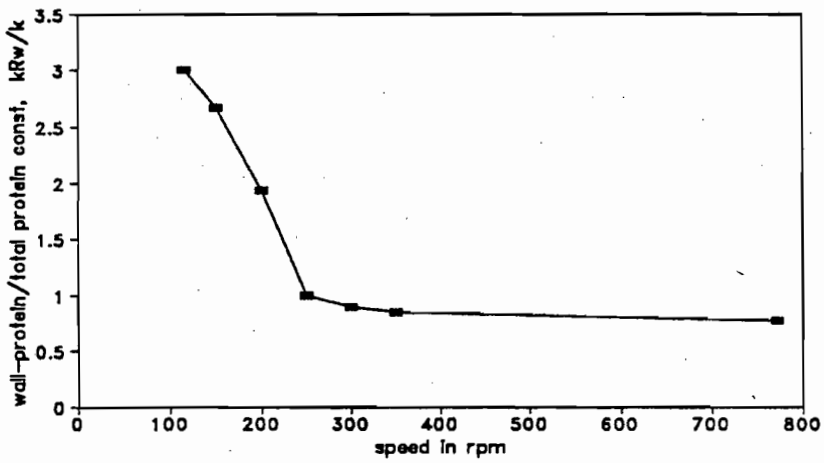

Figure 2.4. **Rate of release of invertase relative to total soluble protein as a function of impeller speed (Pearce 1993).**

Solids volume fraction of 0.20, silica particles with geometric mean particle diameter of 1245 μm, cell dry weight concentration of 50 to 60 kg m^{-3}.

2.2.4 Conclusions

In this review, cell damage and disruption in slurry bioreactors have been considered in terms of whether the solid particles are completely or incompletely suspended. The point of transition between the regimes of incomplete and complete solids suspension is defined by the critical impeller speed. While the effect of completely suspended solids on cell damage has been rigorously investigated in the animal cell-microcarrier system, further research is required into the effect of agitation intensity and impeller flow pattern on the damage to *thiobacilli*, used in minerals bioprocessing, at speeds above the critical impeller speed. In addition, damage to the *thiobacilli* from mechanical stress at high concentrations of suspended solids has

not been rigorously discounted. Studies concerning the effect of completely suspended solids on the disruption of freely suspended cells are limited to the work of Pearce (1993).

Disruption experiments performed by Pearce (1993) using a slurry bioreactor over an agitation intensity range which straddled the critical impeller speed suggested that the functional dependence of the disruption kinetic parameters of *Saccharomyces cerevisiae* on impeller speed differs with respect to the critical impeller speed. However, this requires further investigation since the critical impeller speed was estimated for the work of Pearce (1993), and the dependence of the kinetic parameters on impeller speed was only investigated at a single solids concentration.

This literature review has thus shown that further work is required in determining the effect of incompletely and completely suspended solids on cell disruption. This would provide added understanding and would facilitate the selection of the optimum operating conditions for the slurry systems described in Section 2.1.

Chapter 3: Experimental Materials and Methods

3.1 The Yeast-Silica Model System

3.1.1 Micro-organisms

Saccharomyces cerevisiae (Baker's yeast) was obtained as a stationary phase yeast cream (20 % (w/v) dry weight) from Anchor Yeast (Cape Town, South Africa). The supernatant was removed by centrifugation for 10 minutes in a Beckman TJ-6 centrifuge at 4470 g. The cells were washed and resuspended in phosphate buffered saline solution (Appendix B) to a cell dry weight concentration of 48 to 59 g/l for the disruption experiments. This procedure reduced the interference by the substances in the fermentation broth on the analysis of cell disruption.

3.1.2 Solid Particles

Silica was obtained from CONSOL Sand (Cape Town, South Africa). A particle size fraction of 600-850 μm was achieved using stainless steel sieve screens (20 to 28 mesh). The size of the silica particles was verified by analysis of electron micrographs of the particles, taken using a Standard Scanning Electron Microscope (Cambridge S200) as well as by laser light scattering (Section 3.3.6). The sand particles were first calcined at 500°C for 4 hours to remove organics and impurities from the particle surface (Breytenbach 1995).

3.2 Experimental Apparatus

A stirred tank reactor of standard geometry was used in this study (Bates *et al.* 1966). This consisted of a flat-bottomed, fully baffled (4 baffles with widths of T/10) 3 liter glass beaker, with a working volume of 2.45 liters. As a result of foam formation on breakage of the cells at the high impeller speeds, a perspex extension to the vessel walls was used to prevent a loss of the volume from the system. An overhead Renham 90 W DC motor (Cape Town, South Africa), fitted to the stainless steel impeller shaft, was used to agitate the vessel contents. The apparatus, including vessel geometry, is depicted in Figure 3.1.

Two types of impellers, with an impeller diameter of 0.07 m, were used in this investigation:

- a 6-bladed Rushton turbine (DT)
- a 6-bladed pitched-blade turbine with the pumping action downwards (PTD)

These impellers are shown in Figure 3.2 and Figure 3.3 respectively. The dimensions of the respective impellers are detailed in Table 3.1. Wearing of the stainless steel impellers due to the abrasive action of the sand particles was checked regularly by determining the impeller weight. The impellers were replaced when their weight was reduced by 2%. The variable speed motor allowed the stirrer speed to be adjusted between 200 and 1000 rpm (impeller tip speeds of 0.77 m s^{-1} and 3.87 m s^{-1} respectively). Impeller speeds were measured by using a hand-held tachometer (Series 6611, Veeder-Root, Simsbury, CT). The temperature of the slurry in the stirred tank was kept below 20 °C by attaching an external cooling coil, after the power measurement had been taken.

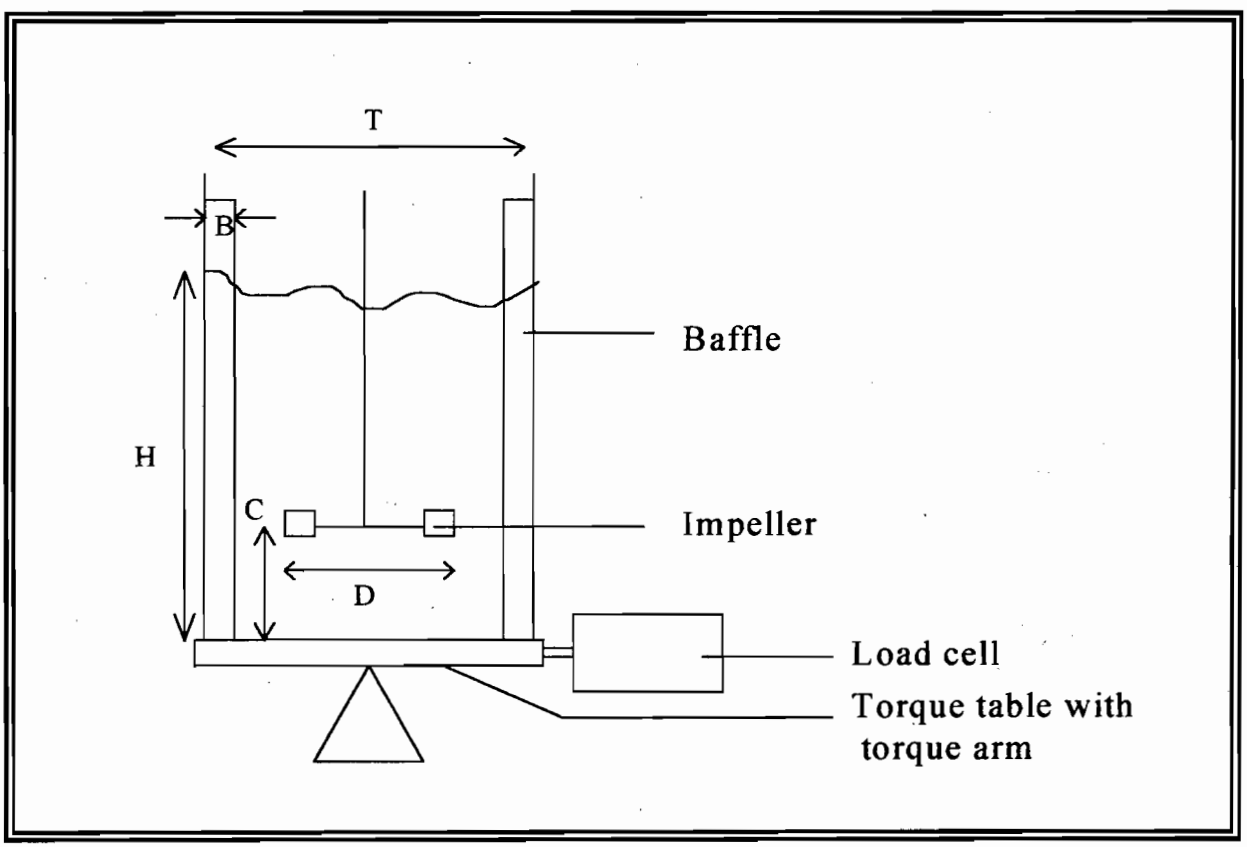

Figure 3.1. Schematic representation of the mechanically agitated contactor used in this study.

Table 3.1. **Geometry of the experimental rig**

Symbols denote the following: T: tank diameter; H: height of liquid in vessel; B: baffle width; C: impeller clearance above the vessel base; D: impeller diameter; L: length of impeller blade; W: width of impeller blade; H_u: length of impeller hub.

Dimension (mm)		**Dimension Ratio**	
Vessel:		**Vessel:**	
T	152.0	H/T	1.00
H	152.0	B/T	0.10
B	15.5	C/T	0.38
C	57.0		
Rushton impeller:		**Rushton impeller:**	
D	74.0	D/T	0.49
L	19.0	L/D	0.26
W	15.5	W/D	0.21
H_u	49.5	H_u/D	0.67
Pitched-blade impeller:		**Pitched-blade impeller:**	
D	75.5	D/T	0.50
L	28.0	L/D	0.37
W	12.0	W/D	0.16
H_u	22.0	H_u/D	0.29
Blade angle	45°		

Power measurements were made by fixing the glass beaker to a frictionless torque table, which was fitted with a torque arm. Rotation of the impeller in the vessel resulted in the torque arm exerting a force on a load cell. The load cell reading was converted to a global power input using the following equation:

$$P = \frac{m\,g\,L\,N\,2\,\pi}{60} \qquad \textbf{Equation 3.1}$$

where m is the mass reading on the load cell (kg), g is the gravitational acceleration (9.81 m s^{-2}), L is the distance from the tip of the torque arm to the centre of the torque table (0.1m), and N is the impeller speed (rpm). By use of a standard reactor geometry (Bates *et al.* 1966) for which correlations of the dimensionless power number as a function of the impeller Reynolds number are available, the measured power inputs could be verified. Appendix C details the method used to verify the accuracy of the power measurements.

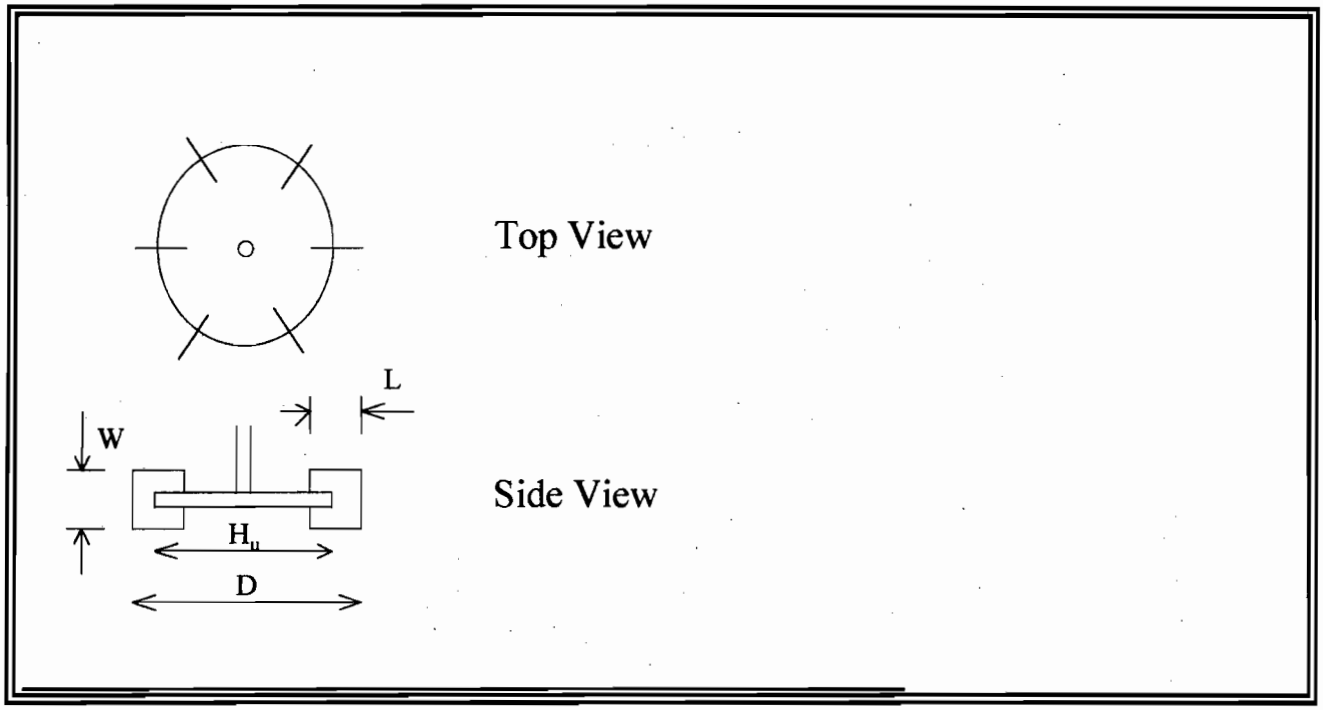

Figure 3.2. **The six-bladed Rushton turbine.**

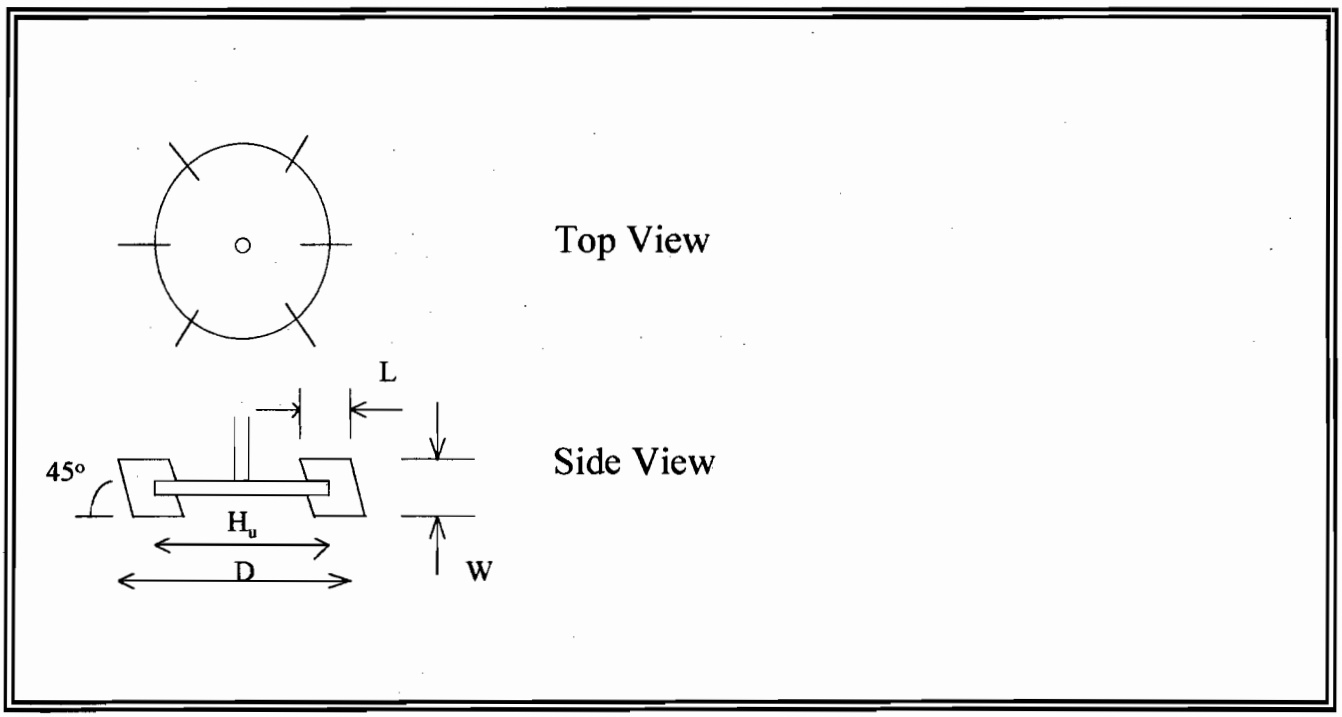

Figure 3.3. **The six-bladed pitched-blade turbine (pumping downwards).**

3.3 Analytical Techniques

3.3.1 Analysis of Cell Disruption by Protein Release

The release of total soluble protein into the supernatant was used as a measure of cell disruption. Samples taken during the cell disruption experiments were centrifuged at 4650 g for 5 minutes and the supernatants were diluted with distilled water. Total soluble protein concentrations were determined using the method of Lowry *et al.* (1951), calibrated with a bovine serum albumin standard (Appendix A). The coefficient of variance in the Lowry assays was typically less than 3%. It was found that freezing of the diluted protein samples had no effect on the Lowry analysis.

In calculating the soluble protein release on disruption of *Saccharomyces cerevisiae* in a Manton Gaulin-APV homogeniser, Hetherington *et al.* (1971) accounted for the volume of the yeast cells. It is shown in Appendix D that the average error incurred by not considering a change in the volume of the aqueous phase on cell disruption (5%) is less than the error incurred in calculating the volume of the aqueous phase (9.7% for the conditions in this work). It is therefore unnecessary to account for the volume of the yeast cells at the relatively low yeast concentrations used in this study.

3.3.2 Biomass Concentration

The biomass concentration of *Saccharomyces cerevisiae* was determined from a cell dry weight analysis. 1ml of undisrupted cell suspension was pipetted into microcentrifuge tubes pre-weighed to four decimal places. The suspension was centrifuged at 4650g for 5 minutes. After removal of the supernatant, the cell residue was dried in an oven at 100°C for 3 days. The cell dry weight concentration was determined from the quotient of the cell mass and the volume of the suspension (1 ml). Each cell dry weight analysis was performed in triplicate. The coefficient of variance of the dry weight analyses was typically less than 2%.

3.3.3 Maximum Soluble Protein Determination

The maximum soluble protein available for disruption (R_M) was determined following its release using the French Press (Manual-fill 20K cell, SLM Instruments) at an operating pressure of 30MPa. The soluble protein released from *Saccharomyces cerevisiae* cells is greater following disruption in a French Press, operated at 30MPa, than by agitation in a slurry reactor at 40% solids volume fraction and 1090 rpm, or by lysis of the yeast cells using *Cytophaga* enzymes (Pearce 1993).

The French Press utilises liquid shear as the disruption mechanism. The yeast cells are disrupted on rapid decompression and extrusion through a narrow capillary. The resultant protein release was determined using the method of Lowry *et al.* (1951) (Appendix A). The method used to operate the French Press is included in Appendix E.

The maximum soluble protein available for disruption, R_M, was established by passing the yeast suspension twice through the French Press. Further passes of the yeast suspension through the French Press did not increase the amount of soluble protein released. Protein release from the yeast cells as a function of the number of passes through the French Press is documented in Appendix E. R_M was measured for each batch of yeast cells and was found to vary in the range 382 mg protein/g cell to 452 mg protein/g cell.

3.3.4 Viscosity and Density of Yeast Suspensions

Yeast viscosity was measured using a British size 'A' U-tube viscometer (Technico, England). The time for flow of a fixed volume through a capillary section is related to viscosity according to:

$$\mu = A \rho t \qquad \textbf{Equation 3.2}$$

where:

	μ	=	dynamic viscosity of yeast suspension (Pa s)
	A	=	constant ($m^2 s^{-2}$)
	ρ	=	density of yeast suspension ($kg m^{-3}$)
	t	=	efflux time (s)

The yeast suspensions give efflux times that fall within the recommended range of 200-800s for the viscometer. Using distilled water to calibrate the viscometer, a value of 3.34×10^{-9} $m^2 s^{-2}$ at 15 °C was obtained for the constant, A, in the viscometer equation. Each viscosity measurement was performed four times and the coefficient of variance of these measurements was typically less than 3%.

Density measurements of the yeast suspensions were made by determining the mass of a pipetted 3 ml volume of the yeast suspension at a particular temperature. Each measurement was performed five times and the coefficient of variance of these measurements was consistently less than 0.4%.

3.3.5 Density of Sand

The density of the sand particles was measured using an Accupyc 1330 Pycnometer (Micromeritics, Georgia, USA). This model is a fully-automatic gas displacement pycnometer which determines the density of a known mass of substance by measuring the pressure change of helium in a calibrated volume.

3.3.6 Particle Size Analysis

A Malvern Mastersizer Analyser (Mastersizer S longbed Ver 2.15, Malvern Instruments, Worcestershire, UK) was used to establish the size of the yeast cells and the particle size distribution of the 600-850 μm silica particle size fraction that was used for the disruption experiments. This instrument exploits the radial light scattering distribution functions of particles. A suspension of particles is passed across the path of a collimated beam of laser light and the radially scattered light is collected by a set of photo detectors that are positioned perpendicular to the optical axis. The scattered light distribution is sampled and processed using the Fraunhofer and Mie scattering models to provide a particle size distribution (Coulson *et al.* 1991, Malvern MAN 0101 January 1996).

3.3.7 Microscopic Observation of the Model System

The disrupted yeast cells from several of the slurry reactor experiments and French Press experiments were visually observed using an Olympus BX40 microscope, connected to an Optimas 5.2 Image Analyser (Optimas Corporation, Washington, USA). The samples were viewed using brightfield illumination and an objective with a magnification of 40x. Methylene blue was used to stain the yeast cells. The images of the cells on the image analyser were enhanced using sharpen-high filtering.

Photographs of the sand particles and the undisrupted yeast cells were taken using a Standard Scanning Electron Microscope (Cambridge S200) to establish the shape and verify the size of the model micro-organism and silica particles. The yeast cells were fixed with glutaraldehyde and dehydrated by treating them with increasingly more concentrated ethanol solutions. After removal of the ethanol by critical point drying, the mounted cells were coated with AuPd. Only the final step needed to be performed in the preparation of the silica particles. A magnification of 14400 and 18.1 fold were used for the yeast cells and the silica particles respectively.

3.4 Experimental Method

3.4.1 Critical Impeller Speed Measurements

The critical impeller speed (N_{JS}) was used as an indicator of the suspension of the silica particles. Critical impeller speed for off-bottom suspension was determined by visual observation and from the maxima in measurements of the power number (N_p) as a function of the impeller Reynolds number (N_{RE}).

3.4.1.1. Visual Observation

The critical impeller speeds were visually determined by placing the beaker on a glass sheet. The vessel base was illuminated and an inclined mirror, placed beneath the vessel, allowed its base to be more easily observed. The speed at which the solid particles were observed not to remain on the vessel base for more than 1 or 2 s was measured using the Veeder-Root tachometer (Zwietering 1958). Critical impeller speeds were determined by visual observation at 5%, 10%, 15%, 20% and 40% solids (v/v) for the Rushton turbine, and at 20% solids (v/v) for the pitched-blade turbine. A yeast suspension, containing 46-60 g/l dry mass, was used as the suspending medium.

3.4.1.2. N_p-N_{RE} Curves

The critical impeller speed was determined by varying the impeller speed between 200 to 800 rpm and recording the corresponding power input. The power number was then plotted as a function of the impeller Reynolds number for each solids loading. The power number (N_p) is defined as follows:

$$N_p = P / (\rho N^3 D^5) \qquad \textbf{Equation 3.3}$$

where:

P	=	power input to vessel measured from load cell readings (W)
N	=	impeller speed (rps)
D	=	impeller diameter (m)

The impeller Reynolds number (N_{RE}) is defined as follows:

$$N_{RE} = \rho N D^2 / \mu \qquad \textbf{Equation 3.4}$$

The viscosity and density of the yeast suspension were used to calculate N_p and N_{RE}, according to the approach of Bohnet and Niesmak (1980). The critical impeller speed corresponds to the local maximum in

the curves of the power number as a function of the impeller Reynolds number (Bohnet and Niesmak 1980, Rewatkar *et al.* 1991). Experiments were performed at 5%, 10%, 15%, 20% and 40% solids (v/v) for the Rushton turbine and at 20% solids (v/v) for the pitched-blade turbine. Yeast suspensions, of dry mass 50 g/l, were used as the suspending medium.

3.4.2 Cell Disruption Experiments

The effect of incompletely and completely suspended solid particles on cell disruption was investigated by performing three types of experiments:

1. A series of experiments was performed over the range of solids volume fractions of 0%, 5%, 10%, 20% and 40% at a fixed impeller speed of 750 rpm (impeller tip speed of 2.91 m s^{-1}). This study was conducted using a Rushton turbine with complete off-bottom suspension, verified by comparison to the critical impeller speed for 40% solids (v/v) (593 rpm).

2. Using the Rushton turbine, the solids loading was fixed at 10% and 20% (v/v) and a series of experiments was performed over the impeller speed range of 200 to 900 rpm (impeller tip speeds of 0.77 m s^{-1} to 3.49 m s^{-1} respectively). This range of impeller speeds straddles the respective critical impeller speeds (N_{JS} = 439 rpm for the 10% solids, N_{JS} = 461 rpm for the 20% solids).

3. Using the pitched-blade turbine, a series of experiments was performed at 20% solids (v/v) over the range of impeller speeds of 440 to 900 rpm (impeller tip speeds of 1.70 m s^{-1} to 3.49 ms^{-1} respectively). This range of impeller speeds straddles the critical impeller speed of 662 rpm.

In each experiment, the cell suspension and the solid particles were agitated at the desired impeller speed in the absence of aeration. Samples were taken at regular intervals to monitor the degree of cell disruption and were kept in ice until they were centrifuged and diluted for the Lowry analysis. The duration of the experiment was determined by the time required to reach the maximum extent of cell disruption at the experimental conditions specified (0.67 to 38.18 hours). In each run, the global power input to the vessel was determined from the force exerted on the load cell, the temperature was noted at intervals and the impeller speed was measured using the Veeder-Root tachometer.

The temperature of the disruption experiments was maintained below 20 °C and the yeast cells were resuspended in phosphate buffered saline solution (PBS), hence yeast growth during the experiments was negligible (Stanier *et al.* 1970). Nevertheless, 10 mg/l of the anti-fungal agent, cycloheximide (Sigma C7698) was used in experiments exceeding 10 hours in duration. Cycloheximide is an antibiotic produced by *Streptomyces griseus* and inhibits the growth of yeasts by preventing the synthesis of new proteins (Ryder *et al.* 1983, Pearce 1993). It is effective for up to 72 hours (Pearce 1993). In Appendix F, it is shown that the growth of the yeast cells was negligible in the disruption experiments run for less than 10 hours. The addition of cycloheximide to these disruption experiments was thus not required.

3.5 Concluding Remarks

In this chapter, the preparation of the *Saccharomyces cerevisiae* suspensions and the silica particles for the disruption experiments has been described and the experimental apparatus used in this study presented. The geometry of the test vessel has been detailed and the method used to measure the global power input into the vessel has been discussed and verified. Analytical techniques that were used to assess the cell disruption in the slurry reactor have also been presented in this chapter. The accuracy of each of these methods has been quantified in terms of a coefficient of variance of the measurements. Finally, the experimental protocol that was used in measuring the critical impeller speeds of the suspensions and the protocol used in the cell disruption experiments have been described. The critical impeller speeds were used to quantify the suspension of the silica particles in the slurries.

Chapter 4: Characterisation of the Yeast-Silica Model System

4.1 Yeast Model System

The cell envelope of micro-organisms forms a biologically active boundary between the micro-organism and its external environment and provides a rigid outer support which protects the cell from osmotic lysis (Engler 1985, Harrison 1991). Since cell disruption involves rupture of the cell envelope, an understanding of its structure is important for the analysis of cell disruption. Hence this section begins with a review of the structure of the envelope of *Saccharomyces cerevisiae*. The size of the yeast cells as well as measurements and predictions of the density and viscosity of the yeast suspensions are also presented in this section. The latter properties were required in the calculations of the power number (N_p) and the impeller Reynolds number (N_{RE}) for determining the critical impeller speeds (Section 5.3), and were also required in modelling the cell disruption in Chapter 7.

4.1.1 Structure of the Yeast Cell Envelope

In discussion of the composition and structure of the yeast cell envelope, the region from the cell wall to the cytoplasmic membrane is considered. Although cell disruption only occurs on rupture of the cell membrane, the structural strength of the cell is provided by the cell wall. Figure 4.1 depicts a model of this region.

The yeast cell wall is one of the most tough and rigid of all microbial cell walls. The wall is approximately 70 nm thick. This thickness increases with yeast cell age (Moor and Muhlethaler 1963). The basic structural components of the cell wall are glucans, mannans and proteins. These biopolymers are arranged in two distinct layers: an inner layer of glucan microfibrils and an outer surface of mannan-protein.

The glucan fibrils make up 55-60 % of the wall and constitute the rigid matrix that gives the cell its shape and protects it from mechanical breakage (Engler 1985, Hunter and Asenjo 1988). Figure 4.2 shows a schematic representation of Baker's yeast glucan. Two glucan fractions can be separated by extraction of the cell wall with alkali solutions. The main structural component of the cell wall is an alkali-insoluble β(1-3) linked glucan with 3-6% β(1-6) branch points. These glucans are aggregated into microfibrils located toward the inner surface of the wall. Alkali-soluble glucan has a similar chemical structure. However, it has

a few more β(1-6) links and is linked to small quantities of mannan oligosaccharides, suggesting an attachment to wall mannan-protein (Hunter and Asenjo 1988).

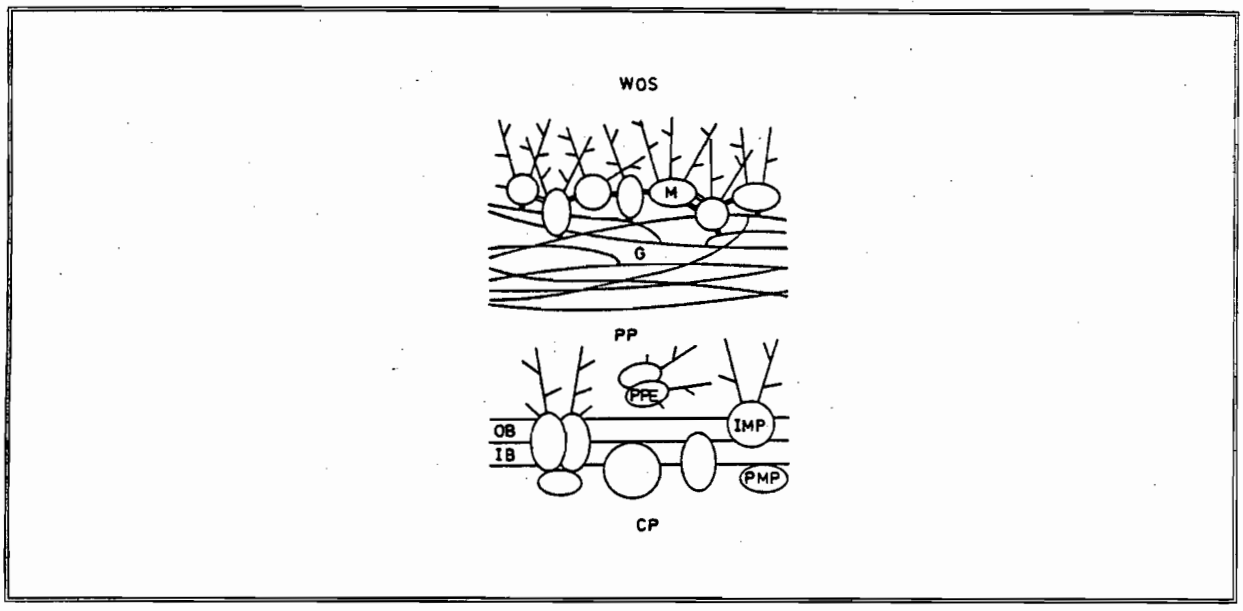

Figure 4.1. Diagram of the yeast cell wall surrounding the cytoplasmic membrane (Schekman and Novick 1982, Zlotnik *et al.* 1984).

Symbols denote the following: CP: cytoplasm; IB, OB: inner and outer halves, respectively, of the plasma membrane bilayer; PMP: peripheral membrane protein; IMP: integral membrane protein; PPE: periplasmic enzyme; PP: periplasmic space; G: glucan; M: mannan-protein; WOS: wall outer surface; (=): S-S thioester bond; (-): covalent bond.

Covering the fibrils is a layer of glycoprotein, and beyond this is the mannan mesh. Figure 4.3 shows the schematic structure of Baker's yeast mannan. Mannans from Baker's yeast cell walls are characterised by a backbone of mannose residues in α(1-6) linkage having short oligosaccharide side chains composed of mannose residues in mostly α(1-2) linkage with a small amount of α(1-3) linkage. The mannan mesh is linked to the glucan fibrils by covalent bonds of an unknown nature (Zlotnik *et al.* 1984) and does not form any crystalline or fibrillar structures in the yeast cell wall (Cabib *et al.* 1982). Within the mannan mesh are mannan-enzyme complexes. It is uncertain as to whether these complexes are covalently attached to the mesh. The outer surface of the mannan mesh, crosslinked by disulphide bonds and intrachain hydrogen bonding, allows the penetration of small molecules but acts as a barrier to enzymes which might hydrolyse the underlying glucan. Zlotnik *et al.* (1984) point out that the mannan and glucan layers in the yeast cell wall are not completely separated since mannan-proteins may penetrate the glucan layer.

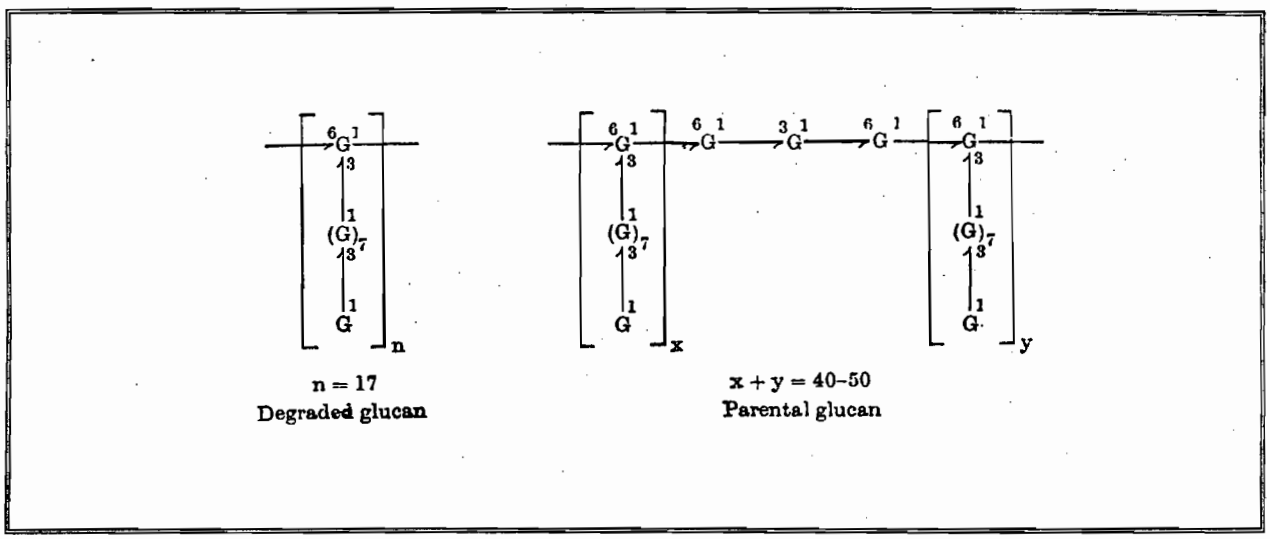

Figure 4.2. **Schematic representation of Baker's yeast glucan (Misaki *et al.* 1969).**
The formula on the left represents native glucan after treatment and resulting cleavage by periodate. G indicates a β-D-glucopyranosyl residue.

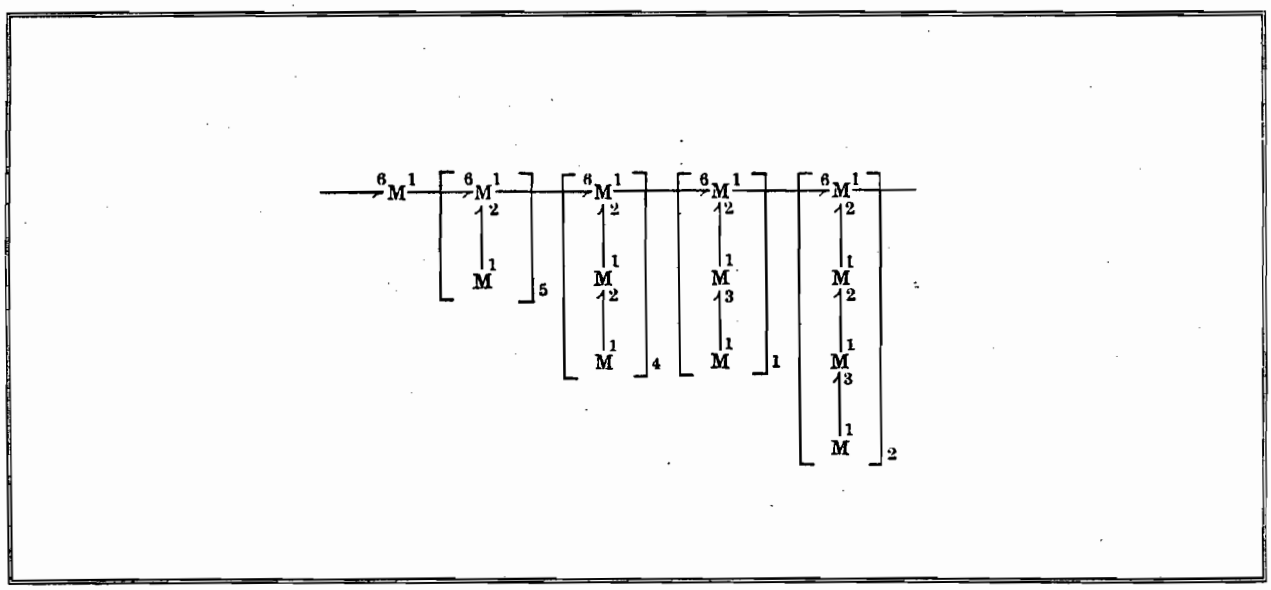

Figure 4.3. **Schematic structure of Baker's yeast mannan (Stewart and Ballou 1968).**
The order in which the side-chains occur is unknown. The subscripts outside the brackets indicate the average molecular proportions of the various types of side-chains. M indicates an α-D-mannopyranosyl residue.

Other compounds located in the cell wall of *Saccharomyces cerevisiae* are less than 4 % chitin (Roberts *et al.* 1983) and about 8.5 % lipid which consists mainly of neutral fat (Northcote and Horne 1952). Chitin is almost entirely restricted to the bud scar (Cabib *et al.* 1982).

Between the cell wall and cytoplasmic membrane is the periplasmic space which contains a number of enzymes as well as sugar and amino acid binding proteins. Most periplasmic enzymes are mannan-proteins (Hunter and Asenjo 1988, Bailey and Ollis 1986). An important enzyme, which is associated with the periplasmic space, is invertase (Tuite and Oliver 1991). Fischer and Kohtes (1951) found that the polysaccharide, mannan, acted as a stabiliser to this enzyme since the invertase activity was rapidly lost when the mannan was resolved by electrophoresis. As a result of its association with the cell wall, invertase is a useful indicator of the extent of damage to the yeast cell wall.

The cytoplasmic membrane is the innermost part of the cell envelope. This membrane keeps the cytoplasm intact and maintains the concentration gradients between the interior and exterior of the cell. The plasma membrane is a lipid bilayer consisting mostly of phospholipids and sterols (Tuite and Oliver 1991). There is evidence that the membrane is not of a uniform composition but that there is a laterally heterologous distribution of membrane components (Steere *et al.* 1980, Kramer *et al.* 1978). Proteins can be found both in the lipid bilayer and on the bilayer surface.

4.1.2 Physical Properties of the Yeast

4.1.2.1. Size Distribution of Yeast

The ellipsoidal cells of *Saccharomyces cerevisiae* are typically 7 to 10 microns in length and 1 to 5 microns in width (Bailey and Ollis 1986). The size distribution of the yeast cells (Figure 4.4), obtained as Baker's yeast cream from Anchor Yeast (Epping, Cape Town), was determined by laser light scattering using the Malvern Mastersizer. On a volume basis, the average cell diameter in this size analysis is 5.1 μm and the mode is 5.5 μm. On a particle number basis, the average cell diameter is 3.8 μm and the mode is 4.5 μm. Figure 4.5 shows an electron micrograph of a budding yeast cell from the yeast cream at a magnification of 14 400x. The diameter of the yeast cell in this electron micrograph is 4.0 μm.

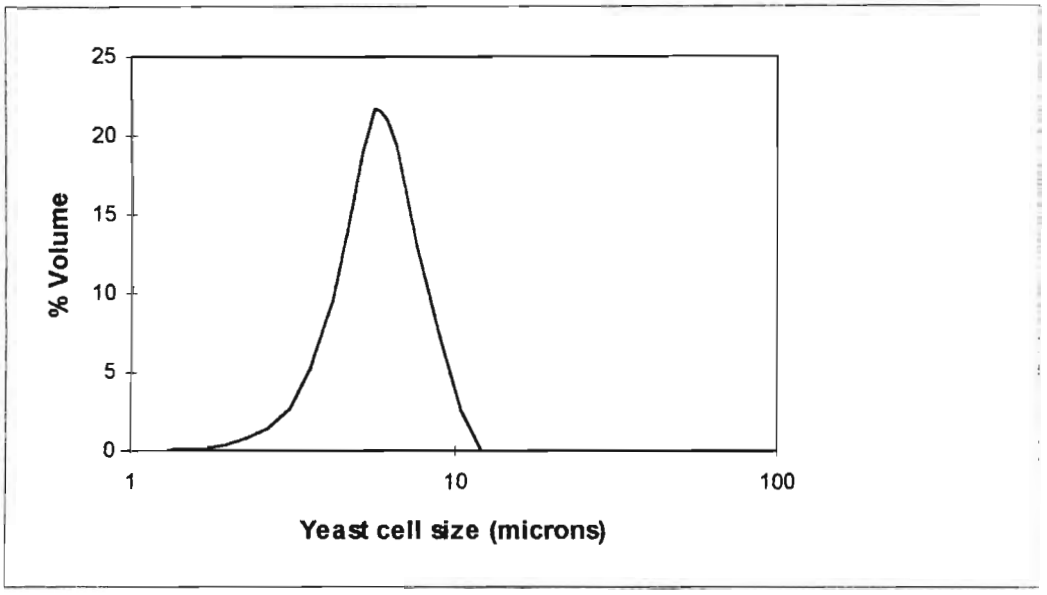

Figure 4.4. **Size distribution of *Saccharomyces cerevisiae* cells (Malvern Mastersizer particle size analysis).**

Figure 4.5. **Electron micrograph of a budding yeast cell from the yeast cream.**
A Standard Scanning Electron microscope (Cambridge S200) was used at a magnification of 14 400x.

c	=	cell dry weight concentration (g / l)
T	=	temperature (°C)
$\mu_{so,20°C}$	=	viscosity of the suspending medium at 20°C (centipoise)

The nonlinear term in the equation of Vand (1948) (Equation 4.2) accounts for the interaction of the yeast cells at higher concentrations. As the volume fraction of the cells decreases, this equation reduces to that of Einstein (1906) (Equation 4.1). Reuss *et al.* (1979) included osmotic pressure (P_{osm}) in their correlation (Equation 4.3) since they found that osmotic pressure significantly affected the viscosity of yeast suspensions. Cell volume fractions in the correlations in Table 4.1 can be determined from the following equation of Reuss *et al.* (1982) which expresses the volume fraction of cells (E_x) as a function of cell dry weight concentration (c) and osmotic pressure (P_{osm}):

$$E_x = 3.05 \times 10^{-3} \exp(-3 \times 10^{-2} P_{osm})\, c \qquad \textbf{Equation 4.5}$$

In Table 4.2, the viscosities measured at 15°C are compared to the values predicted from the correlations in Table 4.1. Using a Micro Osmometer (Model 5004, Precision Systems), the osmotic pressure of PBS, the suspending medium used in the experimental study, was measured as 0.286 Os/kg H_2O, which is equivalent to 6.9×10^{-6} bar. The osmotic pressure of PBS is thus negligible. The viscosity of PBS at 20°C ($\mu_{so,20°C}$) was measured as 1.23×10^{-3} Pa s with a 95% confidence interval of 1×10^{-5} Pa s, as determined from the statistical methods presented in Miller and Freund (1985).

The agreement between the predicted and measured viscosities, over the biomass concentration range of 34.5 to 60.3 g/l, was quantified in terms of a coefficient of variance. The coefficient of variance was defined as:

$$CV = \frac{\sqrt{\dfrac{\sum_{i=1}^{n} (X_{predicted,i} - X_{measured,i})^2}{n-1}}}{\dfrac{\sum_{i=1}^{n} X_{measured,i}}{n}} \qquad \textbf{Equation 4.6}$$

where n is the number of measurements made. The coefficient of variance for each of the correlations is shown in Table 4.2. The measured viscosities of the yeast suspensions compare well with the viscosities predicted by the equations of Einstein (1906), Vand (1948) and Cilliers and Harrison (1996). However,

there is a 41% coefficient of variance between the measured viscosities and the viscosities predicted by the equation of Reuss *et al.* (1979), over the biomass concentration range of 34.5 to 60.3 g/l. Cilliers and Harrison (1996) found that the equation of Reuss *et al.* (1979) overpredicted their measured viscosity data by 20% over the biomass concentration range of 2 to 105 g/l.

Table 4.2 **Comparison of measured and predicted viscosities of yeast suspensions at a temperature of 15°C.**

Measured viscosities are quoted with a 95% confidence interval.

Cell Dry Weight (g/l)	**Viscosity of Yeast Suspension (Pa s)**				
	Einstein (1906)	**Vand (1948)**	**Reuss *et al.* (1979)**	**Cilliers and Harrison (1996)**	**Measured in this Study**
34.5	0.00155	0.00165	0.00208	0.00167	$1.54 \times 10^{-3} \pm 4 \times 10^{-5}$
42.5	0.00162	0.00177	0.00225	0.00182	$1.64 \times 10^{-3} \pm 1 \times 10^{-5}$
51.4	0.00171	0.00193	0.00245	0.00199	$1.81 \times 10^{-3} \pm 7 \times 10^{-5}$
60.3	0.00179	0.00209	0.00267	0.00218	$1.98 \times 10^{-3} \pm 4 \times 10^{-5}$
Coefficient of Variance (%)	7.2	7.7	41.1	11.4	

The data for the curves of the power number (N_p) as a function of the impeller Reynolds number (N_{RE}) (Section 5.3) were obtained at 15 °C and an average cell dry weight concentration of 50 g/l. The viscosity of the yeast suspension was taken as 0.0018 Pa s for the N_{RE} calculations. The average cell concentration and average temperature used in the disruption experiments were 52.8 g/l and 14 °C respectively. The viscosity used in the cell disruption models in Chapter 7 was also 0.0018 Pa s.

4.1.2.3. Density of Yeast Suspensions

The densities of yeast suspensions were measured at biomass concentrations of 34.5 g/l, 42.5 g/l, 51.4 g/l and 60.3 g/l. These measurements were compared to predictions from the following equation:

$$\rho = E_x \rho_x + (1-E_x) \rho_{so}$$ **Equation 4.7**

where: ρ = density of the yeast suspension (kg m^{-3})

ρ_x = density of the yeast cells (kg m^{-3})

ρ_{so} = density of the suspending medium (kg m^{-3})

The volume fraction of the yeast suspensions was determined from Equation 4.5. Densities of yeast cells (ρ_x), suspended in distilled water at 22.5 °C, are summarised in Table 4.3. Since the osmotic pressure of PBS is negligible, the density of yeast in PBS can be approximated by that of yeast in distilled water. The density of PBS (ρ_{so}) was measured as 1021.8 g/l with a 95% confidence interval of 3.0 g/l.

Table 4.3. Densities of yeast cells suspended in distilled water at 22.5°C (Reuss *et al.* 1979).

Proponent	**Yeast Density (kg / l)**
Reuss *et al.* (1979)	1.0952 ± 0.0110
Aiba *et al.* (1962)	1.0725 ± 0.0112
Haddad *et al.* (1953)	1.0870 ± 0.0260

The measured and predicted densities of the yeast suspensions at 15 °C are compared in Table 4.4. Agreement between the measured and predicted yeast densities is quantified in terms of a coefficient of variance (Equation 4.6). The coefficient of variance of 0.62% (Table 4.4) shows that there is good agreement between the measured and predicted values. However, the predicted densities of the yeast suspensions increase with increasing biomass concentration whereas this is not observed for the measured densities (Table 4.4). The predicted increase in the yeast suspension density is, however, within the experimental error. The average of the measured densities over the 34.5 g/l to 60.3 g/l biomass concentration range was used for the calculations in this study. This average is 1035.9 g/l.

Table 4.4. **Comparison of measured and predicted densities of yeast suspensions at a temperature of 15°C.**

Measured densities are quoted with a 95% confidence interval.

Cell Dry Weight (g/l)	Density of Yeast Suspension (g/l)	
	Equation 4.7	**Measured in this Study**
34.5	1028.4	1036.7 ± 3.7
42.5	1030.0	1033.9 ± 2.3
51.4	1031.7	1037.7 ± 3.2
60.3	1033.4	1035.4 ± 1.2
Coefficient of Variance (%)	0.62	

4.2 Silica Model System

The properties of silica which motivated its use in this study are its inertness and hardness (Hardness factor (HF) for silica = 7 on a scale where the HF of montmorillonite = 1 and the HF of corundum = 9 (Roberts *et al.* 1990)). The silica particles are thus not subject to attrition in slurry bioreactors. In this section, the silica model system is characterised in terms of its particle size distribution, the smoothness of the particles and the particle density. Measurements of the size and density of the silica particles were required for the calculations of the critical impeller speeds from correlations (Section 5.4) and for the correlations used in modelling the cell disruption in the slurry reactor (Chapter 7).

4.2.1 Particle Size Distribution

Figure 4.6 shows the size distribution of the silica particles, determined from a Malvern Mastersizer analysis. On a volume basis, the mode is 754 μm and the average diameter of the silica particles is 791 μm. On a particle number basis, the mode of this distribution is 647 μm and the mean particle diameter is 729 μm. To provide verification of these measurements, electron micrographs were taken of the silica particles (Figure 4.7).

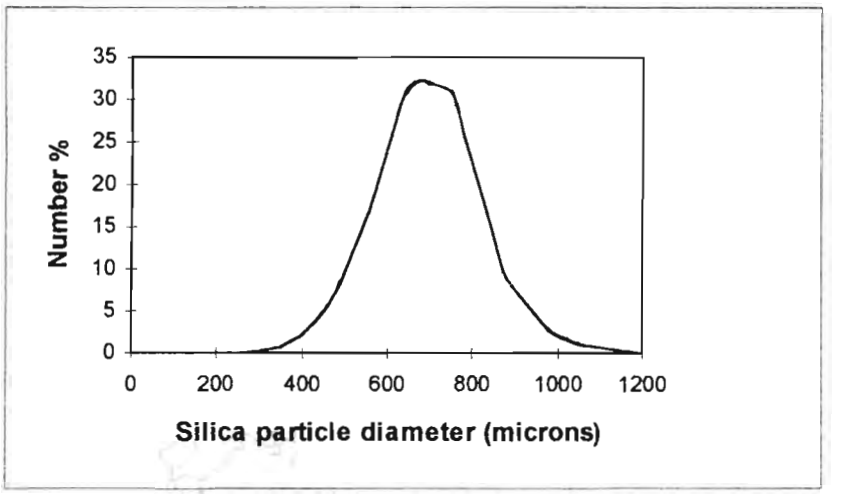

Figure 4.6. **Size distribution of silica particles (Malvern Mastersizer particle size analysis).**

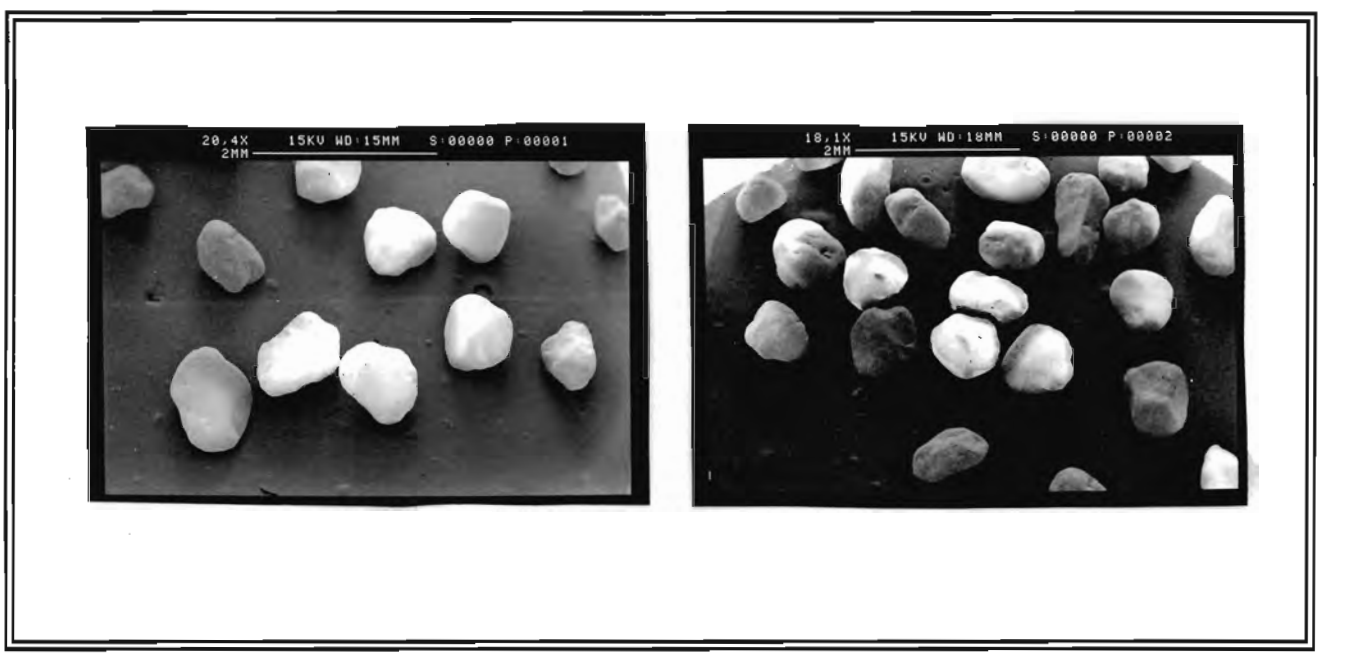

Figure 4.7. **Electron micrographs of the silica particles used in this study.**
A Standard Scanning Electron microscope (Cambridge S200) was used at magnifications of 20.4x and 18.1x respectively.

Figure 4.7 shows that the silica particles are irregularly shaped. Two dimensions of the particles were thus measured from the electron micrographs: the longest dimension of the particles, which was termed the *particle length*, and the dimension of the particles perpendicular to this, which was termed the *particle*

width. These dimensions were determined for 34 particles. This sample size is sufficiently large to assume a normal distribution (Miller and Freund 1985). A bar chart of the frequency distribution of the particle lengths and widths is shown in Figure 4.8. The particle widths range from 450 μm to 850 μm, with the majority of the particles (41.2%) having widths of 650 μm to 750 μm. The particle lengths range from 650 μm to 1200 μm, with the majority of the particles (41.2%) having lengths of 750 to 850 μm. In sieving, the orientation of the particles at the surface of the screens determines whether or not the particles pass through the screen apertures (Coulson *et al.* 1991). The particles with lengths of 850 μm to 1200 μm (50.0% of the particles) passed through the 850 μm screen because their widths were less than 850 μm. Hence the electron micrographs support the sieve analysis. In addition, they verify the measurements of the volume-based equivalent particle diameter from the Malvern Mastersizer analysis.

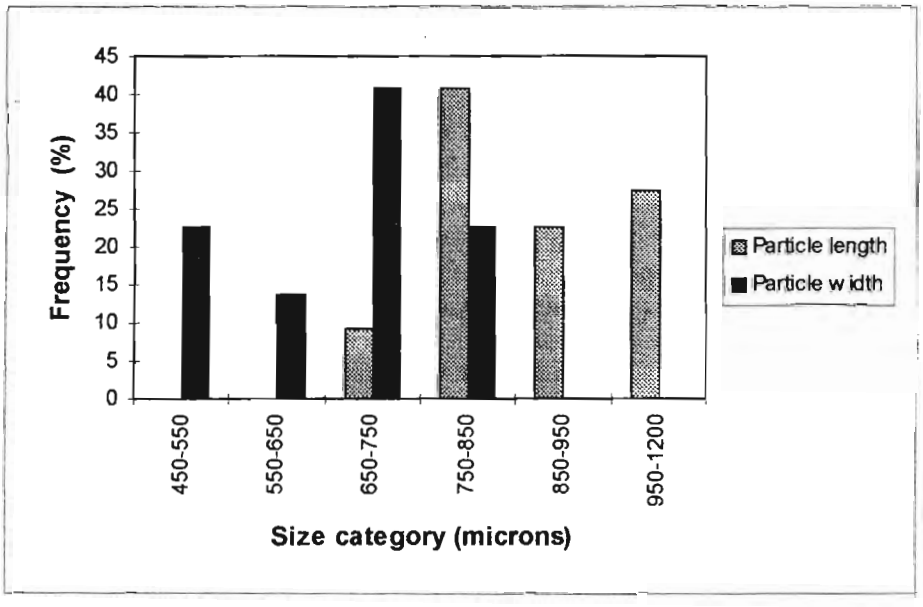

Figure 4.8. **Frequency distribution of the particle lengths and particle widths measured from electron micrographs.**

Since the volume of the silica particles is an important factor in solids suspension and in determining the particle momentum, the Malvern measurement (on a number basis) of the average particle diameter (729 μm) was used for the purposes of the calculations in this work.

4.2.2 Particle Smoothness

The smoothness of the particles was determined qualitatively from electron micrographs of the particles at magnifications of 85.0x and 6 340x. The latter magnification shows the silica particles at the same scale as the yeast cells. Typical electron micrographs of the silica particles at these magnifications are shown in Figure 4.9. It can be seen that at a magnification of 85.0x, the silica particles appear smooth whereas at the same scale as the yeast cells (magnification of 6340x), the surface of the silica particles is rough.

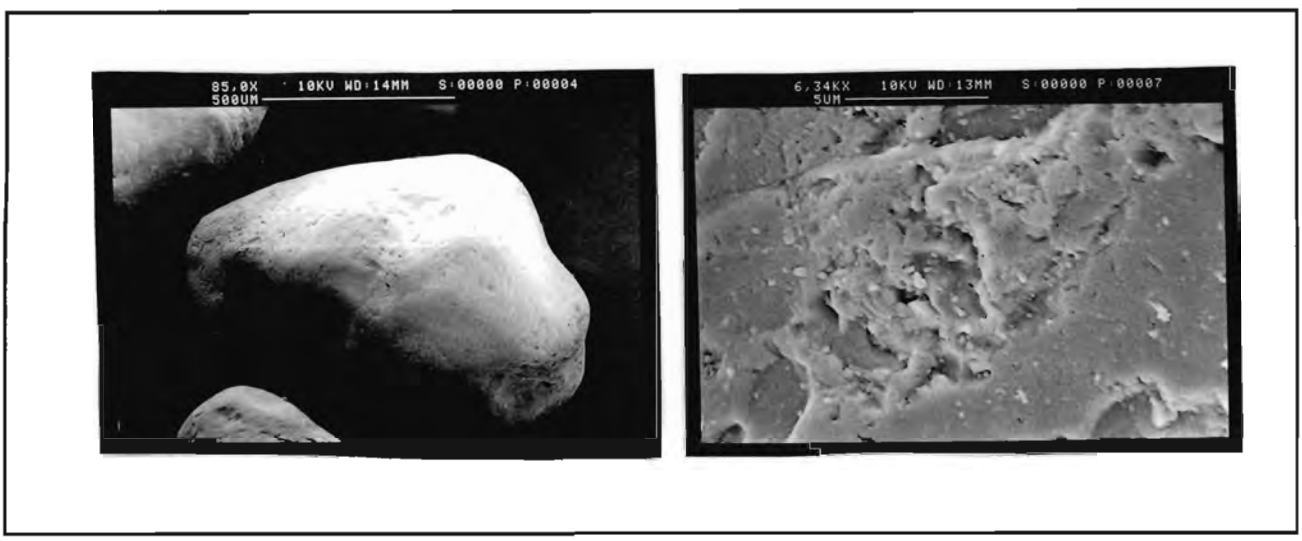

Figure 4.9. **Electron micrographs of the surface of the silica particles used in this study.** A Standard Scanning Electron microscope (Cambridge S200) was used at magnifications of 85.0x and 6 340x respectively.

4.2.3 Particle Density

The average density of the silica particles was measured, using the Micromeritics AccuPyc 1330 Pycnometer, as 2664 kg m^{-3} with a 95% confidence interval of 2 kg m^{-3}. This density measurement corresponds well with the range of 2500 - 2800 kg m^{-3} quoted by Perry *et al.* (1984) for quartz.

4.3 Concluding Remarks

The *Saccharomyces cerevisiae* and silica components of the model system have been characterised in this chapter in terms of their physical properties. The structure of the yeast cell wall has been described since an appreciation of this gives a greater understanding of the mechanism of cell disruption in the slurry reactor. The size of the yeast cells has been determined and the viscosity and density of yeast suspensions have been

measured. The latter properties were required in the calculations of the power number and impeller Reynolds number in Section 5.3, and in the correlations used in the modelling of the cell disruption in Chapter 7. These measurements have been validated by comparing them to literature values.

The silica particles used in this work have been characterised in terms of their particle size distribution, their smoothness and their density. The size and density of the silica particles were needed in the calculations of the critical impeller speeds (Section 5.4) and in the cell disruption models (Chapter 7). The diameter of the silica particles, determined from a Malvern Mastersizer analysis, was verified using electron micrographs of the particles. The density measurements of the particles have been validated by comparing them to literature values.

Chapter 5: Quantifying the Solids Suspension

5.1 Introduction

In order to establish the effect of incompletely and completely suspended solids on the rate and extent of cell disruption, it was necessary to quantify the solids suspension as a function of solids loading and power input. In this chapter, the different degrees of solids suspension and the various methods of quantifying solids suspension are reviewed. Measurement of the solids suspension in this system, in terms of the critical impeller speed, is then presented for the Rushton (DT) and pitched-blade (PTD) turbines and the results obtained are compared to the predicted values from literature equations. The critical impeller speeds are modelled as a function of the solids loading. The latter relationship was required for the modelling of the cell disruption data under incompletely suspended conditions (Chapter 8).

5.2 Quantifying Solids Suspension - A Review

There are essentially four degrees of solids suspension that are observed in solid-liquid systems (Oldshue 1983, Rewatkar *et al.* 1991, Pearce 1993):

1. Fillet formation, but no progressive fillet build-up. Fillets are stationary or stagnant deposits of the solid particles that form at the center and along the periphery of the vessel base in axial and radial flow (Rewatkar *et al.* 1991)
2. Complete on-bottom motion of all particles
3. Complete off-bottom suspension of the particles
4. Complete homogeneity of suspension

These are depicted in Figure 5.1 for the predominantly axial flow pattern of the 6-bladed pitched-blade turbine (pumping downwards). As the impeller speed is increased, a transition from Stage 1 through to Stage 4 is observed. Although homogeneity is approached as the level of agitation increases, it is impossible for Stage 4 to be attained (Nienow 1968, Bohnet and Niesmak 1980).

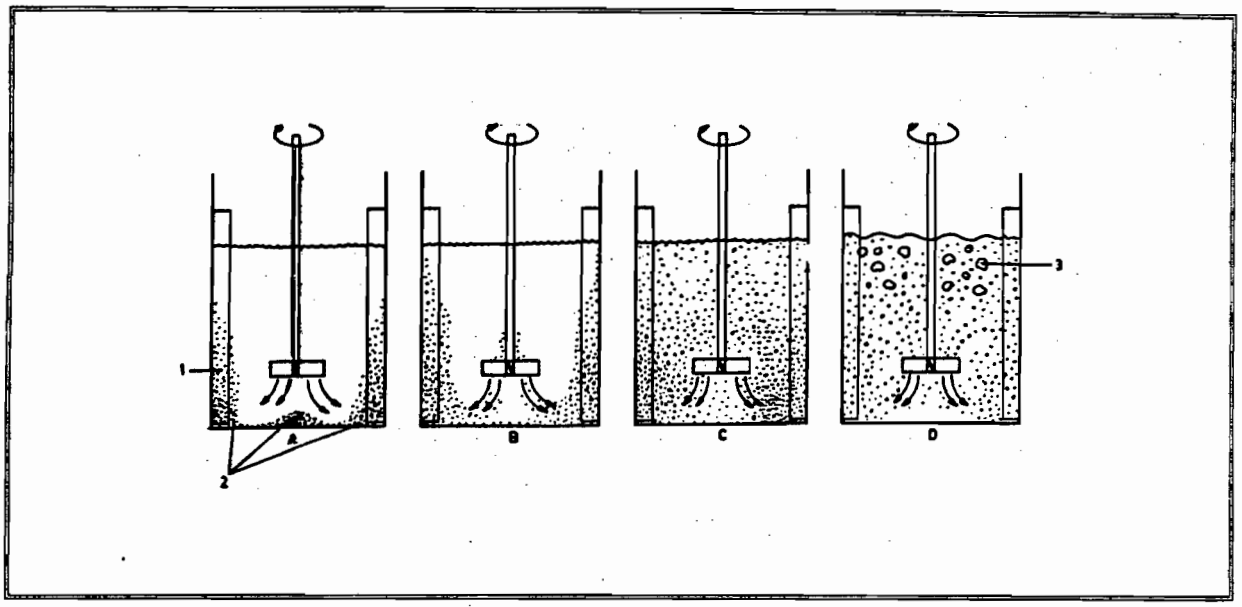

Figure 5.1. **Schematic representation of the degrees of solids suspension of a solid-liquid mixture on agitation with a 6-bladed pitched-blade turbine (pumping downwards) (Rewatkar *et al.* 1991).**

(A) fillet formation, (B) fillet disappearance, (C) complete off-bottom suspension, (D) recirculation of solid-liquid mixture. The number (1) indicates a solid particle, (2) indicates the solid fillets, and (3) indicates a gas bubble.

Solids suspension is quantified in two ways:

1. in terms of the critical impeller speed, *i.e.* the speed at which the solid particles become completely suspended.
2. in terms of the degree of homogeneity that is achieved as the solids are suspended.

The measurement techniques and correlations that have been developed for quantifying solids suspension are presented below.

5.2.1 Critical Impeller Speed

The critical impeller speed appears to be the most commonly used way of quantifying the solids suspension of a mixture. Its most accepted definition is that of Zwietering (1958):

> *The critical impeller speed is the speed at which the solid particles do not remain on the tank bottom for more than 1 or 2 s.*

The critical impeller speed of a system can be measured by visual determination, plotting the power number

as a function of the impeller Reynolds number or the impeller speed, plotting the liquid-phase mixing time as a function of the impeller speed, using a radioactive tracer technique, or plotting the solids concentration just above the base of the vessel as a function of the impeller speed (Zwietering 1958, Bohnet and Niesmak 1980, Wiedmann *et al.* 1980, Chapman *et al.* 1983, Rewatkar *et al.* 1991). Since visual determination and the power number-impeller Reynolds number function are the most widely used ways of determining the critical impeller speed (N_{JS}), these methods are discussed below. The empirical and theoretical expressions developed for the prediction of the critical impeller speed are also presented.

5.2.1.1 Measurement of the Critical Impeller Speed

Visual Determination

One of the easiest methods for determining the critical impeller speed is visually. The bottom of the vessel is observed by illuminating its base and watching an inclined mirror, placed beneath the vessel. The speed at which the solid particles do not remain on the bottom of the vessel for more than 1 or 2 s can then be determined using a tachometer (Zwietering 1958, Chapman *et al.* 1983, Rewatkar *et al.* 1991). The advantage of this method lies in the fact that no disturbance occurs either of the flow pattern or of the solids distribution. This method is also particularly suitable for systematic investigations since no difficulties arise on varying the experimental parameters over a wide range. However, visual observation of the critical impeller speed is subjective. The reproducibility of this method is reported to be 2 to 5 % (Zwietering 1958, Bohnet and Niesmak 1980, Chapman *et al.* 1983, Takahashi *et al.* 1993).

Power Number as a Function of Impeller Reynolds Number

By monitoring power number as a function of the impeller Reynolds number, a simple and objective criterion for determining the critical impeller speed is obtained. The power input into the vessel is determined at a range of impeller speeds for a particular solids loading and solid particle size.

Figure 5.2 shows a typical plot of the power number (N_p) as a function of the impeller Reynolds number (N_{RE}) for different solids loadings. A considerable torque is necessary to start rotation of the stirrer and to set the solids in motion. The power numbers at low impeller speeds are thus high. As the impeller speed increases, the power number decreases considerably (line A-B) as a consequence of the formation of solid fillets along the periphery of the vessel base. As the impeller speed is further increased, the fillets start breaking up (point B) and suspension of the solids is initiated. Along line BC, increasingly more solids become suspended and the power number increases as a result of the increasing suspension density. At point C, complete suspension is achieved. A further increase in the impeller speed results in a slight

decrease in the power number along the line CD as the slurry becomes more homogeneous (Bohnet and Niesmak 1980). The critical impeller speed thus corresponds to the speed at which there is a relative maximum in the N_p-N_{RE} curve.

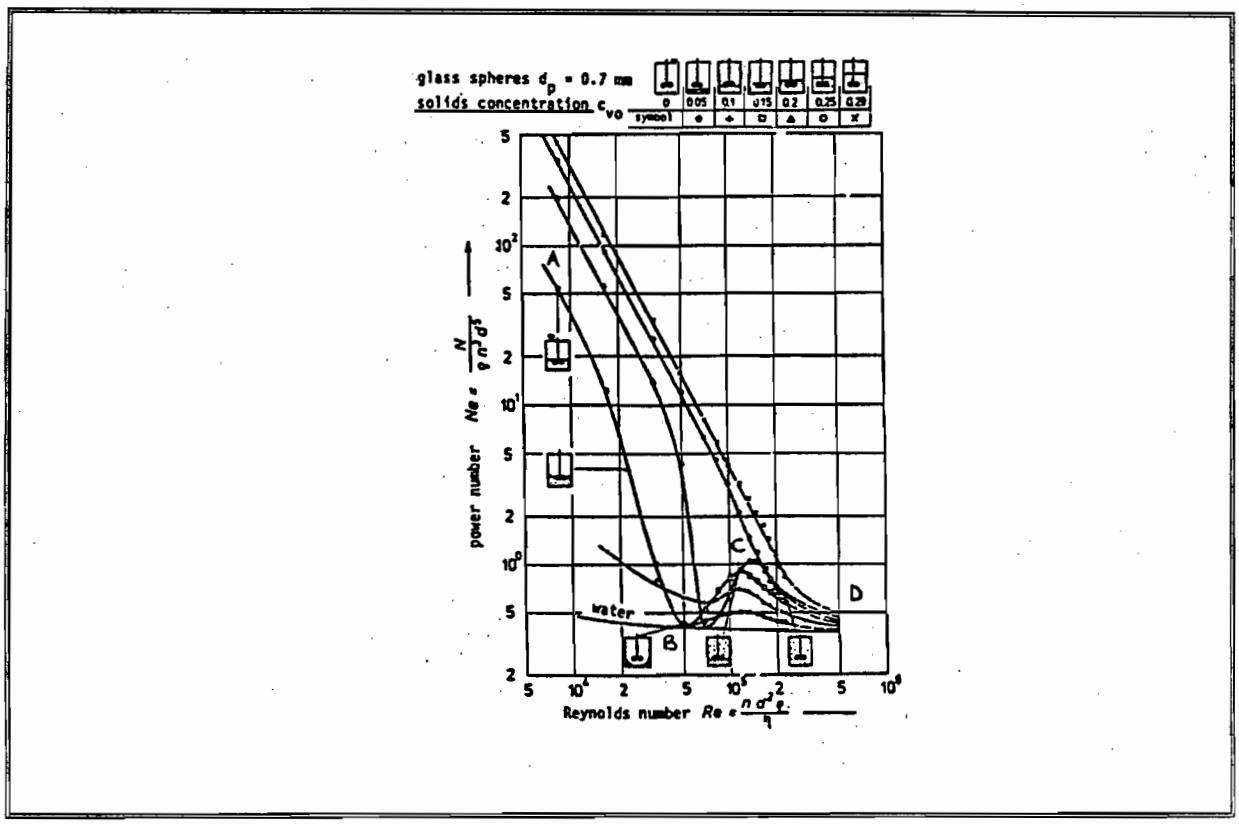

Figure 5.2. **Power number as a function of impeller Reynolds number and solids concentration for a propeller (downward thrust) (Bohnet and Niesmak 1980).**

In application of the N_p-N_{RE} correlation reported in the literature, the physical properties of the liquid are used (Bohnet and Niesmak 1980, Rewatkar *et al.* 1991). The density and viscosity of the yeast suspensions were thus used in the calculation of N_p and N_{RE} in this study. Indeed, in this work, values of the critical impeller speed, determined from curves of the power number as a function of the impeller Reynolds number, were unaffected by whether the density and viscosity of the slurry were used instead of the density and viscosity of the yeast suspension.

The disadvantage of using this method to determine the critical impeller speed is that it breaks down at high solids loadings (> 25% volume fraction) since no maximum is observed in the N_p-N_{RE} plot (Bohnet and Niesmak 1980). Rewatkar *et al.* (1991) report that the values of the critical impeller speed, obtained using this method, were within 5 % of those measured by visual observation.

5.2.1.2 Critical Impeller Speed Expressions

Both empirical and theoretical expressions have been developed to predict the critical impeller speed. The application of the empirical expressions is limited to a particular set of conditions. However, within their subspace, they describe solids suspension well. Although theoretical expressions apply to a more universal set of conditions, their accuracy is limited because of the large number of simplifying assumptions made as a consequence of the complexity of two phase systems.

Empirical Expressions

A large number of empirical expressions have been developed to predict the critical impeller speed. Differences between these expressions exist largely as a result of different ranges that were used for the variables and different suspension criteria used in the various studies (Rewatkar and Joshi 1991).

One of the most complete investigations performed in the development of a correlation for the critical impeller speed (N_{JS}) is that of Zwietering (1958). Zwietering (1958) determined his correlation for N_{JS} from a dimensional analysis of the factors affecting solids suspension. The constants in the expression were determined empirically from the more than 1000 experiments that he performed with sand and water. For a fully baffled vessel, consisting of 4 baffles (each with a width of T/10), and for Reynolds numbers exceeding 3000:

$$N_{JS} = 60\left(\frac{s\,\nu_l^{0.10}\,d_p^{0.20}\,(9.81\Delta\rho/\rho)^{0.45}\,B^{0.13}}{D^{0.85}}\right) \text{ rpm} \qquad \textbf{Equation 5.1}$$

where:

	s	=	dimensionless constant = f(type of stirrer, T/C, T/D)
	T	=	tank diameter (m)
	C	=	impeller clearance above the vessel base (m)
	D	=	impeller diameter (m)
	ν_l	=	liquid kinematic viscosity (m^2/s)
	d_p	=	particle diameter (m)
	$\Delta\rho$	=	density difference between solid and liquid phases (kg/m^3)
	ρ	=	density of the liquid phase (kg/m^3)
	B	=	mass of solids in suspension per mass of liquid, given as a percent (%)

The exponents of the above parameters were found to be independent of the vessel geometry, the impeller

type, the solids loading, the density and diameter of the solid particles, and the density and viscosity of the liquid. Graphs of the constant, *s*, as a function of the impeller type, T/C and T/D, are presented by Zwietering (1958). Nienow (1968) found that the values of *s* for a 6-bladed Rushton turbine were dependent on the impeller clearance ratio and were not the same for C/T in the range of 1/7 to 1, as suggested by Zwietering (1958). At an impeller diameter ratio (D/T) of 0.5 and over the range of impeller clearance ratios (C/T) of 1/7 to 1/3, values of *s* were found to range between 3.6 and 5.6 (Nienow 1968). For the 6-bladed Rushton turbine used in this study at an impeller diameter ratio of 0.5 and an impeller clearance ratio of 0.38, the constant, *s*, was estimated as 5.6. No value of *s* could be found for the 6-bladed pitched-blade turbine (PTD) corresponding to the vessel geometry of this study. However, Ibrahim *et al.* (1992) report a value of 5.7 for *s* for a 6-bladed PTD at an impeller diameter ratio (D/T) of 0.5 and an impeller clearance ratio (C/T) of 0.25. This value was used, although it gives an underestimate of the actual critical impeller speed as a result of the lower impeller clearance ratio used by Ibrahim *et al.* (1992).

A reliable expression for predicting critical impeller speeds for a 6-bladed Rushton turbine has also been developed by Takahashi *et al.* (1993). The form of their correlation is the same as that of Zwietering (1958) but the constants and exponents were determined for a particular system geometry. The geometry of their system was the same as the one used in this study, the only difference being the clearance of the impeller off the vessel base (C/T = 0.25 for Takahashi *et al.*(1993), C/T = 0.38 for this study).

Takahashi *et al.* (1993) found that as the solid particle size (d_p) increased, the critical impeller speeds initially increased but started decreasing or changing slope above a critical particle size (d_p^*). Their critical impeller speed correlation was derived for particle sizes smaller than d_p^*. For $d_p < d_p^* = 18\, D^{0.63}\, \Delta\rho^{-1.0}$:

$$N_{JS} = 60\left(\frac{1.8\,\nu_l^{0.10}\, d_p^{0.05}\,(9.81\,\Delta\rho/\rho)^{0.38}\, B^{0.17}}{D^{0.60}}\right) \qquad \textbf{Equation 5.2}$$

The critical particle size is 2144 μm for the conditions used in this work. Since a particle size fraction of 600-850 μm was used for the disruption experiments, application of the correlation of Takahashi *et al.* (1993) for calculating the critical impeller speeds is valid.

Theoretical Expressions

Several attempts have been made to model theoretically a mechanism describing suspension. Many of these models are based on a force or energy balance in the vicinity of the vessel base. Another approach has been

the consideration of the particle in relation to the boundary layers on the vessel base (Bourne and Zabelka 1980).

Chapman *et al.* (1983) found that the model of Baldi *et al.* (1978) predicted critical impeller speeds closest to the experimental values of Zwietering (1958). Baldi *et al.* (1978) postulated that suspension was due to turbulent eddies of a scale of the order of, or proportional to, the particle size. Although Chapman *et al.* (1983) found that this model represented the best attempt at a theoretical analysis of complete suspension, the model was not suitable for all geometries. It was thus concluded that the empirical correlations of Zwietering (1958) and Takahashi *et al.* (1993) were the most useful and reliable models for prediction of the critical impeller speed.

5.2.2 Degree of Homogeneity

A second way of quantifying the solids suspension of a mixture is by determining the degree of homogeneity through monitoring the solids concentration profile in the vessel. Increased agitation intensity increases the uniformity of this solids concentration profile. Measurement techniques are briefly discussed below. Thereafter, the suspension criteria, which allow the prediction of the degree of homogeneity, are presented.

5.2.2.1 Measurement of the Solids Concentration

The local solids concentration in a mixture can be sampled with a sample tube or a draw-off device (Oldshue 1983). However, this method disrupts the flow pattern within the vessel and changes the slurry composition at the sample point (Gates *et al.* 1976, Oldshue 1983). An alternative method involves the measurement of the change in pressure with liquid depth at a number of positions below the liquid interface (Weisman and Efferding 1960). The pressure was measured by manometer dip tubes and a sensitive differential pressure cell with a porous-tipped probe to exclude slurry from the instrument lead line. Velocity-head effects were eliminated by making measurements during and immediately after mixing. Bohnet and Niesmak (1980) used the extent of adsorption of a light beam passing through the suspension to determine the solids concentration at various points. The light source was a helium-neon laser with an effective power of 7 mW. A silicon photocell was used as the signal modulator to transform the impact radiation to a voltage proportional to the light intensity. The adsorbed light was then related to the solids concentration at that point.

5.2.2.2 Suspension Criteria based on the Solids Concentration

Various criteria used to establish the degree of homogeneity of a suspension are discussed below. Researchers have determined qualitatively the dependence of these suspension criteria, and thus the degree of solids homogeneity, on the impeller speed, impeller type, vessel geometry, solids concentration and solid particle properties (Bohnet and Niesmak 1980, Baldi *et al.* 1981, Barresi and Baldi 1987).

Percent Suspension

The percent suspension is defined in Equation 5.3 (Oldshue 1983). The values calculated from this equation can be above or below 100 %.

$$\%\ Suspension = \frac{Weight\ \%\ solids\ in\ the\ sample\ at\ a\ point}{Total\ \%\ solids\ in\ vessel} \qquad \textbf{Equation 5.3}$$

Quality of Solids Distribution

The quality of solids distribution, σ, is defined as the deviation factor between the local solids concentration and that of a homogeneous suspension (Bohnet and Niesmak 1980):

$$\sigma = \sqrt{\frac{1}{i}\sum\left(\frac{X_v}{X_{vo}} - 1\right)^2} \qquad \textbf{Equation 5.4}$$

where:

	i	=	number of measuring points
	X_v	=	local solids concentration (m^3 / m^3)
	X_{vo}	=	given solids concentration of a homogeneous suspension (m^3 / m^3)

The solids distribution cannot readily be compared by the quality of solids distribution when suspensions with different solids concentrations, X_{vo}, are being compared because the initial values for the total deposited solids at the vessel bottom (X_{vb}) are different. If the extent of improvement of solids distribution is of interest, then it is more useful to employ the relative quality of distribution, φ (Bohnet and Niesmak 1980, Equation 5.5). This criterion reflects not only the average solids concentration of a homogeneous suspension, X_{vo}, but also the maximum concentration of the solid particles deposited on the vessel base, X_{vb}. Both the quality and the relative quality of solids distribution decrease as the impeller speed is increased.

$$\varphi = \sigma \sqrt{\frac{X_{vo}}{X_{vb} - X_{vo}}}$$ **Equation 5.5**

Suspension Impeller Speed

Kolar (1961) defined a suspension impeller speed as the speed at which the solids concentration at heights of 0.25 T and 0.75 T from the tank bottom was the same in both positions (measured by light-adsorption). Nienow (1968) criticises this criterion since he points out that suspension can never be called homogeneous throughout the vessel. He suggests that the equal mean concentrations at these two points may result from highly concentrated particle eddies being flung into the upper regions of the vessel.

5.2.2.3 Degree of Homogeneity Expressions

Empirical Expressions

Weisman and Efferding (1960) found that, when all solids were suspended, the solids concentration increased linearly with the distance below the interface except in the immediate vicinity of the slurry-water interface. Here, a fluctuating boundary between the circulating solid particles and the suspending liquid existed. As the power input was increased, the solids boundary rose until it reached the liquid surface, and the suspension became increasingly more homogeneous (Weisman and Efferding 1960, Wiedmann *et al.* 1980).

Since a solids mixture may be considered as a series of planes of a particular concentration parallel to the vessel base, Weisman and Efferding (1960) used the height of the solids boundary as an index of the degree of slurry dispersion where all the solids were suspended. They developed a mathematical expression to describe the position of the solids boundary as a function of the system geometry and the mixture properties. The constants and the forms of the functions were developed empirically. For a single, 6-bladed paddle located so that C/T exceeded 0.5 and the impeller Reynolds number exceeded 2.5×10^4, the height of the solids boundary above the midplane of the impeller, h, may be determined as follows:

$$\frac{h}{T} = 0.23\,\ell n\left(\frac{g_c\, P\Phi^{\frac{-2}{3}}\left(\frac{D}{T}\right)^{\frac{1}{2}}}{9.81\rho_{sl}\, n\, V_m\, v_{ts}}\right) + 0.1$$ **Equation 5.6**

where:

g_c	=	gravitational constant (=1 for SI units)
P	=	power input by impeller (W)
Φ	=	volume fraction of solids = $M_s/(\rho_p V_m)$
M_s	=	mass of solid particles (kg)
ρ_p	=	particle density (kg/m^3)
V_m	=	system volume below solid boundary (m^3) = $\Pi T^2/4 (h + C)$
ρ_{sl}	=	density of slurry (kg/m^3) = $\Phi \rho_p + (1-\Phi) \rho$
ρ	=	liquid density (kg/m^3)
n	=	number of impellers
v_{ts}	=	particle terminal settling velocity (m/s) = $9.81 d_p^2 (\rho_p - \rho)/(18 \mu)$
μ	=	liquid viscosity (Pa s)

Theoretical Expressions

Theoretical models, developed to predict the homogeneity of solids suspensions, are based either on a force or an energy balance in the bulk region. As a result of the simplifying assumptions made, these models are of limited accuracy and are not widely used (Rewatkar and Joshi 1991).

5.2.3 Conclusions

A primary objective of this study was to determine the effect of incompletely and completely suspended solid particles on the disruption of the *Saccharomyces cerevisiae* in the slurry reactor. A method was thus required for the direct measurement of the transition from the incompletely to the completely suspended solids regimes, and which predicted the volume fraction of solids suspended at a given impeller speed. Use of a correlation describing the critical impeller speed, such as that of Zwietering (1958) (Equation 5.1) or Takahashi *et al.* (1993) (Equation 5.2), allows the prediction of the mass of solids suspended at a given impeller speed. The critical impeller speed further provides a direct measure of the transition between the regimes of incomplete and complete solids suspension and is measured readily by visual observation and from the determination of the power number as a function of the impeller Reynolds number. This approach was thus chosen to quantify solids suspension in this study.

5.3 Measurement of the Critical Impeller Speed

5.3.1 Rushton Turbine

The power number (N_p) was determined as a function of the impeller Reynolds number (N_{RE}) in the reactor system for suspensions with solids loadings of 5%, 10%, 15%, 20% and 40% (v/v). The impeller speed was varied between 200 to 800 rpm. This data is presented in Figure 5.3. Distinct maxima, corresponding to the respective critical impeller speeds, can be observed for the 5%, 10%, 15% and 20 % (v/v) curves. No maximum was observed for the 40% curve. This agrees with the findings of Bohnet and Niesmak (1980). These workers used glass beads of 700 μm diameter and found that above a solids loading of 25% (v/v), no local maximum in the N_p-N_{RE} curve could be observed. The form of the 40% solids curve in Figure 5.3 was not affected by whether the density and viscosity of the slurry or the density and viscosity of the yeast suspension were used in the calculation of the power number (Equation 3.3) and the impeller Reynolds number (Equation 3.4).

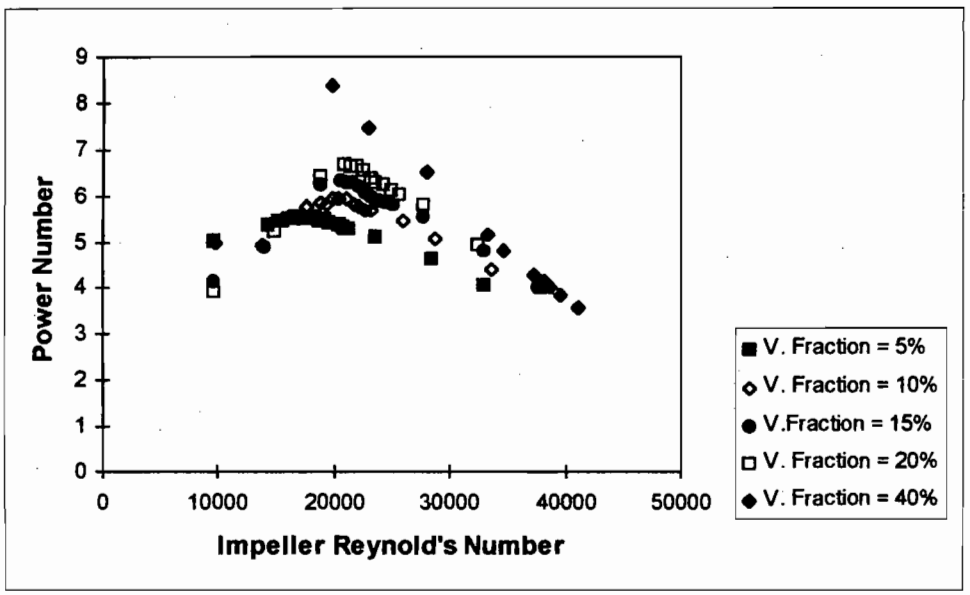

Figure 5.3. Power number (N_p) as a function of the impeller Reynolds number (N_{RE}) measured to determine the critical impeller speeds using the Rushton turbine at solids volume fractions of 5 to 40% (v/v).

Table 5.1 compares the critical impeller speeds determined from the N_p-N_{RE} curves to those found by visual observation. The measurements are quoted with 95% confidence intervals, as determined from the

statistical methods presented in Miller and Freund (1985). Table 5.1 shows that the visually observed critical impeller speeds (N_{JS}) are, on average, 9% higher than those observed from the N_p-N_{RE} curves. This compares well with the 5% difference reported by Rewatkar *et al.* (1991) using a solids concentration range of 0.13% to 28.4% (v/v). It can also be seen from Table 5.1 that the 95% confidence interval on the visually observed critical impeller speed at 40% solids is approximately four times greater than the 95% confidence intervals on the measurements obtained at the lower solids volume fractions. This is attributed to the difficulty in visually assessing the point of complete off-bottom suspension at this high solids concentration. The more objective critical impeller speeds obtained from the power number-impeller Reynolds number curves were used for the Rushton turbine in this study.

Table 5.1. **Comparison of critical impeller speeds from N_p-N_{RE} curves and visual observations for the Rushton turbine.**
Measurements are quoted with 95% confidence intervals.

Volume Fraction of Solids	N_{JS} (rpm) N_p-N_{RE} Curve	N_{JS} (rpm) Visual Observation
0.05	400	451 ± 6
0.10	439 ± 11	474 ± 5
0.15	450	484 ± 5
0.20	461 ± 14	501 ± 4
0.40	-	593 ± 22

5.3.2 Pitched-Blade Turbine

Measurements of the power number as a function of the impeller Reynolds number were also made over the impeller speed range of 200 to 800 rpm for the pitched-blade turbine at a 20% solids loading (v/v). Figure 5.4 shows the data obtained on performing the measurement in triplicate. These are also compared to the N_p-N_{RE} curve obtained for the Rushton turbine at 20% solids (v/v). In contrast to the curve obtained for the Rushton turbine, no maximum is apparent in the N_P-N_{RE} curve for the pitched-blade turbine. Above an impeller Reynolds number of 20 000, the average power number of the pitched-blade turbine is constant at 1.58 with a 95% confidence interval of 0.04.

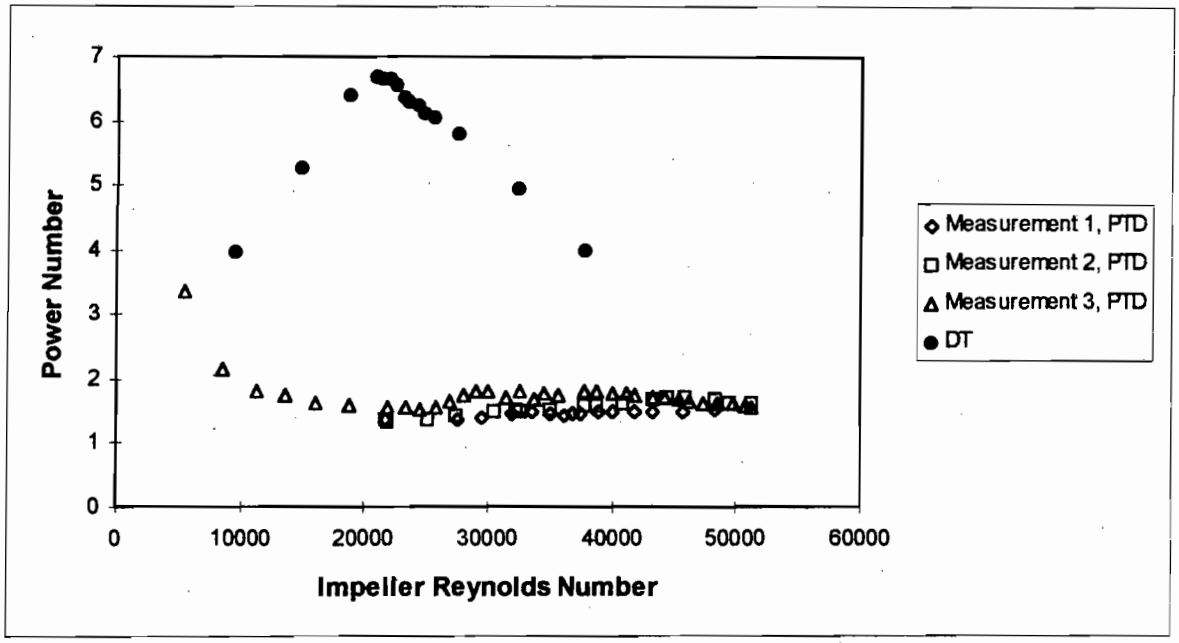

Figure 5.4. **Power number (N_p) as a function of the impeller Reynolds number (N_{RE}) measured to determine the critical impeller speed using the pitched-blade turbine (PTD) at 20% solids (v/v).**

The N_p-N_{RE} curve for the Rushton turbine (DT) at 20% solids (v/v) is included for comparison.

The absence of a maximum in the N_p-N_{RE} curve of the pitched-blade turbine can be explained in terms of its flow pattern. In Figure 5.5, the flow patterns of the Rushton turbine (DT), the PTD and the propeller are presented. The radial flow pattern of the Rushton turbine results in solid fillets forming at the center and along the periphery of the vessel base as the impeller speed is increased. The increase in the power number as a function of the impeller Reynolds number at speeds approaching the critical impeller speed (N_{JS}) (Figure 5.3) results from the suspension of particles in these solid fillets (Rewatkar *et al.* 1991). Similarly, an increase in the power number as a function of the impeller Reynolds number is observed for the axial flow pattern of the propeller at agitation rates below N_{JS}, as solid particles along the periphery of the base are suspended (Bohnet and Niesmak 1980). The absence of a maximum in the N_p-N_{RE} curve of the PTD (Figure 5.4) suggests that the formation of solid fillets at the center and periphery of the vessel base is relatively insignificant for the mixed axial and radial flow pattern of this impeller. This was confirmed by visual observation of the vessel base. Since a maximum in the N_P-N_{RE} curve is not observed for the PTD, this method cannot be used to determine the critical impeller speed for the pitched-blade turbine in this study.

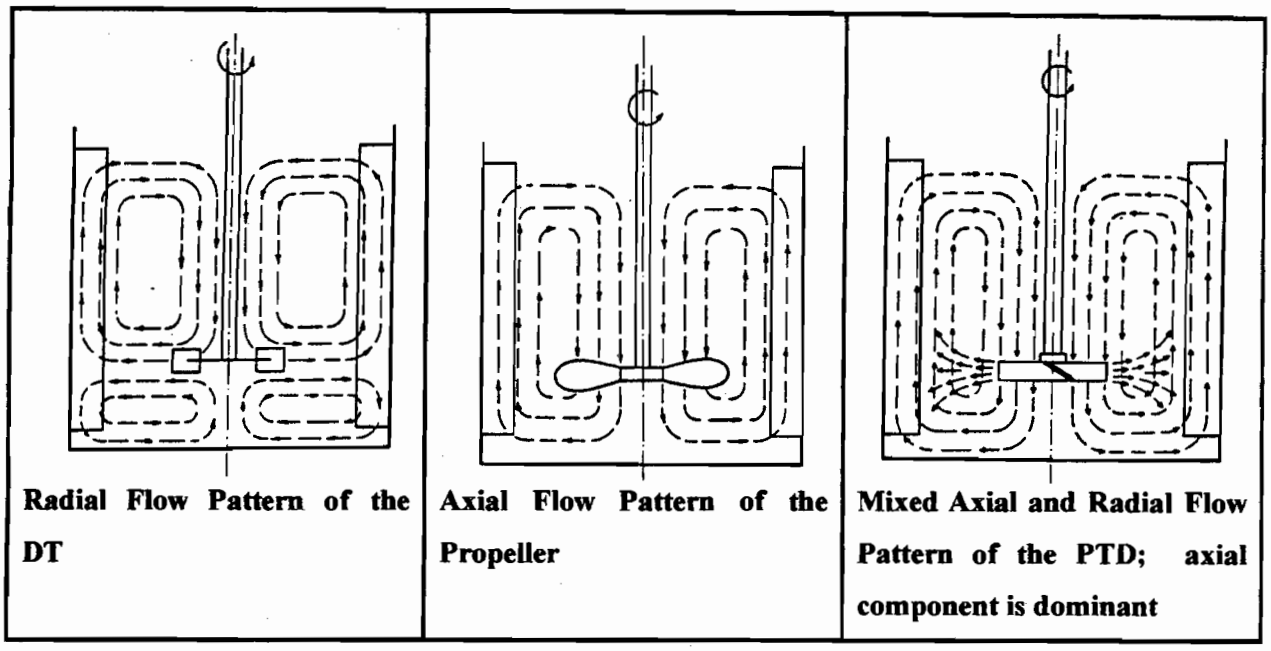

Radial Flow Pattern of the DT

Axial Flow Pattern of the Propeller

Mixed Axial and Radial Flow Pattern of the PTD; axial component is dominant

Figure 5.5. **Flow patterns of the Rushton turbine (DT), propeller and pitched-blade turbine, pumping downwards (PTD) (Joshi *et al.* 1982)**

Rewatkar *et al.* (1991) infer in their paper that they determined the critical impeller speeds of pitched-blade turbines (pumping downwards) from curves of the power number as a function of impeller speed. This contrasts with the findings of this study. To understand this discrepancy, the geometry of their system was compared to the system of this study (Table 5.2). Table 5.2 shows that the primary difference between the system of Rewatkar *et al.* (1991) and the system used in this study is the scale of the vessels and the impellers. The diameters of the vessels used by Rewatkar *et al.* (1991) are 3.8 to 9.9 times larger than the diameter of the stirred tank in this work, and the diameters of the pitched-blade turbines used by Rewatkar *et al.* (1991) are 1.9 to 9.9 times larger than the pitched-blade turbine in this study. Tatterson *et al.* (1980) showed that the flow patterns of pitched-blade turbines differ, depending on the impeller scale. The flow from pitched-blade turbines of 0.1m diameter, similar to the 0.076m diameter impeller in this work, was heterogeneous. The trailing vortices from the outside tips of the blades of these impellers were not coherent and exited the impeller region in a chaotic fashion below or directly into the path of an oncoming blade. However, the flow from pitched-blade turbines of 0.3m diameter, similar to the scale of the PTD impellers used by Rewatkar *et al.* (1991), was well-defined and very coherent in the discharge flow from the impeller region. The reduced heterogeneity of the flow from the 0.3m diameter pitched-blade turbine could allow fillet formation at the center and along the periphery of the vessel base, hence explain why Rewatkar *et al.* (1991) observed maxima in the curves of power number as a function of impeller speed.

Table 5.2. **Comparison of parameter ranges used by researchers in determining the critical impeller speed.**

Proponent	Impeller Type	D (m)	T (m)	D/T	C/T	$\Delta\rho$ (kg m^{-3})	d_p (μm)	B (% by weight)	$\mu \times 10^3$ (Pa s)
Zwietering (1958)	Marine propeller, DT, vaned disc, 2-bladed paddle	0.06-0.20	0.15-0.60	0.17-0.67	0.05-1.00	560-1810	125-850	0.5-20	0.32-9.30
Nienow (1968)	DT	0.036-0.073	0.14	0.26-0.52	0.14-0.33	530-1660	153-9000	0.093-10.0	1.0
Chapman *et al.* (1983)	DT, Angled-blade disc turbine, mixed flow impeller pumping upwards (4 blades), mixed flow impeller pumping downwards (4, 6 blades), marine propeller	0.072-0.902	0.29-1.83	0.25-0.52	0.25	50-1900	80-2800	1-3	1.0
Rewatkar *et al.* (1991)	DT, PTD (pumping downwards, 6 blades), PTD (pumping upwards, 6 blades)	0.14-0.75	0.57-1.50	0.12-0.58	0.33	1520	120-2000	0.34-50	1.0
Takahashi *et al.* (1993)	DT	0.05-0.29	0.10-0.58	0.5	0.25	49-2720	54-4920	0.1-2.0	0.55-1.00
This Study	DT, PTD (pumping downwards, 6 blades)	0.074	0.152	0.49	0.38	1629	600-850	13.5-171.6	1.8

The critical impeller speed of the pitched-blade turbine used in this work was determined by visual observation. The average critical impeller speed measured was 662 rpm with a 95% confidence interval of 4 rpm. Solids suspension occurs at a higher impeller speed for the pitched-blade turbine (662 rpm) compared to the Rushton turbine (501 rpm). In Table 5.3, *s* values (Equation 5.1) for the Rushton turbine and pitched-blade turbine are compared for the following vessel geometry: D/T = 0.5, C/T = 0.25. The ratio of the average *s* value in Table 5.3 for the pitched-blade turbine and the Rushton turbine is 1.38. For a fixed vessel geometry, solids concentration, particle properties and liquid properties, this determines the ratio of the critical impeller speed of the pitched-blade turbine to that of the Rushton turbine. In this work, a ratio of 1.32 was observed at 20% solids (v/v). The agreement between this ratio and the average literature ratio of 1.38 validates the relative magnitude of the critical impeller speeds of the pitched-blade turbine and Rushton turbine at 20% solids (v/v) in this work.

Table 5.3. **Comparison of s values (Equation 5.1) for a 6-bladed pitched-blade turbine (pumping downwards) and a 6-bladed Rushton turbine at an impeller diameter ratio (D/T) of 0.5 and an impeller clearance ratio (C/T) of 0.25.**

Proponent	Pitched-blade Turbine (PTD)	Rushton Turbine (DT)
Zwietering (1958)		4.0
Nienow (1968)		4.7
Chapman *et al.* (1983)	5.8*	4.3
Bujalski *et al.* (1988)	6.4	
Ibrahim *et al.* (1992)	5.7	

* 4-bladed pitched-blade turbine

Although the critical impeller speed of the pitched-blade turbine is 1.32 times greater than that of the Rushton turbine, the power input required for complete suspension with the PTD is lower (P = 5.2 W, N_p = 1.6) than for the DT (P = 6.8 W, N_p = 6.7). This is in agreement with the observations of Chapman *et al.* (1983). These workers suggest that the lower power consumption with which pitched-blade turbines cause suspension can be attributed to the enhanced drag forces of axial flow impellers, resulting from their higher volumetric pumping rate, or the shorter path length between the axial impeller and the point from which the particles are last suspended. The former applies if drag forces are considered to be primarily responsible for the solids suspension while the latter applies if turbulent eddies are considered to be

responsible for the suspension. Less power would be required for the axial flow impeller since the shorter path length reduces the possibility of the turbulent eddies decaying.

5.4 Modelling the Critical Impeller Speed

The requirements of a mathematical expression, relating the measured critical impeller speeds (N_{JS}) to the operating parameters, were that it should describe the measured N_{JS} values and also predict the N_{JS} values below the lowest measured value in this study. Correlations relating the critical impeller speed to the operating parameters are generally of the form of the equations of Zwietering (1958) and Takahashi *et al.* (1993). The exponents of these correlations are broadly supported by many works (Chapman *et al.* 1983, Rewatkar and Joshi 1991). Hence the critical impeller speeds from this study were fitted to expressions with the same exponents. The constants, *s*, were obtained from a Least Squares analysis (see Appendix H for the Least Squares Algorithm). Equations 5.7 to 5.9 respectively represent the expressions obtained using the correlation of Zwietering (1958) for the critical impeller speeds of the Rushton turbine at 5% to 20% solids (v/v), the correlation of Zwietering fitted to the PTD critical impeller speed at 20% solids loading (v/v) and the correlation of Takahashi *et al.* (1993) fitted to the critical impeller speeds of the Rushton turbine at 5% to 20% solids (v/v).

$$N_{JS} = 60\left(\frac{2.33\,\nu_l^{0.1}\,d_p^{0.2}\,(9.81\,\Delta\rho/\rho)^{0.45}\,B^{0.13}}{D^{0.85}}\right) \qquad \textbf{Equation 5.7}$$

$$N_{JS} = 60\left(\frac{3.24\,\nu_l^{0.1}\,d_p^{0.2}\,(9.81\,\Delta\rho/\rho)^{0.45}\,B^{0.13}}{D^{0.85}}\right) \qquad \textbf{Equation 5.8}$$

$$N_{JS} = 60\left(\frac{1.60\,\nu_l^{0.1}\,d_p^{0.05}\,(9.81\,\Delta\rho/\rho)^{0.38}\,B^{0.17}}{D^{0.60}}\right) \qquad \textbf{Equation 5.9}$$

Since these expressions are of the standard form, which has been used to describe critical impeller speeds across the range of solids concentrations of 0.0008 % (v/v) (Baldi *et al.* 1978) to 28 % (v/v) (Raghava Rao *et al.* 1988, Rewatkar *et al.* 1989), it is assumed that it is valid to apply Equations 5.7 to 5.9 to predict the critical impeller speeds below the lowest measured N_{JS} value in this study (corresponding to 5% solids (v/v)). The reliability of a correlation in predicting the measured critical impeller speeds can be quantified in terms of a standard deviation, defined as:

$$\text{Standard Deviation} = \sqrt{\frac{\sum_{i=1}^{n}\left(X_{predicted,i} - X_{measured,i}\right)^2}{n-1}} \qquad \textbf{Equation 5.10}$$

where: n = number of points where measurements were made.

The measured critical impeller speeds, determined from the N_p-N_{RE} curves using the Rushton turbine, were compared to the predictions of N_{JS} from Equation 5.7, Equation 5.9, the correlation of Zwietering (1958) (Equation 5.1) and of Takahashi *et al.* (1993) (Equation 5.2), in terms of a standard deviation (Equation 5.10). These are summarised in Table 5.4. In Figure 5.6, a parity chart is provided for the comparison of the measured and predicted N_{JS} values at 5%, 10%, 15% and 20% solids (v/v) for the Rushton turbine. The solid line represents perfect correlation between the predicted critical impeller speeds and those measured from the N_p-N_{RE} curves.

Table 5.4. **Standard deviation (Equation 5.10) in predictions of the critical impeller speed values for the Rushton turbine.**

Correlation	Standard Deviation (rpm)
Equation 5.7	13
Equation 5.9	24
Correlation of Zwietering (1958)	683
Correlation of Takahashi *et al.* (1993)	67

Table 5.4 and Figure 5.6 show that Equations 5.7 and 5.9 predict the experimental critical impeller speeds well. Since Equation 5.7 has a lower standard deviation than Equation 5.9, it was used in Chapter 8 to predict the critical impeller speeds for the Rushton turbine below the lowest measured N_{JS} value.

Figure 5.6 also shows that the correlation of Zwietering (1958) predicts critical impeller speeds for the Rushton turbine approximately twice as large as the measured values. Calculation of the critical impeller speed for the pitched-blade turbine at 20% solids (v/v), using the correlation of Zwietering (1958), yields 1163 rpm *i.e.* 1.8-fold the visually-observed critical impeller speed of 662 rpm. Takahashi *et al.* (1993) found that the correlation of Zwietering (1958) overpredicted their measured critical impeller speeds for the

Rushton turbine by a factor of two. In addition, Narayanan *et al.* (1969) and Baldi *et al.* (1978) measured critical impeller speeds 22% and 50% lower than the values predicted from the correlation of Zwietering (1958) (Rewatkar *et al.* 1991). In contrast to this, a number of researchers (Nienow 1968, Chapman *et al.* 1983, Rewatkar *et al.* 1991) have obtained critical impeller speed expressions similar to the correlation of Zwietering (1958).

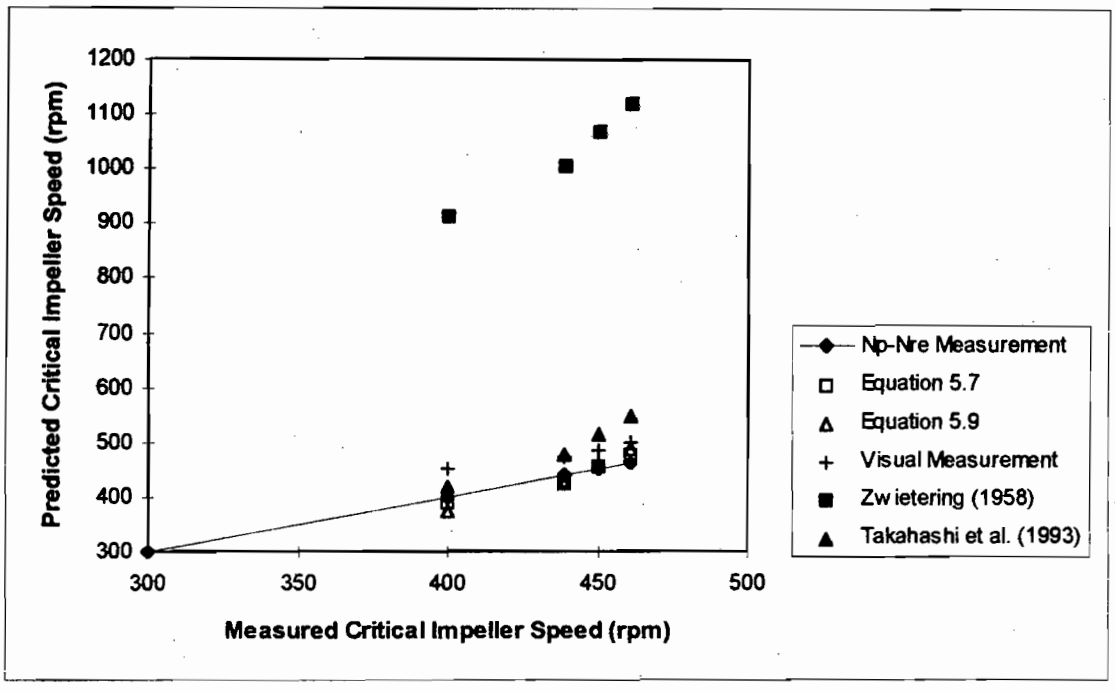

Figure 5.6 **Parity chart of measured and predicted critical impeller speeds for the Rushton turbine at 5%, 10%, 15% and 20% solids (v/v).**

Rewatkar *et al.* (1991) explained the lower critical impeller speeds measured by Narayanan *et al.* (1969) and Baldi *et al.* (1978) in terms of the small vessel diameters (0.114-0.141 m and 0.122-0.229m respectively) used by these researchers. However, as is shown in Table 5.2, Takahashi *et al.* (1993) used a similar range of vessel diameters to Zwietering (1958) and still obtained critical impeller speeds 50% lower than the values measured by Zwietering (1958). Table 5.2 shows that the parameter ranges used by the various researchers are similar and it is thus difficult to establish the reason for the discrepancy in the critical impeller speed measurements. The subjectivity of the visual determinations of the critical impeller speeds by these workers may account for this discrepancy.

The larger standard deviations (Table 5.4) obtained between the measured critical impeller speeds of the Rushton turbine and the critical impeller speeds predicted by the correlations of Zwietering (1958) and Takahashi *et al.* (1993), compared to the fitted expressions (Equations 5.7 and 5.9), may also be attributed

to the solids concentration in this study lying outside the range used by these workers. The correlation of Zwietering (1958) applies to a solids concentration of 0.2% to 8.8% (v/v). The maximum solids loading used by Takahashi *et al.* (1993) was 0.8% (v/v). Despite these differences, the applicability of standard expressions of the form of the correlations of Zwietering (1958) and Takahashi *et al.* (1993) to the experimental data, and the fairly good agreement between the measured N_{JS} values for the Rushton turbine and those predicted by Takahashi *et al.* (1993) (16% coefficient of variance) validate the measured critical impeller speed values in this study.

5.5 Conclusions

In this chapter, quantifying solids suspension in terms of the critical impeller speed and the degree of solids homogeneity has been reviewed. The need for a relationship quantifying the volume fraction of solids suspended at a given impeller speed (Chapter 8) led to the choice of the critical impeller speed. Correlations of the form of Zwietering (1958) and Takahashi *et al.* (1993), which describe the critical impeller speed as a function of the operating parameters, allow the prediction of the volume fraction of solids suspended at a given impeller speed. In addition, the critical impeller speed is a more direct measure of the transition between the regimes of incomplete and complete solids suspension than the degree of solids homogeneity.

The critical impeller speed (N_{JS}) was measured by visual observation and from determining the maxima in curves of the power number (N_P) as a function of the impeller Reynolds number (N_{RE}). For the Rushton turbine, measurements of the critical impeller speeds from the N_p-N_{RE} curves differed from the visually observed values by an average of 9%. The critical impeller speed measurements from the N_P-N_{RE} curves were used for the Rushton turbine (DT) since they are more objective. The N_P-N_{RE} curves did not yield a maximum for the pitched-blade turbine (PTD) used in this study. As a result, the visually observed critical impeller speed was used for this impeller. Although the visually observed critical impeller speed of the pitched-blade turbine at 20% solids (v/v) is 1.32 times greater than that of the Rushton turbine, the power input required for complete suspension with the PTD is 24% lower. This has been validated by reference to the literature.

The measured critical impeller speeds (N_{JS}) of the Rushton turbine and pitched-blade turbine were mathematically related to the operating parameters for the modelling of the cell disruption in Chapter 8. An expression of the form of the correlation of Zwietering (1958) was fitted to describe the N_{JS} data best. The measured critical impeller speeds of the Rushton turbine were compared to the predictions of N_{JS} from the

correlations of Zwietering (1958) and Takahashi *et al.* (1993). Although the correlation of Takahashi *et al.* (1993) described the critical impeller speeds of the Rushton turbine relatively well (coefficient of variance of 16%), the correlation of Zwietering (1958) overpredicted the measured critical impeller speeds by a factor of 2. Possible reasons for this have been discussed.

Chapter 6: The Effect of Completely and Incompletely Suspended Solids on Cell Disruption

6.1 Introduction

The need to quantify microbial cell damage and disruption in slurry systems in the regimes of complete and incomplete solids suspension was highlighted in Chapter 2. In this chapter, results are presented on the effect of completely and incompletely suspended solids on the disruption of *Saccharomyces cerevisiae* in a slurry reactor, as a function of the agitation intensity, solids concentration and impeller flow pattern. The impeller flow pattern was investigated by using either a 6-bladed Rushton turbine or a 6-bladed pitched-blade turbine (pumping downwards) (Section 3.4.2). The transition between the incompletely and completely suspended solids regimes occurs at the critical impeller speed (Chapter 5).

The chapter begins with a discussion of the kinetic expression used to model the disruption of the *Saccharomyces cerevisiae* in terms of soluble protein release. Use of a kinetic expression allowed the cell disruption to be quantified in terms of kinetic parameters. The calculation of these kinetic parameters is described and the duration of the disruption experiments required to determine the true values of these kinetic parameters is discussed. The inter-batch variation in the yeast and the reproducibility of the results are addressed. Finally, results are presented to assess the effect of incompletely and completely suspended solid particles on cell disruption.

6.2 Determination of the Cell Disruption

6.2.1 First Order Kinetics of Protein Release

6.2.1.1 Derivation of First Order Expression

It has been found that cell disruption by mechanical means follows first order kinetics (Chisti and Moo-Young 1986). It is well documented that cell breakage in bead mills shows first order kinetics in which the rate of protein release is directly proportional to the amount of unreleased protein (Engler 1985, Schutte *et al.* 1986, Schutte and Kula 1988, Harrison 1991). Poncelet and Neufeld (1989) and Lu *et al.* (1992) observed first order breakage kinetics when nylon microcapsules were agitated in a bioreactor. The microcapsules were used as a physical model of animal cells in suspension culture. First order kinetics have also been observed for cell disintegration in a high pressure homogeniser (Kula and Schutte 1987) and in the use of ultrasonication to disrupt cells (Chisti and Moo-Young 1986).

The use of a first order expression to describe the release of soluble protein as a function of time has been validated by assuming that the disruption of cells is first order with respect to the concentration of intact cells (Limon-Lason *et al.* 1979, Pearce 1993):

$$-\frac{dN}{dt} = k\ N \qquad \textbf{Equation 6.1}$$

where N is the number of intact cells at time t, and k is the first order disruption rate constant. Integration of Equation 6.1 yields Equation 6.2:

$$\ell n\left(\frac{N_o}{N}\right) = k\ t \qquad \textbf{Equation 6.2}$$

Here, N_o is the initial number of cells. To obtain a cell disruption expression in terms of the soluble protein release, the soluble protein content is substituted for the number of intact cells:

$$R_M = C_p N_o \qquad \textbf{Equation 6.3}$$

$$R = C_p N_o - C_p N \qquad \textbf{Equation 6.4}$$

where R_M is the maximum soluble protein available for release, R is the soluble protein released at time t, and C_p is the protein content of one cell. Rearrangement gives:

$$N = N_o - \frac{R}{C_p} \qquad \textbf{Equation 6.5}$$

$$N = \frac{R_M}{C_p} - \frac{R}{C_p} \qquad \textbf{Equation 6.6}$$

Substituting Equations 6.6 and 6.3 into Equation 6.2 and rearranging gives:

$$\ell n\left(\frac{R_M}{(R_M - R)}\right) = k\ t$$

$$R = R_M(1 - \exp(-k\ t)) \qquad \textbf{Equation 6.7}$$

Equation 6.4 assumes that the cells are instantaneously disrupted to their maximum extent. Measurement of the release of enzymes, located in the cell wall, the cytoplasm and the organelles, is required to validate this assumption.

6.2.1.2 Determining the Kinetic Parameters

Figure 6.1 shows sample data of the soluble protein release as a function of time for the disruption experiments in this study. The first order expression used to model the data is shown in Equation 6.8:

$$R = R_i (1-\exp(-k\ t)) \qquad \textbf{Equation 6.8}$$

where R is the soluble protein released at time t (mg protein / g cell), R_i is the maximum soluble protein released under the specified operating conditions (mg protein/g cell), and k is the first order disruption rate constant (s^{-1}).

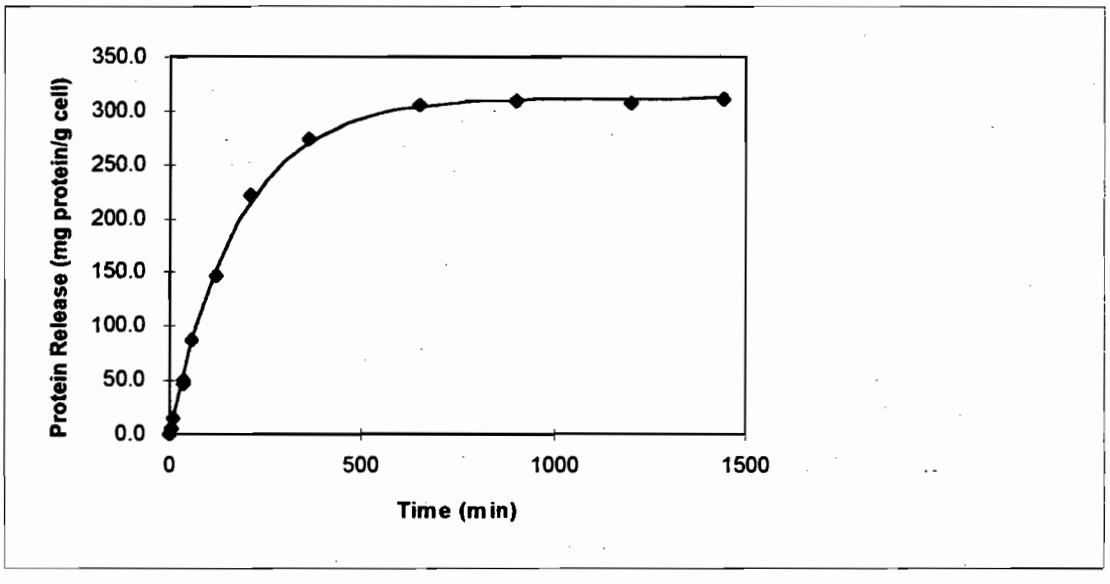

Figure 6.1. **Characteristic curve of protein release as a function of time.**
Solids volume fraction of 20%, Impeller speed of 273 rpm, Rushton turbine (Run #10.39). Symbols indicate measured protein release. Solid line indicates protein release predicted by Equation 6.8.

Equation 6.8 was fitted to each experimental protein release time course by minimising the sum of the squares of the error between the experimental and predicted values. The algorithm used is described and illustrated with a sample calculation in Appendix G. The accuracy of the first order expression in predicting the disruption data was quantified in terms of a coefficient of variance (CV), defined as:

$$CV = \frac{\sqrt{\frac{\sum_{i=1}^{n} (X_{predicted,i} - X_{measured,i})^2}{n-1}}}{\frac{\sum_{i=1}^{n} X_{measured,i}}{n}} \qquad \textbf{Equation 4.6}$$

where X signifies the soluble protein release (R) and n is the number of samples taken. The coefficients of variance for each of the experiments are presented in Appendix G. These values were generally about 4 % and were always less than 8%. The first order expression clearly describes the disruption data well.

The term, R_i, was used to represent the maximum soluble protein release in the slurry reactor (Equation 6.8) to differentiate it from the maximum soluble protein available for release, designated as R_M in this work. This distinction was not made in the bead mill literature. As discussed in Section 3.3.3, Pearce (1993) showed that the soluble protein release from *Saccharomyces cerevisiae* is greater on disruption in a French Press than on agitation in a slurry reactor at 40% solids (v/v) and 1090 rpm, or on lysis of the yeast cells using *Cytophaga* enzymes. The maximum soluble protein available for release (R_M) was thus determined for each batch of yeast cells by passing the yeast suspension twice through the French Press (Appendix E).

Micrographs of the yeast cells prior to disruption, following treatment in the slurry reactor and following 2 passes through the French Press are given in Figure 6.2 (Olympus BX40 microscope, Panasonic RGB 8-bit digital camera). Microscopic observation of the cells confirmed that the yeast cells were completely disrupted in the French Press since only cell debris was observed (Figure 6.2(d)). Although cell debris can be seen in micrographs of the yeast cells following disruption in the slurry reactor using the Rushton turbine (Figure 6.2(b)) and the pitched-blade turbine (Figure 6.2(c)), deformed yeast cells with disrupted cell walls can also be distinguished. The micrographs in Figure 6.2 thus confirm that a greater degree of cell disruption occurs in the French Press compared to the slurry reactor. Micronization of the cell debris in the French Press, with the concomitant release of insoluble complexed protein and other Folin-positive materials, such as peptide, glycopeptide and amino acids, could explain the greater soluble protein release that occurs in the French Press compared to the slurry reactor. The micrographs further indicate that none of the cells stained blue. Methylene blue indicates the presence of intact, non-viable cells (EBC Analytica Microbiologica 1977) and did not stain the cells as a result of the release of the cell cytoplasm into the supernatant on cell breakage.

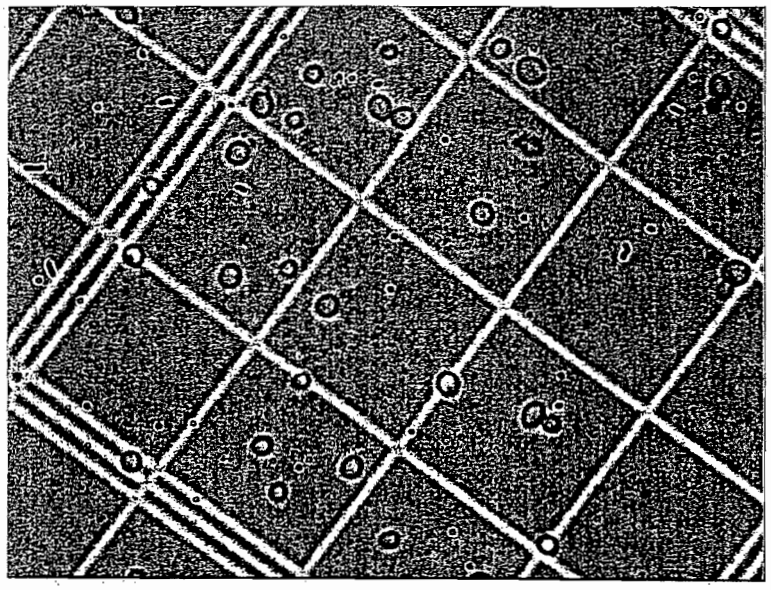

Figure 6.2(a)

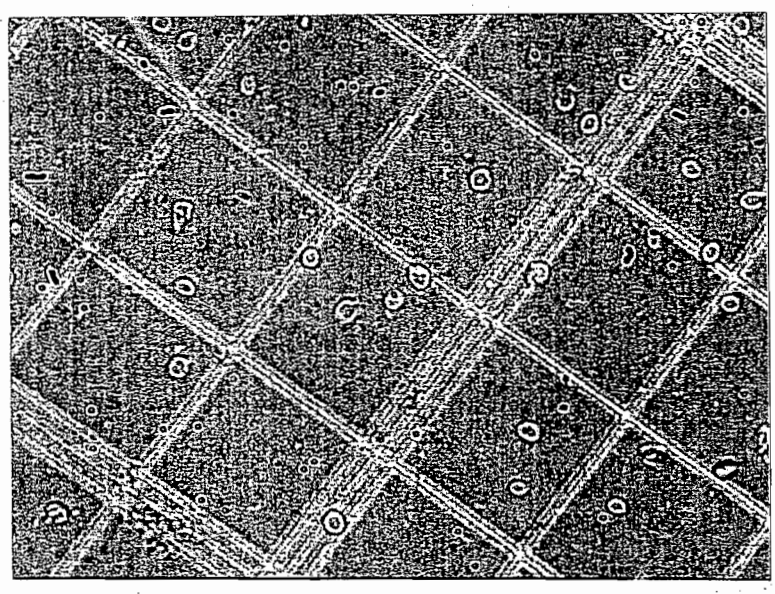

Figure 6.2(b)

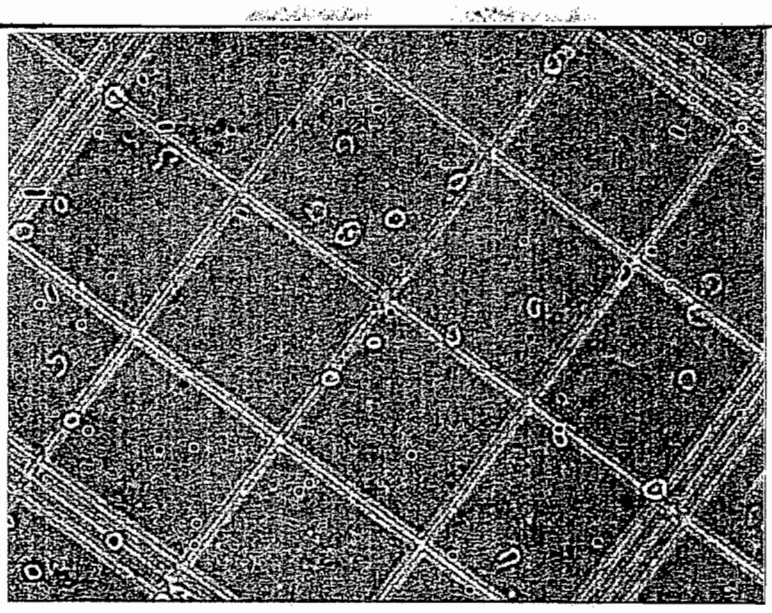

Figure 6.2(c)

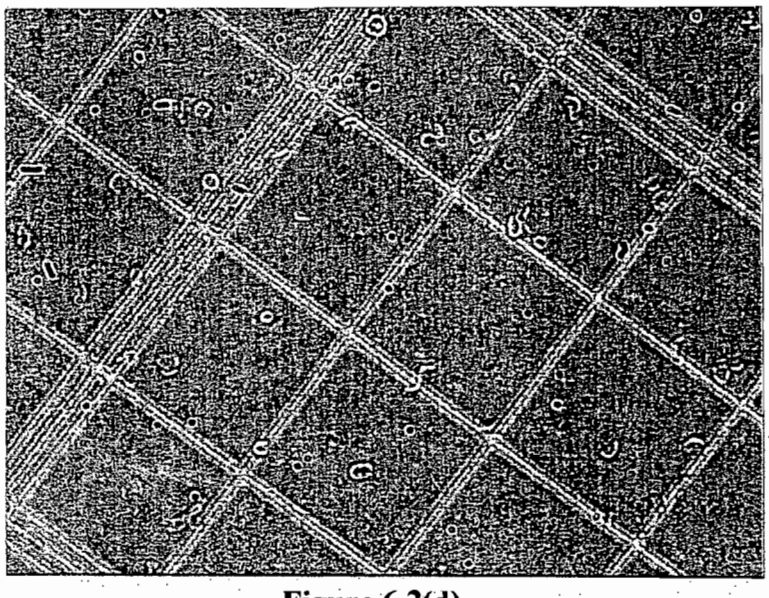

Figure 6.2(d)

Figure 6.2. **Photographs of cell disruption in the slurry reactor and the French Press.**
(Cells mounted on Neubauer Counting Chamber with grid dimensions of 0.05 mm x 0.05mm, Olympus BX40 microscope with Brightfield illumination and 40x magnification, Optimas 5.2 Image Analyser with Sharpen-high filtering): (a) undisrupted cells, (b) disrupted cells after 4 hours agitation with the Rushton turbine at 663.2 rpm and 20% solids (v/v) in the slurry reactor (Run#10.65), (c) disrupted cells after 5 hours agitation with the pitched-blade turbine at 673.6 rpm and 20% solids (v/v) in the slurry reactor (Run#10.64), (d) disrupted cells after 2 passes through the French Press.

The maximum soluble protein released under specified operating conditions in the slurry reactor, R_i, was normalised with respect to the maximum soluble protein available for release, R_M. This normalisation allowed comparison between different yeast batches. The ratio, R_i/R_M, was defined as the maximum extent of disruption under specified conditions.

6.2.2 Duration of Disruption Experiments

In order to determine the required duration of disruption experiments, the first order expression (Equation 6.8) was fitted to data collected over different time intervals, as detailed in Appendix G. In Table 6.1, the kinetic parameters of two disruption experiments, calculated using the soluble protein data collected over 2 hours, 6 hours and till cell disruption was complete, are given. For the disruption experiment performed at 10% solids (v/v) and 360 rpm, errors of 56% and 20% were obtained in k when the first order disruption expression was fitted to the soluble protein data collected over 2 hours and 6 hours respectively. The corresponding R_i values were underpredicted by 30% and 14%. For the disruption experiment performed at 20% solids (v/v) and 273 rpm, the respective absolute errors in k were 17% and 8%, when the first order disruption expression was fitted to the soluble protein data collected after 2 hours and 6 hours. The corresponding R_i values were overpredicted by 12% and 5%.

Table 6.1. **Comparison of kinetic parameters calculated after 2 hours and 6 hours of disruption and after complete cell disruption.**

Complete disruption was achieved for Run #10.37 (10% solids (v/v), 360 rpm) by 38 hours. Complete disruption was achieved for Run #10.39 (20% solids (v/v), 273 rpm) by 24 hours.

Time (hrs)	**10% solids (v/v), 360 rpm (Run #10.37)**			**20% solids (v/v), 273 rpm (Run #10.39)**		
	Fractional Disruption (%)	**k (1/s)**	**R_i (mg/g)**	**Fractional Disruption (%)**	**k (1/s)**	**R_i (mg/g)**
2	21	5.02×10^{-5}	218	49	7.67×10^{-5}	349
6	50	4.00×10^{-5}	267	86	8.50×10^{-5}	329
24				100	9.27×10^{-5}	312
38	100	3.21×10^{-5}	310			

Table 6.1 highlights the importance of ensuring that R_i has reached its maximum value before the first order expression is fitted to the disruption data. For the experimental work presented in this chapter, the duration of the experiments was determined by the time taken for the soluble protein to reach its maximum value. This ranged from 0.67 hours at 40% solids (v/v) and 758 rpm to 38.18 hours at 10% solids (v/v) and 360.3 rpm.

6.2.3 Inter-batch Variation in Yeast

The experiments reported in this study were conducted from January 1995 to January 1997 using different yeast batches from Anchor Yeast. To establish the variation in the first order disruption rate constant (k) and the maximum extent of cell disruption (R_i/R_M) as a result of using different yeast batches, five disruption experiments were repeated during this time period. These experiments are listed in Table 6.2. The protein release as a function of time for each of these experiments is detailed in Appendix G. Also presented in Table 6.2 are the average values, the standard deviations and the coefficients of variance in k and R_i/R_M from the repeated experiments at each of the experimental conditions. The coefficient of variance is defined as the quotient of the standard deviation and the average, and provides a relative measure of the agreement in the repeated measurements of the kinetic parameters.

Table 6.2. **Average values, standard deviations (SD) and coefficients of variance (CV) in k and R_i/R_M for the repeated experiments in this study.**

Experimental Conditions	Number of Repeats	k			R_i/R_M		
		Average (1/s)	SD (1/s)	CV (%)	Average (1/s)	SD (1/s)	CV (%)
Rushton turbine:							
• 10% solids, 360 rpm	5	2.61×10^{-5}	4.92×10^{-6}	18.9	78.7	0.7	0.9
• 20% solids, 273 rpm	2	9.08×10^{-5}	2.69×10^{-6}	3.0	80.4	2.0	2.5
• 20% solids, 474 rpm	2	4.12×10^{-4}	7.07×10^{-7}	0.2	81.2	5.3	6.5
• 20% solids, 745 rpm	2	7.44×10^{-4}	8.49×10^{-6}	1.1	77.8	2.3	3.0
Pitched-blade Turbine:							
20% solids, 674 rpm	4*	4.51×10^{-4}	3.68×10^{-5}	8.2	84.0	5.9	7.0

* Physiologically changed yeast

Table 6.2 shows that, with the exception of the disruption experiment performed at 10% solids (v/v) and 360 rpm, the coefficients of variance in k are less than 8.2%. Although the coefficient of variance for the 10% solids experiment at 360 rpm is relatively large (18.9%), the standard deviation for this experiment is of the same order of magnitude as the other repeated experiments. It is the small average k value of this experiment that gives rise to the comparably larger coefficient of variance. Table 6.2 further shows that the coefficients of variance in the maximum extent of disruption (R_i/R_M) are less than 7.0% for all the repeated experiments. The good reproducibility in k and R_i/R_M validates the comparison of the disruption results from the different yeast batches used in this work.

During the period over which the disruption experiments were performed, a physiological change in the yeast cells, obtained from Anchor Yeast (Epping, Cape Town), was observed. This physiological change was confirmed by repetition of the disruption experiment performed with the Rushton turbine at 20% solids (v/v) and an agitation intensity of 663 rpm. At these conditions, a first order disruption rate constant of 6.54×10^{-4} s^{-1} was obtained using the initial yeast batches in this work (Run #10.43; coefficient of variance less than 8.2%, Table 6.2). Using the physiologically changed yeast, an average first order disruption rate constant of 8.22×10^{-4} s^{-1}, with a coefficient of variance of 7.6%, was obtained from 3 disruption experiments (Runs #10.50, 10.53, 10.65) performed at these conditions. The difference between these k values is statistically significant within a 95% confidence interval, as determined from the statistical methods presented in Miller and Freund (1985). Despite the 26% increase in the first order disruption rate constant on using the physiologically changed yeast, the maximum extent of cell disruption (R_i/R_M) was consistent with that of the initial yeast batches. The disruption experiments shown in Table 6.2, that were performed with the physiologically changed yeast, are denoted by an asterisk.

The larger first order disruption rate constants observed using the physiologically changed yeast indicate the reduced strength of the cell wall for this yeast (Engler 1985, Harrison *et al.* 1991a). This may be attributed to a change in the medium composition for the growth of the micro-organisms (Gray *et al.* 1972) or a difference in the growth phase of the cells when they were harvested (Harrison *et al.* 1991b). Gray *et al.* (1972) found that cell disruption was more readily accomplished following cell growth on a simple synthetic medium than on a complex medium. The increased sensitivity of exponentially growing cells over stationary phase bacteria to cell disruption has been demonstrated on high pressure homogenisation (Harrison *et al.* 1991b), on disruption by bead mills, ultrasound or autolysis (Cumming *et al.* 1985), on enzymatic lysis (Fish and Lilly 1984), and on osmotic shock (Felix 1982). The increased sensitivity of the exponentially growing cells to cell disruption results from the formation of discontinuities in the cell wall as

the cells grow. These discontinuities are formed by hydrolytic enzymes to allow for the insertion of new wall material into the older portions of the cell wall (Bayer 1967).

6.3 The Effect of Solids Loading at a Constant Impeller Speed using the Rushton turbine

6.3.1 Experimental Conditions

In the first set of experiments, the solids volume fraction was varied across the range of 0.00 to 0.40 using a Rushton turbine at a constant impeller speed of 750 rpm (impeller tip speed of 2.91 m/s). This impeller speed is greater than the critical impeller speed of 593 rpm for the solids volume fraction of 0.40. These disruption experiments show the effect of increasing suspended solids on the cell disruption at a constant particle momentum.

6.3.2 Results

The resultant disruption, in terms of soluble protein release, is summarised in Figure 6.3. The disruption data of each of the experiments and the conditions at which they were performed are presented in Appendix G. Figure 6.3 shows that the curves of soluble protein release tend to a common maximum value and that this maximum value is attained more quickly at the higher solids volume fractions. In addition, over the time period investigated, negligible cell disruption occurs in the slurry reactor in the absence of solid particles. A number of mechanisms have been proposed to describe the damage to cells in systems where cells and solid particles are present: interactions between the cells and fluid eddies, interactions between the cells and solid particles, interactions between the cells and gas bubbles, and interactions between the cells and reactor components (Croughan *et al.* 1987, 1988, 1989; Cherry and Papoutsakis 1988). These mechanisms are comprehensively reviewed in Chapter 7 of this work. The negligible cell disruption in the absence of solid particles suggests that the dominant cell disruption mechanism in the slurry reactor is interaction between the cells and solid particles.

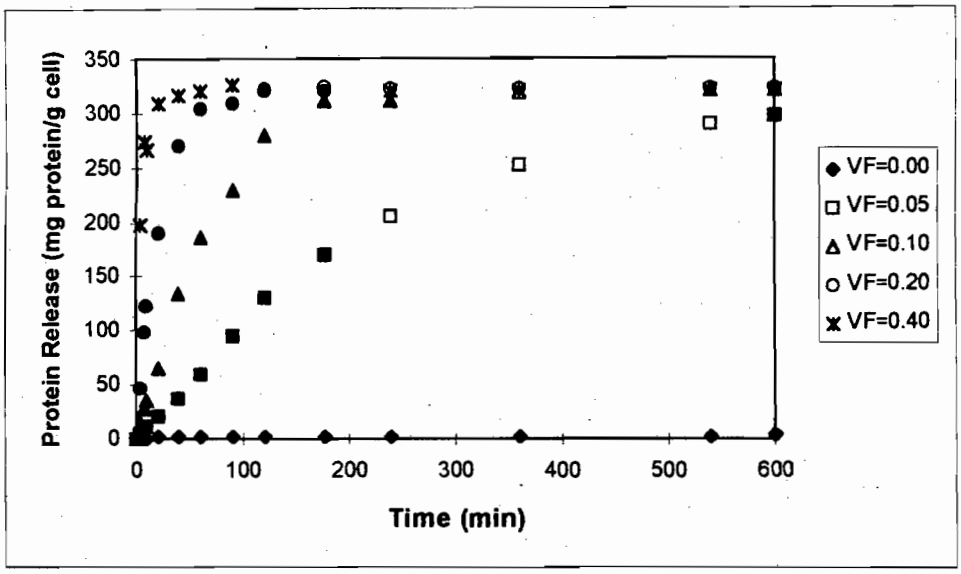

Figure 6.3. **Soluble protein release as a function of time and solids loading on agitation with the Rushton impeller.**

Impeller speed of 750 rpm, cell dry weight concentration of 52.8 kg m^{-3}. VF signifies the solids volume fraction. Closed symbols designate measured data, open symbols designate data extrapolated using Equation 6.8.

The results presented in Figure 6.3 can be more readily interpreted by examination of the kinetic parameters, R_i and k, as a function of the solids volume fraction. The values of the kinetic parameters are presented in Appendix G and are shown as a function of the solids volume fraction in Figure 6.4. Over the range of volume fractions investigated, the maximum extent of breakage in the slurry reactor (R_i/R_M) is constant with an average value of 79.1% at a 95% confidence interval of 0.3%. The first order disruption rate constant, k, increases in a power law fashion with the solids volume fraction (Φ). This power law relationship is described by Equation 6.9 with a correlation coefficient (R^2) of 0.992 (Figure 6.4). The modelling of the variation of k with solids volume fraction is discussed in detail in Chapter 7.

$$k = 0.0202\ \Phi^{1.92} \qquad \textbf{Equation 6.9}$$

cell disruption rate. In this study, the disruption rate of *Saccharomyces cerevisiae* at an agitation intensity of 750 rpm (impeller tip speed of 2.91 m s^{-1}) was found to vary from 7.08 x 10^{-5} s^{-1} at 5% (v/v) inert solids, to 4.05 x 10^{-3} s^{-1} at 40% inert solids (v/v), in a power law fashion. The functional dependence of the cell disruption rate constant on the solids concentration consequently differs in this work from that observed by Croughan *et al.* (1988). This may be attributed to the low solids concentrations that these researchers used, the different mechanisms of cell disruption in the two systems (discussed in detail in Section 7.5.2) or the location of the cells relative to the solid particles.

The disruption kinetic parameters presented in this section were also compared to the results of Pearce (1993), described in Section 2.2.3. Pearce (1993) investigated the effect of solids concentration on the disruption of *Saccharomyces cerevisiae* over the range of 5 to 40% solids (v/v) at an impeller speed of 772 rpm (impeller tip speed of 2.18 m s^{-1}). At this impeller speed, the solid particles at each of the solids volume fractions were completely suspended. Silica particles with a geometric mean particle diameter of 1245 μm were used, the cell dry weight concentration was 50 to 60 kg m^{-3} and the stirred tank employed was geometrically similar to the system used in this study. A 6-bladed Rushton turbine was used for the disruption experiments. The kinetic parameters of cell disruption obtained by Pearce (Figure 2.1) on fitting a first order disruption expression to the data of soluble protein release as a function of time are compared in Figure 6.5 to the kinetic parameters obtained in this work.

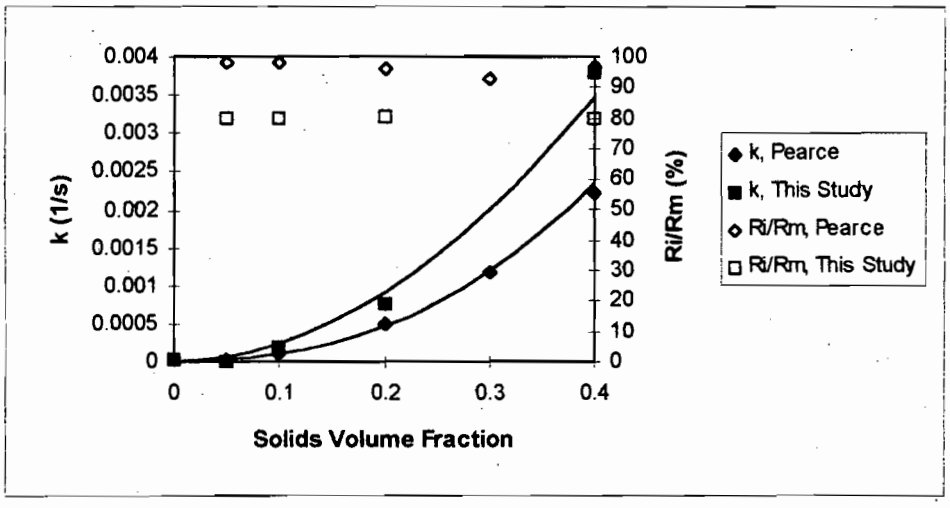

Figure 6.5. **Comparison of disruption kinetic parameters of *Saccharomyces cerevisiae* obtained by Pearce (1993) and in this work as a function of the solids volume fraction.**
Rushton turbine; Pearce: N = 772 rpm, $d_{p,\,mean}$ = 1245 μm, c = 50-60 kg m^{-3}; This study: N = 750 rpm, $d_{p,\,mean}$ = 714 μm, c = 52.8 kg m^{-3}. Solid lines represent the k values predicted by Equation 2.1 (Pearce) and Equation 6.9 (this study).

Despite the higher impeller speed used by Pearce (1993), the power input per unit volume was 36% higher in this work (Pearce: P/V is 7430 W m^{-3}; This study: P/V is 10 079 W m^{-3}). For particles larger than 500 μm in diameter, particle diameter does not affect k (Figure 2.2). It was therefore anticipated that the k values would be higher in this study. In agreement with this study, Pearce found a power law dependence of k on solids volume fraction (Equation 2.1). The constants in this equation are similar to those in Equation 6.9.

$$k = 0.0198\,\Phi^{2.33} \qquad \textbf{Equation 2.1}$$

Pearce (1993) also found that the maximum extent of cell disruption (R_i/R_M) was constant over 5 to 40% (v/v) solids concentration. An average R_i/R_M value of 96.4% with a 95% confidence interval of 2.9% was reported whereas the average R_i/R_M value in this work was found to be 79.1% with a 95% confidence interval of 0.3%. This difference may be attributed to the larger bead diameter used by Pearce (1993) (Figure 2.2).

6.4 The Effect of Agitation Intensity at a Constant Solids Loading using the Rushton turbine

6.4.1 Experimental Conditions

In this set of experiments, the Rushton turbine was used and the solids loading was fixed at either 10% or 20% (v/v). At each of these solids concentrations, a series of experiments was performed over the impeller speed range of 200 to 900 rpm (impeller tip speeds of 0.77 to 3.49 m s^{-1}). This range of speeds straddles the respective critical impeller speeds (N_{JS} = 439 rpm for 10% solids, N_{JS} = 461 rpm for 20% solids). Increasing the impeller speed, below N_{JS}, at a constant solids concentration results in an increase in the degree of solids suspension and an increase in the particle momentum. These experiments thus directly show the effect of incompletely ($N \leq N_{JS}$) and completely ($N \geq N_{JS}$) suspended solids on cell disruption as a function of the agitation intensity at solids volume fractions of 0.10 and 0.20.

6.4.2 Results

In Figures 6.6 and 6.7, curves of the soluble protein release are presented as a function of time at selected impeller speeds at 0.10 and 0.20 solids volume fractions respectively. The data from all the experiments is tabulated in Appendix G. Figure 6.6 and Figure 6.7 show that the soluble protein release curves tend to the same maximum extent of cell disruption. This maximum in the extent of cell disruption is attained more

quickly as the agitation intensity is increased and is attained more rapidly at 20% solids (v/v) than at 10% solids (v/v).

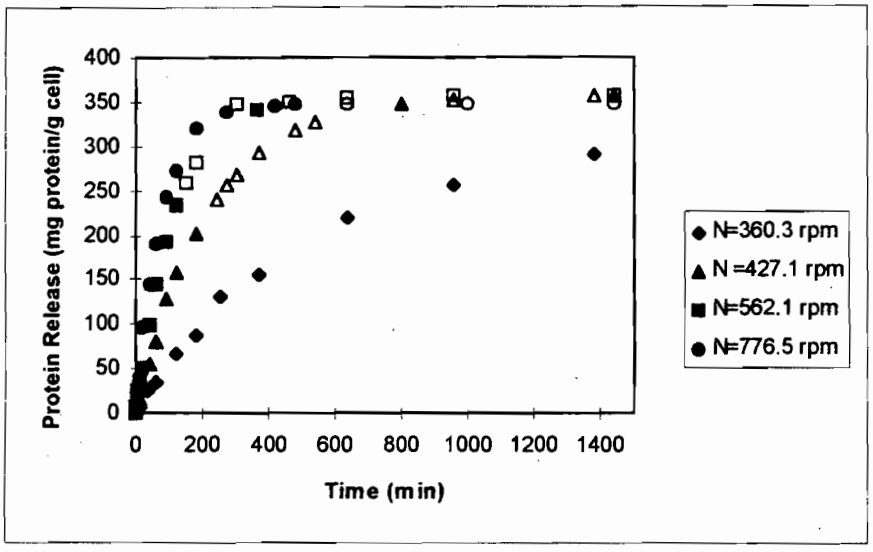

Figure 6.6. **Soluble protein release as a function of time and impeller speed on agitation with the Rushton turbine at 10% solids (v/v).**

Cell dry weight concentration of 52.8 kg m^{-3}. Closed symbols designate measured data, open symbols designate data extrapolated using Equation 6.8.

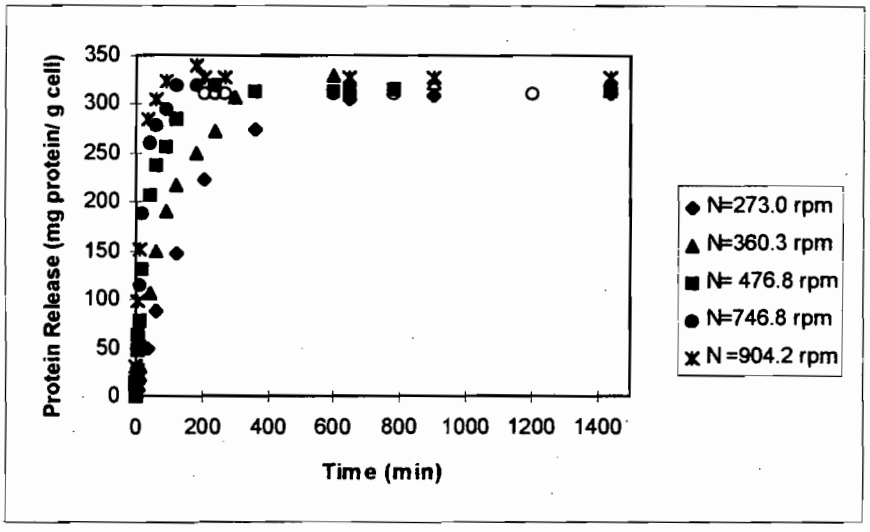

Figure 6.7. **Soluble protein release as a function of time and impeller speed on agitation with the Rushton turbine at 20% solids (v/v).**

Cell dry weight concentration of 52.8 kg m^{-3}. Closed symbols designate measured data, open symbols designate data extrapolated using Equation 6.8.

The kinetic parameters from all the disruption experiments performed in this set of experiments are presented in Figure 6.8 as a function of the impeller speed at the two solids volume fractions. Figure 6.8 illustrates clearly that the maximum extent of cell disruption (R_i/R_M) is constant over the range of impeller speeds of 200 to 900 rpm for the 10% and 20% solids (v/v) experiments. For the 10% solids experiments, the average value of R_i/R_M is 80% with a 95% confidence interval of 2%. For the 20% solids experiments, the average value of R_i/R_M is 81% with a 95% confidence interval of 3%. The difference between these R_i/R_M values is not significant within a 95% confidence interval, as determined from the statistical methods presented in Miller and Freund (1985). In addition, within a 95% confidence interval, the difference between these R_i/R_M values and those presented in Section 6.3.2 is not statistically significant. This shows that irrespective of whether the yeast cells are agitated in the presence of incompletely or completely suspended solids, the same maximum extent of cell disruption ultimately results.

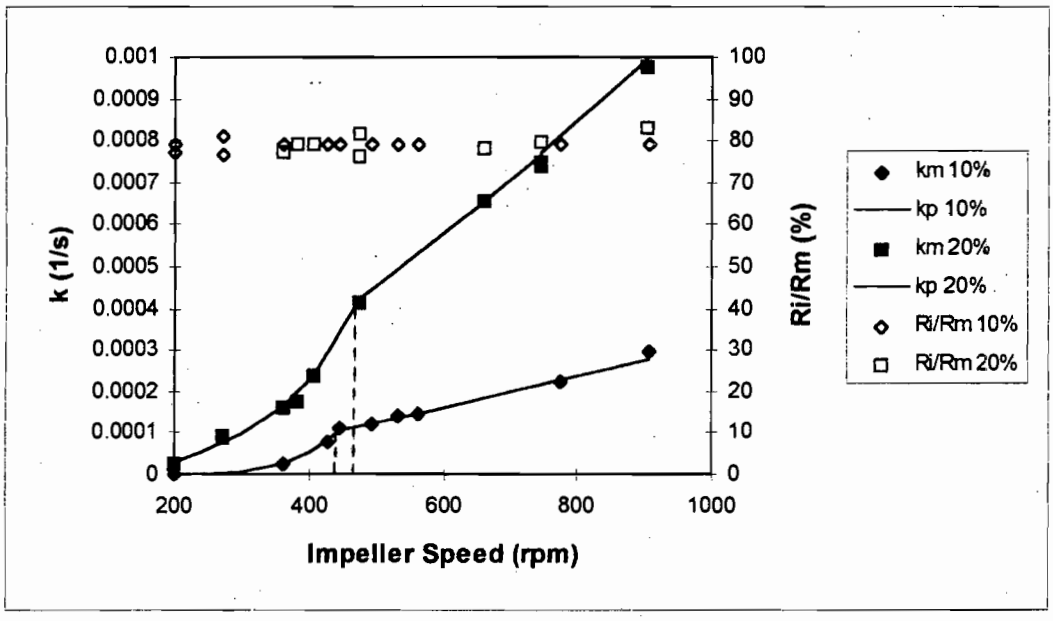

Figure 6.8. Cell disruption kinetic parameters as a function of impeller speed at 10% and 20% solids loadings (v/v) on agitation with the Rushton turbine.

Cell dry weight concentration of 52.8 kg m^{-3}. k_m signifies the measured k values. Solid lines indicate the predicted k values (k_p), using a power law function for $N \leq N_{JS}$ (Equation 6.10 for 10% solids, Equation 6.11 for 20% solids), and a linear function for $N \geq N_{JS}$ (Equation 6.12 for 10% solids, Equation 6.13 for 20% solids). Broken lines indicate the critical impeller speeds.

Figure 6.8 shows that the first order disruption rate constant, k, is a function of both the impeller speed and the solids loading. As observed on comparison of Figure 6.6 and Figure 6.7, the rate constants are greater

for the 20% solids concentration than for the 10% solids concentration over the impeller speed range. The difference between them becomes more significant above the critical impeller speed. In addition, the relationship between the rate constant and the impeller speed at 10% and 20% solids differs in relation to the critical impeller speed (N_{JS}). Below N_{JS}, the rate constant exhibits a power law dependence on impeller speed, which is described by Equation 6.10 and Equation 6.11 for the 0.10 and 0.20 solids volume fractions respectively. The respective correlation coefficients of the power law fits are 0.901 and 0.963. Above N_{JS}, the rate constant has a linear dependence on the impeller speed. This relationship is described by Equation 6.12 and Equation 6.13 for the 0.10 and 0.20 solids volume fractions with respective correlation coefficients of 0.991 and 0.997. The good agreement between the measured k values and those predicted by Equations 6.10 to 6.13 is further shown in Figure 6.8. The power law dependence of the rate constant on the impeller speed below N_{JS} was anticipated owing to the increase in volume fraction of suspended solids with increasing impeller speed (Figure 6.4). Above N_{JS}, the volume fraction of suspended solids remains constant. The dependence of the rate constant on the impeller speed and the solids volume fraction is analysed in detail in Chapters 7 and 8.

$$k = 2.63 \times 10^{-13} N^{3.20} \qquad \textbf{Equation 6.10}$$

$$k = 8.16 \times 10^{-12} N^{2.86} \qquad \textbf{Equation 6.11}$$

$$k = 4.07 \times 10^{-7} N - 8.1 \times 10^{-5} \qquad \textbf{Equation 6.12}$$

$$k = 1.29 \times 10^{-6} N - 2.1 \times 10^{-4} \qquad \textbf{Equation 6.13}$$

6.4.3 Discussion

As discussed in Section 2.2, the effect of agitation intensity on cell damage has been investigated at speeds greater than the critical impeller speed in the minerals bio-oxidation and animal cell-microcarrier systems. In the minerals bio-oxidation system, Hackl *et al.* (1989) found, in their pilot plant testwork, that an impeller tip speed of 5.3 m s^{-1} was detrimental to the *thiobacilli*. However, when the tip speed of the Rushton turbine was reduced to 3.3 m s^{-1}, normal leach rates were observed. Pearce (1993) studied the growth of *thiobacilli* in the presence of 10% (w/v) or 2% (v/v) pyrite at the laboratory scale. A tip speed of 2.6 m s^{-1} for a 6-bladed Rushton turbine was found to inhibit the cell growth, whereas an impeller tip speed of 1.4 m s^{-1} was not detrimental to the cells. In the laboratory scale animal cell-microcarrier system, low agitation intensities of 0.1 to 0.2 m s^{-1} were found to have no effect on the cell growth, even when the inert solids concentration was increased to 2.9% (v/v) and the fluid viscosity was increased to 2.6 cp (Croughan *et al.* 1988, 1989; Lakhotia and Papoutsakis 1992). However, at high agitation intensities of 0.3 to 0.6 ms^{-1}, the apparent cell growth rate is reduced even at low microcarrier concentrations of 0.02% (v/v) (Croughan

et al. 1989). The decrease in the cell growth rate is magnified as the inert solids concentration is increased to 2.9% (v/v) (Croughan *et al.* 1988).

In contrast to the studies in minerals bio-oxidation and in animal cell-microcarrier systems, it can be seen from Figure 6.8 that the entire range of agitation intensities above the critical impeller speed (1.70 to 3.49 m s^{-1} for 10% (v/v) solids; 1.79 to 3.49 m s^{-1} for 20% (v/v) solids) gives rise to significant disruption of the *Saccharomyces cerevisiae*. This may be attributed to the higher solids concentrations used in this work, corresponding to higher critical impeller speeds. A higher range of agitation intensities were thus used in this study compared to the work on animal cell-microcarrier systems or the work of Pearce (1993). In agreement with the study of Croughan *et al.* (1988), the disruption of the *Saccharomyces cerevisiae* at these agitation intensities is magnified as the solids concentration is increased.

The cell disruption observed in this set of disruption experiments was also compared to the results of Pearce (1993), where the disruption of *Saccharomyces cerevisiae* was investigated over the range of 150 to 1090 rpm (impeller tip speeds of 0.42 to 3.08 m/s), using a slurry reactor. This range of impeller speeds straddled the critical impeller speed of 685 rpm. In these disruption experiments, silica particles with a geometric mean particle diameter of 1245 μm at a solids volume fraction of 0.20 were employed. The cell concentration was 50 to 60 kg dry weight m^{-3}. The kinetic parameters obtained by Pearce (1993) were presented in Figure 2.3. However, the data of Pearce was collected over a 2 hour period of agitation, with the result that the maximum extent of cell disruption was only attained for the disruption experiments performed at 772 and 1090 rpm. The kinetic parameters shown in Figure 2.3 are the maximum extent of cell disruption (R_i/R_M), calculated using the soluble protein release over 2 hours, and the first order disruption rate constant (k), calculated from Equation 6.8 using R_M instead of R_i. To enable the direct comparison of the results of Pearce with the results of this study, the values of R_i and k, using both R_i and R_M in Equation 6.8, were recalculated from the data of Pearce. The method presented in Appendix G was used in the calculation of these kinetic parameters. The resultant values are summarised in Figure 6.9.

Figure 6.9 shows that there is a large amount of scatter in the values of $k(R_i)$ and the corresponding R_i/R_M values below 350 rpm. It was shown in Section 6.2.2 that if the disruption data under mild conditions was collected over 2 hours and fitted with a first order expression, erroneous values of the kinetic parameters were obtained. The values of the maximum extent of disruption and the $k(R_i)$ values, summarised in Figure 6.9, are consequently not reliable.

6.5 The Effect of Agitation Intensity at a Constant Solids Loading using the Pitched-blade turbine

6.5.1 Experimental Conditions

The effect of incompletely ($N \leq N_{JS}$) and completely ($N \geq N_{JS}$) suspended solids on cell disruption was also investigated as a function of agitation intensity using the pitched-blade turbine. A solids volume fraction of 0.20 was used for these disruption experiments and the agitation intensity was varied over the range of 440 to 900 rpm (impeller tip speeds of 1.70 to 3.49 m s^{-1}), straddling the critical impeller speed of 662 rpm. These disruption experiments were performed to establish whether the impeller flow pattern would alter the functional dependence of the kinetic parameters on the agitation intensity in the incompletely and completely suspended solids regimes.

6.5.2 Results

The kinetic parameters, obtained for the pitched-blade turbine at 20% solids (v/v), are plotted as a function of the impeller speed in Figure 6.10. For ease of comparison, the kinetic parameters obtained from the Rushton turbine at 20% solids (v/v) (Figure 6.8) are also plotted in Figure 6.10. Direct comparison of the cell disruption resulting from agitation with the Rushton turbine and the pitched-blade turbine is not possible since a physiological change in the yeast cells, obtained from Anchor Yeast (Epping, Cape Town), was observed for the disruption experiments performed with the pitched-blade turbine compared to the yeast used for the Rushton turbine experiments. The reduced resilience of the physiologically changed yeast resulted in larger k values compared to the initial yeast batches. However, the maximum extent of disruption observed using the physiologically changed yeast was the same as that of the initial batches (Section 6.2.3).

Figure 6.10 shows that the maximum extent of cell disruption (R_i/R_M) for the pitched-blade turbine is constant across the critical impeller speed and that it is, on average, 87% with a 95% confidence interval of 4%. Hence, as with the Rushton turbine, the cells ultimately tend to the same maximum extent of cell disruption, irrespective of whether the solid particles are incompletely or completely suspended. In Section 6.4, it was shown that, over the impeller speed range of 200 to 900 rpm at 20% solids (v/v) and using the Rushton turbine, the maximum extent of cell disruption is constant at 81% ± 3% (at a 95% confidence interval). The difference between the R_i/R_M values for the Rushton and pitched-blade turbines is not significant within a 99% confidence interval, indicating that the same maximum extent of cell disruption occurs in the slurry reactor, irrespective of the flow pattern.

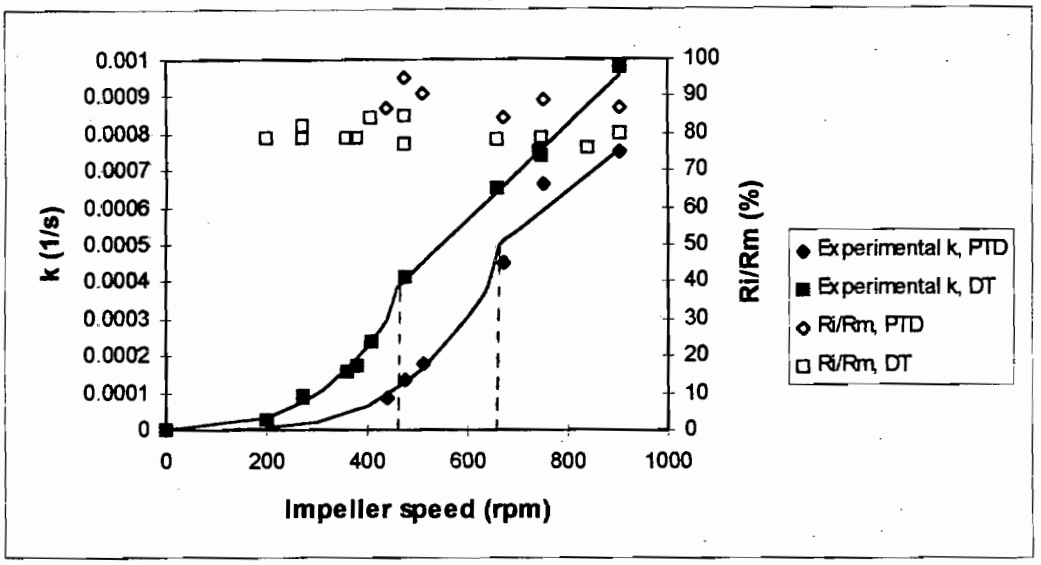

Figure 6.10. **Comparison of the cell disruption kinetic parameters for the pitched-blade turbine (PTD) and Rushton turbine (DT) as a function of impeller speed at 20% solids volume fraction.**

Cell dry weight concentration of 52.8 kg m^{-3}. Solid lines indicate the predicted k values, using a power law function for $N \leq N_{JS}$ (Equation 6.11 for the DT, Equation 6.14 for the PTD), and a linear function for $N \geq N_{JS}$ (Equation 6.13 for the DT, Equation 6.15 for the PTD). Broken lines indicate the critical impeller speeds.

Figure 6.10 further shows that the first order disruption rate constants (k) of the pitched-blade turbine exhibit a power law dependence on the impeller speed, below the critical impeller speed (N_{JS}). This relationship is described by Equation 6.14 with a correlation coefficient of 0.982. Above N_{JS}, the first order disruption rate constants exhibit a linear dependence on the impeller speed, which is described by Equation 6.15 with a correlation coefficient of 0.825. Although the linear expression does not describe the k values of the pitched-blade turbine, at speeds above the critical impeller speed, as accurately as the k values of the Rushton turbine (Equation 6.13, R^2=0.997), it appears that the functional dependence of k on the impeller speed is similar for the Rushton and pitched-blade turbines in the regions of incomplete and complete solids suspension.

$$k = 1.40 \times 10^{-14} N^{3.72} \qquad \textbf{Equation 6.14}$$

$$k = 1.0 \times 10^{-6} N - 2.1 \times 10^{-4} \qquad \textbf{Equation 6.15}$$

6.5.3 Discussion

Since disruption experiments performed with the physiologically changed yeast resulted in increased first order disruption rate constants compared to the original yeast batches used, the k values of the Rushton turbine in Figure 6.10 would be larger if all the disruption experiments were repeated using the physiologically changed yeast. It is thus evident that, at a given impeller speed below or above the critical impeller speed, the rate of cell disruption is less for the pitched-blade turbine than for the Rushton turbine. The observations in this study confirm the findings of Hackl *et al.* (1989) and Pearce (1993), which were made at a single impeller speed of 5.3 m s^{-1} and 2.6 m s^{-1} respectively, in the minerals bio-oxidation system. As described in Section 2.2.1, pitched-blade turbines have a higher pumping capacity than Rushton turbines and for a given impeller speed, require less power and produce a lower turbulence intensity (Chapman *et al.* 1983, Hackl *et al.* 1989). The lower k values for the pitched-blade turbine, at a given impeller speed, can be attributed to this lower power input.

6.6 Conclusions

In determining the effect of completely and incompletely suspended solids on the disruption of *Saccharomyces cerevisiae* in a slurry reactor, cell disruption was monitored in terms of the soluble protein release as a function of time. This profile is described well by a first order disruption expression with kinetic parameters, R_i (representing the maximum soluble protein release under the operating conditions) and k (representing the rate of cell disruption). A distinction needs to be made between R_i and R_M, the maximum soluble protein available for release, determined by disrupting the cells in a French Press. Normalisation of the R_i values with respect to R_M, allowed the disruption results from different yeast batches to be compared. This ratio (R_i/R_M) was defined as the maximum extent of cell disruption.

The importance of ensuring that R_i reached its maximum value in the cell disruption experiments before fitting the first order expression to the disruption data was highlighted in this chapter. Inaccurate kinetic parameters are obtained if the experiments are not run for a sufficiently long period of time, especially at low agitation rates and low solids loadings. The validity of using different batches of yeast from Anchor Yeast for the disruption experiments in this work was shown by the good reproducibilty of the kinetic parameters from replicate experiments.

Negligible cell disruption occurred in the slurry reactor in the absence of solid particles over a 10 hour period. However, significant cell disruption was observed over a solids concentration range of 5% to 40% solids (v/v). This suggests that the dominant cell disruption mechanism in the slurry reactor is interaction

between the cells and solid particles. In the presence of solid particles, a constant maximum extent of cell breakage (81% ± 1%) occurred at equilibrium conditions on agitation with either the Rushton or pitched-blade turbine at all the hydrodynamic conditions investigated. This study therefore shows that, irrespective of whether the solid particles are incompletely or completely suspended, the cells ultimately tend to the same maximum extent of cell disruption in the slurry reactor.

Disruption experiments performed in the completely suspended solids regime using the Rushton turbine over the solids concentration range of 5% to 40% (v/v) and a constant impeller speed of 750 rpm (impeller tip speed of 2.91 m s^{-1}) showed that the first order disruption rate constant (k) exhibits a power law dependence on the solids volume fraction. However, at a constant solids concentration and over the agitation intensity range of 200 to 900 rpm (impeller tip speeds of 0.77 to 3.49 m s^{-1}), using the Rushton or pitched-blade turbine, the functional dependence of k on the impeller speed differs in relation to the critical impeller speed. Increasing the agitation intensity in these disruption experiments increased the particle momentum and, below the critical impeller speed, increased the degree of solids suspension. At impeller speeds below the critical impeller speed, k exhibits a power law dependence on the impeller speed in accordance with the increase in volume fraction of suspended solids. At impeller speeds above the critical impeller speed, k has a linear dependence on impeller speed. Above the critical impeller speed, the volume fraction of suspended solids is constant and only the effect of agitation intensity on cell disruption is observed. These disruption results were compared to the cell damage observed in the minerals bio-oxidation and the animal cell-microcarrier systems, and to the disruption of *Saccharomyces cerevisiae* observed by Pearce (1993) using a slurry reactor.

Comparison of the first order disruption rate constants of the Rushton turbine and pitched-blade turbine revealed that for a given impeller speed, below or above the critical impeller speed, cell disruption is less for the pitched-blade turbine. This was attributed to the lower power input of this impeller at a given impeller speed.

Chapter 7: Modelling Cell Disruption when the Solids are Completely Suspended

7.1 Introduction

In Section 6.4, it was shown that the functional dependence of the first order disruption rate constant on the impeller speed differed in relation to the critical impeller speed. In modelling the cell disruption in the slurry reactor, the regions of complete and incomplete solids suspension were thus considered separately. This chapter concerns the modelling of the first order disruption rate constants in terms of the solids volume fraction (Φ) and the impeller speed (N) in the region of complete solids suspension.

Modelling of the cell disruption in the slurry reactor is required to predict cell disruption under particular operating conditions. A number of models have been proposed to describe cell damage and disruption in systems where the solids are completely suspended. These models are presented either in terms of the physical parameters of the system (Reuss 1988, Lilly *et al.* 1992, Pearce 1993) or in terms of the mechanisms of cell damage (Croughan *et al.* 1987, 1988, 1989; Cherry and Papoutsakis 1988, Lakhotia and Papoutsakis 1992). Mechanistic models have the advantage that they allow the significance of the different mechanisms of cell damage and disruption to be elucidated. In this chapter, the physical parameter models and mechanistic models are reviewed and are applied to the cell disruption data generated in this work on agitation with the Rushton turbine. Three new models are then presented which describe the cell disruption with the Rushton turbine. These new models are validated by applying them to the cell disruption data for the pitched-blade turbine and to cell damage in animal cell-microcarrier systems.

7.2 Physical Parameter Models presented in the Literature

Physical parameters with which cell damage and disruption have been modelled include the solids loading, the agitation intensity, the solids particle size and the energy or power input into the system (Reuss 1988, Lilly *et al.* 1992, Pearce 1993). The physical parameter models are reviewed in this section in two categories, using single physical parameters and dimensionless groupings of the physical parameters respectively.

7.2.1 Correlations with the System Parameters

The correlation of the first order disruption rate constant of *Saccharomyces cerevisiae* with the system parameters was investigated by Pearce (1993). As discussed in Section 2.2.3, Pearce studied the disruption of freely suspended *Saccharomyces cerevisiae* agitated with a 6-bladed Rushton turbine in a slurry reactor, which was geometrically similar to the reactor system used in this study. Pearce (1993) investigated the use of mathematical expressions such as the power law function, the logistic function and the logarithmic model to correlate the first order disruption rate constant with the solids volume fraction, impeller speed and solids particle size.

The power law expression, represented by Equation 2.1, described the dependence of the first order disruption rate constant (k) on the solids volume fraction (Φ) over the range of 0.00 to 0.40 at a constant impeller speed of 772 rpm (impeller tip speed of 2.2 m s^{-1}) and a geometric mean particle diameter of 1245 μm (Pearce 1993). The correlation coefficient (R^2) of this expression was 0.999. The exponent of Φ in Equation 2.1 is close to 2 which suggests the importance of solid-cell-solid collisions (c Φ^2) as a cell disruption mechanism in the slurry reactor (Abrahamson 1975).

$$k = 0.0198\,\Phi^{2.33} \qquad \textbf{Equation 2.1}$$

Pearce (1993) evaluated the use of a power law and a logistic expression to model the dependence of k on the agitation intensity (N) over the range of 150 to 1090 rpm (impeller tip speeds of 0.4 to 3.1 m s^{-1}). This impeller speed range straddles the critical impeller speed of 685 rpm. A constant volume fraction of 0.20 of silica particles with a geometric mean particle diameter of 1245 μm was used. The data was described by the logistic and power law expressions in Equations 7.1 and 2.2 respectively with respective correlation coefficients of 0.923 and 0.953. Both expressions describe the disruption rate constants well at low impeller speeds and provide poor fits to the data at speeds greater than the estimated critical impeller speed. This highlights the need to model separately the cell disruption in the regions of complete and incomplete solids suspension.

$$\ell n\left(\frac{k}{k_{max}-k}\right) = 0.0061N - 3.6135 \qquad \textbf{Equation 7.1}$$

$$k = 1.278x10^{-9}\ N^{1.906} \qquad \textbf{Equation 2.2}$$

Correlation of the first order disruption rate constant (k) with the diameter (d_p) of the inert solid particles was also investigated by Pearce (1993). The geometric mean diameter of the silica particles was varied between 114 and 1245 μm at 20% solids (v/v) and an impeller speed of 772 rpm. The applicability of a logarithmic and a logistic equation to this disruption data was examined (Equations 7.2 and 7.3 respectively). Respective correlation coefficients of 0.945 and 0.852 were obtained, indicating satisfactory fits to the experimental data.

$$k = -0.00117 + 2.46x10^{-4}\,\ell n\left(d_p\right) \qquad \textbf{Equation 7.2}$$

$$\ell n\left(\frac{k}{k_{max} - k}\right) = 0.0061 d_p - 2.011 \qquad \textbf{Equation 7.3}$$

Pearce (1993) further considered correlation between the disruption rate constant and the impeller power input, and correlation between the extent of cell disruption (R/R_M) and the energy input. These relationships are represented in Figures 7.1 and 7.2. Although a general increase in the cell disruption rate and extent with power and energy input respectively were observed, the exact mathematical form of these relationships was not ascertained.

In addition to the work of Pearce (1993), changes in the relative metabolic activity and integrity of plant, insect and animal cells have been related to the total energy dissipation per unit volume by Dunlop and Namdev (1993). However, since the maximum energy dissipation rate per unit fluid mass in a stirred tank occurs in the impeller discharge zone and is between 5 and 30 times the average energy dissipation rate per unit fluid mass (Okamoto *et al.* 1981, Costes and Couderc 1988, Zhang and Thomas 1993), the majority of cell damage and disruption occurs in the impeller region. Reuss (1988) therefore only considered the impeller region and correlated the first order disruption rate constant of a solid-free suspension of *Tetrahymena pyriformis* and the extent of disruption (R/R_M) of *Saccharomyces cerevisiae* in a bead mill with the energy input per pass through the impeller zone per unit volume of the vessel ($P\ t_c/V$). The correlation applied, irrespective of the geometric configuration of the system. The form of this relationship was the same as that observed by Pearce (1993) (Figure 7.2). Lilly *et al.* (1992) successfully correlated the penicillin production rate and the mean main hyphal length of *Penicillium chrysogenum*, during the penicillin production phase, with a term accounting for the power dissipation in the impeller region (P/D^3) and the frequency with which the mycelia passed through this zone of high shear ($1/t_c$).

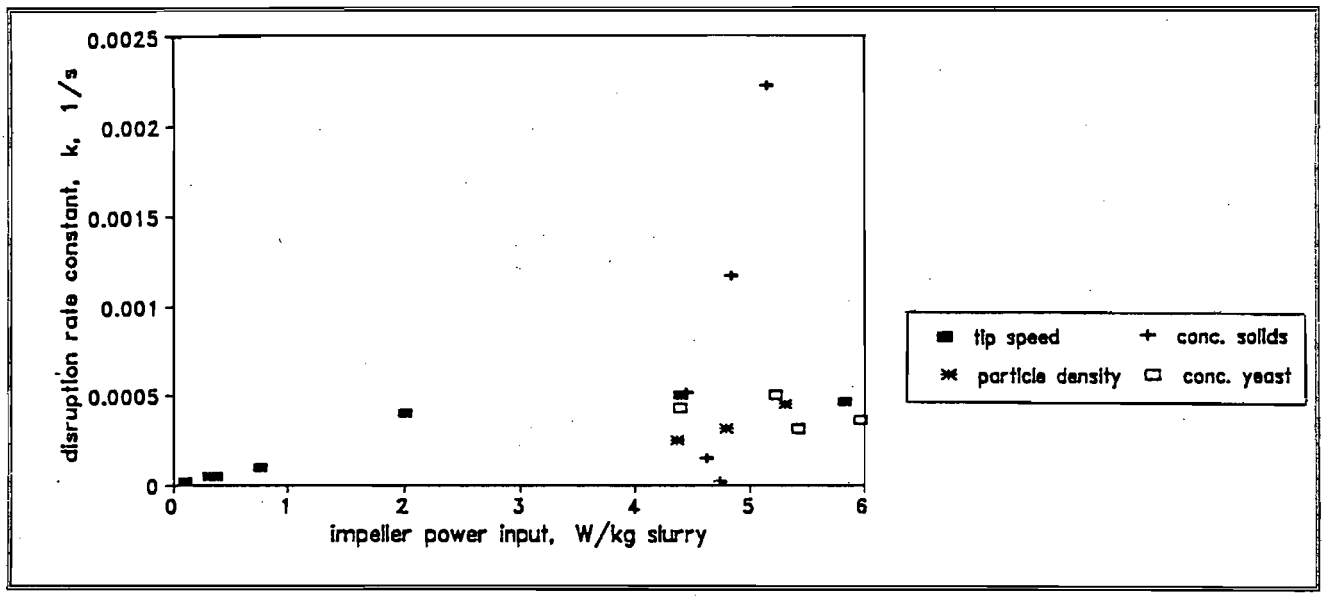

Figure 7.1 **The relationship between the disruption rate constant of *S.cerevisiae* and the impeller power input per unit mass of slurry (Pearce 1993).**

Impeller speed, solids concentration, solids density and biomass concentration were varied in the ranges 150 to 1090 rpm (impeller tip speeds of 0.42 to 3.08 m s^{-1}), 0.05 to 0.40, 1600 to 4500 kg m^{-3}, and 20 to 130 kg m^{-3} respectively.

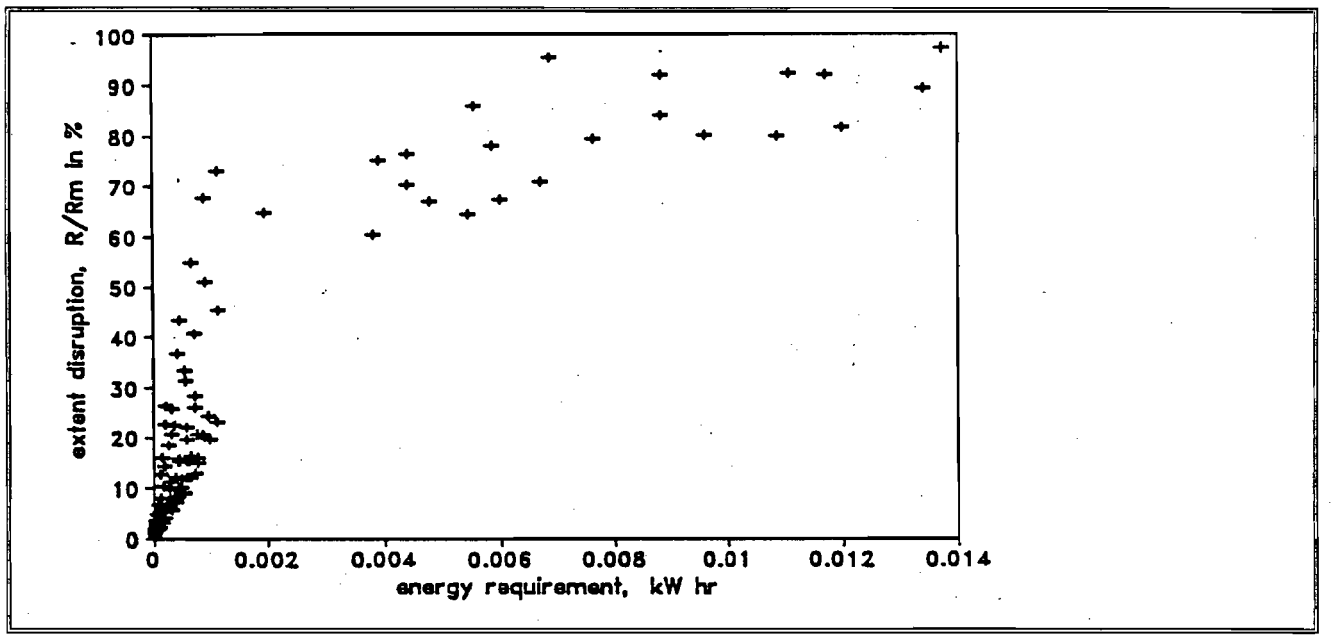

Figure 7.2 **The relationship between the extent of disruption of *S.cerevisiae* and the energy requirement for disruption (Pearce 1993).**

The applicability of the above models to the first order disruption rate constants (k) obtained in this study was investigated. As discussed in Section 6.3, a power law expression (Equation 6.9), with a correlation coefficient of 0.992, was fitted to the disruption experiments performed over the solids volume fraction range of 0.00 to 0.40 at a constant impeller speed of 750 rpm:

$$k = 0.0202\ \Phi^{1.92} \qquad \textbf{Equation 6.9}$$

As with Equation 2.1 (Pearce 1993), the exponent of Φ in Equation 6.9 is close to 2, highlighting the importance of solid-cell-solid collisions in the cell disruption mechanism (Abrahamson 1975). This expression, however, does not account for any variation in agitation intensity.

A power law expression, of the form of Equation 7.4, was used to model the relationship between the first order disruption rate constants obtained in this study and the agitation intensity at impeller speeds above the critical impeller speed. Data from the disruption experiments performed at a constant solids concentration of 10% or 20% (v/v) were used (Section 6.4). Table 7.1 shows that a power law expression describes the k values at constant solids concentrations well. As expected, it provides a poor description when all the data is regressed together since it does not account for variations in the solids concentration. It is thus clear that both impeller speed and solids concentration need to be accounted for in modelling the cell disruption.

$$k = A\,N^{b} \qquad \textbf{Equation 7.4}$$

Table 7.1. Constants and correlation coefficients of power law expression (Equation 7.4) applied to k values from agitation intensity experiments

Data Set	A	b	R^2
10 % Data	2.65×10^{-8}	1.36	0.990
20 % Data	1.09×10^{-7}	1.34	0.999
10 % and 20 % Data	3.95×10^{-9}	1.76	0.337

Hence an expression of the form of Equation 7.5 was applied to the data obtained at 10% and 20% solids (v/v). The exponent of Φ was obtained from Equation 6.9.

$$k = A\,N^{b}\Phi^{1.92} \qquad \textbf{Equation 7.5}$$

Using the cell disruption data at agitation intensities greater than the critical impeller speed, values of 2.77×10^{-6} and 1.32 for A and b respectively were found by minimising the sum of the squares of the difference between the experimental and the predicted values (Appendix H). Equation 7.5 describes the cell disruption data with a coefficient of variance (Equation 4.6) of 6.1%. The close agreement between the predicted and measured disruption rate constants is further seen in the parity chart in Figure 7.3. However, the exponent over Φ in Equation 7.5 strictly applies at a constant impeller speed of 750 rpm. In Section 7.4.1, Equation 7.5 is extended to apply to the range of impeller speeds and solids concentrations used in the fully suspended solids regime of this work.

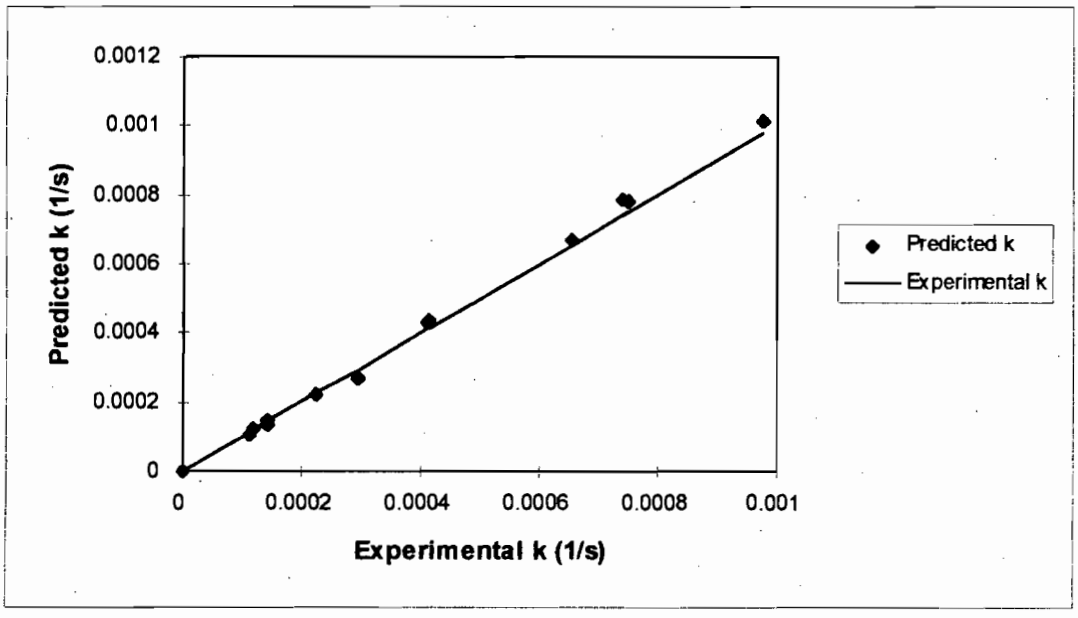

Figure 7.3. **Parity chart comparing predictions of k from Equation 7.5 and experimental k values** The solid line represents perfect correlation between the model and the data.

To regress the first order disruption rate constants from the agitation intensity experiments (Section 6.4) with the parameter of Reuss (1988), $P\ t_c/V$, the circulation time, t_c, was estimated from Reed *et al.* (1977). For a 6-bladed Rushton turbine in a fully baffled, cylindrical vessel:

$$t_c = V / Q = V / (0.75\ N\ D^3) \qquad \textbf{Equation 7.6}$$

Figure 7.4 shows the correlation of the first order disruption rate constants, measured above the critical impeller speed, with the parameter of Reuss (1988). Although an increase in k was observed with $P\ t_c/V$,

two distinct lines were obtained: one for the 0.10 volume fraction data and one for the 0.20 volume fraction data. This was attributed to the solids concentration not being accounted for in the expression of Reuss (1988). The parameter of Reuss was thus altered to account for the effect of solids concentration and the k values were correlated with the resultant expression, $Pt_c\Phi^{1.92}$ / V. A single curve was obtained for both the 0.10 and 0.20 volume fraction data. Using a Least Squares analysis (Appendix H), the relationship, represented in Equation 7.7, was established between k and $Pt_c\Phi^{1.92}$ / V with a coefficient of variance of 9.9%. The relatively good agreement between the predicted and measured k values is shown in Figure 7.5.

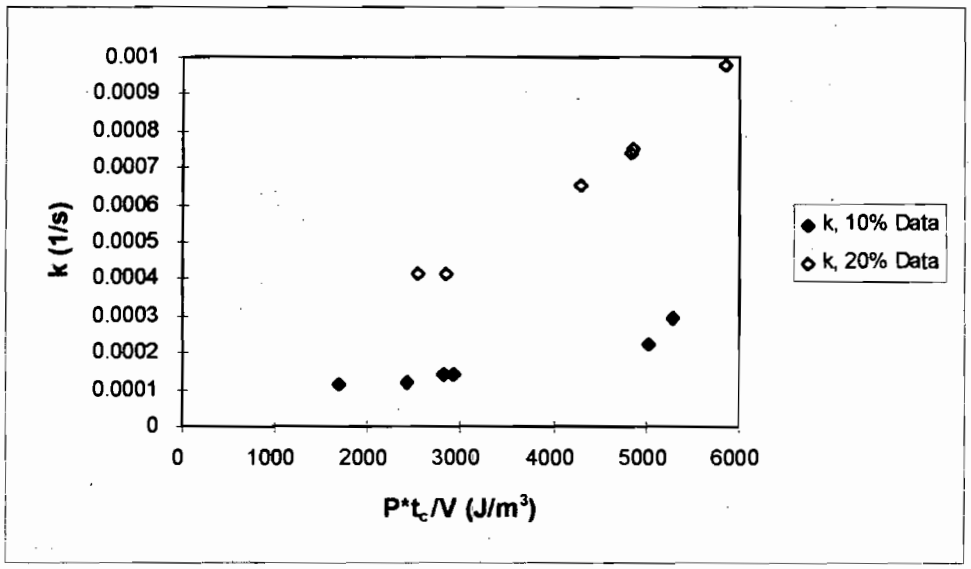

Figure 7.4. **Correlation of k with the parameter of Reuss (1988), P t_c/ V.**

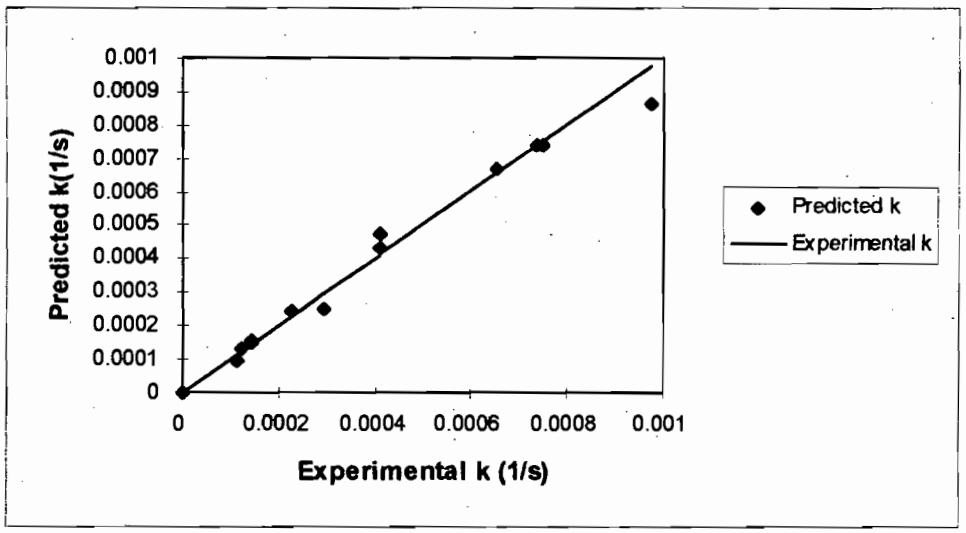

Figure 7.5. **Parity chart comparing predictions of k from Equation 7.7 and experimental k values.**

$$k = 8.54 x 10^{-6} \left(\frac{P t_c \Phi^{1.92}}{V} \right)^{0.83}$$

Equation 7.7

Based on the work of Lilly *et al.* (1992), the term, $P/(D^3 t_c)$, was used to correlate the first order disruption rate constants obtained in this work at speeds greater than the critical impeller speed (Figure 7.6). The separate curves obtained for the k values at 10% and 20% solids (v/v) suggested that the effect of the solids volume fraction on cell disruption ($\Phi^{1.92}$) needed to be accounted for in the parameter, $P/(D^3 t_c)$. Figure 7.7 shows the relationship between the k values and $P\Phi^{1.92}/(D^3 t_c)$. Separate curves are obtained for the 0.10 and 0.20 volume fraction data, although the curves lie closer together than in the correlation of k with $P/(D^3 t_c)$. Correlation of the first order disruption rate constants in this study with the rate of power dissipation in the impeller region ($P/(D^3 t_c)$) is thus not successful, even when accounting for the effect of solids concentration ($\Phi^{1.92}$) on the cell disruption.

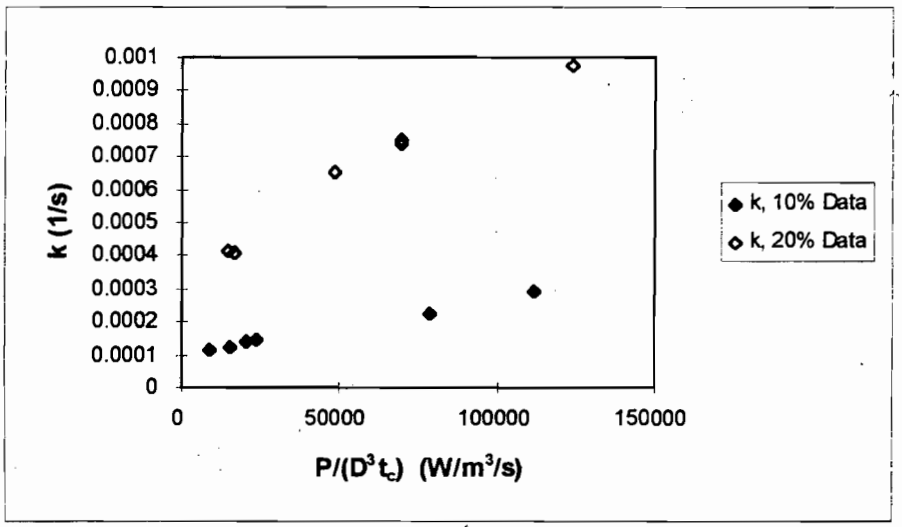

Figure 7.6. Correlation of k with the parameter of Lilly *et al.* (1992), $P/(D^3 t_c)$

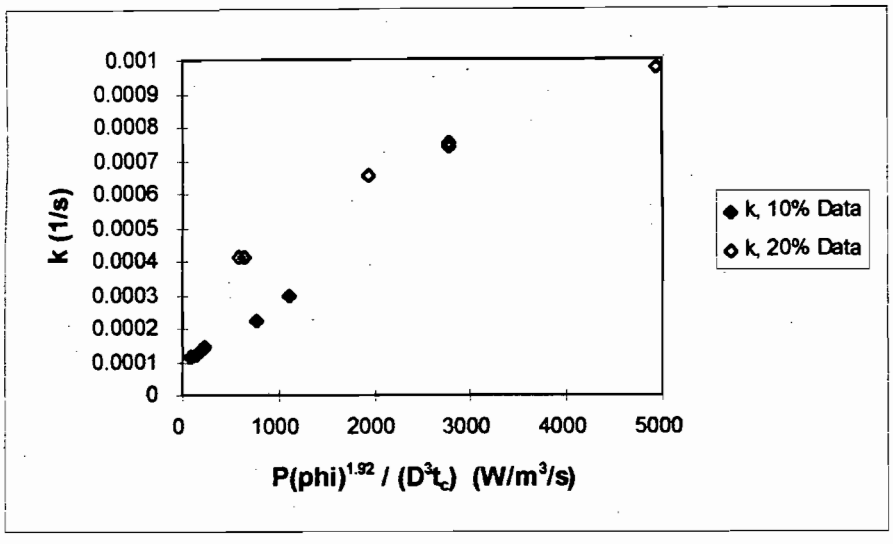

Figure 7.7. **Correlation of k with the modified parameter of Lilly *et al.* (1992), $P\Phi^{1.92}/(D^3 t_c)$**

7.2.2. Correlations with Dimensionless Groupings of the System Parameters

The second category of physical parameter models involves the correlation of the cell damage or disruption with dimensionless groupings of the physical parameters. The correlation of the first order disruption rate constant (k) with the impeller Reynolds number (N_{RE}) and the power number (N_p) was investigated by Pearce (1993), studying the disruption of *Saccharomyces cerevisiae* in a slurry reactor. The relationship between the first order disruption rate constant and the impeller Reynolds number at a solids volume fraction of 0.20 is shown in Figure 7.8, for varying agitation intensity (straddling the critical impeller speed), solid particle density and biomass concentration. The solid line in Figure 7.8 represents the linear expression (Equation 7.8), fitted to the data of Pearce (1993) by a Least Squares analysis. A correlation coefficient of 0.659 was obtained, indicating that the linear expression provides a relatively poor description of the relationship between k and the impeller Reynolds number (N_{RE}) over the widely varying conditions.

$$k = 1.92 \times 10^{-9} N_{RE} + 6.12 \times 10^{-5} \qquad \textbf{Equation 7.8}$$

Figure 7.9 shows the relationship observed by Pearce (1993) between the first order disruption rate constants and the power number. No trend was observed in the k values on variation of the power number over the widely varying conditions.

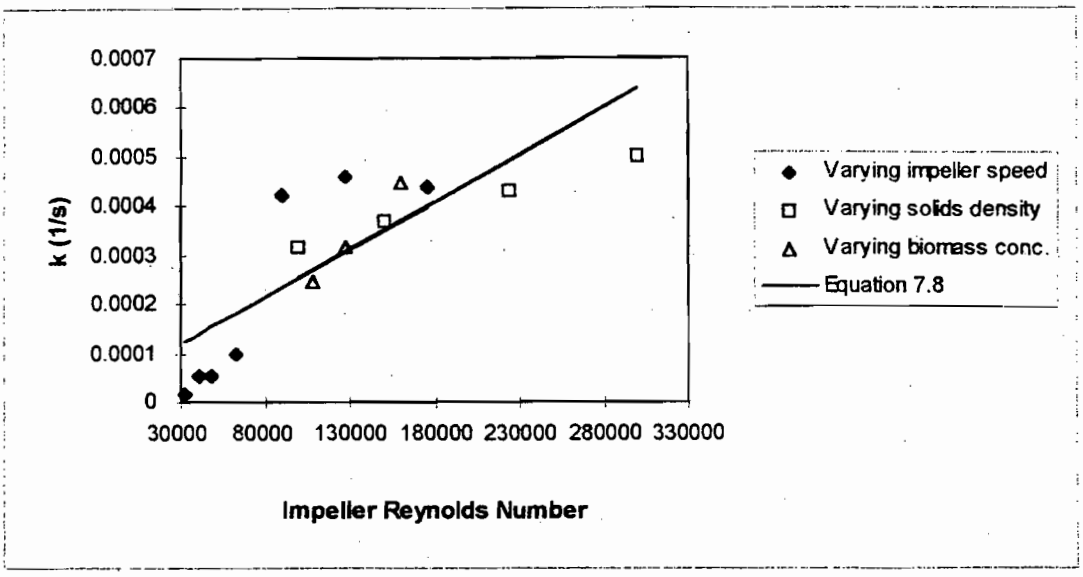

Figure 7.8. **Relationship between the disruption rate constant of *S.cerevisiae* and the impeller Reynolds number (Pearce 1993).**

Solids volume fraction = 20%. Impeller speed, solids density and biomass concentration were varied in the ranges 150 to 1090 rpm (impeller tip speeds of 0.42 to 3.08 m s^{-1}), 1600 to 4500 kg m^{-3}, and 20 to 130 kg m^{-3} respectively.

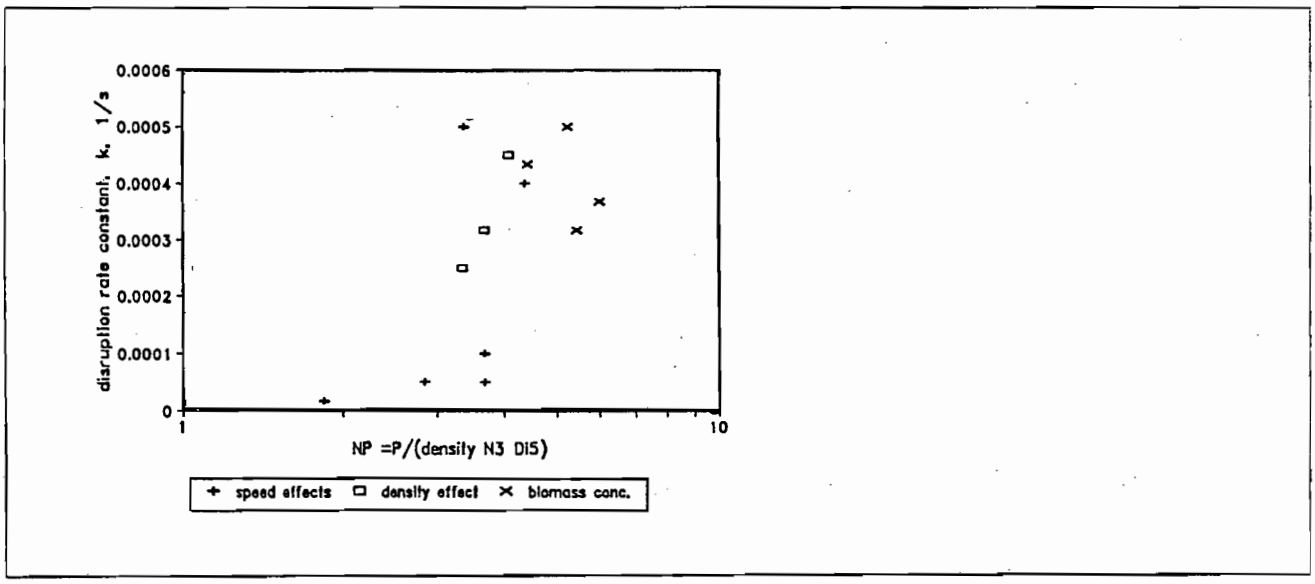

Figure 7.9. **Relationship between the disruption rate constant of *S.cerevisiae* and the power number (Pearce 1993).**

Solids volume fraction = 20%. Legends indicate the parameter that was varied in each set of disruption experiments.

disruption experiments above the critical impeller speed at constant solids density and biomass concentration, as discussed previously.

$$k = -1.0 \times 10^{-4} N_P + 6.0 \times 10^{-4} \quad \textbf{Equation 7.11}$$

$$k = -2.3 \times 10^{-4} N_P + 1.7 \times 10^{-3} \quad \textbf{Equation 7.12}$$

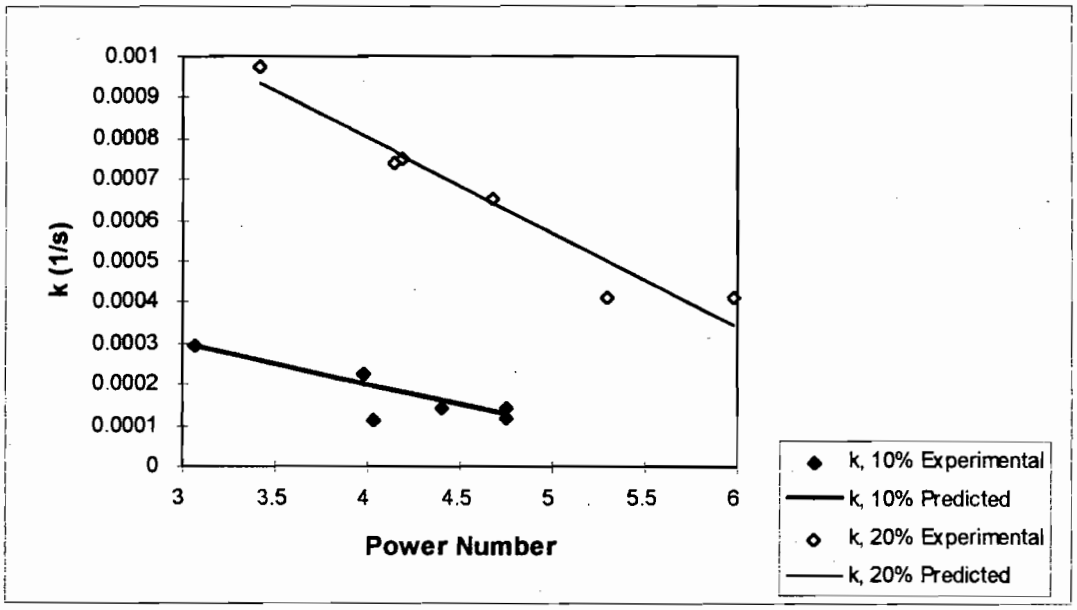

Figure 7.11 **Relationship between the disruption rate constant of *S.cerevisiae* and the power number.**

Solid lines represent Equation 7.11 (10% solids (v/v) data) and Equation 7.12 (20% solids (v/v) data).

Correlation of the k values with the impeller Reynolds number and the power number does not account for the effect of solids concentration on cell disruption, illustrated by separate curves for the 0.10 and 0.20 volume fraction data in Figures 7.10 and 7.11. To account for the effect of solids concentration, the term, $\Phi^{1.92}$, was included in the correlation parameters (Section 7.2.1). Correlation of k with $N_{RE}\ \Phi^{1.92}$ yielded a single curve. Using a Least Squares analysis, the relationship represented by Equation 7.13 was established between k and $N_{RE}\ \Phi^{1.92}$ with a coefficient of variance of 10.3%. The good agreement between the experimental and predicted disruption rate constants can be seen in Figure 7.12.

$$k = 5.65 \times 10^{-7} (N_{RE}\ \Phi^{1.92})^{0.96} \quad \textbf{Equation 7.13}$$

$$= 5.65 \times 10^{-7} (N\ D^2\ \rho\ \Phi^{1.92} / \mu)^{0.96}$$

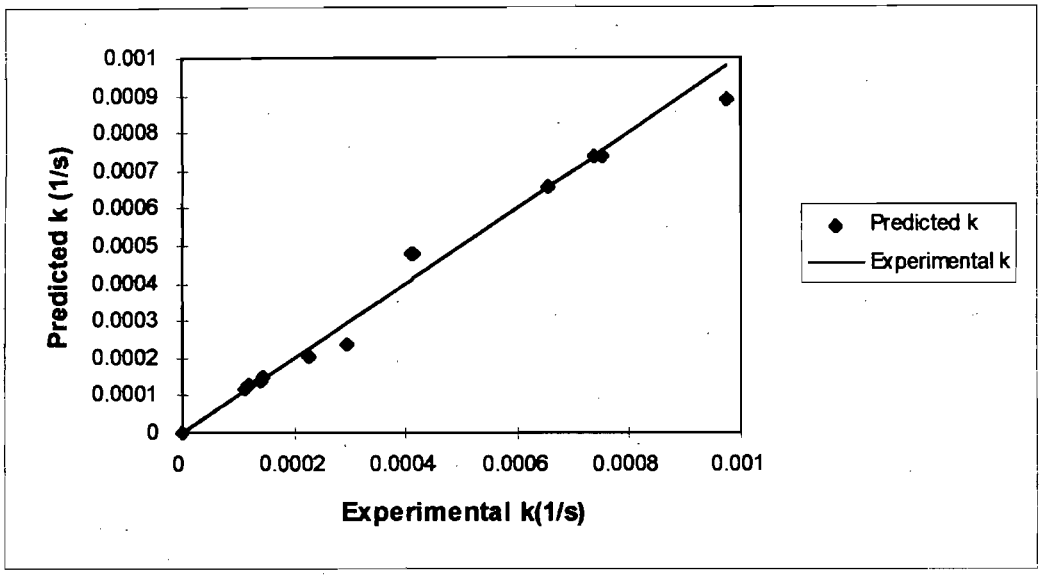

Figure 7.12. **Parity chart comparing predictions of k from Equation 7.13 and experimental k values.**

The correlation of k with $N_P\Phi^{1.92}$ can be seen in Figure 7.13. Despite the use of the $\Phi^{1.92}$ term in the correlation parameter, $N_P\Phi^{1.92}$, separate curves were obtained for the 0.10 and 0.20 volume fraction data. The power number is thus not a suitable correlation parameter for the cell disruption observed in the slurry reactor.

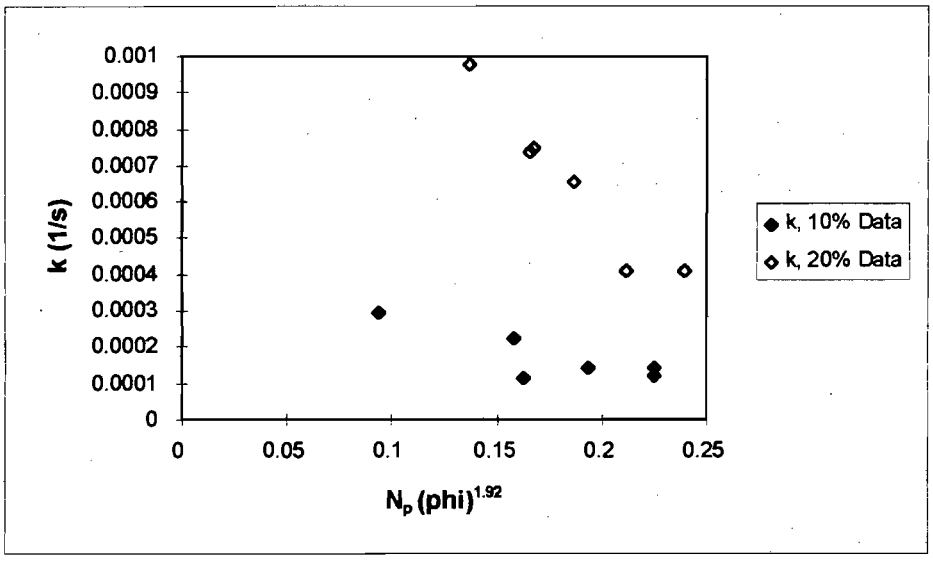

Figure 7.13. **Correlation of k with $N_P\ \Phi^{1.92}$**

7.2.3 Conclusions drawn from Physical Parameter Models

In Section 7.2, it has been shown that the existing physical parameter models are generally simplistic and inadequate in their description of the first order disruption rate constants (k) in this work, since they do not account for the effect of both the solids concentration and the agitation intensity on the cell disruption. It was found that the term, $\Phi^{1.92}$, accounted for the effect of solids concentration on k, suggesting that solid-cell-solid collisions are important in the cell disruption mechanism in the slurry reactor (Hinze 1971, Abrahamson 1975). Physical parameter models that were modified to include the term, $\Phi^{1.92}$, and that included either the impeller speed (Equation 7.5, Equation 7.13: $N_{RE} = N D^2 \rho/\mu$) or the energy input per unit volume (Equation 7.7), described the first order disruption rate constants well. The first order disruption rate constants could not be correlated with the rate of power input per unit volume (Figure 7.7) or the power number (Figure 7.13), even on inclusion of the term, $\Phi^{1.92}$, in the correlation.

7.3 Mechanistic Models presented in the Literature

In mechanistic modelling of cell damage or disruption, the potential mechanisms of the damage or disruption are related to measurable operating parameters of the system. The terms of the model have meaning and thus contribute further to the understanding of the system. As discussed in Section 6.3, a number of mechanisms are potentially responsible for the damage to cells in bioreactors: interactions between the cells and fluid eddies, interactions between the cells and solid particles, interactions between the cells and bubbles, and interactions between the cells and the reactor components. Cell damage in animal cell-microcarrier cultures has been related successfully to these mechanisms (Croughan *et al.* 1987, 1988, 1989; Cherry and Papoutsakis 1988). In this section, the mechanistic models developed to describe the damage to animal cell-microcarrier cultures are reviewed and applied to the cell disruption observed in the slurry reactor on agitation with the Rushton turbine.

7.3.1 Interactions between the Cells and Fluid Eddies

Interactions between cells and fluid eddies in the turbulent flow field in bioreactors can result from both time-fluctuating and time-average velocity components. Strong hydrodynamic forces, damaging to cells, can be created if the fluctuating velocity components change rapidly with time or position. Changes in the time-average velocity components over small intervals in position can also give rise to strong shear stresses which damage the cells (Croughan *et al.* 1987). The cell damage from interactions with fluid eddies is reviewed in terms of these time-fluctuating and time-average velocity components.

7.3.1.1 Damage to Cells from Fluctuating Velocity Components

In the turbulent flow field in a bioreactor, short-term hydrodynamic forces arise through the motion of turbulent eddies. The turbulent flow field consists of a range of eddy sizes. These eddy size ranges are shown in the energy spectrum of isotropic turbulent flow in Figure 7.14. Hydrodynamic energy is transferred from large energy-containing eddies, generated behind the impeller blades in a stirred tank, to eddies gradually decreasing in size and energy content. At sufficiently high Reynolds numbers, there is a range of small eddies that is completely independent of external conditions and is determined only by the amount of energy input into the system and the viscous dissipation. This range of eddies is termed the universal equilibrium range. Viscous effects in these eddies become strong when the eddy Reynolds number ($N_{RE,eddy}$) becomes less than unity. The eddy size at which the $N_{RE,eddy}$ is unity is termed the Kolmogorov microscale (Kolmogorov 1941, Hinze 1975). The size and velocity of this microscale were defined in a model proposed by Kolmogorov (1941):

Length of Kolmogorov microscale $= \eta$

$$= \left(\frac{\nu^3}{\varepsilon}\right)^{0.25} \qquad \textbf{Equation 7.14}$$

Velocity of Kolmogorov microscale $= v$

$$= (\varepsilon \nu)^{0.25} \qquad \textbf{Equation 7.15}$$

where: ε = turbulent power dissipation per mass of liquid (W / kg)

ν = kinematic viscosity of the medium (m^2 / s)

Eddies smaller than the Kolmogorov microscale belong in the viscous dissipation subrange, where the kinetic energy of the fluid is dissipated as heat. Eddies larger than the Kolmogorov microscale, but still belonging to the universal equilibrium range, are termed the inertial convection subrange. The nomenclature of these subranges is in accordance with the predominating forces (van Suijdam and Metz 1981, Kawase and Moo-Young 1990).

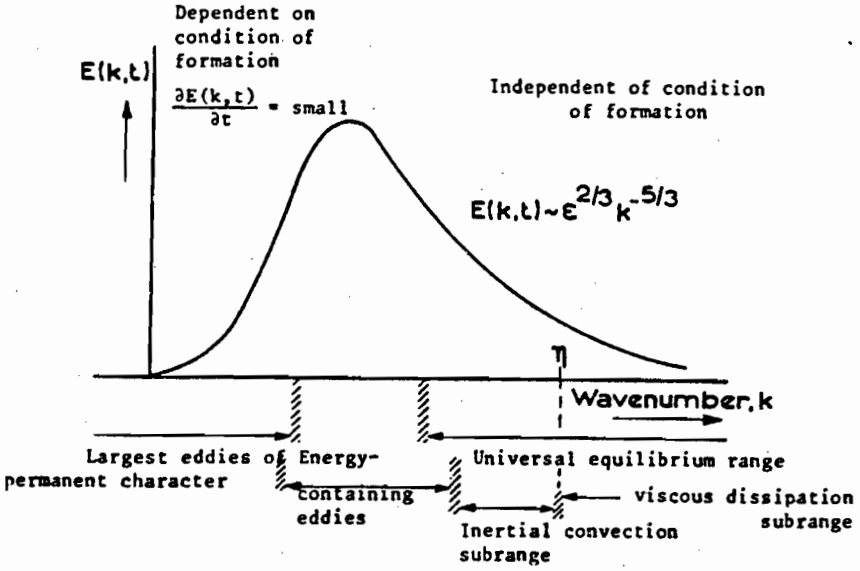

Figure 7.14. **Energy spectrum of isotropic turbulent flow, showing the eddy size ranges (van Suijdam and Metz 1981).**

E(k,t) denotes the energy of the eddies as a function of the time (t) and the wavenumber (k). The size of the eddies is inversely proportional to the wavenumber. ε denotes the turbulent power dissipation per mass of liquid (W / kg).

The size of the fluid eddies is of significance to cell damage. Eddies larger than suspended cells or solids, to which cells are attached, tend to entrain the cells or the solids, rotating and translating them in a manner that reduces the net forces on their surface. Eddies smaller than the suspended cells or the solids are dissipated on the surface of the suspended or immobilised cells, and are thus more likely to damage the individual cells (Croughan *et al.* 1987, Jobses *et al.* 1991).

Experimental data on the damage to immobilised animal cells can be analysed by comparing the microcarrier size to the Kolmogorov eddy length (Papoutsakis 1991). However, this analysis is valid only if certain conditions apply. The first condition is that the eddies exist in a state of isotropic, statistical equilibrium. Although the energy-containing eddies and the overall turbulence in a stirred tank is anisotropic and nonhomogeneous, at high bulk Reynolds numbers, the terminal eddies at the Kolmogorov scale can be considered isotropic at the local level (Kawase and Moo-Young 1990). This first condition is thus met for the Kolmogorov eddies if the bulk Reynolds number is large and the eddies in the viscous dissipation regime are much smaller than the energy-containing eddies. In typical animal cell-microcarrier

cultures, the eddies in the viscous dissipation regime are over an order of magnitude smaller than the energy-containing eddies (Croughan *et al.* 1987). The Kolmogorov eddy size and velocity estimations also assume that there is no disturbance of the small scale turbulence structure by the particles. This is questionable if the beads are much larger and more massive than the smallest turbulence (Cherry and Papoutsakis 1988). The microcarriers used in animal cell cultures are neutrally buoyant and are of a comparable size to the Kolmogorov eddy length (Croughan *et al.* 1987). The conditions for application of the Kolmogorov theory are thus met in animal cell-microcarrier cultures.

Damage to immobilised animal cells, in terms of the specific cell death rate, the relative specific growth rate, the relative growth extent of the cells and the maximum attached cell concentration, has been successfully correlated with the Kolmogorov eddy length (Sinskey *et al.* 1981, Hu 1983, Croughan *et al.* 1989). In the cases where this correlation has been applied, the concentration of microcarriers was low, typically in the range of 0.02 to 0.29 % (v/v) (Croughan *et al.* 1987, 1989). At these conditions, interactions between the cells and fluid eddies predominate as the damage mechanism. As an example of this correlation, the relative growth extent of FS-4 cells immobilised on microcarriers is shown as a function of the Kolmogorov eddy length scale in Figure 7.15 (Croughan *et al.* 1987). Figure 7.15 shows that damage to cells from interactions with fluid eddies occurs at a Kolmogorov length scale below 130 μm, approximately 70% of the average microcarrier diameter of 185 μm. This substantiates the theory that only eddies smaller than the microcarrier diameter are damaging to the individual cells (Croughan *et al.* 1987). The correlation appears to apply, regardless of the system geometry.

Croughan *et al.* (1987) consequently developed the following model:

$$q = k_1\left(\frac{1}{\eta}\right)^a \qquad \textbf{Equation 7.16}$$

$$= k_1\left(\left(\frac{\varepsilon}{\nu^3}\right)^{0.25}\right)^a$$

where: q = cell death rate (hr^{-1})

k_1 = constant ($m^3\ hr^{-1}$)

This equation only applies to turbulent eddies smaller than a critical size. Croughan *et al.* (1987) found a value of *a* of approximately 3 for attached FS-4 cells which had been damaged as a result of interactions

between the cells and fluid eddies. The exponent of 3 for the inverse of the Kolmogorov eddy length in Equation 7.16 implies that the cell death rates are proportional to the eddy concentration. Vessel geometry did not appear to have a strong effect on the value of k_1.

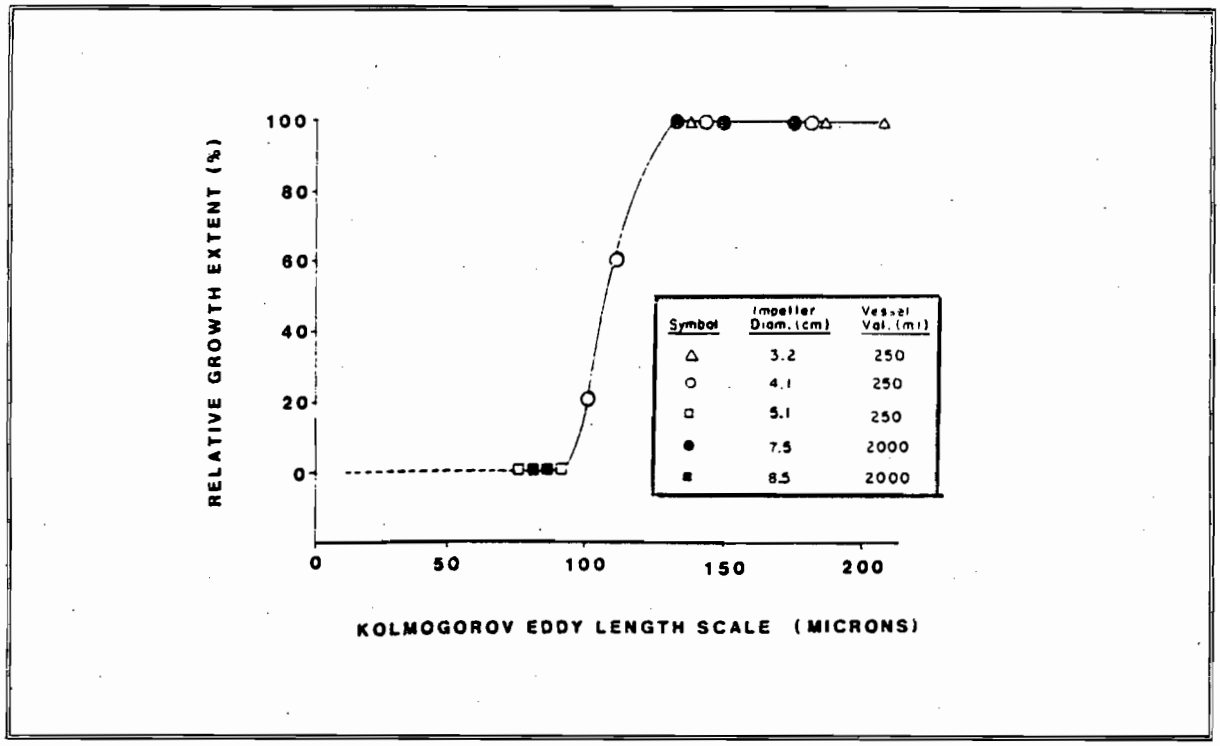

Figure 7.15 **Relative growth extent of FS-4 cells on microcarriers as a function of the Kolmogorov eddy length scale, calculated from the data of Hu (1983) (Croughan *et al.* 1987).**

Damage to cultures of freely suspended animal cells under typical bioreactor conditions in the absence of solid particles appears to be negligible. The unattached cells of 10-15 μm are considerably smaller than the Kolmogorov microscale of turbulence. They are consequently entrained by the turbulent eddies and exist within an environment characterised as laminar shear (Kunas and Papoutsakis 1990, Cherry and Kwon 1990).

The impeller Reynolds numbers at the critical impeller speeds at 10% and 20% solids (v/v) were calculated as 17 294 and 13 620 respectively. Since these impeller Reynolds numbers are greater than 10 000, the disruption experiments performed at speeds above the critical impeller speed in this study were in the turbulent regime (Rushton *et al.* 1950). Correlation of the disruption of the *Saccharomyces cerevisiae* in the slurry reactor with the Kolmogorov length scale, as defined by Equation 7.14, is not valid at the conditions used in this work (solid particle diameter of 600 to 850 μm, solid particle density of 2664 kgm^{-3},

solids concentration of 5 to 40% (v/v)) since at these conditions, the particles modify the fluid turbulence structure.

The effect of solid particles on fluid turbulence has been rigorously reviewed by Caulet *et al.* (1996). They point out that below a solids volume fraction of 2%, the effect of solid particles on the fluid turbulence structure is negligible. At solids concentrations between 2% and 10% (v/v), the particles create small-scale turbulence owing to the wakes induced by their relative velocity in the fluid. This increase in the fluid turbulence at high wave numbers is accompanied by an increase in the viscous dissipation rate of the turbulent energy and an increase in the rate of energy transfer by fluid-fluid interactions from the large-scale eddies. The presence of particles in the turbulent flow field thus revises the energy cascade process (Figure 7.14) and results in a reduction in the Kolmogorov eddy size. Gore and Crowe (1989) observed this enhancement of the fluid turbulent energy in pipe and jet flows only when the ratio of the particle diameter to the length of the energy-containing eddies was greater than 0.1. Hetsroni (1989) defined a particle Reynolds number of 400 as the lower limit for the increase in turbulence in pipe and jet flows on the addition of solid particles. Elghobashi and Truesdell (1993) contested the importance of these characteristic parameters since their simulation of a decaying homogeneous isotropic turbulence showed that even particles smaller than the Kolmogorov microscale augmented the turbulence energy at high wave numbers.

At solids volume fractions greater than 20 to 30%, the mechanism controlling the flow in solid-liquid systems changes from that of fluid-particle interactions to particle-particle interactions (Caulet *et al.* 1996, Crowe *et al.* 1996). As a result, viscous effects dominate the flow and the effect of the particles on the turbulent structure differs from that discussed in the preceding paragraph. The increase in the apparent viscosity of the suspension at high solids concentrations decreases the particle response time, with the result that the particles are better able to follow the fluid motions. This decrease in the particle relative velocity reduces the formation of the small-scale turbulent eddies. As a result and since the kinetic energy is primarily dissipated into heat in highly loaded suspensions, there is a reduction in the energy transfer in the energy cascade, and the Kolmogorov eddies are of a larger scale than those predicted by Equation 7.14.

Nouri *et al.* (1987) measured the mean and fluctuating velocities of particles in a descending solid-liquid turbulent flow in a vertical pipe. They used acrylic particles with a diameter of 270 μm at solids volume fractions of 0.1 to 14%. The ratio of the particle density to the fluid density was 1.32. Nouri *et al.* found that increasing the solids concentration resulted in the overall changes of the mean flow being reduced by the inertia of the particles. A flattening of the mean velocity profiles was observed at increased solids concentrations and the size of the recirculation zone, downstream of an axisymmetric baffle in the pipe, was

reduced by 24% at 8% solids (v/v). The fluctuating velocities of the particles were reduced to 35 to 90% of the fluctuations of single phase flow in the baffled pipe at solids concentrations of 3 to 8%. The study of Nouri *et al.* (1987) shows that although the turbulence is reduced at a solids concentration of 10%, the small-scale motions of the particles are still significant. A solids volume fraction of 10% can thus reasonably be considered to be in the transition zone between the regimes where fluid-particle and particle-particle interactions dominate the flow (Caulet *et al.* 1996).

The majority of the cell disruption experiments in this work were performed at solids concentrations of 10% and 20% (v/v). These experiments are thus in the transition regime, with viscous effects being significant for the experiments performed at 20% solids. It is thus anticipated that the Kolmogorov eddy length, at the conditions in this study, will be of the order of the value predicted by Equation 7.14 at 10% solids, and larger than the value predicted by Equation 7.14 at 20% solids. As a lower bound of the length of the Kolmogorov eddies in this study, Equation 7.14 was applied to the disruption experiment operated at the highest impeller speed (N = 904.2 rpm). This yielded a Kolmogorov eddy length of 28.8 μm. Since the true Kolmogorov length scale at 904.2 rpm will be of the order of or larger than 28.8 μm, and since this value is larger than the average yeast cell size of 5.1 μm (Section 4.1.2.1), the yeast cells will be entrained by the turbulent eddies in the slurry reactor. Kolmogorov eddies are thus not a cause of cell disruption in the slurry reactor.

7.3.1.2 Damage to Cells from Time-Averaged Velocity Components

Evaluation of the effect of time-averaged velocity components on cell damage involves determining the position-dependent time-averaged flow profile around the cells and solid particles as they circulate through various time-averaged velocity fields in the stirred tank. This approach is a difficult fluid-mechanical problem and as a result, the role of average and maximum time-averaged shear rates on the cell damage has been considered at various locations in a stirred reactor (Hu 1983; Croughan *et al.* 1987, 1989). These shear rates are given by the spatial derivatives of the time-averaged velocity components.

In liquid systems, shear forces are determined by the impeller flow pattern, the agitation intensity and the position in the stirred tank (Croughan *et al.* 1989, Hackl *et al.* 1989, Gormely and Branion 1989, Prokop and Bajpai 1992). Since the maximum energy dissipation rate per unit fluid mass in a stirred tank occurs in the impeller discharge zone, the greatest shear stresses and consequently the majority of cell damage and disruption from shear forces are expected to occur in this region. Expressions for the average and maximum time-averaged shear rates and shear stresses, at various locations in a stirred tank, are summarised

in Table 7.2 for liquid systems where no solid particles are present. In animal cell cultures, the microcarrier diameter is typically of the order of the Kolmogorov eddy length and the microcarriers are neutrally buoyant. As a result, the microcarriers primarily follow the fluid streamlines (Kuboi *et al.* 1974). Since there is no difference between the mean velocities of the microcarriers and the bulk fluid, the microcarriers do not alter the single-phase fluid shear rates (Caulet *et al.* 1996). Application of the expressions summarised in Table 7.2 to the cell damage in animal cell-microcarrier systems is thus valid.

Hu (1983) and Croughan *et al.* (1987, 1989) have investigated the significance of the maximum time-averaged shear rate in the bulk flow (Equation 7.17) on the damage to FS-4 cells immobilised on microcarriers. Both these workers found that damage to animal cells on microcarriers does not correlate with this parameter. Correlation of the cell damage with the maximum time-averaged shear rate or impeller tip speed does not account for the system geometry, with the result that maximum cell growth or zero cell growth can be observed at the same impeller tip speed (Hu 1983). The work of Reuss (1988) and Cherry and Kwon (1990) supports this finding.

The effect of the average time-averaged shear rate in the bulk flow (Equation 7.18) on the damage to immobilised FS-4 cells was investigated by Croughan *et al.* (1987). The relative growth extent of immobilised FS-4 cells could be correlated with this parameter (Figure 7.16). For the FS-4 cells, the growth declines sharply at approximately 3 inverse seconds. Time-averaged shear stresses are only significant as a cause of cell damage in animal cell-microcarrier systems if the viscosity of the medium is greatly increased and if strong time-averaged shear rates are generated, for example if there is a small clearance between the impeller and a stationary vessel component (Croughan *et al.* 1989).

The shear rate expressions for a stirred tank, presented in Table 7.2, cannot be applied to the cell disruption observed in this study. The large density (2664 kg m^{-3}) and size (600 to 850 μm) of the silica particles result in significant inertial lag and gravitational forces acting on the particles (Kuboi *et al.* 1974). The difference in motion between the particles and fluid eddies increases the effective shear rates in the fluid (Hinze 1971, Caulet *et al.* 1996). Expressions of the time-averaged shear rate, corresponding to the conditions in this study, could not be found in the literature. Hence their effect on the cell disruption in the slurry reactor was not established.

Table 7.2. **Summary of shear rate (γ) and shear stress (τ) expressions of liquids agitated in a stirred tank**

Shear Rate / Shear Stress Expression	Conditions for Application of Expression	Reference	Equation Number
Bulk Flow:			
$\gamma_{max} = K \pi N D$		Nagata (1975) Oldshue (1983)	**7.17**
$\gamma_{ave} = \frac{112.8\, N\, D^{1.8}\, (T^{0.2} - D^{0.2})\, R^{1.8}}{T^2 - D^2}$ $R = N_{RE} / (1000+1.6\, N_{RE})$	Unbaffled vessel $N_{RE}>1000$	Croughan *et al.* (1987)	**7.18**
On Impeller Blades:			
$\gamma_{max} = 3.3N \left(\frac{N D^2}{\nu_z}\right)^{0.5}$ ν_z = zero shear kinematic viscosity	Rushton turbine $100<N_{RE}<29\,000$ for water and 0.5 and 1% polyox solutions	Robertson and Ulbrecht (1986)	**7.19**
$\gamma_{max} = N(1+5.3\beta)^{\frac{1}{\beta}} N_{RE}^{\frac{1}{(1+\beta)}}$ $\beta = 1$ for Newtonian Fluid	Baffled, agitated tank in standard configuration using 6-bladed disc-style turbine. $10<N_{RE}<10^5$	Wichterle *et al.* (1984)	**7.20**
On the Vessel Base and Walls:			
$\tau_{max} = \frac{16(\rho\mu)^{0.5}\, N^{1.5}\, D^3}{T^2}$	Standard 6-bladed Rushton turbine $0.15<D/T<0.57$ $C/T = 0.33$ $250<N_{RE}<2.35 \times 10^4$ Newtonian liquids	Wichterle *et al.* (1985)	**7.21**
$\tau_{max} = \frac{10(\rho\mu)^{0.5}\, N^{1.5}\, D^3}{(D+C)^2}$	Pitched blade turbine (Downward pumping) $0.2<D/T<0.4$ $0.2<C/T<0.4$ $6000<N_{RE}<110\,000$	Wichterle *et al.* (1988)	**7.22**

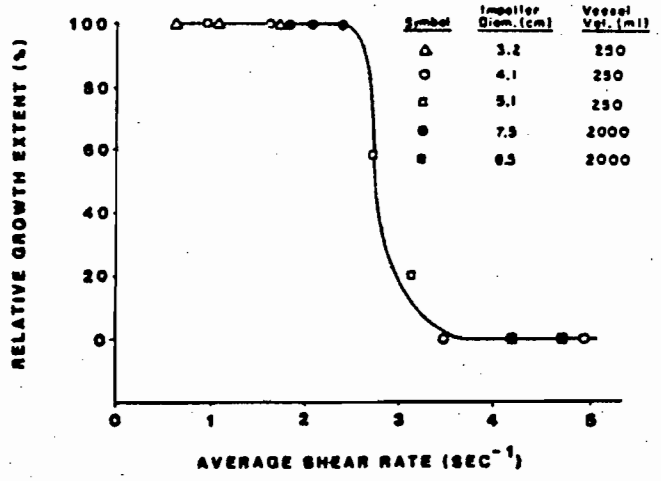

Figure 7.16. **Relative growth extent of FS-4 cells on microcarriers as a function of the average time-averaged shear rate in the bulk flow, calculated from the data of Hu (1983) (Croughan *et al.* 1987).**

7.3.2 Interactions between the Cells and the Solid Particles

The contribution of interactions between the cells and solid particles to cell damage in animal cell-microcarrier cultures has been well-established (Cherry and Kwon 1990, Croughan *et al.* 1989, Cherry and Papoutsakis 1988). Cells are damaged either when the microcarrier particles, on which the cells are immobilised, collide or when the microcarriers pass each other in close proximity (Croughan *et al.* 1988). Croughan *et al.* (1988) used 125 ml spinner vessels to determine that this mechanism is only of significance above solids concentrations of approximately 0.5% (v/v) at relatively high agitation intensities of 150 rpm (impeller tip speed of 0.42 m s^{-1}).

The important parameters that need to be considered in mechanistically modelling the interactions between the cells and solid particles are the frequency and force of the collisions. Quantifying these parameters has proven a difficult fluid-mechanical problem with the result that they have only been estimated in an approximate manner (Papoutsakis 1991). The various mechanistic models that have been proposed to describe damage to animal cells from interactions between the cells and solid particles are described below.

7.3.2.1 Turbulent Collision Severity

Cherry and Papoutsakis (1988) suggested the use of a factor, called the *Turbulent Collision Severity* (TCS), for correlating the damage to animal cells from interactions between the microcarriers. The TCS was defined as the product of the collision kinetic energy and the collision frequency of the microcarriers. The following approximate expression for the collision frequency of the solid particles per unit volume of suspension was developed by Hinze (1971):

$$\begin{pmatrix} Collision\ frequency\ per \\ unit\ suspension\ volume \end{pmatrix} = O\left(\frac{v_{rel}\Phi^2}{d_p^{\,4}}\right) \qquad \textbf{Equation 7.23}$$

where O signifies "of the order of", v_{rel} is the relative velocity between colliding microcarriers (m s^{-1}), Φ is the microcarrier volume fraction, and d_p is the microcarrier diameter (m). Using this expression for the collision frequency and converting to collisions per bead rather than per volume, Cherry and Papoutsakis (1988) developed the following relationship for the TCS:

$$\text{TCS} = (\text{kinetic energy})\left(\frac{collisions}{(suspension\ volume)(time)}\right)\left(\frac{suspension\ volume}{no.\ of\ beads}\right)$$

$$= O\left[\left(\frac{mv_{rel}^{\,2}}{2}\right)\left(\frac{v_{rel}\Phi^2}{d_p^{\,4}}\right)\left(\frac{(4\Pi/3)(d_p/2)^3}{\Phi}\right)\right] \qquad \textbf{Equation 7.24}$$

where m is the mass of a microcarrier bead (kg). Experimental and theoretical evidence suggest that eddies of the order of the size of the solid particles and smaller are responsible for creating the relative motion between the particles (Kuboi *et al.* 1974, Lakhotia and Papoutsakis 1992, Caulet *et al.* 1996). Since the Kolmogorov eddy length is typically of the order of the microcarrier diameter (Lakhotia and Papoutsakis 1992), the velocity of the Kolmogorov eddies (Equation 7.15) was used by Cherry and Papoutsakis (1988) as an order of magnitude estimate of the relative bead velocity. Substitution of Equation 7.15 into Equation 7.24 yields Equation 7.25.

Velocity of Kolmogorov microscale, $v = (\varepsilon\nu)^{0.25}$ **Equation 7.15**

Hence: $$TCS = O\left[(\varepsilon\nu)^{0.75}\left(\frac{\Pi^2\rho_s\Phi d_p^{\,2}}{72}\right)\right]$$

$$= O\left[\left(\frac{N_p N^3 D^5 \nu}{V}\right)^{0.75}\left(\frac{\Pi^2\rho_s\Phi d_p^{\,2}}{72}\right)\right] \qquad \textbf{Equation 7.25}$$

where ρ_s is the density of the microcarrier beads (kg m^{-3}), N_p is the power number, N is the impeller speed (rps), D is the impeller diameter (m), and V is the bioreactor liquid volume (m^3). Cherry and Papoutsakis (1988) successfully correlated the death rate, apparent growth rate, growth extent and maximum population of immobilised animal cells with the TCS. They found that by replacing the bioreactor liquid volume (V), in Equation 7.25, with D^3, representing an impeller zone, a single correlation could be obtained for all impeller sizes used (Figure 7.17). It is more meaningful to use D^3 in the TCS expression since the majority of the cell damage occurs in the impeller region.

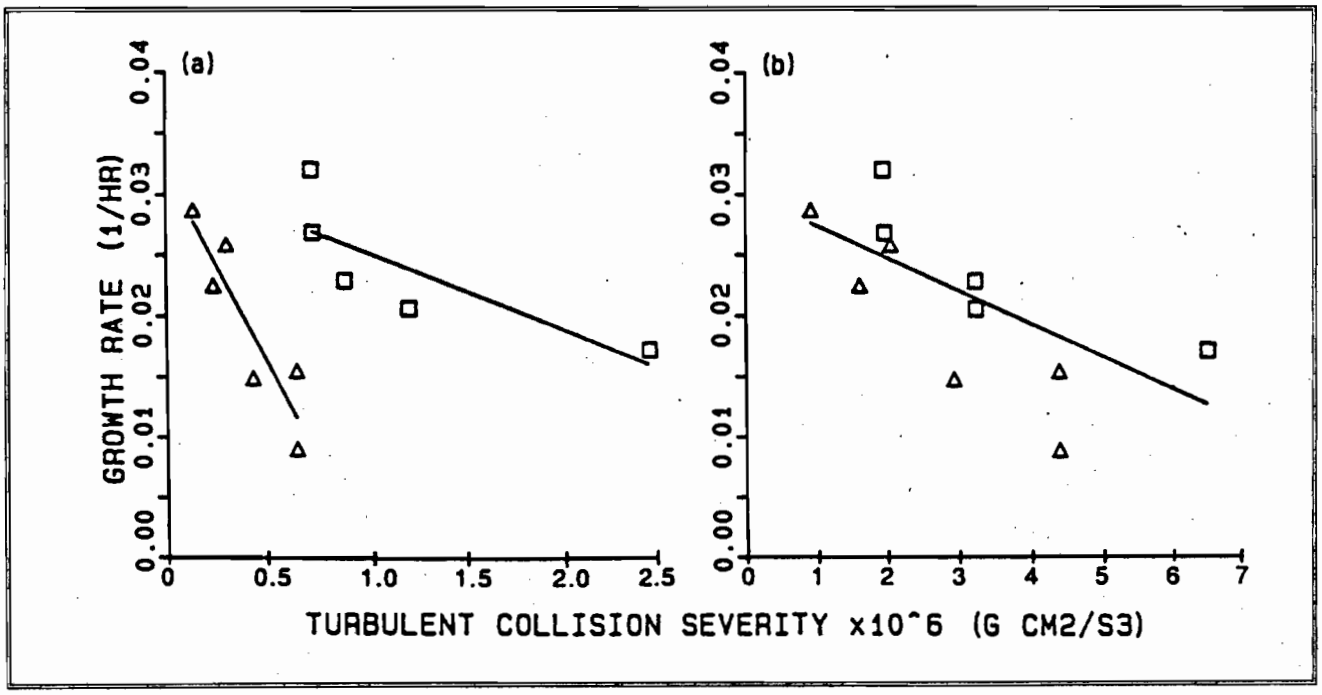

Figure 7.17. **Apparent growth rate of immobilised bovine embryonic kidney cells as a function of the Turbulent Collision Severity (TCS) (Cherry and Papoutsakis 1988).**
Lines are least-squares fits for (Δ) 4 cm and (□) 6 cm 2-bladed pitched-blade turbines. TCS values are calculated (a) using V in Equation 7.25, and (b) using D^3 in Equation 7.25.

To apply the TCS model of Cherry and Papoutsakis (1988) to the slurry reactor data, the particle relative velocity (v_{rel}) required calculation. The particle relative velocity is determined by the physical properties of the solid particles and the fluid (Table 7.3). As a result of the large density difference between the solid particles and the fluid in this study and the large size of the particles used, the relative velocity of the silica particles is determined by the action of turbulent eddies as well as by the inertial and gravitational forces acting on the particles (Kuboi *et al.* 1974).

Table 7.3 **Physical properties of the solid particles and fluid in the slurry reactor system and the animal cell-microcarrier system**

Parameter	Slurry Reactor System	Animal Cell-Microcarrier System
Particle Size (μm)	600-850	185
Particle Density (kg m^{-3})	2664	1030
Density Difference between the Solid Particles and the Fluid (kg m^{-3})	1628	20

An order of magnitude estimate of the particle relative velocity was made. Nouri *et al.* (1987) showed that the inertia of solid particles reduces the particle fluctuating velocity to a particular fraction of the fluid fluctuating velocity. In this work, the fluid fluctuating velocity was estimated from the Kolmogorov eddy velocity since this provides a lower bound of the eddy velocities which affect the particle motion. It is, however, recognised that the Kolmogorov eddy velocity would be lower in this work than that predicted by Equation 7.15 because of the effect of the particles on the fluid turbulence (Section 7.3.1.1). The fraction of the fluid fluctuating velocity required to calculate the particle fluctuating velocity would be incorporated in the constant relating k to TCS. Equation 7.25 was therefore used to calculate the TCS in this work.

Figure 7.18 shows the correlation of the first order disruption rate constants of this study with the TCS expression (Equation 7.25). Separate curves were obtained for the k values measured at 10% and 20% solids (v/v), indicating that the TCS expression does not account adequately for the frequency of the interactions between the cells and solid particles. Since the cells in this work are freely suspended, the collision frequency term in the TCS expression was redefined as the number of collisions per unit volume of suspension per unit time (Equation 7.26) instead of the number of collisions per bead per unit time. A single curve was obtained in correlating the k values at 10% and 20% solids (v/v) with the redefined TCS expression (TCS*).

$$TCS^{*} = (\text{kinetic energy})\left(\frac{collisions}{(suspension\ volume)(time)}\right)$$

$$= O\left[\left(\frac{mv_{rel}^{2}}{2}\right)\left(\frac{v_{rel}\Phi^{2}}{d_p^{4}}\right)\right]$$

$$= O\left[8.32x10^{-2}(v\varepsilon)^{0.75}\left(\frac{\rho_s\Phi^{2}\Pi}{d_p}\right)\right] \qquad \textbf{Equation 7.26}$$

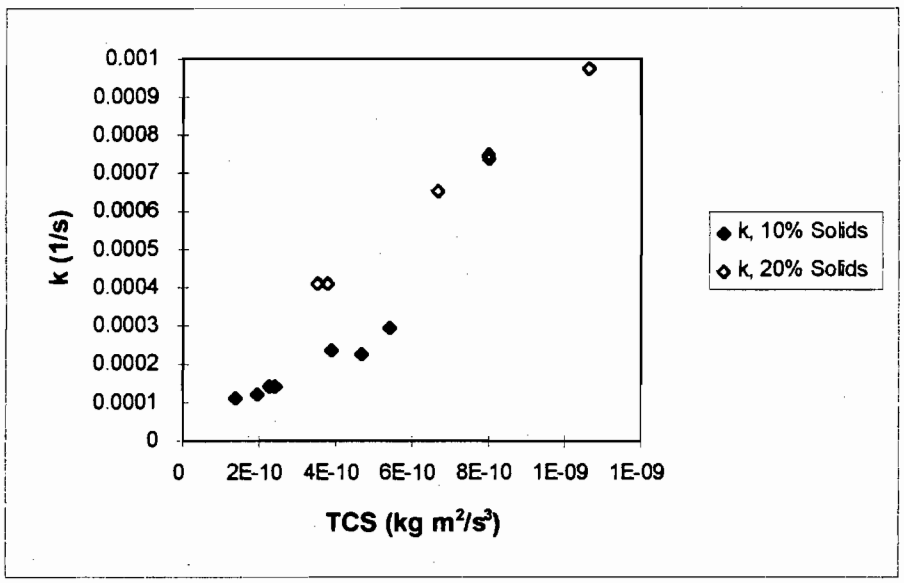

Figure 7.18 **Correlation of the first order disruption rate constants at 10% and 20% solids (v/v) with the Turbulent Collision Severity.**

A power law relationship, shown in Equation 7.27, was fitted to the k values as a function of the redefined TCS expression (Equation 7.26). The parity chart, illustrating the good agreement between the measured k values and those predicted by Equation 7.27, is shown in Figure 7.19. The coefficient of variance between the measured and predicted k values is 6.0%. The good correlation of k with the redefined TCS expression, which includes the terms Φ^2 and the power input per unit fluid mass (ε), supports the form of the modified physical parameter models presented in Section 7.2. Equation 7.27 also highlights the importance of accounting for the frequency and force of solid-cell-solid collisions in the cell disruption mechanism in the slurry reactor.

$$k = 9.00 \times 10^{-4}(TCS^{*})^{0.84} \qquad \textbf{Equation 7.27}$$

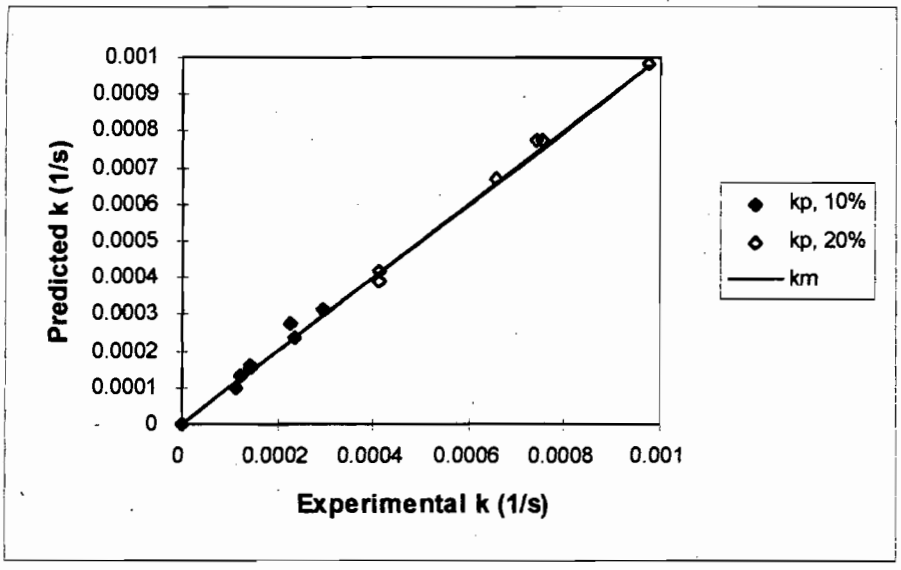

Figure 7.19 **Parity chart comparing predictions of k from Equation 7.27 and the experimental k values.**

k_m denotes the experimental k values. k_p signifies the predicted k values at 10% and 20% solids (v/v).

The essential differences in the TCS (Equation 7.25) and TCS* (Equation 7.26) expressions are their functional dependence on the solids volume fraction (Φ) and the particle diameter (d_p). Cherry and Papoutsakis (1988) investigated the effect of increasing agitation intensity (impeller tip speeds of 0.16 to 0.43 m s^{-1}) on the growth rates of bovine embryonic kidney cells immobilised on microcarriers at a constant microcarrier concentration of 0.5% (v/v). Since only ε was varied in their work, their data cannot be used to discriminate between the two expressions. The form of the relationship between the growth rate and TCS, and the growth rate and TCS^{*} was therefore anticipated to be the same. This is shown in Figure 7.20.

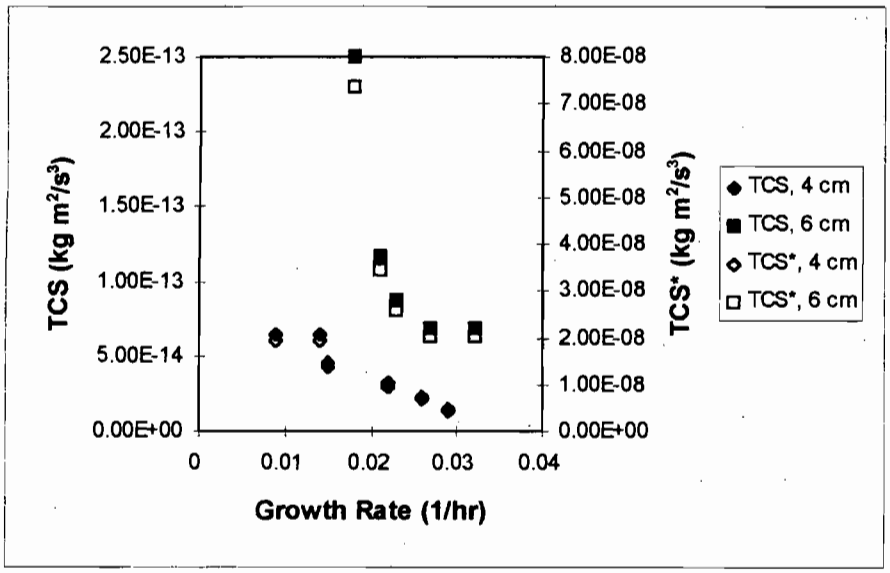

Figure 7.20. **Correlation of the growth rate of bovine embryonic kidney cells immobilised on microcarriers (Cherry and Papoutsakis 1988) with TCS and TCS*.**
Correlations of the growth rate, using both 4 cm and 6 cm paddle-type impellers in a 2 liter reactor, are shown.

7.3.2.2 Eddy Concentration-Collision Frequency Model

Croughan *et al* (1988) developed a model to describe the damage to immobilised FS-4 cells at relatively high solids concentrations of 0.1% to 3.1% (v/v) and a relatively high agitation intensity of 150 rpm (impeller tip speed of 0.42 m s^{-1}). Under these conditions, cell death occurs as a consequence of interactions between the cells and eddies, and interactions between the cells and solid particles. This model is an extension of the one developed by Croughan *et al.* (1987) to describe cell damage at low solids concentrations in terms of interactions between the cells and eddies alone (Equation 7.16).

Croughan *et al.* (1988) assumed that almost all relative motion between two neighbouring microcarriers would arise from the action of turbulent eddies of the order of or smaller than the microcarrier size. The frequency of interactions between the microcarriers was thus considered to be first order in the concentration of Kolmogorov eddies and second order in microcarrier concentration (Hinze 1971, Abrahamson 1975):

$$F = k_2 (\varepsilon / \nu^3)^{0.75} C_M^2 \qquad \textbf{Equation 7.28}$$

where F is the number of interactions between the microcarriers per unit time and volume (m^{-3} hr^{-1}), k_2 is a

constant (m^6 kg^{-2} hr^{-1}), and C_M is the microcarrier concentration (kg m^{-3}). If each microcarrier-cell-microcarrier interaction resulted in cell death with a probability of k_3, the rate of change in the immobilised cell concentration would be given by:

$$dc/dt = -k_3 k_4 N_0 F$$
$$= -k_5 \varepsilon^{0.75} c C_M \qquad \textbf{Equation 7.29}$$

where:

k_4 = fraction of each microcarrier surface exposed to each collision or close encounter

N_0 = number of cells per microcarrier (kg cells / kg microcarrier)

k_5 = $k_2 k_3 k_4 / \nu^{2.25}$ (m^3 $W^{-0.75}$ $kg^{-0.25}$ hr^{-1})

c = attached cell concentration (kg m^{-3} suspension)

To establish the effect of bead concentration on the damage to the immobilised FS-4 cells, Croughan *et al.* (1988) used inert solid particles (Section 2.2.2). Collisions between a microcarrier and an inert solid particle with no cells, were considered to cause, on average, half the cell damage caused on collision between two microcarriers. The overall model, describing cell death from interactions between the attached cells and eddies, microcarrier-cell-microcarrier interactions and microcarrier-cell-inert solid particle interactions, was of the following form:

$$dc/dt = \mu c - q_1 c - q_2 C_M c - (q_2 / 2) C_i c \qquad \textbf{Equation 7.30}$$

where:

μ = intrinsic cell growth rate (hr^{-1})

q_1 = $k_1 (\varepsilon / \nu^3)^{0.75}$ **Equation 7.16**

= cell death rate as a result of interactions between the cells and eddies (hr^{-1})

q_2 = $k_5 \varepsilon^{0.75}$ **Equation 7.29**

= cell death rate as a result of interactions between the cells and solid particles ($m^3 kg^{-1} hr^{-1}$)

C_i = concentration of inert solid particles (kg m^{-3})

Equation 7.30 only applies to turbulent eddies smaller than a critical size. The excellent agreement between the measured apparent growth rates of immobilised FS-4 cells and those predicted by Equation 7.30 is shown as a function of the inert solid particle concentration in Figure 7.21 (Croughan *et al.* 1988). Equation

7.30 also allows the relative significance of the damage mechanisms to be elucidated. By plotting the total specific death rate, $q_1 + q_2 C_M + (q_2/2) C_i$, against the sum of the microcarrier and inert solid particle concentrations, it was found that at solids concentrations below 0.5% (v/v), cell damage resulting from interactions between the cells and eddies is predominant. At solids concentrations above 0.5% (v/v), the microcarrier-cell-microcarrier and microcarrier-cell-inert solid particle mechanisms become more significant.

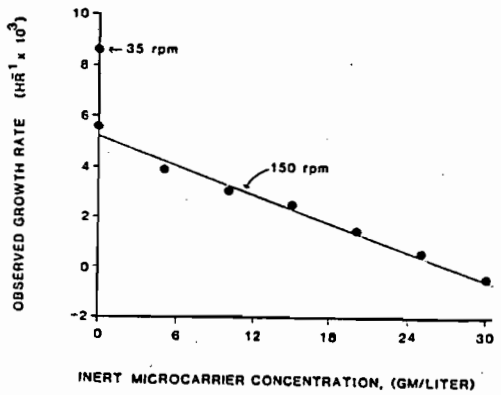

Figure 7.21. **Comparison of measured apparent growth rates of FS-4 cells immobilised on Cytodex 1 microcarriers, and apparent growth rates predicted by Equation 7.30, as a function of the inert solid particle concentration (Croughan *et al.* 1988).**
Measured and predicted apparent growth rates are represented by the data points and the solid line respectively.

Croughan *et al.* (1988) considered q_1, the cell death rate as a result of interactions between the cells and eddies, to be independent of the solid particle concentration. This was possible because the solid particle spacing was greater than the distance over which viscous dissipation occurs, when an eddy interacts with a solid support.

The model of Croughan *et al.* (1988) (Equation 7.30) was applied to the disruption of *Saccharomyces cerevisiae* observed in the slurry reactor. As discussed in Section 6.3.3, the death rate of FS-4 cells is essentially a measure of their disruption rate. Hence application of Equation 7.30 to the first order disruption rate constants, k, is valid. The first order disruption rate constant was thus considered to be the sum of the disruption rates of the potential mechanisms of cell disruption (Equation 7.31).

$$k = \sum_i k_{mechanism,i}$$

Hence: $k = q_1 + q_2 C_M + (q_2/2) C_i$ **Equation 7.31**

Since the contribution of interactions between the cells and eddies to the cell disruption in the slurry reactor is negligible (Section 7.3.1.1), the term, q_1, can be neglected. In addition, the second term in Equation 7.31 can be disregarded since freely suspended cells were used in the slurry reactor. Equation 7.31 was thus rewritten as:

$$k = (q_2/2)\, C_i \quad \textbf{Equation 7.32}$$
$$= k_6\, \varepsilon^{0.75}\, C_i$$

Figure 7.22 shows the correlation of the k values with $\varepsilon^{0.75}\, C_i$. Separate curves for the 0.10 and 0.20 volume fraction data were obtained. This was anticipated since the physical parameter models in Section 7.2 and the redefined TCS expression (Equation 7.26) show that k approaches a quadratic dependency on solids volume fraction. Although Croughan *et al.* (1988) assumed that the frequency of microcarrier-cell-microcarrier interactions had a quadratic dependency on microcarrier concentration (Equation 7.28), this dependency was lost on incorporating the collision frequency term into the cell death rate expression (Equation 7.29). The model of Croughan *et al.* (1988) thus does not adequately account for the collision frequency in the slurry reactor.

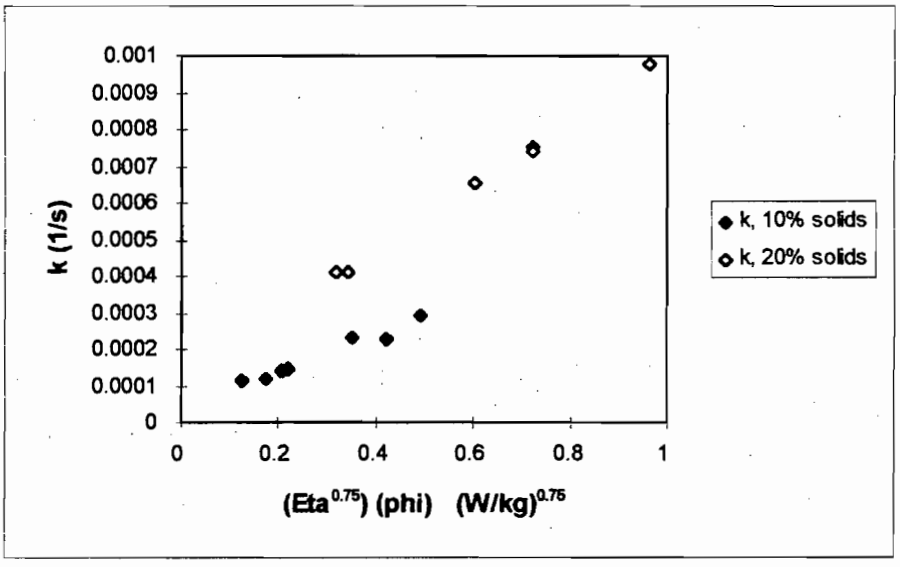

Figure 7.22. Correlation of k with Equation 7.32 as a function of the solids volume fraction.

7.3.2.3 Turbulent Energy Model

In animal cell-microcarrier systems, the dependency of the cell damage mechanisms of interaction between cells and solids and interaction between cells and fluid eddies on the bioreactor variables has been determined in terms of the Turbulent Collision Severity and the ratio of Kolmogorov eddy length to bead diameter respectively. The fractional contribution of each of these mechanisms to the overall cell damage was determined by Croughan *et al.* (1988) as a function of solids loading at an agitation intensity of 150 rpm (impeller tip speed of 0.42 m s^{-1}). However, fluid-mechanical considerations suggest that the fractional contribution of each of these two mechanisms to the overall cell damage will vary with agitation intensity, bead size and possibly other bioreactor parameters (Papoutsakis 1991, Lakhotia and Papoutsakis 1992).

To account for this, Lakhotia and Papoutsakis (1992) modelled the damage to bovine embryonic kidney cells, immobilised on microcarriers, in terms of the turbulent energy responsible for both the interactions between the cells and solid particles and the interactions between the cells and fluid eddies. Their model accounts for both types of interactions simultaneously and uses the properties of a spectrum of eddies smaller than the microcarrier diameter, instead of the Kolmogorov-scale eddy size alone.

The one-dimensional energy spectrum of the universal equilibrium subrange of isotropic turbulence was used to construct the model (Figure 7.14). The universal equilibrium subrange of isotropic turbulence includes both the inertial convection subrange and the viscous dissipation subrange. The turbulence in this regime is independent of external conditions and is determined only by the energy input into the system and the viscous dissipation (van Suijdam and Metz 1981, Kawase and Moo-Young 1990, Lakhotia and Papoutsakis 1992). The Pao-Corrsin model (Equation 7.33) was used by Lakhotia and Papoutsakis (1992) to describe the one dimensional energy spectrum of the universal equilibrium range of isotropic turbulence.

$$E(k) = 1.7\,\varepsilon^{2/3} k^{-5/3} \exp(-2.55\,\nu\,\varepsilon^{-1/3} k^{4/3}) \qquad \textbf{Equation 7.33}$$

where: $E(k)$ = one-dimensional energy distribution function for turbulent eddies

k = wavenumber of turbulent eddy (m^{-1})

The average energy of the interactions between the cells and solid particles and the cells and fluid eddies was taken as the integral of Equation 7.33. The specific cell death rate, q, was considered to be proportional to this integral:

$$q = B \int_{kc}^{\infty} 1.7\,\varepsilon^{2/3} k^{-5/3} \exp(-2.55\,\nu\,\varepsilon^{-1/3} k^{4/3})\,dk \qquad \textbf{Equation 7.34}$$

where B is a constant (sm^{-2}) and k_c is the wavenumber corresponding to the largest eddy size that is damaging to the cells (m^{-1}). Lakhotia and Papoutsakis (1992) successfully used this model to explain and predict the varying functional dependence of the specific death rate of immobilised bovine embryonic kidney (BEK) cells on the medium viscosity at agitation intensities of 120 to 160 rpm (impeller tip speeds of 0.26 to 0.35 m s^{-1}) at a solids concentration of 0.5% (v/v). Spinner flasks were used in the cell damage experiments. Figure 7.23 is a parity chart comparing the measured specific death rates of BEK cells, suspended in maintenance medium, and the specific death rates predicted by the model of Lakhotia and Papoutsakis (1992). Figure 7.23 shows that the model agrees well with the data despite the 10-15% error in the experimental data (Lakhotia and Papoutsakis 1992).

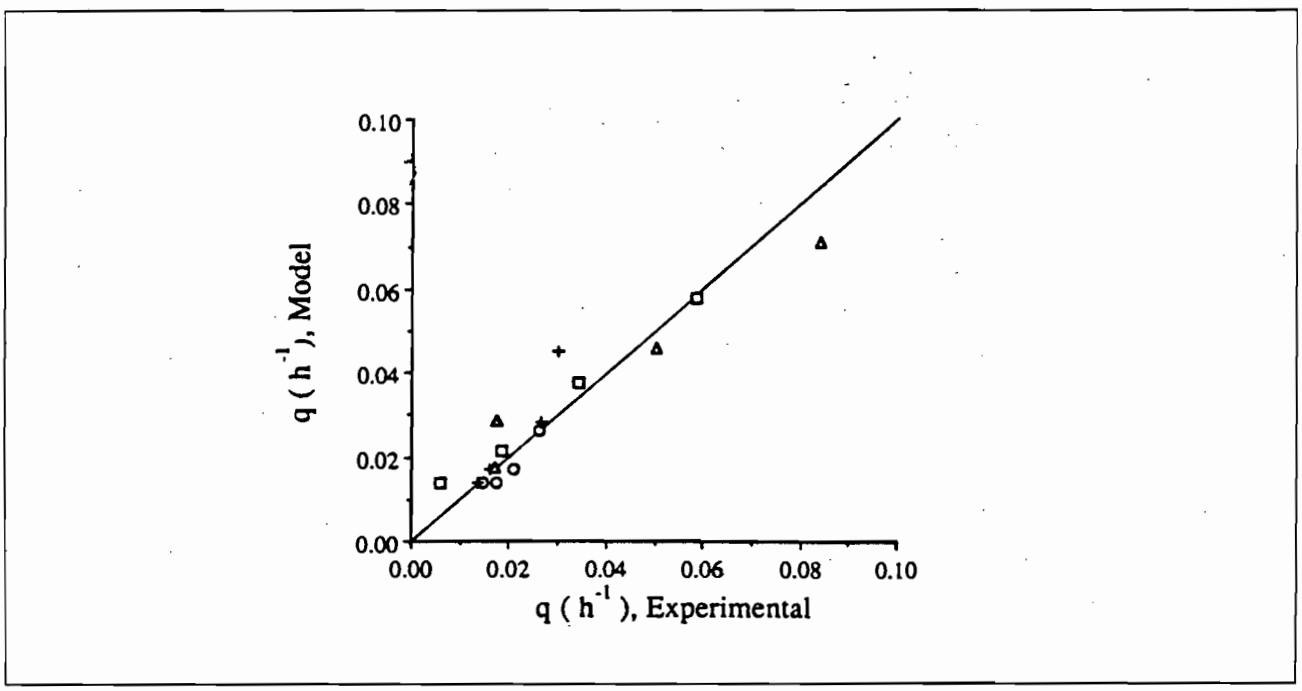

Figure 7.23. **Parity chart comparing the measured specific death rates of immobilsed bovine embryonic kidney cells and the specific death rates predicted by the model of Lakhotia and Papoutsakis (1992) (Lakhotia and Papoutsakis 1992).**
The cells were suspended in maintenance medium. Each data point shown is the average of duplicate measurements. (O)120 rpm; (+)140 rpm; (□)150 rpm; (Δ)160 rpm.

The Pao-Corrsin model (Equation 7.33) strictly applies to one-phase systems only. However, the

proportionality between the one-dimensional energy distribution function for turbulent eddies, E(k), and $\varepsilon^{2/3}k^{-5/3}$ has been verified for dilute two-phase systems, similar to the animal cell-microcarrier cultures (Kuboi *et al.* 1974). This proportionality relationship is not valid for the slurry reactor system in this study because of the high solids concentrations used. As discussed in Section 7.3.1.1, the presence of solids at concentrations greater than 2% (v/v), modifies the energy spectrum of the fluid in the high wave number region (Hinze 1971, Caulet *et al.* 1996). Since an expression for E(k) at the conditions in this study could not be found, the turbulent energy model (Equation 7.34) of Lakhotia and Papoutsakis (1992) was not applied to the cell disruption in the slurry reactor.

7.3.3 Interactions between the Cells and Bubbles

Bubble rupture at the free gas-liquid interface has been shown to be the dominant cause of animal and insect cell damage when the cells interact with bubbles in gas-liquid systems (Handa-Corrigan *et al.* 1989, Kunas and Papoutsakis 1990, Papoutsakis 1991, Trinh *et al.* 1994, Michaels *et al.* 1996). Bubble break-up at the medium surface is significant to cell damage because cells become adsorbed onto the bubble surfaces, either because of hydrophobic interactions between the cells and the bubbles or because the cells are captured by the wakes behind moving bubbles. Cells trapped in the rupturing film of bubbles may be killed by large compressional forces which occur when the rupturing rim breaks into threads (Chalmers and Bavarian 1991, Kowalski 1991). Furthermore, the hydrodynamic forces due to shear in the boundary layer around the walls of the bubble cavity are sufficiently large to kill the cells (Chalmers and Bavarian 1991). The breaking bubble may also release its built-up surface energy in a potentially damaging shockwave (Yang *et al.* 1990).

The specific cell death rate in a gas-liquid system was related to the interactions between cells and bubbles by Yang and Wang (1992). Their mathematical model was based on the postulation that cells were killed or damaged if they were in the close vicinity of a deformed bubble as it underwent break-up or coalescence. The model of Yang and Wang (1992) makes no distinction where bubble break-up and coalescence take place: at the point of the sparger, at the medium surface or in the impeller stream region, where the intense eddy-bubble interaction creates a high density of deformed bubbles. However, as discussed above, other workers have shown that bubble break-up at the medium interface is most damaging to cells.

Surface aeration was used in the animal cell-microcarrier cultures of Cherry and Papoutsakis (1988) and Croughan *et al.* (1988) to achieve the required dissolved oxygen concentrations. The models developed by these workers to describe the damage to the immobilised animal cells only considered the effect of interactions between the cells and the fluid eddies (Section 7.3.1.1) and interactions between the cells and

the microcarriers (Section 7.3.2). The good agreement achieved between the measured and predicted cell damage in these systems, without accounting for the effect of interactions between the cells and bubbles, suggests that interactions between the cells and bubbles are relatively insignificant as a damage mechanism.

Although the vessel in this study was not sparged, surface aeration of the slurry occurred at the high impeller speeds. Interactions between the cells and bubbles are thus a possible cause of cell disruption. However, the cell disruption experiments, presented in Section 6.3, suggested that interactions between the freely suspended cells and the solid particles are the dominant cause of cell disruption in the slurry reactor. Hence interactions between the cells and bubbles, entrained from surface aeration, are relatively insignificant as a disruption mechanism. This is verified by the applicability of the models presented in Section 7.4, which only account for collisions between the cells and solid particles as the disruption mechanism.

7.3.4 Interactions between the Cells and the Reactor Components

A final mechanism that has been proposed to account for the damage to animal cells in bioreactors is collisions between the particles supporting the cells, and the solid components of the vessel, especially the impeller (Croughan *et al.* 1988, 1989; Cherry and Papoutsakis 1988). Cherry and Papoutsakis (1988) defined an *Impeller Collision Severity* (ICS) to characterise the rate of energy input to each solid support particle as a result of collisions of the beads with the impeller. As with the Turbulent Collision Severity, the ICS was defined as the product of the collision kinetic energy and the collision frequency. The microcarriers were assumed to collide with the impeller only if they passed within one bead radius of the impeller surface. The region defined by this area, where collisions between the microcarriers and the impeller occur, was termed the "window area". The collision frequency was estimated from the time that the microcarriers take to flow through the entire reactor volume along the set of streamlines that are in the window area. The ICS was consequently expressed as:

$$ICS = (kinetic\ energy)(collision\ frequency)$$

$$ICS = (kinetic\ energy)\left[\frac{(window\ area)(velocity\ past\ blade)}{(reactor\ volume)}\right]$$

Hence: $$ICS = O\left[\left(\frac{m v_{av}^{\,2}}{2}\right)\left(\frac{(n_b D d_p / 2) v_{av}}{V}\right)\right] \qquad \textbf{Equation 7.35}$$

where O signifies "of the order of ", m is the mass of a microcarrier (kg), v_{av} is the average velocity of the

medium over the impeller blade (m s^{-1}) and n_b is the number of impeller blades. Cherry and Papoutsakis (1988) estimated v_{av} as 75% of the impeller tip speed (πND). Substituting for v_{av} and m ($\rho_s \pi d^2/6$) into Equation 7.35 yields the following order of magnitude estimate of ICS:

$$ICS = O\left[\frac{9\Pi^4 \rho_s n_b N^3 D^4 d_p{}^4}{512V}\right] \qquad \textbf{Equation 7.36}$$

Cherry and Papoutsakis (1988) found that the death rate, apparent growth rate, growth extent and maximum population of animal cells correlated well with the ICS. However, they failed to obtain a single correlation for the 4cm and 6 cm pitched-blade turbines (two-bladed) when using either the bioreactor fluid volume, V, or the impeller zone volume (α D^3). Cherry and Papoutsakis (1988) concluded that, for their experimental conditions, collisions of the microcarriers with the impeller were not the primary mechanism of damage. Croughan *et al.* (1989) suggest that interactions between the microcarriers and the reactor components are unimportant as a damage mechanism because the microcarriers do not rapidly penetrate the boundary layers surrounding the reactor internals.

Cherry and Papoutsakis (1988) note that the ICS is only an approximation to the actual energy input rate to each microcarrier because the inertial deviation of the particle trajectories from the fluid streamlines was not considered. This would not affect the animal cell-microcarrier system significantly since the neutrally buoyant microcarriers primarily follow the fluid streamlines (Kuboi *et al.* 1974). However, the inertial deviation of the silica particles of this study from the fluid streamlines is significant owing to their large size (600 to 850 μm) and density (2664 kg m^{-3}). The inaccuracies in correlating the cell disruption observed in this study with the ICS are thus greater than in the animal cell-microcarrier system.

Cherry and Papoutsakis (1988) did not consider the effect of the solids loading on the collision frequency of the microcarriers with the impeller (Equation 7.35). When the cell disruption observed in this study was correlated with the ICS, separate curves were obtained for the 0.10 and 0.20 solids volume fractions (Figure 7.24). As discussed in the preceding paragraph, the ICS is not an accurate description of the interactions between the solids of this study and the impeller. It is thus difficult to draw meaningful conclusions from Figure 7.24.

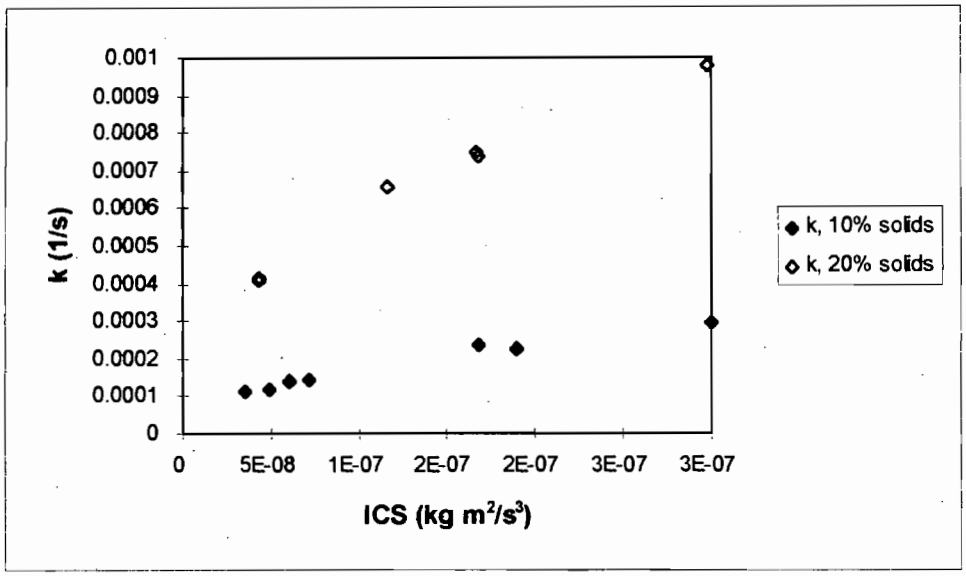

Figure 7.24. **Correlation of k with the Impeller Collision Severity of Cherry and Papoutsakis (1988) as a function of the solids volume fraction.**

7.3.5 Conclusions drawn from Mechanistic Models

Direct application of the animal cell mechanistic models to the cell disruption observed in the silica slurry reactor is limited. The microcarriers used in the animal cell cultures were small (185 μm), neutrally buoyant and used at solids concentrations lower than 3.1% (v/v). The silica particles used in this study were large (600 to 850 μm), dense ($\Delta\rho$ = 1628 kg m^{-3}) and used at solids volume fractions of 0.10 and 0.20. At the conditions used in this work, the particles affect the fluid turbulence structure and as a result of the inertial and gravitational forces acting on the particles, their response to the fluid eddies is reduced. In contrast to this, the microcarriers do not affect the fluid turbulence structure and primarily follow the fluid streamlines.

The limited applicability of the animal cell mechanistic models to the cell disruption in the slurry reactor motivated the development of new models, presented in Section 7.4. However, in this review of the mechanistic models, it was shown from the literature that interactions between the cells and the fluid eddies are insignificant as a disruption mechanism at the conditions in this work. Furthermore, cell disruption from interaction between the cells and entrained bubbles is negligible. In addition, it was shown that the cell disruption observed in this study correlated well with a redefined Turbulent Collision Severity (TCS) expression (Equation 7.26), which accounts for both the energy and frequency of the interactions between the cells and solid particles. The collision energy term in Equation 7.26 is a function of the power input per

unit fluid mass (ε), and the collision frequency term is a function of the solids volume fraction (Φ) and ε. The relationship between the k values and the redefined TCS expression supports the form of the modified Physical Parameter models, presented in Section 7.2, as well as the experimental observation that interactions between the cells and solid particles are the primary cause of cell disruption in the slurry reactor.

7.4 Modelling Cell Disruption in the Slurry Reactor

In this section, three new models are presented to describe the cell disruption in the slurry reactor resulting from agitation with the Rushton turbine. In these models, only collisions between the cells and solid particles are considered as the disruption mechanism. This is validated in Section 7.4.1. The first two models are generalised forms of the Physical Parameter models, modified to account for both the solids concentration and the impeller speed (Section 7.2). The first of these models is a modified mass transfer-type model which expresses the first order disruption rate constant in terms of the solids volume fraction and the power input per unit volume. The second model is similar to the first, but uses an energy input term instead of a power input term. The third model is a mechanistic model which describes the types of collisions between the cells and solid particles that are responsible for the cell disruption. It also accounts for the magnitude of the collision force between the cells and the solids. The equivalence of these models is shown in this section.

7.4.1 Modified Mass Transfer-Type Model

In Section 7.2, it was shown that the following modified Physical Parameter models described the first order disruption rate constants well:

$$k = 2.77 \times 10^{-6} N^{1.32} \Phi^{1.92} \qquad \textbf{Equation 7.5}$$

$$k = 8.54 \times 10^{-6} \left(\frac{P t_c \Phi^{1.92}}{V} \right)^{0.83} \qquad \textbf{Equation 7.7}$$

$$k = 5.65 \times 10^{-7} (N_{RE} \Phi^{1.92})^{0.96} \qquad \textbf{Equation 7.13}$$

All these models account for the effect of the impeller speed ($P \propto N^3$; $N_{RE} = N D^2 \rho/\mu$) and the solids volume fraction (Φ) on the cell disruption. However, in fitting these models to the cell disruption data in

the slurry reactor, the exponent of Φ was fixed at 1.92. In Equations 7.7 and 7.13, the exponents of $\Phi^{1.92}$ and P or N were forced to the same value.

Here, the dependence of the first order disruption rate constant on P/V (or N since $P \alpha N^3$) and Φ is generalised to an expression of the following form:

$$k = A (P/V)^b \Phi^c \qquad \textbf{Equation 7.37}$$

The cell concentration is not explicitly shown in Equation 7.37 since it was maintained at a constant average value of 52.8 kg m^{-3} in the disruption experiments. A Least Squares analysis (Appendix H) was used to establish the constants in Equation 7.37, yielding Equation 7.38. The coefficient of variance between the measured k values and those predicted by Equation 7.38 is 4.7%. The excellent agreement between the experimental and predicted k values can be seen in the parity chart represented by Figure 7.25.

$$k = 7.11 \times 10^{-5} (P/V)^{0.56} \Phi^{1.64} \qquad \textbf{Equation 7.38}$$

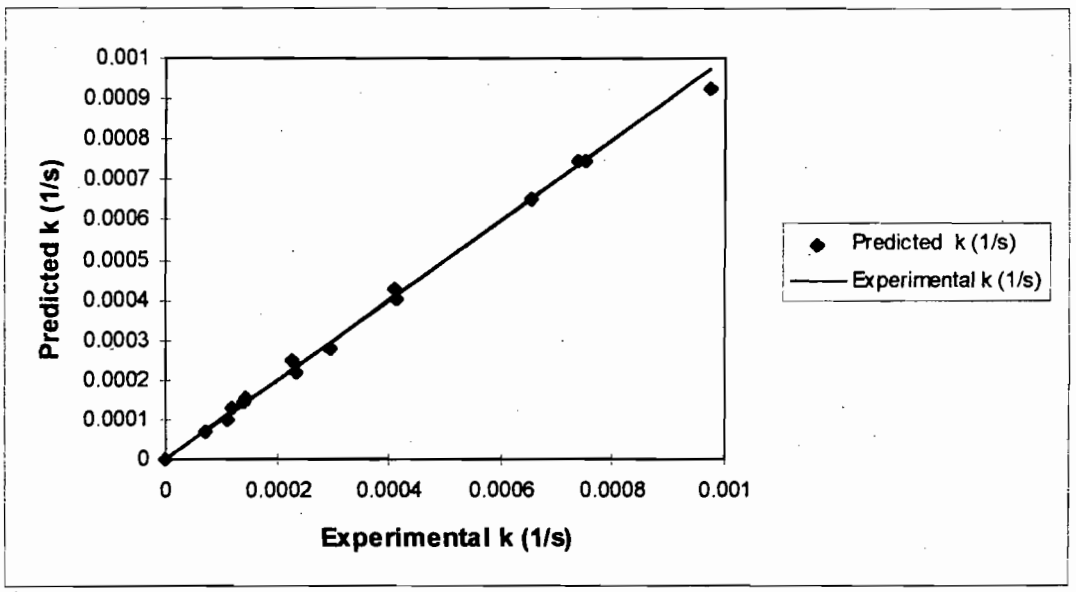

Figure 7.25. **Parity Chart comparing predictions of k from Equation 7.38 and experimental k values.**

The parity chart includes data from the disruption experiments performed at both 10% and 20% solids (v/v) and at speeds above the respective critical impeller speeds.

Equation 7.38 is termed a modified mass transfer-type model since it is analogous to the empirical expression describing the rate of oxygen mass transfer, k_la, in stirred tanks. The form of the expression relating k_la to the power input per unit volume and the superficial gas velocity, v_G, is shown in Equation 7.39 (Van't Riet 1983):

$$k_la = A (P/V)^b v_G^c \qquad \textbf{Equation 7.39}$$

Equation 7.38 describes the rate of protein release from the cells into the supernatant as the cells are disrupted, whereas Equation 7.39 describes the rate of oxygen mass transfer from the gas bubbles into the liquid. Both the first order disruption rate constant of cell breakage (k) and the oxygen mass transfer coefficient (k_la) are a function of the power input per unit volume. The superficial gas velocity term in Equation 7.39 is essentially a measure of the bubble concentration.

Typical values of *A*, *b* and *c* in Equation 7.39 are listed in Table 7.4 and are compared to the corresponding parameters for the first order disruption rate constant expression in Equation 7.38. Table 7.4 shows that although the values of *A* and *c* in the expressions of k and k_la differ, these expressions have similar dependencies on the power input per unit volume (value of *b*).

Table 7.4. **Comparison of values of *A*, *b* and *c* for the first order disruption rate constant expression (Equation 7.38) and the empirical oxygen mass transfer expression (Equation 7.39) (Nielsen and Villadsen 1994).**

Parameter values for Equation 7.39 are for a coalescing (air-water) dispersion.

Equation	Agitator	A*	b	c	Reference
7.38	6-bladed Rushton turbine	7.11×10^{-5}	0.56	1.64	This study
7.39	6-bladed Rushton turbine	2.5×10^{-2}	0.4	0.5	Moo-Young and Blanch (1981)
		4.95×10^{-3}	0.593	0.4	Linek *et al.* (1987)
	Not specified	2.6×10^{-2}	0.4	0.5	Van't Riet (1983)

*The units of *A* vary for each correlation depending on the values of *b* and *c*. The power input per unit volume is measured in W m^{-3} and the superficial gas flowrate is measured in m s^{-1}.

In Section 7.3.2.1, it was shown that the first order disruption rate constants (k), obtained on disruption of the yeast cells in the slurry reactor, correlated well with a redefined Turbulent Collision Severity expression (Equation 7.26). This expression accounted for both the kinetic energy ($\alpha\ v_{rel}^2 \propto \varepsilon^{0.5}$) and the frequency ($\alpha\ v_{rel}\ \Phi^2$ or $\varepsilon^{0.25}\ \Phi^2$) of the collisions between the cells and solid particles which give rise to the cell disruption. The first order disruption rate constant (k) was thus shown to be a function of $(v_{rel}^3\ \Phi^2)^{0.84}$. Equation 7.38 describes k as a function of $(P/V)^{0.56}\ \Phi^{1.64}$. The similarity of these expressions shows that Equation 7.38 also accounts for both the kinetic energy ($\alpha\ (P/V)^{0.37}$) and the frequency ($\alpha\ (P/V)^{0.19}\ \Phi^{1.64}$) of the collisions between the cells and solid particles. The excellent correlation of the first order rate constants in this work by Equation 7.38 therefore verifies that the primary cell disruption mechanism in the slurry reactor is collision between the cells and solid particles.

An energy balance was performed to calculate the maximum value of the exponent of (P/V) in Equation 7.38 and hence to determine the validity of the best-fit value (0.56). The energy balance was performed on the fluid adjacent to the 6-bladed Rushton turbine in the stirred tank and is only approximate since it neglects drag coefficient dependence on Reynolds number and it assumes the quantitative transfer of energy from the impeller to the particles via liquid:

Let F denote the force acting on the fluid adjacent to the impeller in the stirred tank.

$$\text{Then} \quad F = c_D\,(\text{Area})\,(0.5)\,\rho\,v^2$$

$$= c_D\,f(D^2)\,(0.5)\,\rho\,(\pi N D)^2 \qquad \textbf{Equation 7.40}$$

where c_D is the drag coefficient associated with the impeller and $f(D^2)$ denotes that the area on which the force acts is a function of the square of the impeller diameter. Now energy is the product of force and displacement. Therefore, for a fixed impeller type and fixed system geometry, the maximum energy transferred from the impeller to the solid particles in the slurry reactor, resulting in collisions between these solid particles and the cells, is given by the following expression:

$$\text{Maximum Collision Energy} \quad \alpha \quad N^2 \qquad \textbf{Equation 7.41}$$

It was shown previously in this section that the first order disruption rate constant (k) is proportional to the collision kinetic energy. Hence:

$$k \quad \alpha \quad \textit{Maximum Collision Energy} \quad \alpha \quad N^2 \qquad \textbf{Equation 7.42}$$

For a 6-bladed Rushton turbine in a stirred tank

$$P \quad \alpha \quad N^3 \qquad \textbf{Equation 7.43}$$

Hence:

$$k \quad \alpha \quad N^2 \quad \alpha \quad P^{2/3} \qquad \textbf{Equation 7.44}$$

Thus, for a 6-bladed Rushton turbine in a stirred tank, the maximum value of the exponent of (P/V) is 0.67. This is greater than the best-fit value of 0.56 in Equation 7.38, thereby establishing its validity. Energy from the impeller is also dissipated at the bubble interface (from gas entrainment) and as heat in the slurry reactor. The latter necessitated the use of a cooling coil (Section 3.2) in the disruption experiments to prevent protein denaturation.

The modified Physical Parameter models (Section 7.2) and the redefined Turbulent Collision Severity expression (Equation 7.26) indicated that the rate of cell disruption in the slurry reactor approaches a quadratic dependency on the solids volume fraction. Hence it was anticipated that the exponent of Φ in Equation 7.38 should lie close to 2. The significance of it being slightly less than 2 is discussed in terms of the mechanistic model (Section 7.4.3).

7.4.2 Energy Input Model

In this section, a model is presented which describes the k values in terms of the energy input per unit volume and the solids volume fraction. The following model between k and the modified parameter of Reuss (1988), $Pt_c\Phi^{1.92} / V$, was presented in Section 7.2.1:

$$k = 8.54\,x\,10^{-6}\left(\frac{P\,t_c\,\Phi^{1.92}}{V}\right)^{0.83} \qquad \textbf{Equation 7.7}$$

Since the exponent of Φ in Equation 7.7 was fixed at 1.92, this expression strictly only applies to an impeller speed of 750 rpm. Equation 7.7 was thus generalised to the following form:

$$k = A\,(P\,t_c / V)^b\,\Phi^c \qquad \textbf{Equation 7.45}$$

The constants in Equation 7.45 were determined by fitting the expression to the cell disruption data using a Least Squares analysis (Appendix H). From this analysis:

$A = 4.76 \times 10^{-6}$

$b = 0.90$

$c = 1.61$

The coefficient of variance between the experimental k values and those predicted by Equation 7.45 is 8.7%, indicating good agreement between them. The parity chart for this fit is shown in Figure 7.26. The energy input term in Equation 7.45 represents the energy input to the solid particles per pass through the impeller zone (Section 7.2.1). This suggests that cell disruption, as a result of collisions between the cells and the solid particles, primarily occurs in the impeller region.

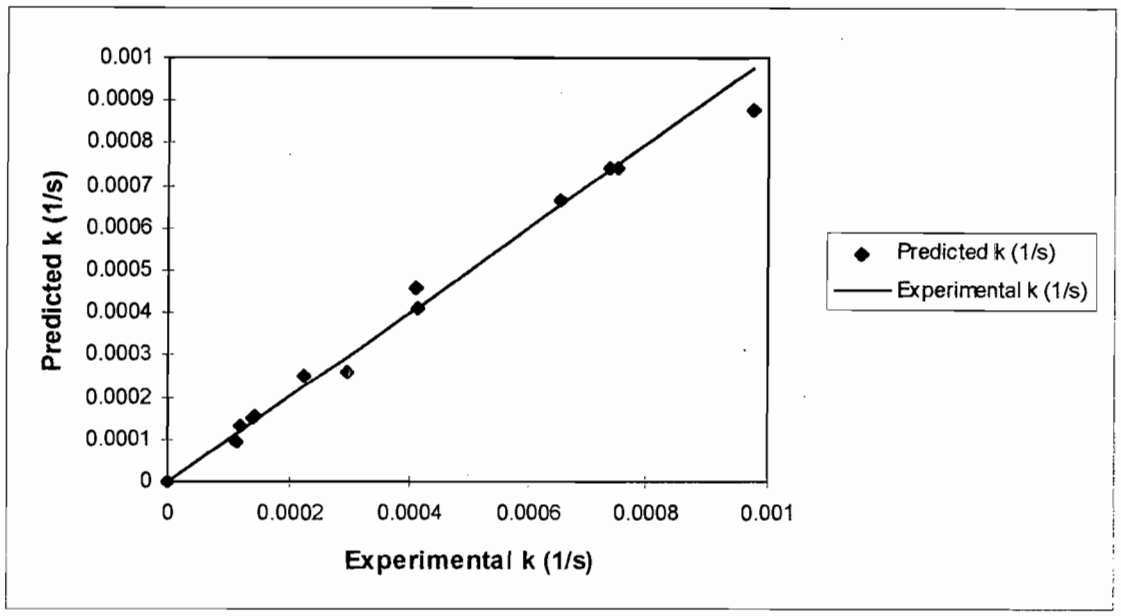

Figure 7.26. **Parity chart comparing predictions of k from Equation 7.45 and the experimental k values**

The parity chart includes data from the disruption experiments performed at both 10% and 20% solids (v/v) and at speeds above the respective critical impeller speeds.

Comparison of the energy input model (Equation 7.45) to the mass transfer-type model (Equation 7.38) shows that the value of 1.61 for the exponent of Φ in Equation 7.45 corresponds very closely with the value of 1.64 in Equation 7.38. To compare the relative magnitude of b in these models, the maximum value of b was determined for Equation 7.45:

$$\textit{Maximum Collision Energy} \quad \propto \quad N^2 \quad \propto \quad P^{2/3} \qquad \textbf{\textit{Equation 7.44}}$$

Now: $$t_c = \frac{V}{0.75\, N\, D^3} \qquad \textbf{\textit{Equation 7.6}}$$

$$t_c = \frac{V\, N_p\, \rho\, N^2\, D^2}{0.75\, P}$$

Hence, for a fixed system geometry:

$$t_c \quad \propto \quad \frac{N^2}{P} \quad \propto \quad \frac{P^{2/3}}{P} \qquad \textbf{\textit{Equation 7.46}}$$

Substitution of Equation 7.46 into Equation 7.44 yields Equation 7.47.

$$\textit{Maximum Collision Energy} \quad \propto \quad (P\, t_c) \qquad \textbf{\textit{Equation 7.47}}$$

Hence:

$$k \quad \alpha \quad \textit{Maximum Collision Energy} \quad \alpha \quad (P\, t_c) \qquad \textbf{\textit{Equation 7.48}}$$

Hence the maximum value of b in Equation 7.45 is unity which is greater than the Least Squares value of 0.90 for b in Equation 7.45. The closeness in agreement between the maximum and best-fit values for the exponent of (P/V) in Eqiuations 7.38 and 7.45 corresponds well with the value of 84% predicted by Equation 7.38. Since the dependency of the k values on the collision frequency and force is essentially the same in Equation 7.38 and Equation 7.45, it can be concluded that these models are equivalent in their description of cell disruption in the slurry reactor. Cell disruption in the slurry reactor is thus correlated well by expressions which account for either the energy input per pass through the impeller zone per unit volume (Pt_c/V) or the power input per unit volume (P/V).

7.4.3 Mechanistic Model

The mass transfer type-model (Section 7.4.1) and the energy input model (Section 7.4.2) accounted for the force and frequency of the collisions between the cells and solid particles. However, they did not describe fully the mechanisms responsible for the cell disruption. Potential mechanisms of cell disruption include cell-eddy interactions, solid-cell-solid collisions, solid-cell collisions and solid-cell-reactor collisions, respectively represented in Equation 7.49. Here, the $c\Phi$ term represents the solid-cell and the solid-cell-reactor collision mechanisms.

$$k = A\,(\varepsilon / \nu^3)^{3/4} + B\,c\,\Phi^2\,N^n + D\,c\,\Phi\,N^n \qquad \textbf{Equation 7.49}$$

where A, B, D and n are constants and c is the biomass concentration (kg m^{-3}). With freely suspended microbial cells ($d_p \leq 5$ μm), cell-eddy interactions do not contribute significantly to cell disruption (Section 7.3.1.1). Hence only the last two terms in Equation 7.49 were considered. The relative significance of these disruption mechanisms was tested by fitting the expressions listed in Table 7.5 to the first order disruption rate constants. A value of 1.68 was used for the exponent of N in Equations 7.50-7.52. This is based on Equation 7.38, where k is proportional to $P^{0.56}$. For a 6-bladed Rushton turbine in a stirred tank, the power input is proportional to N^3 (Equation 7.43), hence k is proportional to $N^{1.68}$. The cell concentration (c) is not explicitly shown in the equations in Table 7.5 since it was not varied in the cell disruption experiments. A Least Squares analysis (Appendix H) was used to calculate the constants in each of the equations. The agreement between the measured k values and those predicted by each of these equations is quantified in terms of a coefficient of variance.

Table 7.5. **Mechanistic models applied to the cell disruption data obtained on agitation with a Rushton turbine in the slurry reactor**

Expression	Coefficient of Variance (%)	Equation Number
$k = 2.83 \times 10^{-7}\,\Phi^2\,N^{1.68}$	9.5	**7.50**
$k = 5.17 \times 10^{-8}\,\Phi\,N^{1.68}$	23.3	**7.51**
$k = 2.27 \times 10^{-7}\,\Phi^2\,N^{1.68} + 1.05 \times 10^{-8}\,\Phi\,N^{1.68}$	7.8	**7.52**

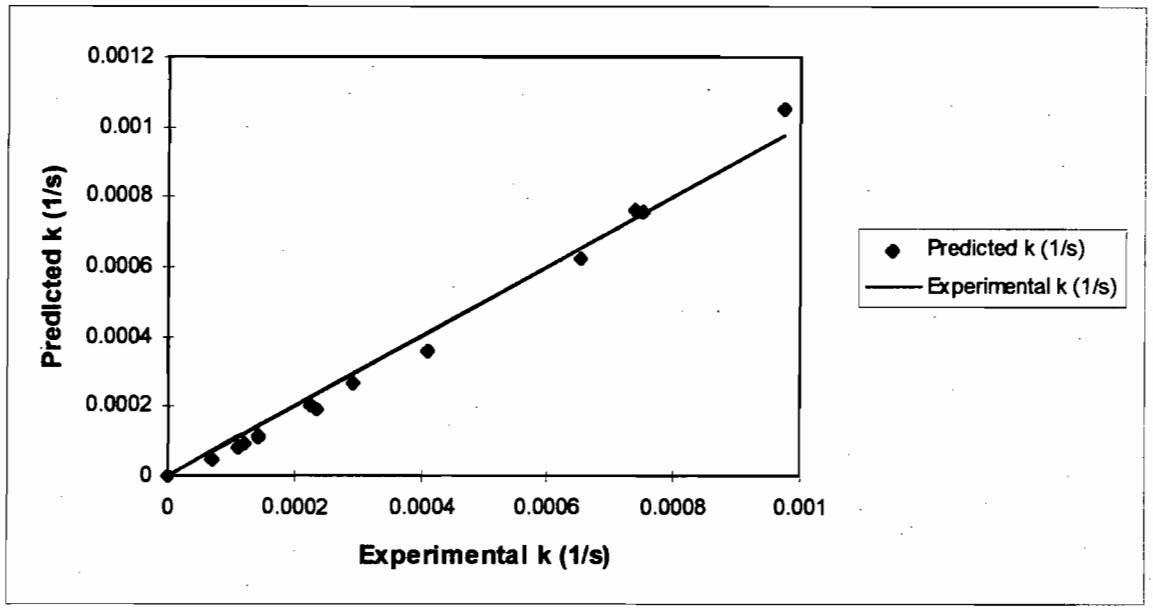

Figure 7.27. **Parity chart comparing experimental k values to the predictions of k from Equation 7.50: $k = 2.83 \times 10^{-7} \Phi^2 N^{1.68}$.**

The parity chart includes data from the disruption experiments performed at both 10% and 20% solids (v/v) and at speeds above the respective critical impeller speeds.

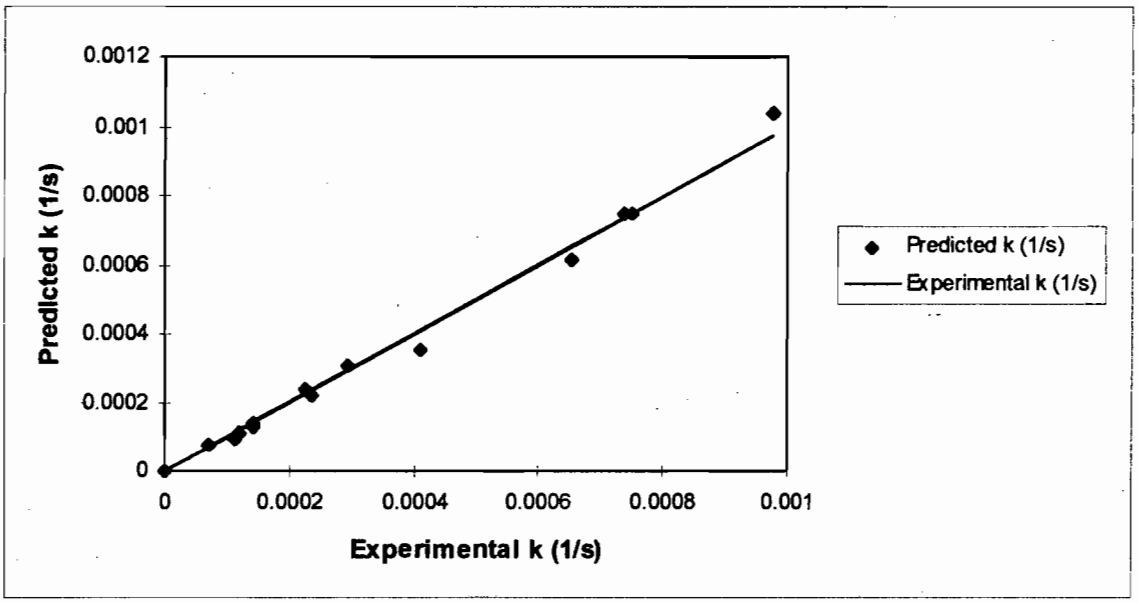

Figure 7.28. **Parity chart comparing experimental k values to the predictions of k from Equation 7.52: $k = 2.27 \times 10^{-7} \Phi^2 N^{1.68} + 1.05 \times 10^{-8} \Phi N^{1.68}$.**

The parity chart includes data from the disruption experiments performed at both 10% and 20% solids (v/v) and at speeds above the respective critical impeller speeds.

Table 7.5 shows that Equation 7.51 describes the cell disruption in the slurry reactor poorly. Cell disruption in the slurry reactor therefore cannot be described by solid-cell collisions and solid-cell-reactor collisions alone. Since the coefficients of variance are similar for Equation 7.50 and Equation 7.52, their parity charts are compared in Figures 7.27 and 7.28 respectively. Both Equations 7.50 and.7.52 describe the cell disruption adequately, however, Equation 7.50 slightly underpredicts the experimental data, suggesting the need to consider solid-cell-solid collisions, solid-cell collisions and solid-cell-reactor collisions in the disruption mechanism.

The relative significance of each term in Equation 7.52 was investigated. For a particular solids concentration, the contribution of each of the terms was constant, irrespective of the agitation intensity. The contributions of the terms to k at solids volume fractions of 0.10 and 0.20 are summarised in Table 7.6. The solid-cell-solid collision term is dominant at both solids concentrations. However, its dominance is greater at 20% solids (v/v). The relative significance of the two disruption mechanisms can thus be altered by adjusting the solids concentration but not the power input to the system.

Table 7.6. **Contributions of terms in Equation 7.52 to k at solids volume fractions of 0.10 and 0.20.**

Solids Volume Fraction	Contribution of solid-cell-solid collision term to k (%)	Contribution of solid-cell collision and solid-cell-reactor collision term to k (%)
0.10	68.4	31.6
0.20	81.2	18.8

Since the solid-cell-solid collision term is dominant for both the 0.10 and 0.20 solids volume fractions, it follows that the exponent of Φ in Equation 7.38 and Equation 7.45 should lie closer to 2 than 1. It remains less than 2 because, as shown in this section, solid-cell collisions and solid-cell-reactor collisions cannot be discounted as a cause of cell disruption.

7.5 Application of Cell Disruption Models of Section 7.4 to Other Particulate Systems

The cell disruption models, described in Section 7.4, were further validated by applying them to the cell disruption data from the pitched-blade turbine (PTD) in the slurry reactor and to the cell damage data from the animal cell-microcarrier system, obtained by Croughan *et al.* (1988, 1989) and Croughan and Wang (1989).

7.5.1 Application of Model to Cell Disruption from the PTD in the Slurry Reactor

As discussed in Section 6.2.3, a physiological change in the *Saccharomyces cerevisiae* was observed during the course of the experimental work. The models presented in Section 7.4 were developed to describe the disruption data from the Rushton turbine experiments where the initial yeast batches were used. Equation 7.38 was re-fitted to the disruption experiments performed with the Rushton turbine using the physiologically changed yeast (Runs #10.50, 10.53, 10.65). The exponents of P/V and Φ in Equation 7.38 do not change with a change in the physiological state of the yeast cells since neither the collision frequency nor the fraction of kinetic energy, transferred from the impeller to the solid particles, is altered. The Least Squares fit using the physiologically changed yeast is shown in Equation 7.53. The increased value of the constant, A, in Equation 7.53, compared to Equation 7.38, reflects the increased first order disruption rate constants obtained with the physiologically changed yeast.

$$k = 8.92 \times 10^{-5} (P/V)^{0.56} \Phi^{1.64} \qquad \textbf{Equation 7.53}$$

$$k = 7.11 \times 10^{-5} (P/V)^{0.56} \Phi^{1.64} \qquad \textbf{Equation 7.38}$$

Equation 7.53 was applied to the k values of the pitched-blade turbine (PTD), determined using the physiologically changed yeast at speeds above the critical impeller speed. The parity chart, showing the agreement between the measured k values and those predicted from Equation 7.53, is presented in Figure 7.29. The coefficient of variance of this fit is 6.2%. This compares well with the coefficient of variance of 4.7% obtained for the fit of Equation 7.38 using the Rushton turbine data (Section 7.4.1).

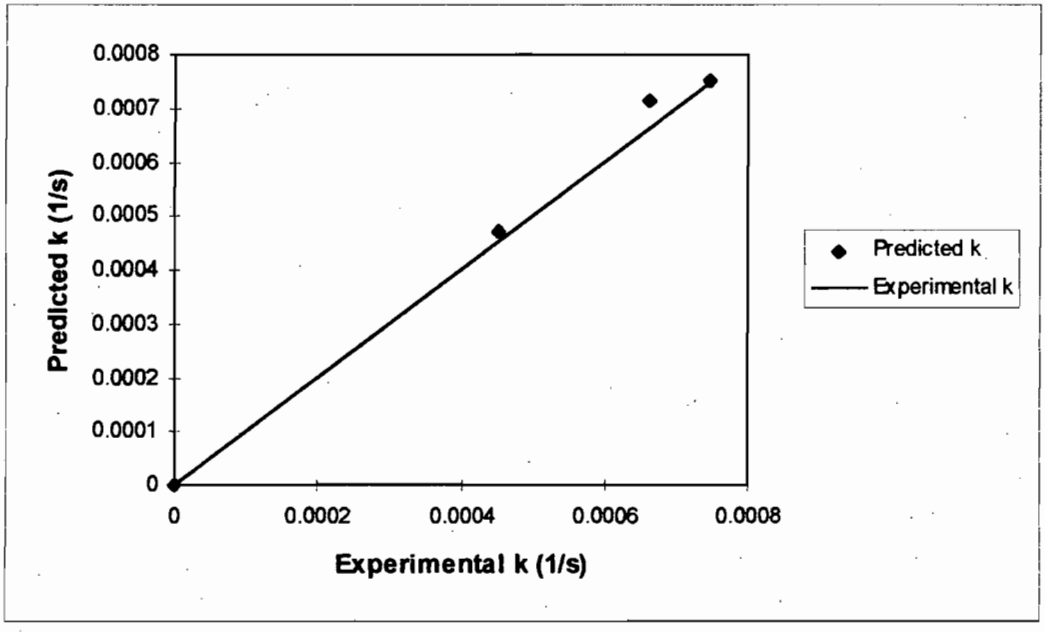

Figure 7.29. **Parity chart comparing experimental k values of the pitched-blade turbine to the predictions of k from Equation 7.53.**

The data in the parity chart was obtained at 20% solids (v/v) and at speeds above the critical impeller speed for the pitched-blade turbine (N_{JS} = 662rpm).

Equation 7.38 and Equation 7.53 can thus be used to predict the k values for both the Rushton turbine and the pitched-blade turbine, at speeds above the critical impeller speed. This implies that for a given power input above the critical impeller speed, the same cell disruption rate results independently of the flow pattern type. Furthermore, the k values from the pitched-blade turbine have the same dependency as the k values from the Rushton turbine on the energy and frequency of the collisions between the cells and solid particles, indicating that the same mechanism of cell disruption applies.

7.5.2 Application of Model to Cell Damage in Animal Cell-Microcarrier Systems

In animal cell-microcarrier systems, the dominant cell disruption mechanisms have been identified as cell-eddy interactions and collisions between solids bearing cells (microcarriers) and solids without attached cells (inert solid particles) (Croughan *et al.* 1987, 1988, 1989; Lakhotia and Papoutsakis 1992). Since Equation 7.38 only considers collisions between the cells and solid particles as the disruption mechanism, it cannot be applied to the animal cell-microcarrier data. Equation 7.49 was thus applied but was first modified to differentiate between the microcarrier (Φ_M) and the inert solid particle (Φ_i) volume fractions.

Microcarrier-cell-reactor interactions were not considered since they are negligible in the animal cell-microcarrier system (Cherry and Papoutsakis 1988, Croughan *et al.* 1989).

$$k = A (\varepsilon / \nu^3)^{3/4} + B c^2 \Phi_M^2 N^n + D c \Phi_M \Phi_i N^n \qquad \textbf{Equation 7.54}$$

This equation was applied to the cell death rate data, obtained by Croughan *et al.* (1988, 1989) and Croughan and Wang (1989), for FS-4 cells immobilised on Cytodex 1 microcarriers. This data set represents the most complete investigation into the effect of solids concentration and agitation intensity on the death rates of animal cells (Table 2.2). Values of these death rates are included in Appendix I. Application of Equation 7.54 to the animal cell death rates is justified since the death rate of the animal cells is essentially a measure of their disruption rate (Section 6.3.3).

At the low microcarrier concentration of 0.02% (v/v) and over the range of agitation intensities of 35 to 220 rpm (impeller tip speeds of 0.10 to 0.61 m s^{-1}) used by Croughan *et al.* (1989), the last two terms in Equation 7.54 are negligible. Hence Equation 7.55 is obtained. This equation describes the data well with a coefficient of variance of 3.3%.

$$k = 1.06 \times 10^{-9} (\varepsilon / \nu^3)^{3/4} \qquad \textbf{Equation 7.55}$$

The cell death rate data of Croughan *et al.* (1988) was measured at a constant microcarrier concentration of 0.1% (v/v) and an impeller speed of either 35 rpm or 150 rpm (impeller tip speeds of 0.10 and 0.42 ms^{-1} respectively). In these experiments, the inert solids concentration was varied up to 2.9% (v/v). At 35 rpm, negligible cell death rates were observed. Qualitatively, this is predicted by Equation 7.54 since at this low agitation intensity, each of the terms is small. At 150 rpm, significant cell damage occurred and since only Φ_i was varied, Equation 7.54 reduces to Equation 7.56. A Least Squares analysis yielded values of 0.187 and 0.003 for E and F, respectively, with a coefficient of variance of 4.5% for this fit. Equation 7.56 thus explains the linear dependence of the cell death rate on the inert solids concentration that Croughan *et al.* (1988) observed (Section 6.3.3).

$$k = E \Phi_i + F \qquad \textbf{Equation 7.56}$$

In the experiments of Croughan and Wang (1989), performed at a moderately high microcarrier concentration of 0.5% (v/v) and over the agitation intensity range of 35 to 150 rpm (impeller tip speeds of 0.10 to 0.42 m s^{-1}), cell damage was only observed at the sufficiently high impeller speed of 150 rpm. Cell

damage at 150 rpm results from both cell-eddy interactions and interactions between the attached cells and microcarriers. It was, however, not possible to determine the values of B and n in Equation 7.54 from a single data point.

Despite the fact that the values of B, D and n in Equation 7.54 could not be determined from the available cell damage data, Equation 7.54 is consistent with the trends in the cell death rate data of Croughan *et al.* (1988, 1989). The mechanistic model, presented in Section 7.4.3, can thus be applied to the animal cell-microcarrier system when the model is altered to account for both the inert solid and microcarrier concentrations.

7.6 Conclusions

In the development of a model which describes the first order disruption rate constants (k) from the slurry reactor in the region of complete solids suspension, the applicability of existing cell damage and disruption models was assessed. Models describing cell disruption in terms of the physical parameters of the system predicted the measured first order disruption rate constants (k) in this work well, when modified to account for both the solids concentration ($\Phi^{1.92}$) and either the impeller speed or the energy input per unit volume. The alteration of the fluid turbulence structure at solids concentrations of 10% and 20% (v/v) and the reduced response of the relatively large, dense silica particles to fluid eddies precluded the direct application of existing mechanistic models to the cell disruption in the slurry reactor. These mechanistic models were developed to describe the damage to animal cells immobilised on relatively small, neutrally buoyant microcarriers (Croughan *et al.* 1987, 1988; Cherry and Papoutsakis 1988, Lakhotia and Papoutsakis 1992, Yang and Wang 1992). However, a literature review (Nouri *et al.* 1987, Croughan *et al.* 1988, Caulet *et al.* 1996) indicated that interaction between the cells and fluid eddies is insignificant as a cell disruption mechanism in this work. In addition, cell disruption from interaction between the cells and entrained bubbles is negligible. Correlation of the first order disruption rate constants in this study with a redefined Turbulent Collision Severity (TCS) expression (accounting for both the energy ($\alpha\ \varepsilon^{0.5}$) and the frequency ($\alpha\ \varepsilon^{0.25}\Phi^2$) of the collisions between the cells and solid particles) supports the experimental observation that interactions between the cells and solid particles are the primary mechanism of cell disruption in the slurry reactor.

Three new models were developed to describe the first order disruption rate constants (k) obtained on agitation with the Rushton turbine using the slurry reactor. A modified mass transfer-type expression

describes the first order disruption rate constant in terms of the solids volume fraction and the power input per unit volume. In the second model, the power input term of the first model is replaced by a term quantifying energy input per circulation through the impeller zone. The third model is a mechanistic model, describing the types of collisions between the cells and solid particles that are responsible for the cell disruption. It accounts for the frequency and magnitude of the collision force between the cells and the solid particles. The excellent correlation of the k values in this work by these models verified that the primary cell disruption mechanism in the slurry reactor is collisions between the cells and particulates.

Examination of the terms in the three new models allows the following conclusions to be drawn:

1. The circulation time term (t_c) in the energy input expression of the second model suggests that cell disruption primarily occurs in the impeller region.
2. When the solids are completely suspended, cell disruption results from solid-cell-solid collisions, solid-cell collisions and solid-cell-reactor collisions.
3. The solid-cell-solid collision mechanism is dominant in the slurry reactor as a cause of cell disruption. The significance of this mechanism increases as the solids loading is increased and remains unaffected by changes in the agitation intensity.

These models were further validated by applying them to the cell disruption data generated using the pitched-blade turbine in the slurry reactor, and to cell damage data from the animal cell-microcarrier system (Croughan *et al.* 1988, 1989; Croughan and Wang 1989). The applicability of the mass transfer-type model to the first order disruption rate constants (k) from the pitched-blade turbine implies that for a given power input above the critical impeller speed, the same cell disruption rate results independently of the flow pattern type. It further indicates that the same mechanism of cell disruption applies to cell breakage from the two impellers in the regime of complete solids suspension.

Application of the new cell disruption models to the death rates of animal cells is justified since the death rate of the animal cells is essentially a measure of their disruption rate (Section 6.3.3). The new mechanistic model can be applied to the animal cell-microcarrier system when the model is altered to differentiate between inert solids and microcarrier particles. It was not possible to establish all the constants in the model as a result of insufficient cell damage data at impeller tip speeds above 0.3 ms^{-1} and solids concentrations

above 0.5% (v/v). However, the model describes the trends in the cell death rate data of Croughan *et al.* (1988, 1989) well.

Chapter 8: Modelling Cell Disruption when the Solids are Incompletely Suspended

8.1 Introduction

In this chapter, modelling of the first order disruption rate constant (k), in terms of the solids volume fraction (Φ) and the power input per unit volume (P/V), is discussed for the region of incomplete solids suspension. Models are developed for two systems: the slurry reactor in this study operated at speeds below the critical impeller speed, and the bead mills (Section 2.1.4) used by Mogren *et al.* (1974), Rehacek and Schaefer (1977) and Schutte *et al.* (1986). Although both these systems involve the use of inert solid particles to disrupt freely suspended cells, they differ with respect to the degree of suspension of the solid particles. In the slurry reactor, at impeller speeds below the critical impeller speed, the solid particles are only partially suspended. An increase in the agitation intensity below the critical impeller speed, increases the ratio of suspended solids to solids remaining on the vessel base. At the high solids volume fractions of approximately 45% (excluding interstitial volume) used in bead mills, all the solid particles are unsuspended. Kinetic energy is imparted to the solid particles by the motion of a number of discs mounted on the central shaft of a horizontally or vertically oriented grinding chamber (Section 2.1.4). The solid particles are accelerated in a radial direction, forming stream layers of different velocity. Cell disruption is achieved by the combined action of collisions and grinding between these stream layers of solid particles (Rehacek and Schaefer 1977, Kula and Schutte 1987).

The chapter begins with a review of the existing cell disruption models for the slurry reactor in the incompletely suspended solids regime. The mechanisms of cell disruption in this regime are discussed. These are used to develop a predictive model which describes the first order disruption rate constants obtained in this study on agitation with the Rushton turbine or the pitched-blade turbine. Modelling of cell disruption in bead mills is then addressed. An existing model, developed to describe the extent of cell disruption in a bead mill, is presented and is extended to include the effects of solids concentration and cell concentration. The applicability of a mass transfer-type model to describe the rate of cell disruption in a bead mill is also assessed.

8.2 The Slurry Bioreactor

8.2.1 Literature Models of Cell Disruption

A literature search of models, developed to describe cell disruption in slurry reactors in the regime of incomplete solids suspension, revealed that the only model was that of Pearce (1993). As discussed in Section 2.2.3, Pearce (1993) determined a power law relationship between the first order disruption rate constants (k) of *Saccharomyces cerevisiae* in a slurry reactor and the impeller speed, over a range which straddled the critical impeller speed (Equation 2.2). Although the model describes the first order disruption rate constants below the critical impeller speed relatively well ($R^2 = 0.953$), it only applies to a 20% solids volume fraction.

$$k = 1.278 \times 10^{-9} N^{1.906} \qquad \textbf{Equation 2.2}$$

The inadequacy of an expression of the form of Equation 2.2 was further illustrated by application to the k values in this work, determined on agitation with the Rushton turbine at speeds below the critical impeller speed. The expression was fitted to three data sets: agitation at 10% solids (v/v), agitation at 20% solids (v/v), and the combination of these two data sets. The constants obtained and the respective correlation coefficients are presented in Table 8.1. The power law expression describes the first order disruption rate constants relatively well at a constant solids volume fraction. However, the poor fit of this expression to the combined 10% and 20% solids (v/v) data confirms the need to account for both the impeller speed and the total solids concentration in the cell disruption model. Comparison of the correlation coefficients in Table 8.1 at either 10% or 20% solids (v/v) with those of the corresponding expressions for the completely suspended solids regime (Table 7.1) shows that an expression of the form of Equation 2.2 provides a poorer fit to the data at speeds below the critical impeller speed. This may result because the model does not account for the relative quantity of unsuspended solids as a function of the impeller speed. It is shown in Section 8.2.3 that this is an important consideration in modelling the cell disruption in the slurry reactor in the incompletely suspended solids regime.

Table 8.1. **Constants and correlation coefficients of power law expression, $k = A N^b$, applied to k values from agitation intensity experiments.**

Data Set	A	b	R^2
10% Data	2.63×10^{-13}	3.20	0.901
20% Data	8.16×10^{-12}	2.86	0.963
10% and 20% Data	5.51×10^{-18}	5.22	0.516

8.2.2 Mechanisms of Cell Disruption

The suitability of the mass transfer-type model, developed for the completely suspended solids regime, was assessed. This model is presented in Equation 7.38 and Equation 7.53 (Chapter 7) for the two physiological states of yeast used. In applying this model to the k values below the critical impeller speed, the total solids volume fraction (Φ_T) of either 0.10 or 0.20 was used for the Φ term. Figure 8.1 represents the parity chart, comparing the measured and predicted k values for both the Rushton and pitched-blade turbines. Equation 7.38 and Equation 7.53 overpredict the measured k values in the incompletely suspended solids regime. This was anticipated since these equations describe the cell disruption in terms of collisions between the cells and suspended solid particles (Section 7.4.1). In the incompletely suspended solids regime, only a fraction of the solid particles are suspended and this fraction varies with the agitation intensity.

$$k = 7.11 \times 10^{-5} (P/V)^{0.56} \Phi^{1.64} \qquad \textbf{Equation 7.38}$$

$$k = 8.92 \times 10^{-5} (P/V)^{0.56} \Phi^{1.64} \qquad \textbf{Equation 7.53}$$

The applicability of Equation 7.38 and Equation 7.53 was re-assessed in the incompletely suspended solids regime, using the volume fraction of suspended solids (Φ) for the Φ term. To estimate the volume fraction of suspended solids as a function of the impeller speed, Equation 5.7 and Equation 5.8, respectively, were used for the Rushton and pitched-blade turbines to calculate B, the percentage mass of solids in suspension per mass of liquid (Section 5.4). Equation 8.1 was used to convert B to the volume fraction of suspended solids (Φ).

$$B = \frac{\rho_s \Phi (100)}{\rho (1 - \Phi)}$$ **Equation 8.1**

where ρ is the density of the yeast suspension (kg/m^3) and ρ_s is the density of the silica particles (kg/m^3). Figure 8.2 represents the parity chart which compares the measured k values to those predicted by Equations 7.38 and 7.53 when the volume fraction of suspended solids (Φ) is used for the Φ term. There is poor agreement between the measured and predicted first order disruption rate constants. To understand this, the percentage of suspended solids, calculated using Equation 8.2, was plotted as a function of the impeller speed for the Rushton and pitched-blade turbines (Figure 8.3).

$$\% \ Solids \ Suspended = \frac{Volume \ fraction \ of \ suspended \ solids}{Total \ volume \ fraction \ of \ solids} x100$$

$$= \frac{\Phi}{\Phi_T} x\,100$$ **Equation 8.2**

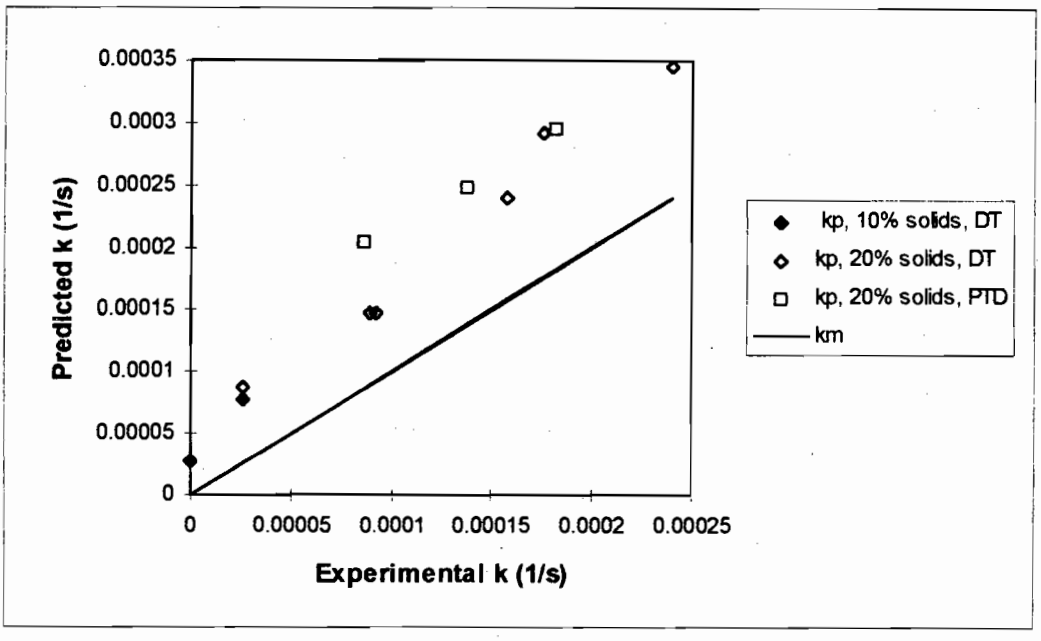

Figure 8.1. **Parity chart comparing experimental k values and those predicted by Equation 7.38 (initial yeast batches) and Equation 7.53 (physiologically changed yeast).**
k_p signifies the predicted k values, k_m signifies the measured k values. The total solids volume fraction of either 0.10 or 0.20 was used for the Φ term in the calculation of k_p.

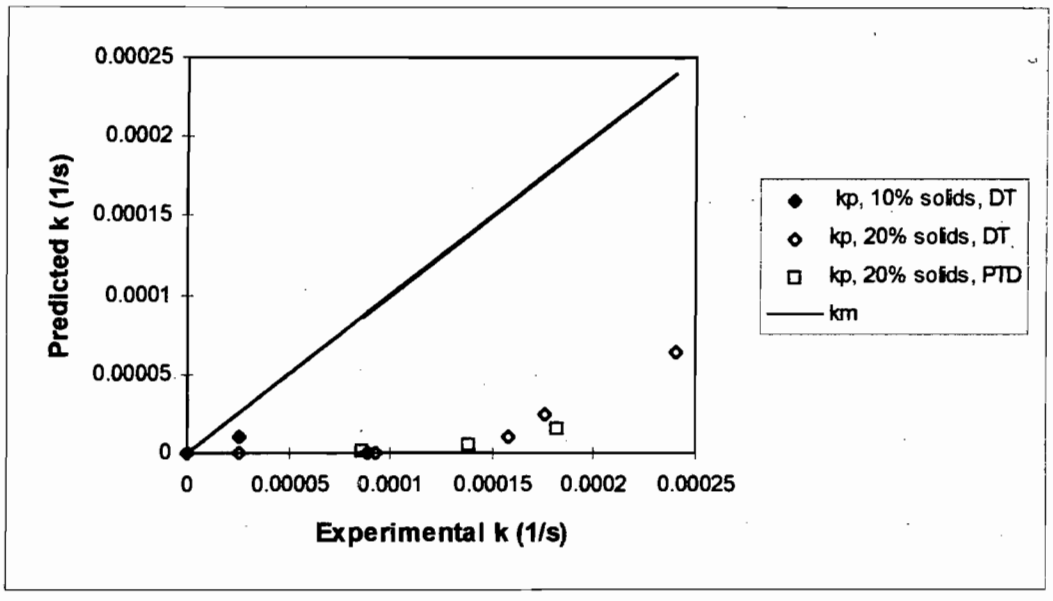

Figure 8.2. **Parity chart comparing experimental k values and those predicted by Equation 7.38 and Equation 7.53.**

k_p signifies the predicted k values, k_m signifies the measured k values. The volume fraction of suspended solids was used for the Φ term in the calculation of k_p.

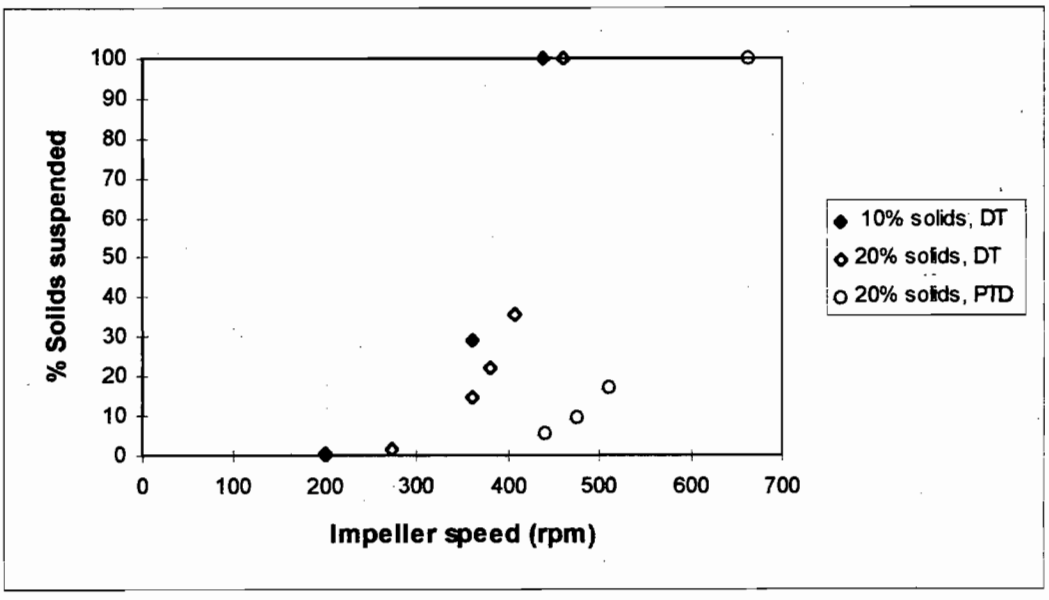

Figure 8.3. **Percent solids suspended for the Rushton (DT) and pitched-blade (PTD) turbines as a function of the impeller speed.**

Data at both 10% and 20% (v/v) total solids are included.

Figure 8.3 shows that for both the Rushton and pitched-blade turbines, less than 36% of the solid particles are suspended at the impeller speeds used in this study below the respective critical impeller speeds. These suspended solids contribute less than 40% to the overall cell disruption rate constant (Figure 8.2). This suggests that the unsuspended solid particles contribute significantly to the cell disruption in the slurry reactor. It is postulated that the mechanism by which this occurs is the grinding action of adjacent unsuspended solid particles. The existence of a grinding mechanism betweeen layers of adjacent particles of different velocity is supported by the work of Funk and Dinger (1994). At speeds below the critical impeller speed, the slurry reactor can thus be considered to consist of two regions which are characterised by different cell disruption mechanisms: an upper region, where all the solid particles are suspended and where cell disruption results from solid-cell-solid collisions, solid-cell collisions and solid-cell-reactor collisions (Section 7.4.3), and a lower region, where the solids are not suspended and where cell disruption results from the grinding action of adjacent solid particles.

8.2.3 Modelling the Cell Disruption

In this section, a predictive model is developed to describe the first order disruption rate constants (k) from the slurry reactor at speeds below the critical impeller speed. Factors that affect the first order disruption rate constant in the incompletely suspended solids regime are discussed before the model is presented. In Section 8.2.2, the suitability of the mass transfer-type model, developed for the completely suspended solids regime, was assessed for the k values measured at speeds below the critical impeller speed. Since Equation 7.38 and Equation 7.53 did not describe the k values well (Figure 8.1), a generalised form of the mass transfer-type expression was applied to the k values at 0.10 and 0.20 total solids volume fractions (Φ_T):

$$k = A\,(P/V)^b\,(\Phi_T)^c \qquad \textbf{Equation 7.37}$$

A Least Squares analysis (Appendix H) yielded values of 2.89×10^{-5}, 1.24 and 4.16 for *A*, *b* and *c* respectively. A coefficient of variance of 73.5% was obtained for this fit. The poor agreement between the measured and predicted k values, especially at the larger values of k, is illustrated in the parity chart (Figure 8.4). At the lower k values, few of the solid particles are suspended (Figure 8.3) and it is therefore not necessary to differentiate between the suspended and unsuspended solid particles. Use of a total solids volume fraction (Φ_T) describes the data relatively well. However, at the larger k values, the power input per unit volume is greater with the result that the suspended solids are more significant (Figure 8.3). The poor agreement of this model with the larger k values therefore suggests that, in the model, the volume fraction of suspended solids needs to be considered separately from the unsuspended solids in the slurry reactor.

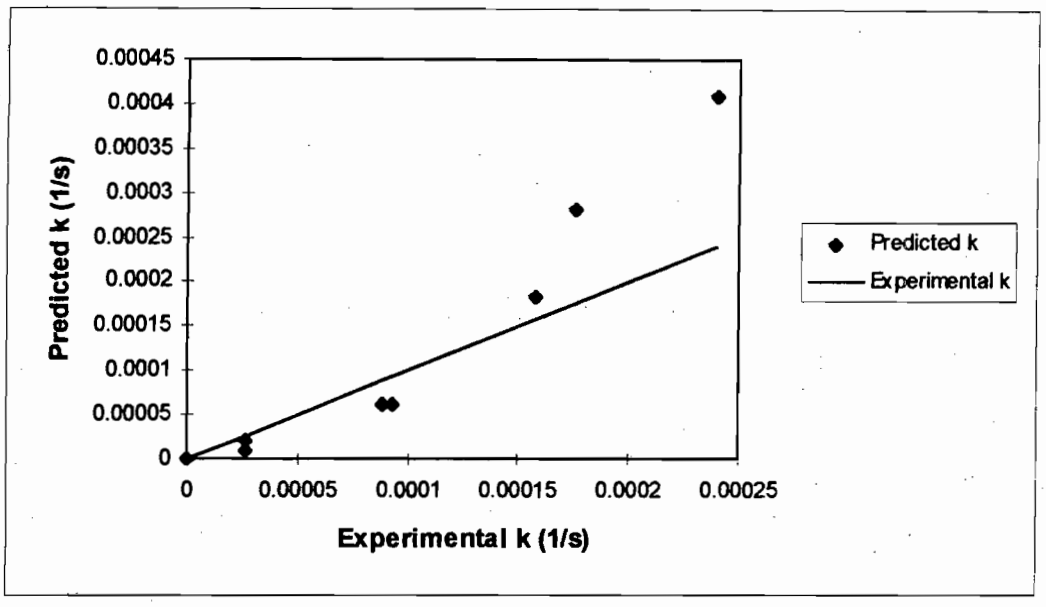

Figure 8.4. **Parity chart comparing experimental k values and those predicted by the expression, $k = 2.89 \times 10^{-5} (P/V)^{1.24} (\Phi_T)^{4.16}$.**
Data from the disruption experiments, performed with the Rushton turbine at 0.10 and 0.20 total solids volume fraction (Φ_T), are shown.

To distinguish between the volume fraction of suspended and unsuspended solids, the contribution to the first order disruption rate constant from collisions between the cells and suspended solid particles ($k_{collision}$) was differentiated from the rate of cell disruption from the grinding action of adjacent unsuspended solid particles (k_{grind}). Equation 7.38 and Equation 7.53 were used to quantify $k_{collision}$ (depending on the yeast batch used). The volume fraction of suspended solid particles (Φ) was used for the Φ term in this calculation (Section 8.2.2). k_{grind} was defined as the difference between the measured k values and the corresponding values of $k_{collision}$.

Figure 8.5 shows the variation of the k_{grind} values as a function of the volume fraction of unsuspended solid particles for the disruption experiments performed with the Rushton turbine at 0.10 and 0.20 total solids volume fraction (Φ_T). The volume fraction of unsuspended solids was calculated from Equation 8.3.

$$\begin{pmatrix} Volume\ fraction\ of \\ unsuspended\ solids \end{pmatrix} = \begin{pmatrix} Total\ solids \\ volume\ fraction \end{pmatrix} - \begin{pmatrix} Volume\ fraction\ of \\ suspended\ solids \end{pmatrix}$$

Hence:

$$\begin{pmatrix} Volume\ fraction\ of \\ unsuspended\ solids \end{pmatrix} = \Phi_T - \Phi \qquad \textbf{Equation 8.3}$$

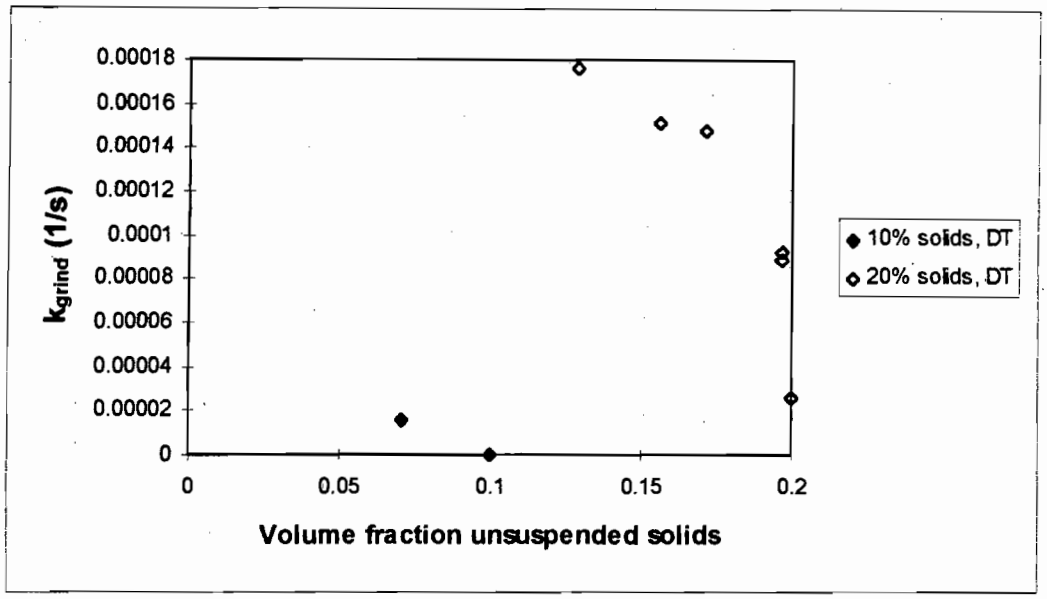

Figure 8.5. **Rate of cell disruption from grinding of the cells by adjacent unsuspended solid particles (k_{grind}) as a function of the volume fraction of unsuspended solids.**
Data from disruption experiments, performed using the Rushton turbine (DT) at 10% and 20% (v/v) total solids, are shown.

The discontinuity in Figure 8.5 between the data at 0.10 and 0.20 total solids volume fraction (Φ_T) results from the difference in the power input per unit volume. At a 0.13 volume fraction of unsuspended solid particles and a total solids volume fraction of 0.20, the power input per unit volume is 1878 W m^{-3}. However, at a 0.10 volume fraction of unsuspended solids and a total solids volume fraction of 0.10 (negligible solids suspension), the power input per unit volume is 163 W m^{-3}. Visual observation of the unsuspended solid particles in the tank showed that approximately 85% of the unsuspended solid particles were stationary at 163 W m^{-3}, whereas the entire bed of unsuspended solid particles was involved in grinding at the data point where the power input per unit volume was 1878 W m^{-3}. This, in addition to the greater momentum of the solid particles at 1878 W m^{-3}, account for the larger value of k_{grind} at this point. The existence of stagnant regions in the unsuspended solid bed at low values of the power input per unit volume also explains the decrease of k_{grind} with increasing volume fraction of unsuspended solids at a constant total solids volume fraction (Figure 8.5). As the power input per unit volume is increased, solids

suspension increases and a greater fraction of the unsuspended solid particle bed is involved in the grinding action.

To describe the first order disruption rate constants (k) in the incompletely suspended solids regime, it is necessary to account for different impeller flow patterns. To overcome the effect of the physiological change in the yeast on the first order disruption rate constants (k) (Section 6.2.3), the ratio, $k_{collision}/k_{total}$, was considered, where k_{total} is the measured first order disruption rate constant. Since expressions for $k_{collision}$ were developed for the initial (Equation 7.38) and physiologically changed (Equation 7.53) yeast batches, use of the ratio, $k_{collision}/k_{total}$, allows comparison to be made between the cell disruption from the Rushton and pitched-blade turbines.

The relationship between the ratio, $k_{collision}/k_{total}$, and the power input per unit volume is shown in Figure 8.6 for the Rushton and pitched-blade turbines. An increase in the power input per unit volume increases the volume fraction of suspended solids (Figure 8.7). It has been shown that $k_{collision}$ increases with both the power input per unit volume and the volume fraction of suspended solids (Section 7.4.1). Figure 8.6 also shows that at a fixed power input per unit volume and a total solids volume fraction of 0.20, the ratio, $k_{collision}/k_{total}$, is slightly greater for the pitched-blade turbine than for the Rushton turbine. This accords with the slight increase in solids suspension ($\approx$ 3%) found on using the pitched-blade turbine at a fixed power input below the critical impeller speed, compared to the Rushton turbine (Figure 8.7). Comparison of the values of $k_{collision}/k_{total}$ in Figure 8.6 for the Rushton turbine at 10% and 20% (v/v) total solids, at a fixed power input per unit volume, shows that $k_{collision}/k_{total}$ is greater at 10% total solids concentration. At a fixed power input per unit volume at these two total solids concentrations, Equations 5.7 and 8.1 predict the same volume fraction of suspended solids. Hence the values of $k_{collision}$ (Equation 7.38) are the same. This suggests that the contribution of the grinding mechanism to the cell disruption is greater at 20% total solids (v/v). At this solids loading, the impeller is partially submerged in the stationary silica bed (C = 57 mm (Section 3.2); silica bed depth $\approx$ 57 mm). However, at 10% total solids, the impeller clearance above the top of the stationary bed is 28 mm. Hence a greater amount of grinding occurs at 20% total solids.

A predictive model was developed which describes the values of $k_{collision}/k_{total}$ for the Rushton and pitched-blade turbines in terms of the volume fraction of suspended solids (Φ) and the operating parameters: the total solids volume fraction (Φ_T) and the power input per unit volume (P/V). The former was calculated using Equations 5.7, 5.8 and 8.1 (Section 8.2.2). An expression of the form:

$$\frac{k_{collision}}{k_{total}} = 60.4\left(\frac{\Phi}{\Phi_T - 1.18x10^{-2}\left(P/V\right)^{0.24}}\right)^{1.36} \qquad \textbf{Equation 8.4}$$

was found to fit the values of $k_{collision}/k_{total}$ with a coefficient of variance of 4.1%. The parity chart, showing the excellent agreement between the calculated and predicted values of $k_{collision}/k_{total}$, is shown in Figure 8.8. Hence knowing the impeller power input and impeller speed at a total solids volume fraction of 0.10 to 0.20, and the impeller type (to enable calculation of suspended solids), the value of $k_{collision}/k_{total}$ can be predicted. Since the value of $k_{collision}$ can be calculated from either Equation 7.38 or Equation 7.53, the value of k_{total} can then be determined. The constraint of Equation 8.4 is that it can only be applied at impeller speeds below the respective critical impeller speeds.

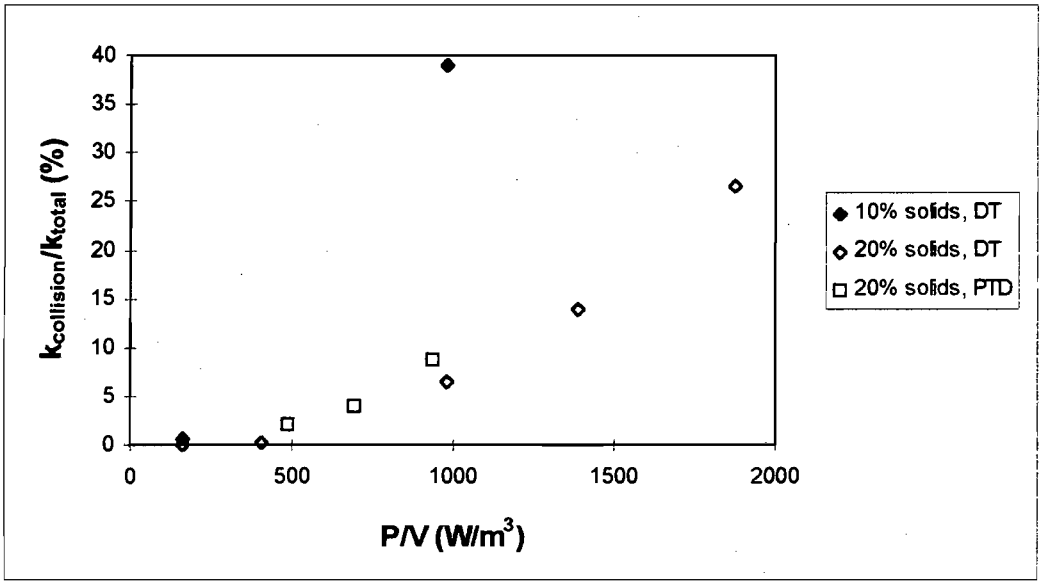

Figure 8.6. **Relationship between the ratio, $k_{collision}/k_{total}$, and the power input per unit volume for the Rushton (DT) and pitched-blade (PTD) turbines.**
Data from disruption experiments performed at both 10% and 20% (v/v) total solids are included.

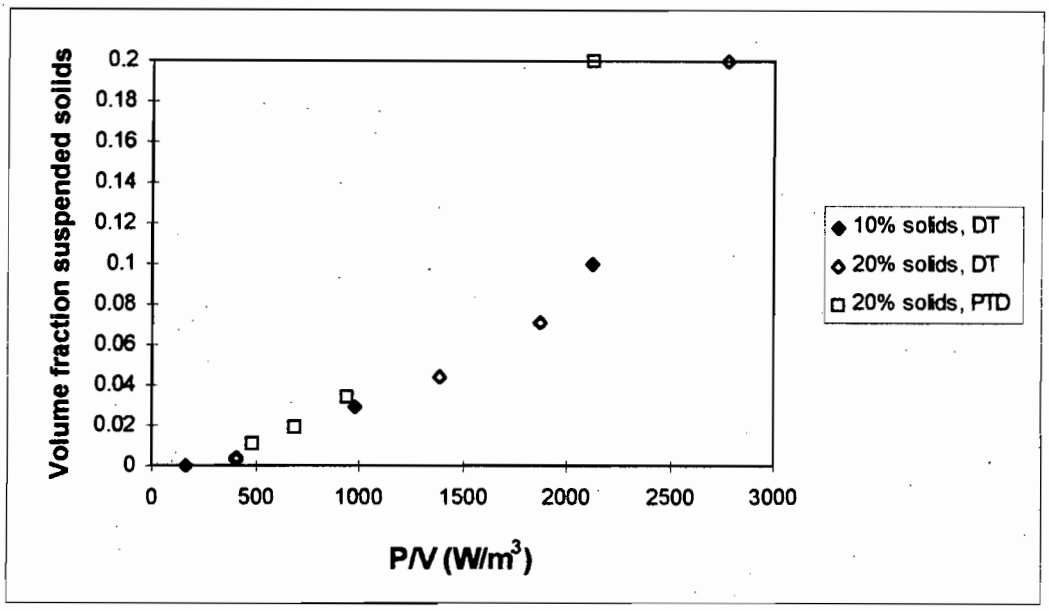

Figure 8.7. **Volume fraction of suspended solids as a function of the power input per unit volume for the Rushton (DT) and pitched-blade (PTD) turbines.**

Volume fraction of suspended solids is calculated according to Equations 5.7, 5.8 and 8.1.

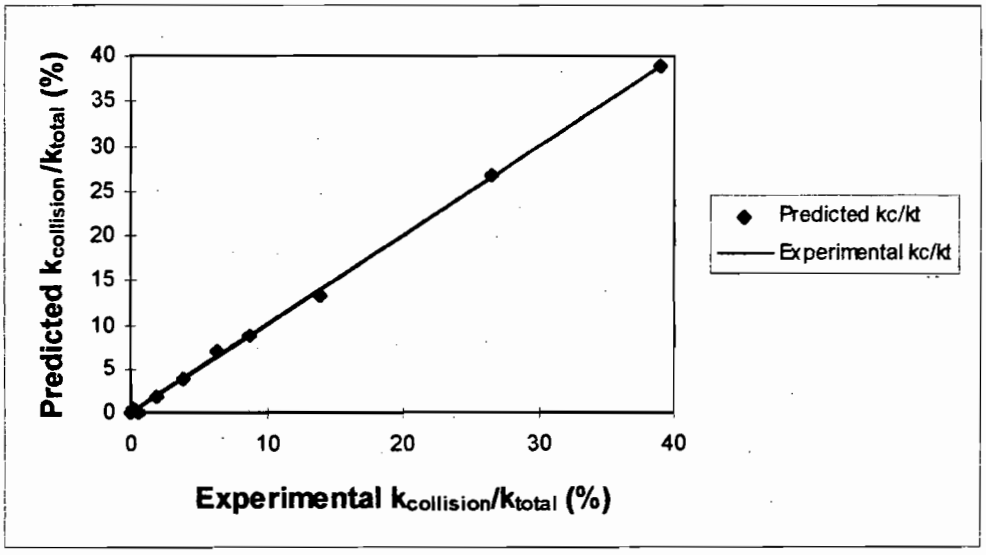

Figure 8.8. **Parity chart comparing calculated values of $k_{collision}/k_{total}$ and those predicted by Equation 8.4.**

Data from the disruption experiments performed at 10% and 20% (v/v) total solids, and using the Rushton or pitched-blade turbines, are included.

8.3 Bead Mills

As mentioned in Section 8.1, bead mills are fundamentally different from slurry reactors in that all the solid particles are unsuspended and cell disruption is caused by collisions and grinding between stream layers of solid particles of different velocity (Kula and Schutte 1987). In the slurry reactor system, when the solid particles are partially suspended, cell disruption is caused by collisions between the cells and suspended solid particles and by the grinding action of adjacent unsuspended solid particles (Section 8.2.2). However, as in the slurry reactor system, cell breakage in bead mills follows first order kinetics with respect to protein release (Engler 1985, Schutte *et al.* 1986, Harrison 1991). In bead mills operated in batch mode, this is represented by:

$$\ell n\left(\frac{R_i}{R_i - R}\right) = k\,t$$

OR $R = R_i\,(1-\exp(-k\,t))$ **Equation 6.8**

where R is the soluble protein released at time t (mg protein / g cell), R_i is the maximum soluble protein released under the operating conditions (mg protein / g cell), and k is the first order disruption rate constant (s^{-1}). For continuous operation, the kinetics of cell disruption has been expressed by viewing the mill as a series of CSTRs (Limon-Lason *et al.* 1979):

$$\left(\frac{R_i}{R_i - R}\right) = \left(1 + \frac{k\,\tau}{j}\right)^j$$

OR $$\left(\frac{1}{1 - R/R_i}\right) = \left(1 + \frac{k\,\tau}{j}\right)^j$$ **Equation 8.5**

where τ is the mean residence time (s) and j is the number of CSTRs in series.

8.3.1 Literature Models of Cell Disruption

A review of the bead mill literature showed that no model has been developed to describe the first order disruption rate constant, k, in terms of the system parameters, such as the power input per unit volume and the solids concentration. However, the degree or extent of cell disruption, R/R_i, in bead mills has been successfully correlated with the energy input per unit volume (E) by Reuss (1988). In continuously

operated systems, this is defined as the ratio of the power input (P) to the biosuspension flow rate through the mill (Q) whereas in systems operated in batch mode, the energy input per unit volume is calculated as Pt/V. Here, V is the reactor volume and t is the time of cell disruption. Figure 8.9 shows the relationship between R/R_i and P/Q obtained by Reuss (1988), using the cell disruption data of Mogren *et al.* (1974). The mathematical form of this relationship was not presented by Reuss. Reuss (1988) also did not account for the variation of the cell concentration (c) in this correlation since this effect contributed less than 10% to the overall value of R/R_i. The correlation of Reuss (1988) is extended in Section 8.3.2.2 to account for the effect of biomass concentration.

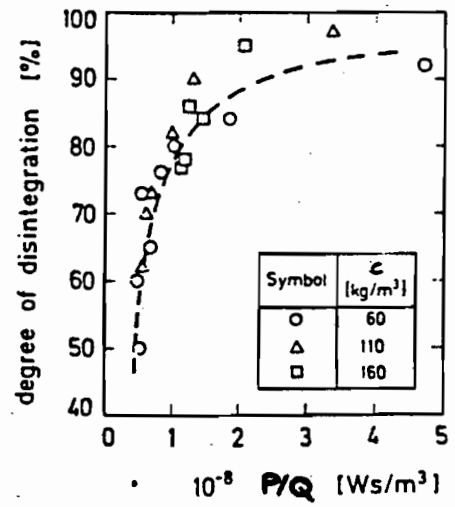

Figure 8.9. **Correlation between the extent of disruption of *Saccharomyces cerevisiae* in a bead mill and the energy input per unit volume (P/Q) (Reuss 1988).**
Correlation determined using experimental data of Mogren *et al.* (1974). c signifies the cell dry weight concentration in kg m^{-3}.

A shortcoming in the correlation of Reuss (1988) is that it does not account for the solids concentration, which has a significant effect on cell disruption in bead mills (Currie *et al.* 1972). As a result, it does not adequately describe the extent of cell disruption in bead mills where the solids volume fraction is varied. This is illustrated in Figure 8.10, where the correlation of Reuss (1988) has been applied to the data of Rehacek and Schaefer (1977). These workers investigated the disruption of *Saccharomyces cerevisiae* in a Netzsch LM20 bead mill over the solids concentration range of 46 to 54% (v/v) and a biosuspension flow

rate range of 1.39×10^{-5} to 5.56×10^{-5} m^3 s^{-1}. This shortcoming in the correlation of Reuss is addressed in Section 8.3.2.2.

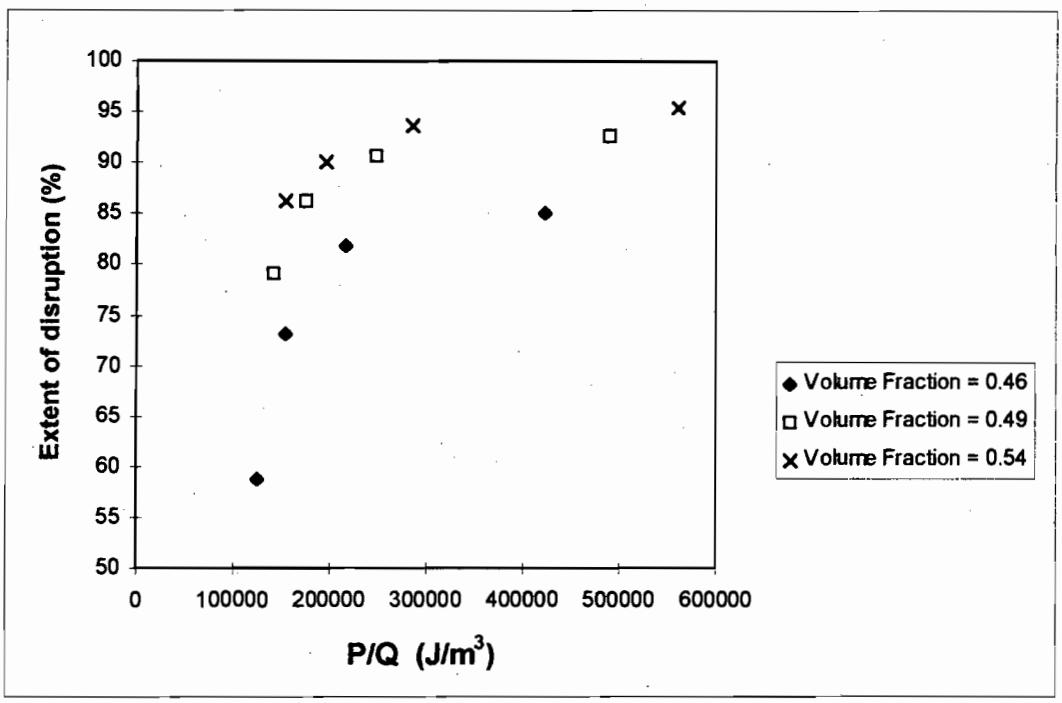

Figure 8.10. **Correlation of bead mill data of Rehacek and Schaefer (1977) with the parameter of Reuss (1988).**

8.3.2 Modelling the Cell Disruption

8.3.2.1 Modelling the First Order Disruption Rate Constant

The applicability of an expression of the form of the mass transfer-type model (Equation 7.37) to the first order disruption rate constants measured in bead mills was assessed. Since the solid particles are unsuspended in bead mills, the solids volume fraction is denoted by Φ_U in this expression to differentiate it from the volume fraction of suspended solids (Φ), used in modelling the cell disruption in the slurry reactor.

$$k = A\,(P/V)^b\,\Phi_U^c \qquad \textbf{Equation 7.37}$$

No data could be found in the bead mill literature where the solids volume fraction and agitation intensity were varied simultaneously at a constant biosuspension flowrate, particle size, impeller configuration and cell concentration. Currie *et al.* (1972) determined the first order disruption rate constants of

Saccharomyces cerevisiae over a solids concentration range of 21 to 47% (v/v) at a constant impeller speed, biosuspension flow rate, particle size, impeller configuration, cell concentration and temperature. However, Equation 7.37 cannot be applied to the data of Currie *et al.* (1972) since these workers do not present the total power consumption data of the bead mill as a function of the solids concentration (Engler 1985). The only suitable data found for the application of Equation 7.37 was that of Schutte *et al.* (1986). These workers established the effect of agitation intensity, over the range of 700 to 4500 rpm (impeller tip speeds of 5.1 to 15.0 ms^{-1}), on the first order disruption rate constants of *Saccharomyces cerevisiae* at a constant solids loading, biosuspension flow rate, glass bead diameter, impeller configuration and cell concentration. Equation 7.37 was thus applied to two of the bead mills used by Schutte *et al.* (1986): a Netzsch Molinex LME 20 bead mill and a Netzsch Molinex LME 20 "double disc" bead mill. The Netzsch Molinex LME 20 bead mill consists of 16 agitator discs, arranged eccentrically on the central shaft as shown in Figure 8.11 (a). In the Netzsch Molinex LME 20 "double disc" bead mill, two agitator discs are used to form one double disc. A total of 10 double discs are arranged on the stirrer shaft (Figure 8.11 (b)).

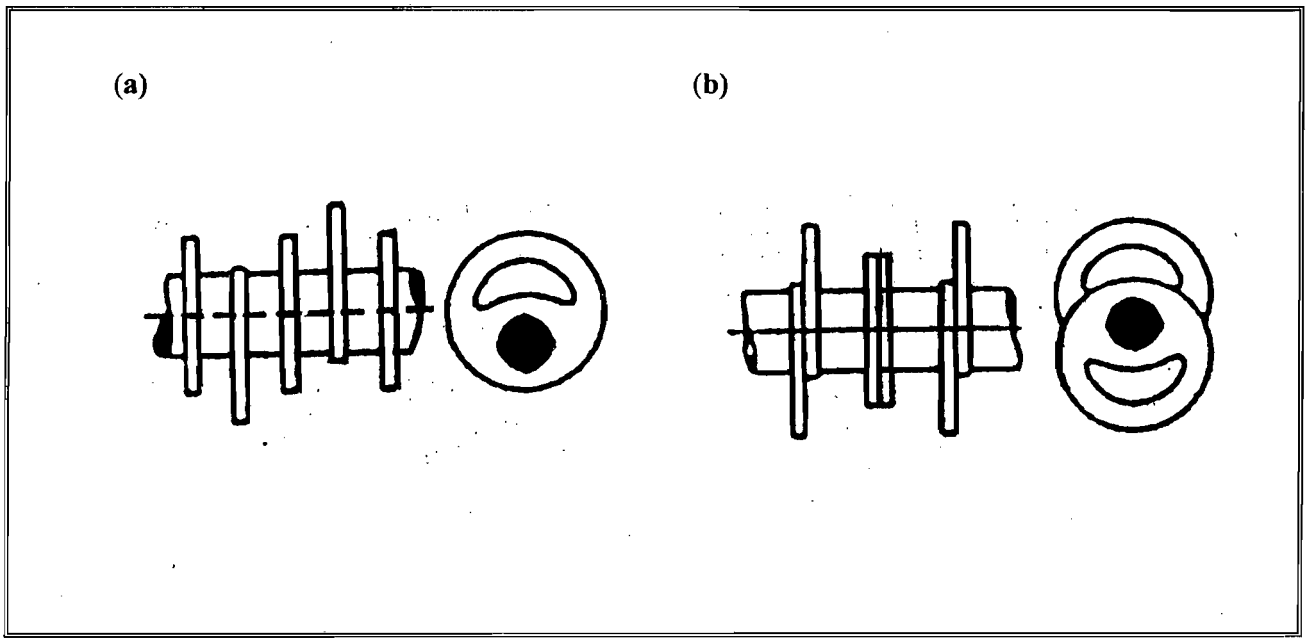

Figure 8.11. Impeller configuration in (a) the Netzsch Molinex LME 20 bead mill and (b) the Netzsch Molinex LME 20 "double disc" bead mill (Schutte *et al.* 1986).

The regressions obtained from Least Squares fits (Appendix H) of Equation 7.37 to the data of Schutte *et al.* (1986) are summarised in Table 8.2 with their corresponding coefficients of variance. The data of Schutte *et al.* (1986), used in these regressions, are included in Appendix J. Table 8.2 shows that a mass transfer-type expression describes the first order disruption rate constants of Schutte *et al.* (1986) well.

Energy balances were performed to determine the maximum values of the exponents of (P/V) in Equations 8.6 and 8.7 and hence to validate the respective best-fit values of 0.66 and 1.04. For the sixteen impellers of the Netzsch Molinex LME 20 bead mill, the impeller speed (N) is directly proportional to $P^{0.79}$ (Schutte *et al.* 1986). If all the energy were transferred from the impellers to the solid particles in the bead mill, the first order disruption rate constant (k) would be proportional to N^2 (Equation 7.42). This implies that the maximum value of the exponent of (P/V) for the Netzsch Molinex LME 20 bead mill is 1.58. Similarly, for the twenty impellers of the Netzsch Molinex LME 20 "double disc" bead mill, the impeller speed (N) is directly proportional to $P^{0.80}$ (Schutte *et al.* 1986) and the maximum value of the exponent of (P/V) is 1.60. The greater magnitude of these calculated maximum values compared to the respective best-fit values in Equations 8.6 and 8.7 verifies their magnitude.

The greater exponent of (P/V) for the Netzsch Molinex LME 20 "double disc" bead mill, compared to the Netzsch Molinex LME 20 bead mill, may be attributed to the greater number of impellers in the former mill. The geometrical design and configuration of the impellers in the bead mills also affect the transfer of kinetic energy to the grinding elements and the mean residence time of the suspension in the grinding chamber (Kula and Schutte 1987). Therefore, although the grinding chambers and biosuspension flow rates are identical for the two bead mills of Schutte *et al.* (1986), the mean residence time of the suspension is greater for the "double disc" impeller configuration (Schutte *et al.* 1986) and consequently more energy is transferred from the agitators per unit volume of suspension. The different exponents obtained for the (P/V) term in Equation 7.37 for different impeller configurations in bead mills contrasts with the slurry reactor system where the same exponent of (P/V) was obtained for the Rushton and pitched-blade turbines (Section 7.5.1) at speeds above the critical impeller speed.

Table 8.2 **Application of Equation 7.37 to the bead mill data of Schutte *et al.* (1986).**

Model Properties	**Netzsch Molinex LME 20 bead mill**	**Netzsch Molinex LME 20 "double disc" bead mill**
Data source	Schutte *et al.* (1986)	Schutte *et al.* (1986)
Conditions	Volume = 0.0227 m^3 4625 ≤ P ≤ 7625 W $\Phi_U = 0.45$ Q = 4.93 x 10^{-5} m^3 s^{-1} d_p = 500-850 μm c = 400 kg m^{-3} *	Volume = 0.0227 m^3 4375 ≤ P ≤ 6500 W $\Phi_U = 0.45$ Q = 4.93 x 10^{-5} m^3 s^{-1} d_p = 500-850 μm c = 400 kg m^{-3} *
Model	$k = 5.55 \times 10^{-6} (P/V)^{0.66}$	$k = 8.84 \times 10^{-7} (P/V)^{1.04}$
Coefficient of Variance (%)	0.9	1.7
Equation Number	**8.6**	**8.7**

* Wet weight

8.3.2.2 Modelling the Extent of Cell Disruption

In the previous section, it was shown that the first order disruption rate constants (k) in bead mills, determined at a constant biosuspension flow rate, glass bead diameter, impeller configuration and cell concentration, are described by a mass transfer-type model. In the bead mill literature, cell disruption has also been reported in terms of an extent of cell disruption (R/R_i) as opposed to a rate (k) of cell disruption (Mogren *et al.* 1974, Rehacek and Schaefer 1977, Schutte *et al.* 1983). In continuously operated bead mills, these parameters are related by Equation 8.5. However, since the residence time distributions are not presented for a number of these bead mills, it is not possible to determine the equivalent number of CSTRs

in series (j) and hence to convert R/R_i to k. The correlation of Reuss (1988) (Section 8.3.1) was thus extended in this work to describe the extent of cell disruption (R/R_i) in terms of the solids volume fraction (Φ_U), the biomass concentration (c) and the energy input per unit volume (P/Q). This relationship was applied to the data of Mogren *et al.* (1974) and Rehacek and Schaefer (1977) (refer to Appendix J for data as a function of the operating parameters) and to the extent of cell disruption determined in this study using the slurry reactor and the Rushton turbine at 10% and 20% total solids (v/v) and at speeds greater than the critical impeller speed (Section 6.4).

A Weibull function with an exponent of 3 (Equation 8.9) described the data of Mogren *et al.* (1974) and Rehacek and Schaefer (1977) well and provided a relatively good description of the extent of cell disruption from the slurry reactor at speeds greater than the critical impeller speed. The Weibull function is suitable for describing "S" shaped curves and the "S" shaped dependence of R/R_i on $\ln(P/Q^{a/Xspan}\ \Phi^{b/Xspan}\ c^{d/Xspan})$ for each of the data sets is clearly seen in Figure 8.12. The two parameters of Equation 8.8 have physical meaning: X_{min} is the value of the x-intercept; and X_{span} is a parameter that determines the width of the "S" function. However, in fitting the Weibull function to the data using a Least Squares Analysis (Appendix H), it was not possible to decouple these parameters (Equation 8.9). Values of the parameters in Equation 8.9 are shown in Table 8.3 for each data set with the corresponding coefficient of variance from fitting this expression.

$$\frac{R}{R_i} = 100\left\{1 - \exp\left[-\left(\frac{\ln\left((P/Q)^a\ \Phi^b\ c^d\right) - X_{\min}}{X_{span}}\right)^3\right]\right\} \qquad \textbf{Equation 8.8}$$

$$\frac{R}{R_i} = 100\left\{1 - \exp\left[-\left(\ln\left((P/Q)^{a/Xspan}\ \Phi^{b/Xspan}\ c^{d/Xspan}\right) - \frac{X_{\min}}{X_{span}}\right)^3\right]\right\} \qquad \textbf{Equation 8.9}$$

Direct comparison of the model parameters (Table 8.3) for the three data sets is not possible as a result of the difficulty in decoupling X_{min} and X_{span} and hence in calculating the values of *a*, *b* and *c*. However, the ratio of b/X_{span} to a/X_{span} for the slurry reactor (1.65) (Table 8.3) is consistent with the ratio of the corresponding exponents (1.79) in the Energy Input Model (Section 7.4.2). Table 8.2 indicates that the exponent of (P/V) is of a similar order of magnitude for bead mills and the slurry reactor, despite variations in the geometric configuration of the bead mills. The large value of 5.99 for the ratio of b/X_{span} to a/X_{span}

for the bead mill of Rehacek and Schaefer (1977) (Table 8.3) therefore suggests that the value of b is larger in this system than in the slurry reactor system, operated in the region of complete solids suspension. The value of b indicates the types of interactions between the cells and solid particles responsible for cell disruption (Section 7.4.3). It is therefore postulated that the larger value of b for the bead mill system of Rehacek and Schaefer (1977) results from both collisions and shear forces between the stream layers of solid particles contributing to the cell disruption. The exponent of the biomass concentration term (d/X_{span}), obtained on regressing the bead mill data of Mogren *et al.* (1974), is 4% of the exponent of the energy input term (a/X_{span}). This accords with the small effect of cell concentration on the extent of cell disruption, reported in the bead mill literature (Limon-Lason *et al.* 1979, Kula and Schutte 1987).

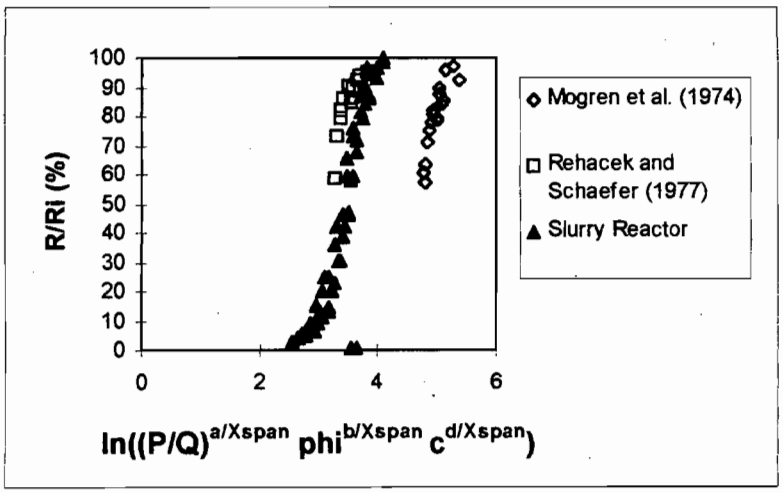

Figure 8.12. **Relationship between the extent of disruption (R/R_i) and $\ln((P/Q)^{a/X_{span}} \Phi^{b/X_{span}} c^{d/X_{span}})$ for the bead mills of Mogren *et al.* (1974) and Rehacek and Schaefer (1977) and the slurry reactor of this study, operated at speeds above the critical impeller speed.**

Parameters defined in nomenclature.

Table 8.3 **Constants and coefficients of variance of Equation 8.9, applied to the extents of cell disruption from bead mills (Mogren *et al.* 1974, Rehacek and Schaefer 1977) and from the slurry reactor of this work.**

Model Properties	**Dyno-Muhle KD-5 bead mill**	**Prototype I of Netzsch LM 20 bead mill**	**Slurry reactor (Rushton turbine, $N>N_{JS}$)**
Data source	Mogren *et al.* (1974)	Rehacek and Schaefer (1977)	This Study
Conditions	Volume = 0.0044 m^3 $5650 \le P \le 12\,370$ W $\Phi_U = 0.50$ $1.64\times10^{-5} \le Q \le 1.36\times10^{-4}$ $m^3\,s^{-1}$ d_p = 500-750 μm $60 \le c \le 160$ kg m^{-3}	Volume = 0.019 m^3 $5880 \le P \le 8560$ W $0.46 \le \Phi_U \le 0.54$ $1.39\times10^{-5} \le Q \le 5.56\times10^{-5}$ $m^3\,s^{-1}$ d_p = 318-418 μm c = 150 kg m^{-3}	Volume = 0.00245 m^3 $3.8 \le P \le 26.8$ W $0.10 \le \Phi \le 0.20$ $5.24\times10^{-8} \le V/t \le 2.04\times10^{-5}$ m^3s^{-1} d_p = 600-850 μm c = 52.8 kg m^{-3}
Model			
a/X_{span}	0.27	0.23	0.27
b/X_{span}	-	1.39	0.44
d/X_{span}	0.01	-	-
X_{min}/X_{span}	3.79	2.23	2.56
Coefficient of Variance (%)	4.9	4.3	12.9

8.4 Conclusions

Modelling the first order disruption rate constants, determined at speeds below the critical impeller speed in the slurry reactor, was first approached by applying a model developed by Pearce (1993). The inapplicability of this model to the combined disruption data at 10% and 20% (v/v) solids motivated the development of a new model. Application of the mass transfer-type model (Section 7.4.1), developed for the completely suspended solids regime, to the first order disruption rate constants measured below the critical impeller speed indicated that unsuspended solid particles in the slurry reactor contribute significantly to the cell disruption. At speeds below the critical impeller speed, the slurry reactor was therefore considered to consist of two regions, characterised by different cell disruption mechanisms: an upper region where all the solid particles are suspended and cell disruption results from collisions between the cells and solid particles; and a lower region where the solid particles are not suspended and cell disruption results from the grinding action of adjacent particles.

In the incompletely suspended solids regime in the slurry reactor, an increase in impeller speed increases the volume fraction of suspended solids as well as the fraction of the unsuspended solid bed involved in grinding. In addition, at a fixed global power input to the slurry reactor when using the Rushton turbine, the mass of unsuspended solids involved in grinding is greater at 20% total solids (v/v) than at 10% total solids (v/v). A mechanistic model of the cell disruption needs to account for these factors, in addition to the momentum of the solid particles and the fact that the pitched-blade turbine suspends more solids than the Rushton turbine at a fixed power input.

A predictive model was developed which describes the overall first order disruption rate constants for both the Rushton and pitched-blade turbines as a function of the rate of cell disruption from collisions between the cells and suspended solid particles ($k_{collision}$), the volume fraction of suspended solids (Φ) and the operating parameters: the total solids volume fraction (Φ_T) and the power input per unit volume (P/V). This relationship has been validated at a total solids volume fraction of either 0.10 or 0.20.

A literature review showed that no models have been developed to describe the first order disruption rate constants (k) in bead mills as a function of the operating parameters. The applicability of a mass transfer-type expression to the k values, determined by Schutte *et al.* (1986) for the Netzsch Molinex LME 20 bead mill and the Netzsch Molinex LME 20 "double disc" bead mill, was therefore assessed. This expression describes the variation in the k values with the power input per unit volume well. The scarcity of data in the

bead mill literature describing k as a function of the solids concentration and the power input per unit volume precluded the application of this expression to other bead mill systems. The exponent of the power input per unit volume term is a function of the number, geometrical design and configuration of the impellers.

Cell disruption in the bead mill literature is also expressed in terms of the extent of cell disruption (R/R_i). Conversion of R/R_i to k in continuously operated systems requires the residence time distribution of the bead mill. The lack of residence time distribution data for a number of bead mill systems motivated the development of a model which would describe R/R_i in terms of the operating parameters. The correlation of Reuss (1988), describing R/R_i as a function of the energy input per unit volume (E), was extended in this work to include the effect of solids concentration and biomass concentration. Using the bead mill data of Mogren *et al.* (1974) and Rehacek and Schaefer (1977), a Weibull function with an exponent of 3 was found to describe this relationship. This function further provided a relatively good description of the extent of cell disruption from the slurry reactor using the Rushton turbine at speeds greater than the critical impeller speed and total solids concentrations of 10% and 20% (v/v).

Although it was not possible to decouple all the parameters in the Weibull function, the ratio of the exponents of the energy input and solids concentration terms for the slurry reactor data was consistent with the corresponding ratio in the Energy Input Model (Section 7.4.2). The larger exponent of the solids concentration term, obtained for the bead mill system compared to the slurry reactor system in the completely suspended solids regime, was attributed to the additional mechanism of grinding in bead mills. Cell concentration had a small effect on the extent of cell disruption in bead mills.

Chapter 9: Conclusions and Recommendations

The damage to and disruption of microbial cells by hydrodynamic stress is an important consideration in biological processes owing to the detrimental effect on the productivity of processes where cells are cultivated. Furthermore, cell disruption may be required in downstream processing for the release of intracellular products. This dissertation has been concerned with a study of the disruption of freely suspended *Saccharomyces cerevisiae* using biologically inert silica particles in a stirred tank reactor in the absence of aeration. The results from this study find application in bead mill systems, minerals bioprocessing, soil bioremediation and immobilised biocatalyst systems, where cells and particulates are used. While the effect of completely suspended solid particles on cell damage and disruption is relatively well understood in animal cell-microcarrier cultures and immobilised cell systems, little work has been performed to investigate the effect of incompletely suspended solids on cell disruption. This work provides added understanding and modelling of the disruption kinetics of freely suspended cells in the incompletely and completely suspended solids regimes, as a function of the solids loading, agitation intensity and impeller flow pattern. The major findings from this investigation are summarised in this chapter. Thereafter, recommendations regarding solids suspension and cell disruption in a slurry reactor are made. Areas in which additional research may yield fruitful results on cell damage and disruption in particulate systems are discussed.

9.1 Conclusions

To establish the effect of incompletely and completely suspended solid particles on cell disruption, the solids suspension in the stirred tank needed to be quantified as a function of the solids loading, agitation intensity and impeller flow pattern. A literature review revealed that solids suspension could be quantified either in terms of the degree of solids homogeneity or the critical impeller speed. The critical impeller speed is defined as the speed at which the transition from the incompletely to the completely suspended solids regimes occurs. Since the critical impeller speed is a more direct and easier measure of this transition point, it was chosen as the method to quantify solids suspension in this study. The critical impeller speed can also be related to the operating parameters using correlations of the form of Zwietering (1958) and Takahashi *et al.* (1993). An expression relating the volume fraction of suspended solids to the impeller speed was required in modelling the cell disruption.

For the Rushton turbine, the critical impeller speed (N_{JS}) was measured at 5%, 10%, 15%, 20% and 40% solids (v/v) by visual observation and from the maxima in curves of the power number (N_p) as a function of

the impeller Reynolds number (N_{RE}). Measurements of the critical impeller speed using these two methods agreed to within 9%. When using the pitched-blade turbine at 20% solids (v/v), the critical impeller speed could only be measured by visual observation since the N_p-N_{RE} curve did not yield a maximum, owing to the flow pattern of this impeller. Expressions, based on the form of the Zwietering equation, were developed for both the Rushton and pitched-blade turbines to relate the critical impeller speed to the volume fraction of suspended solids.

Cell disruption was measured in terms of soluble protein release into the supernatant. A first order disruption expression described the profile of protein release as a function of time and allowed the cell disruption to be quantified in terms of the kinetic parameters: the rate constant (k) and the maximum soluble protein released under the operating conditions (R_i). Measurement of the soluble protein release and microscopic observation of the disrupted cells (Olympus BX40 microscope) indicated a greater degree of cell disruption using the French Press compared to the slurry reactor. The maximum available soluble protein for release (R_M) was therefore measured for each yeast batch using the French Press. For each disruption experiment, R_i was normalised with respect to R_M. This ratio (R_i/R_M) was defined as the maximum extent of cell disruption.

Inaccurate kinetic parameters were obtained when the first order expression was fitted to cell disruption data obtained before R_i had reached its maximum value. The duration of the cell disruption experiments was therefore determined by the length of time taken for the soluble protein release to reach its maximum value under the particular operating conditions. The use of different yeast batches in determining the disruption kinetic parameters was validated.

Although cell disruption over a 10 hour period in the slurry reactor was negligible in the absence of solid particles, significant cell disruption occurred at 5% to 40% (v/v) solids, indicating that interaction between the cells and solid particles is the dominant cell disruption mechanism. Furthermore, since a constant maximum extent of cell disruption was observed using the Rushton and pitched-blade turbines at all the hydrodynamic conditions investigated in the presence of solid particles, it was concluded that the level of solids suspension does not affect the maximum extent of cell disruption.

At 5 to 40% solids (v/v) and using the Rushton turbine at 750 rpm (impeller tip speed of 2.91 m s^{-1}), the first order disruption rate constant (k) exhibits a power law dependence on the solids volume fraction. The impeller speed used in this set of disruption experiments exceeded the critical impeller speed for all conditions used. The cell disruption experiments performed over 200 to 900 rpm (impeller tip speeds of

(P). The third model is a mechanistic model which describes the types of collisions between the cells and solid particles responsible for cell disruption. The equivalence of the three models was shown. In these models, only collisions between the cells and solid particles are considered as the disruption mechanism. The excellent correlation of the rate constants in this work by these models verified that the primary cell disruption mechanism in the slurry reactor is collision between the cells and solid particles.

A number of conclusions can be drawn from examination of the terms in the new models, regarding the process of cell disruption in the slurry reactor in the completely suspended solids regime. Correlation of the first order disruption rate constants with the energy input per pass through the impeller zone (Pt_c) suggests that cell disruption from collisions between the cells and solid particles primarily occurs in the impeller region. Cell disruption in the slurry reactor results from solid-cell-solid collisions, solid-cell collisions and solid-cell-reactor collisions. The solid-cell-solid collision mechanism is dominant. Its significance increases as the solids loading is increased and remains unaffected by changes in the agitation intensity.

The validity of the new models was further assessed by applying them to the cell disruption data from the pitched-blade turbine in the slurry reactor, and to the cell damage data, obtained by Croughan *et al.* (1988, 1989) and Croughan and Wang (1989), for the animal cell-microcarrier system. The mass transfer-type model satisfactorily describes the first order disruption rate constants (k) from the pitched-blade turbine at speeds above the critical impeller speed. This implies that, in the completely suspended solids regime, the cell disruption mechanism is the same for both the Rushton and pitched-blade turbines and that for a given power input, the same disruption rate is observed for these impellers. The new mechanistic model describes trends in the cell death rates of animal cells, immobilised on microcarriers, when the model is altered to account for both the microcarrier and inert solid particle concentrations. However, as a result of insufficient cell damage data at impeller tip speeds above 0.3 m s^{-1} and solids concentrations above 0.5% (v/v), the constants in the model could not be determined.

A literature review of existing models which describe the cell disruption in slurry reactors in the regime of incomplete solids suspension revealed only the model of Pearce (1993). The inability of this model to describe the first order disruption rate constants from the slurry reactor at varying total solids concentrations motivated the development of a new model. In modelling the cell disruption in the slurry reactor in the regime of incomplete solids suspension, the slurry reactor was considered to consist of two regions: an upper region, where the solid particles are suspended and cell disruption results from collisions between the cells and solid particles; and a lower region, where the solid particles are not suspended and cell disruption results from the grinding action of adjacent solid particles.

It was shown that a mechanistic model of the cell disruption in the slurry reactor, at speeds below the critical impeller speed, needs to account for the volume fraction of suspended solids, the particle momentum and the fraction of the unsuspended solid bed involved in grinding. Furthermore, the effect of the flow patterns of the pitched-blade turbine and the Rushton turbine must be considered. A predictive model was developed which allows the calculation of the first order disruption rate constants for both the Rushton and pitched-blade turbines as a function of the volume fraction of suspended solids (Φ) and the operating parameters: the total solids volume fraction (Φ_T) and the power input per unit volume (P/V).

The bead mill system is an example of a system where all the solid particles are unsuspended. Cell disruption in bead mills is achieved by the combined action of collisions and grinding between stream layers of solid particles of different velocity (Kula and Schutte 1987). The final objective of this dissertation was to develop a model which describes the cell disruption in bead mills, and to compare this model to those developed for the cell disruption in slurry reactors. A mass transfer-type expression was found to fit the first order disruption rate constants (k) determined by Schutte *et al.* (1986) for the Netzsch Molinex LME 20 bead mill and the Netzsch Molinex LME 20 "double disc" bead mill. Application of this expression to other bead mill systems was not possible owing to the scarcity of data in the bead mill literature on disruption rate as a function of the solids concentration and the power input per unit volume. The exponent of the power input per unit volume term was shown to be a function of the number, geometrical design and configuration of the impellers.

Cell disruption in the bead mill literature is also expressed in terms of the extent of cell disruption (R/R_i). Reuss (1988) has developed a correlation to describe the extent of cell disruption in continuously operated bead mills as a function of the energy input per unit volume of suspension (P/Q). This correlation was extended in this work to include the effect of solids concentration and biomass concentration on R/R_i. A Weibull function with an exponent of 3 described this relationship for the bead mill data of Mogren *et al.* (1974) and Rehacek and Schaefer (1977) and further provided a relatively good description of the extent of cell disruption determined using the slurry reactor at speeds greater than the critical impeller speed.

Although it was not possible to decouple all the parameters in the Weibull function, a good correspondence between the ratio of the exponents of the solids concentration and energy input terms in the Weibull

function and the Energy Input Model (Section 7.4.2) was found for the slurry reactor operated at speeds above the critical impeller speed. The Weibull function further indicated that the exponent of the solids concentration term is larger in the bead mill system than in the slurry reactor system operated in the completely suspended solids regime. This was attributed to the additional mechanism of grinding in bead mills. The small exponent obtained for the biomass concentration term in the bead mill system reflects its negligible effect on the extent of cell disruption in bead mills (Limon-Lason *et al.* 1979, Kula and Schutte 1987).

9.2 Recommendations

From this study, the following recommendations are made regarding solid suspension and cell disruption in the slurry reactor:

i. Visual observation and curves of the power number as a function of the impeller Reynolds number are suitable for determining the critical impeller speeds using the Rushton turbine. However, when using pitched-blade turbines at the scale in this study, the critical impeller speed can only be measured by visual observation.

ii. A first order kinetic expression is appropriate for describing the profile of soluble protein release as a function of time in the slurry reactor.

iii. If the objective of the process is to maximise the cell disruption rate, the slurry reactor should be operated at high solids volume fractions (>20%) and at high impeller speeds, above the critical impeller speed. The Rushton turbine should be used for agitation.

iv. If the objective of the process is to minimise the disruption of the cells, low solids loadings (<10% (v/v)) and low impeller speeds should be employed. The optimum choice of the operating parameters would involve a trade-off between minimising cell disruption and maximising the mass transfer of oxygen and nutrients to the cells. The pitched-blade turbine should be used in preference to the Rushton turbine to minimise cell disruption.

9.3 Areas for Further Research

The following areas of research offer promise for the further understanding of cell disruption in the presence of particulates:

i. This study investigated the disruption of stationary phase *Saccharomyces cerevisiae* in the presence of inert particulates. However, in many industrial processes, micro-organisms are cultivated in the presence of particulates. It would therefore be fruitful to investigate the effect of particulates on the

metabolic rate, the metabolic pathway and the morphology of micro-organisms of industrial importance, as a function of the solids concentration, agitation intensity and impeller flow pattern.

ii. The growth of micro-organisms in the presence of particulates requires sparging of the slurry to achieve a sufficiently high oxygen concentration for the cell growth. The contribution of sparging to the damage and disruption of cells in particulate systems needs to be assessed.

iii. To fully understand the mechanism and extent of cell disruption in the slurry reactor as a function of time, the hypothesis of incremental cell breakage during the process of cell disruption needs to be investigated by measurement of the release of marker enzymes as a function of time. Examples of marker enzymes characteristically found in the cell wall, cytoplasm and mitochondria of *Saccharomyces cerevisiae* are invertase, glucose-6-phosphate dehydrogenase and fumarase respectively (Tuite and Oliver 1991).

References

Abrahamson, J. 1975. Collision rates of small particles in a vigorously turbulent fluid. ***Chem. Eng. Sci.* 30:** 1371-1379.

Aiba, S., Kitai, S., Ishida, N. 1962. ***J. Gen. Appl. Microbiol.* 9:** 103-108. In: M. Reuss, D. Josic, M. Popovic and W.K. Bronn. 1979. Viscosity of yeast suspensions. ***Eur. J. Appl. Microbiol. Biotechnol.* 8:** 167-175.

Atkinson, B., Black, G.M., Lewis, P.J.S., Pinches, A. 1979. Biological particles of given size, shape, and density for use in biological reactors. ***Biotechnol. Bioeng.* 21:** 193-200.

Atkinson, B., Black, G.M., Pinches, A. 1981. p 75. In: P.F. Cooper and B. Atkinson (eds). ***Biological Fluidised Bed Treatment of Water and Wastewater.*** Ellis Horwood, Chichester. In: G.M. Black, C. Webb, T.M. Matthews and B. Atkinson. 1984. Practical reactor systems for yeast cell immobilisation using biomass support particles. ***Biotechnol. Bioeng.* 26:** 134-141.

Bailey, A.D. 1993. ***An Assessment of Oxygen Availability, Iron Build-up and the Relative Significance of Free and Attached Bacteria, as Factors Affecting Bio-oxidation of Refractory Gold-bearing Sulphides at High Solids Concentrations.*** Ph.D. thesis, Department of Chemical Engineering, University of Cape Town, South Africa.

Bailey, J.E., Ollis, D.F. 1986. ***Biochemical Engineering Fundamentals.*** 2nd edition. McGraw-Hill, Singapore.

Baldi, G., Conti, R., Alaria, E. 1978. Complete suspension of particles in mechanically agitated vessels. ***Chem. Eng. Sci.* 33:** 21-25.

Baldi, G., Conti, R., Gianetto, A. 1981. Concentration profiles for solids suspended in a continuous agitated reactor. ***AIChE J.* 27:** (6), 1017-1020.

Bandyopadhyay, K.K., Ghose, T.K. 1982. Studies on immobilised *Saccharomyces cerevisiae*. III. Physiology of growth and metabolism on various supports. ***Biotechnol. Bioeng.* 24:** 805-815.

Barresi, A., Baldi, G. 1987. Solid dispersion in an agitated vessel. ***Chem. Eng. Sci.* 42:** (12), 2949.

Barrett, J., Hughes, M.N., Karavaiko, G.I., Spencer, P.A. 1993. ***Metal Extraction by Bacterial Oxidation of Minerals.*** J.Burgess and E. Horwood (eds.). Ellis Horwood Ltd, England.

Bates, R.L., Fondy, P.L., Fenic, J.G. 1966. Impeller characteristics and power, Chapter 3. In: V.W Uhl and J.B Gray (eds.). ***Mixing: Theory and Practice.*** Academic Press, New York.

Bayer, M.E. 1967. Response of cell walls of *Escherichia coli* to a sudden reduction of the environmental osmotic pressure. ***J. Bacteriol.*** **93:** (3), 1104-1112.

Beyer, M., Ebner, H.G., Klein, J. 1986. Influence of pulp density and bioreactor design on microbial desulphurisation of coal. ***Appl. Microbiol. Biotechnol.*** **24:** 342-346.

Black, G.M., Webb, C., Matthews T.M., Atkinson, B. 1984. Practical reactor systems for yeast cell immobilisation using biomass support particles. ***Biotechnol. Bioeng.*** **26:** 134-141.

Bohnet, M., Niesmak, G. 1980. Distribution of solids in stirred suspensions. ***Ger. Chem. Eng.*** **3:** 57-65.

Boon, M., Hansford, G.S., Heijnen, J.J. 1995. The role of bacterial ferrous oxidation in the bio-oxidation of pyrite. In: T. Vargas, C.A. Jerez, J.V. Wiertz and H. Toledo (eds.). ***Biohydrometallurgical Processing.*** Vol 1. University of Chile.

Bourne, J.R., Zabelka, M. 1980. ***Chem. Eng. Sci.*** **35:** 533. In: N Harnby, M.F. Edwards and A.W. Nienow (eds.). 1992. ***Mixing in the Process Industries.*** 2nd edition. Chapter 16. Butterworth-Heinemann Ltd, Oxford.

Bradford, M.L., Krishnamoorthy, R.A.J. February 1991. Consider bioremediation for waste site cleanup. ***Chem. Eng. Prog.*** 80-85.

Breytenbach, J.N. 1995. ***An Investigation of Particle Collection Efficiency in Different Particle-bubble Contacting Environments in Flotation.*** MSc thesis, Department of Chemical Engineering, University of Cape Town, South Africa.

Brierley, J.A. 1978. Thermophilic iron-oxidising bacteria found in copper leaching dumps. 1978. ***Appl. Environ. Micro.*** **36:** (3), 523-535.

Brierley, J.A., Wan, R.Y., Hill, D.L., Logan, T.C. 1995. Bio-oxidation heap pretreatment technology for processing lower grade refractory gold ores. In: T. Vargas, C.A. Jerez, J.V. Wiertz and H. Toledo (eds.). ***Biohydrometallurgical Processing.*** University of Chile.

Bujalski, W., Konno, M., Nienow, A.W. 1988. ***Proc. 6th European Conference on Mixing.*** BHRA. Cranfield, pp 389-398. In: N. Harnby, M.F. Edwards and A.W. Nienow (eds.). 1992. ***Mixing in the Process Industries.*** 2nd edition. Chapter 16. Butterworth-Heinemann Ltd, Oxford.

Burrows, S. 1970. Baker's Yeast, Chapter 7. In: A.H. Rose and J.S. Harrison (eds.). ***The Yeasts: Yeast Technology.*** Vol 3. Academic Press, London.

Cabib, E., Roberts, R., Bowers, B. 1982. Synthesis of the yeast cell wall and its regulation. ***Annu. Rev. Biochem.*** **51:** 763-793.

Cabral., J.M.S., Novias, J.M., Kennedy, J.F. 1986. Immobilisation studies of whole microbial cells on transition metal activated inorganic supports. ***Appl. Microbiol. Biotechnol.*** **23:** 157-162.

Calderbank, P.H., Moo-Young, M.B. 1959. ***Trans. Inst. Chem. Eng.*** **37:** 28. In: A. Prokop and R.K. Bajpai. 1992. The sensitivity of biocatalysts to hydrodynamic shear stress. ***Adv. Appl. Microbiol.*** **37:** 165-232.

Caulet, P.J.C., van der Lans, R.G.J.M., Luyben, K.Ch.A.M. 1996. Hydrodynamical interactions between particles and liquid flows in biochemical applications. ***Chem. Eng. J.*** **62:** 193-206.

Chalmers, J.J., Bavarian, F. 1991. Microscopic visualisation of insect cell-bubble interactions II: The film and bubble rupture. ***Biotechnol. Prog.*** **7:** (2), 151-159.

Chapman, C.M., Nienow, A.W., Cooke, M., Middleton, J.C. 1983. Particle-gas-liquid mixing in stirred vessels. Part 1: Particle-liquid mixing. ***Chem. Eng. Res. Des.*** **61:** 71-81.

Cherry, R.S., Papoutsakis, E.T. 1988. Physical mechanisms of cell damage in microcarrier cell culture bioreactors. ***Biotechnol. Bioeng.*** **32:** 1001-1014.

Cherry, R.S., Kwon, K.Y. 1990. Transient shear stresses on a suspension cell in turbulence. ***Biotechnol. Bioeng.*** **36:** 563.

Chisti, Y., Moo-Young, M. 1986. Disruption of microbial cells for intracellular products. ***Enzyme Microb. Technol.*** **8:** 194-204.

Cilliers, J.J., Harrison, S.T.L. 1996. The effect of viscosity on the recovery and concentration of micro-organisms using mini-hydrocyclones, pp 123-133. In: D. Claxton, L. Svarovsky and M. Thew (eds.). ***Hydrocyclones '96***. MEP, UK.

Cook, T.M. 1964. Growth of *Thiobacillus thiooxidans* in shaken culture. ***J. Bacteriol.*** **88:** (3), 620-623.

Costes, J., Couderc, J.P. 1988. Study by laser Doppler anemometry of the turbulent flow induced by a Rushton turbine in a stirred tank: influence of the size of the units - II. Spectral analysis and scales of turbulence. ***Chem. Eng. Sci.*** **43:** (10), 2765-2772.

Coulson, J.M., Richardson, J.F,. Backhurst, J.R., Harker, J.H. 1991. ***Chemical Engineering: Particle Technology and Separation Processes***. Vol 2. 4th edition. Pergamon Press, Oxford.

Croughan, M.S., Hamel, J.F.P., Wang, D.I.C. 1987. Hydrodynamic effects on animal cells grown in microcarrier cultures. ***Biotechnol. Bioeng.*** **29:** 130-141.

Croughan, M.S., Hamel, J.F.P., Wang, D.I.C. 1988. Effects of microcarrier concentration in animal cell culture. ***Biotechnol. Bioeng.*** **32:** 975-982.

Croughan, M.S., Sayre, E.S., Wang, D.I.C. 1989. Viscous reduction of turbulent damage in animal cell culture. ***Biotechnol. Bioeng.*** **33:** 862-872.

Croughan, M.S., Wang, D.I.C. 1989. Growth and death in over-agitated microcarrier cultures. ***Biotechnol. Bioeng.*** **33:** 731-744.

Crowe, C.T., Troutt, T.R., Chung, J.N. 1996. Numerical models for two-phase turbulent flows. ***Annu. Rev. Fluid Mech.*** **28:** 11-43.

Cumming, R.H., Tuffnell, J., Street, G. 1985. The dependence of protein release from *Bacillus amyloliquefaciens* on the growth phase in batch culture. ***Biotechnol. Bioeng.*** **27:** 887-889.

Currie, J.A., Dunnill, P., Lilly, M.D. 1972. Release of protein from Baker's yeast (*Saccharomyces cerevisiae*) by disruption in an industrial agitator mill. ***Biotechnol. Bioeng.*** **14:** 725-736.

Dew, D. 1997. Gencor's commercialisation of biotechnology for metals recovery from sulphide ores, pp 15-16. In: ***Biotech SA '97.*** Grahamstown, South Africa.

Dias, S.M.M., Novias, J.M., Cabral, J.M.S. 1982. Immobilisation of yeasts on Titanium activated inorganic supports. ***Biotechnol. Lett.*** **4:** (3), 209-214.

Doran, P.M., Bailey, J.E. 1986. Effects of immobilisation on growth, fermentation properties, and macromolecular composition of *Saccharomyces cerevisiae* attached to gelatin. ***Biotechnol. Bioeng.*** **28:** 73-87.

Dunlop, E.H., Namdev, P.K. 1993. Effect of fluid forces on plant cell suspensions, pp 447-455. In: ***Third International Conference on Bioreactor and Bioprocess Fluid Dynamics***. BHR Group Ltd. Cambridge, UK.

Dunlop, E.H., Ye, S.J. 1990. Micromixing in fermenters: metabolic changes in *Saccharomyces cerevisiae* and their relationship to fluid turbulence. ***Biotechnol. Bioeng.*** **36:** 854-864.

EBC Analytica Microbiologica. 1977. ***J. Inst. Brew.*** **83:** 109-118.

Einstein, A. 1906. ***Ann. Phys. Paris IV.*** **19:** 289-306. In: M. Reuss, D. Josic, M. Popovic and W.K. Bronn. 1979. Viscosity of yeast suspensions. ***Eur. J. Appl. Microbiol. Biotechnol.*** **8:** 167-175.

Elghobashi, S., Truesdell, G.C. 1993. On the two-way interaction between homogeneous turbulence and dispersed solid particles. I: Turbulence modification. ***Phys. Fluids A.*** **5:** (7), 1790-1801.

Engler, C.R. 1985. Disruption of microbial cells, pp 305-324. In: M. Moo-Young (ed.). ***Comprehensive Biotechnology***. Vol 2. Pergamon Press.

Felix, H. 1982. Permeabilised cells. ***Anal. Biochem***. **120:** 211-234.

Fischer, E.H., Kohtes, L. 1951. ***Helv. Chim. Acta.*** **34:** 1132. In: A.H. Cook (ed.). 1958. ***The Chemistry and Biology of Yeasts.*** Academic Press, New York.

Fish, N.M., Lilly, M.D. July 1984. The interactions between fermentation and protein recovery. ***Bio/Technology***. 623-627.

Follows, M., Hetherington, P.J., Dunnill, P., Lilly, M.D. 1971. Release of enzymes from Baker's yeast by disruption in an industrial homogeniser. ***Biotechnol. Bioeng.*** **13:** 549-560.

Fraleigh, J.B., Beauregard, R.A. 1990. ***Linear Algebra***. 2nd edition. Addison-Wesley, USA.

Funk, J.E., Dinger, D.R. 1994. ***Predictive Process Control of Crowded Particulate Suspensions; Applied to Ceramic Manufacturing***. Kluwer, Boston, MA. In: P.J.C. Caulet, R.G.J.M. van der Lans and K.Ch.A.M. Luyben. 1996. Hydrodynamical interactions between particles and liquid flows in biochemical applications. ***Chem. Eng. J.*** **62:** 193-206.

Garcia-Briones, M.A., Chalmers, J.J. 1993. Analysis of hydrodynamic information obtained from computer solutions of the rupture of a gas bubble in relation to animal cell damage in sparged bioreactors, pp 191-209. In: ***Third International Conference on Bioreactor and Bioprocess Fluid Dynamics***. BHR Group Ltd. Cambridge, UK.

Gates, L.E., Morton, J.R., Fondy, P.L. 1976. ***Chemical Engineering***. **83:** 102. In: N Harnby, M.F. Edwards and A.W. Nienow (eds.). 1992. ***Mixing in the Process Industries***. 2nd edition. Chapter 16. Butterworth-Heinemann Ltd, Oxford.

Gore, R.A., Crowe, C.T. 1989. Effect of particle size on modulating turbulent intensity. ***Int. J. Multiphase Flow***. **15:** (2), 279-285.

Gormely, L.S., Branion, R.M.R. 1989. Engineering design of microbiological leaching reactors, pp 499-515. In: ***Proc. International Symposium on Biohydrometallurgy***. Wyoming, USA.

Gray, P.P., Dunnill, P., Lilly, M.D. 1972. The continuous-flow isolation of enzymes, pp 347-351. In: G. Terui (ed.). ***Fermentation Technology Today***. Society for Fermentation Technology, Japan.

Hackl, R.P., Wright, F.R., Gormely, L.S. 1989. Bioleaching of refractory gold ores - out of the lab and into the plant, pp 533-549. In: ***Proc. International Symposium on Biohydrometallurgy***. Wyoming, USA.

Haddad, S.A., Lindegren, C.C. 1953. ***Appl. Microbiol.*** **1:** 153-156. In: M. Reuss, D. Josic, M. Popovic and W.K. Bronn. 1979. Viscosity of yeast suspensions. ***Eur. J. Appl. Microbiol.***

***Biotechnol.* 8:** 167-175.

Handa-Corrigan, A., Emery, A.N., Spier, R.E. 1989. Effect of gas-liquid interfaces on the growth of suspended mammalian cell: mechanisms of cell damage by bubbles. ***Enzyme Microb. Technol.* 11:** 230-235.

Hansford, G.S., Bailey, A.D. 1993. Oxygen transfer limitation of bio-oxidation at high solids concentration. In: ***International Biohydrometallurgy Symposium***. Jackson Hole, Wyoming, USA.

Harrison, S.T.L. 1991. Bacterial cell disruption: a key unit operation in the recovery of intracellular products. ***Biotechnol. Adv.* 9:** 217-240.

Harrison, S.T.L., Dennis, J.S., Chase, H.A. 1991a. Combined chemical and mechanical processes for the disruption of bacteria. ***Bioseparation*. 2:** 95-105.

Harrison, S.T.L., Chase, H.A., Dennis, J.S. 1991b. The disruption of *Alcaligenes eutrophus* by high pressure homogenisation: key factors involved in the process. ***Bioseparation*. 2:** 155-166.

Hedenskog, G., Ebbinghaus, L. 1972. ***Biotechnol. Bioeng*. 14:** 447. In: Y. Chisti and M. Moo-Young. 1986. Disruption of microbial cells for intracellular products. ***Enzyme Microb. Technol*. 8:** 194-204.

Heslot, H., Gaillardin, C. 1991. ***Molecular Biology and Genetic Engineering of Yeasts.*** CRC Press, Boca Raton, FL. In: C.-H. Shu and S.-T. Yang. 1996. Effect of particle loading on GM-CSF production by *Saccharomyces cerevisiae* in a three-phase fluidised bed reactor. ***Biotechnol. Bioeng.* 51:** (2), 229-236.

Hetherington, P.J., Follows, M., Dunnill, P., Lilly, M.D. 1971. Release of protein from Baker's yeast (*Saccharomyces cerevisiae*) by disruption in an industrial homogeniser. ***Trans. Inst. Chem. Eng.* 49:** 142-148.

Hetsroni, G. 1989. Particles-turbulence interaction. ***Int. J. Multiphase Flow.* 15:** (5), 735-746.

Hetsroni, G., Sokolov, M. 1971. Distribution of mass, velocity and intensity of turbulence in a two-phase turbulent jet. ***Trans. ASME J. Appl. Mech*. 38:** 315-327.

Hinze, J.O. 1971. Turbulent fluid and particle interaction. ***Prog. Heat Mass Transfer.* 6:** 433-452.

Hinze, J.O. 1975. ***Turbulence.*** 2nd edition. McGraw-Hill, New York.

Hirtenstein, M., Clark, J. 1980. ***Tissue Culture in Medical Research***. R. Richards and K. Rajan (eds.). Pergamon, Oxford. p 97. In: M.S. Croughan, J.F. Hamel and D.I.C. Wang. 1987. Hydrodynamic effects on animal cells grown in microcarrier cultures. ***Biotechnol. Bioeng.* 29:** 130-141.

Hoeppel, R.E., Hinchee, R.E., Arthur, M.F. 1991. Bioventing soils contaminated with petroleum hydrocarbons. ***J. Ind. Microbiol.*** **8:** 141-146.

Hu, W.S. 1983. ***Quantitative and Mechanistic Analysis of Mammalian Cell Cultivation on Microcarriers***. Ph.D. thesis, Massachusetts Institute of Technology, Cambridge, MA. In: M.S. Croughan, J.F.P. Hamel and D.I.C. Wang. 1987. Hydrodynamic effects on animal cells grown in microcarrier cultures. ***Biotechnol. Bioeng.*** **29:** 130-141.

Hunter, J.B., Asenjo, J.A. 1988. A structured mechanistic model of the kinetics of enzymatic lysis and disruption of yeast cells. ***Biotechnol. Bioeng.*** **31:** 929-930.

Ibrahim, S., Nienow, A.W., Chatwin, S. 1992. The 1992 I. Chem. E. Research Event, UMIST. ***I. Chem. E.*** Rugby. In: N. Harnby, M.F. Edwards and A.W. Nienow (eds.). 1992. ***Mixing in the Process Industries***. 2nd edition. Chapter 16. Butterworth-Heinemann Ltd, Oxford.

Jobses, I., Martens, D., Tramper, J. 1991. Lethal events during gas sparging in animal cell culture. ***Biotechnol. Bioeng.*** **37:** 484-490.

Joshi, J.B., Pandit, A.B., Sharma, M.M. 1982. Mechanically agitated gas-liquid reactors. Review article Number 7. ***Chem. Eng. Sci.*** **37:** (6), 813-817.

Kanayama, H., Sode, K., Karube, I. 1988. Continuous hydrogen evolution by immobilised recombinant *E. coli* using a bioreactor. ***Biotechnol. Bioeng.*** **32:** 396-399.

Kawase, Y., Moo-Young, M. 1990. Mathematical models for design of bioreactors: applications of Kolmogoroff's theory of isotropic turbulence. ***Chem. Eng. J.*** **43:** B19-B41.

Kennedy, J.F., Cabral, J.M.S. 1990. Use of Titanium species for the immobilisation of cells. ***Transition Met. Chem.*** **15:** 197-207.

Kleijntjens, R.H., van der Lans, R.G.J.M., Luyben, K.Ch.A.M. 1992. Design of a three phase slurry reactor for soil processing. ***Trans. Inst. Chem. Eng.*** **70:** (B), 84-92.

Kolar, V. 1961. ***Colln. Czech. Chem. Comm.*** **26:** 613. In: A.W. Nienow. 1968. Suspension of solid particles in turbine agitated baffled vessels. ***Chem. Eng. Sci.*** **23:** 1453-1459.

Kolmogorov, A.N. 1941. The local structure of turbulence in incompressible viscous fluid for very very large Reynolds numbers. ***CR. Acad. Sci. USSR.*** **30:** 299-303.

Kowalski, A.J. 1991. ***Microscale Fluid Dynamic Effects in Suspension Processing and Attrition of Cell Cultures***. Ph.D. thesis, University of Birmingham, UK. In: J.M. Boulton-Stone and J.R. Blake. 1993. Bursting bubbles at a free-surface, pp 163-173. In: ***Third International Conference on Bioreactor and Bioprocess Fluid Dynamics***. BHR Group Ltd. Cambridge, UK.

Kramer, R., Kopp, F., Niedermeyer, W., Fuhrmann, G.F. 1978. Comparative studies of the structure and composition of the plasmalemma and the tonoplast in *Saccharomyces cerevisiae*. ***Biochim. Biophys. Acta***. **507:** 369-380.

Kuboi, R., Komasawa, I., Otake, T. 1974. Fluid and particle motion in turbulent dispersion - II. Influence of turbulence of liquid on the motion of suspended particles. ***Chem. Eng. Sci.*** **29:** 651-657.

Kula, M.-R., Schutte, H. 1987. Purification of proteins and the disruption of microbial cells. ***Biotechnol. Prog.*** **3:** (1), 31-42.

Kunas, K.T., Papoutsakis, E.T. 1990. Damage mechanisms of suspended animal cells in agitated bioreactors with and without bubble entrainment. ***Biotechnol. Bioeng.*** **36:** 476-483.

Lakhotia, S., Papoutsakis, E.T. 1992. Agitation induced cell injury in microcarrier cultures. Protective effect of viscosity is agitation intensity dependent: experiments and modelling. ***Biotechnol. Bioeng.*** **39:** 95-107.

Lemoine, F., Wolff, M., Lebouche, M. 1996. Simultaneous concentration and velocity measurements using combined laser-induced fluorescence and laser Doppler velocimetry: Application to turbulent transport. ***Exp. Fluids***. **20:** 319-327.

Lilly, M.D., Ison, A., Shamlou, P.A. 1992. The influence of the physical environment in fermenters on antibiotic production by micro-organisms, pp 219-222. In: ***Harnessing biotechnology for the 21st century***, Proc. Ninth International Biotechnology Symposium and Exposition. Crystal City Virginia.

Limon-Lason, J., Hoare, M., Orsborn, C.B., Doyle, D.J., Dunnill, P. 1979. Reactor properties of a high-speed bead mill for microbial cell rupture. ***Biotechnol. Bioeng.*** **21:** 745-774.

Linek, V., Vacek, V., Benes, P. 1987. A critical review and experimental verification of the correct use of the dynamic method for the determination of the oxygen transfer in aerated agitated vessels to water, electrolyte solutions and viscous liquids. ***Chem. Eng. J.*** **34:** 11-34.

Liu, M.S., Branion, R.M.R. 1988. The effects of ferrous iron, dissolved oxygen and inert solids concentrations on the growth of *Thiobacillus ferrooxidans*. ***Can. J. Chem. Eng.*** **66:** 450.

Lowry, O.H., Roseborough, N.J., Farr, A.L., Randall, R.J. 1951. Protein measurement with the Folin reagent. ***J. Biol. Chem.*** **193:** 265-275.

Lu, G.Z., Thompson, B.G., Gray, M.R. 1992. Physical modelling of animal cell damage by hydrodynamic forces in suspension cultures. ***Biotechnol. Bioeng.*** **40:** 1277-1281.

Lyons, E.J. 1967. Suspension of solids, Chapter 9. In: V.W Uhl and J.B. Gray (eds.). ***Mixing: Theory and Practice***. Academic Press, London.

Marffy, F., Kula, M.-R. 1974. Enzyme yields from cells of Brewer's yeast disrupted by treatment in a horizontal disintegrator. ***Biotechnol. Bioeng.*** **16:** 623-634.

Michaels, J.D., Mallik, A.K., Papoutsakis, E.T. 1996. Sparging and agitation-induced injury of cultured animal cells: do cell-to-bubble interactions in the bulk liquid injure cells? ***Biotechnol. Bioeng.*** **51:** 399-409.

Miller, I., Freund, J.E. 1985. ***Probability and Statistics for Engineers***. 3rd edition. Prentice-Hall, Inc., Englewood Cliffs, New Jersey.

Misaki, A., Johnson, Jr. J., Kirkwood, S., Scaletti, J.V., Smith, F. 1969. ***Carb. Res.*** **6:** 150-164. In: A.H. Rose and J.S. Harrison (eds.). 1971. ***The Yeasts: Physiology and Biochemistry of Yeasts***. Vol 2. Academic Press, London.

Mogren, H., Lindblom, M., Hedenskog, G. 1974. Mechanical disintegration of micro-organisms in an industrial homogeniser. ***Biotechnol. Bioeng.*** **16:** 261-274.

Moor, H., Muhlethaler, K. 1963. Fine structure in frozen-etched yeast cells. ***J. Cell. Biol.*** **17:** 609-628.

Moo-Young, M., Blanch, H.W. 1981. Design of biochemical reactors. Mass transfer criteria for simple and complex systems. ***Adv. Biochem. Eng.*** **19:** 1-69.

Nagata, S. 1975. ***Mixing: Principles and Applications***. Halstead, New York.

Narayanan, S., Bhatia, V.K., Guha, D.K., Rao, M.N. 1969. Suspension of solids by mechanical agitation. ***Chem. Eng. Sci.*** **24:** 223. In: V.B. Rewatkar and J.B. Joshi. 1991. Critical impeller speed for solid suspension in mechanically agitated three-phase reactors. 2. Mathematical model. ***Ind. Eng. Chem. Res.*** **30:** 1784-1791.

Navarro, J.M., Durand, G. 1977. Modification of yeast metabolism by immobilisation onto porous glass. ***Eur. J. Appl. Microbiol.*** **4:** 243-254.

Nielsen, J., Villadsen, J. 1994. ***Bioreaction Engineering Principles***. Plenum Press, New York.

Nienow, A.W. 1968. Suspension of solid particles in turbine agitated baffled vessels. ***Chem. Eng. Sci.*** **23:** 1453-1459.

Nienow, A.W. 1992. The suspension of solid particles, Chapter 16. In: N. Harnby, M.F. Edwards and A.W. Nienow (eds.). ***Mixing in the Process Industries***. 2nd edition. Butterworth-Heinemann Ltd, Oxford.

Northcote, D.H., Horne, R.W. 1952. ***Biochem. J.*** **51:** 232-236. In: A.H. Rose and J.S. Harrison (eds.). 1971. ***The Yeasts: Physiology and Biochemistry of Yeasts***. Vol 2. Academic Press, London.

Nouri, J.M., Whitelaw, J.H., Yianneskis, M. 1987. Particle motion and turbulence in dense two-phase flows. ***Int. J. Multiphase Flow***. **13:** (6), 729-739.

Oguz, H., Brehm, A., Deckwer, W.-D. 1987. Gas/liquid mass transfer in sparged agitated slurries. ***Chem. Eng. Sci***. **42:** (7), 1815-1822.

Okamoto, Y., Nishikawa, M., Hashimoto, K. 1981. Energy dissipation rate distribution in mixing vessels and its effect on liquid-liquid dispersion and solid-liquid mass transfer. ***Int. Chem. Eng.*** **21:** 88-94.

Oldshue, J.Y. 1983. ***Fluid mixing technology***. McGraw-Hill, New York.

Papoutsakis, E.T. 1991. Fluid-mechanical damage of animal cells in bioreactors. ***Reviews***. **9:** 427-437.

Pearce, K., Snyman, H., van Heerden, H., Greben, H., Oellermann, R.A. 1995. ***Bioremediation Technology for the Treatment of Contaminated Soil in South Africa***. Final report to the Water Research Commission, South Africa.

Pearce, S.A.J. 1993. ***Disruption of Micro-organisms due to Agitation in Slurries of Fine Particles***. MSc. thesis, Department of Chemical Engineering, University of Cape Town, South Africa.

Perry, R.H., Green, D.W., Maloney, J.O. 1984. ***Perry's Chemical Engineers' Handbook***. 6th edition. McGraw-Hill, Singapore. p 3-96.

Petersen, J.F., McIntire, L.V., Papoutsakis, E.T. 1990. Shear sensitivity of hybridoma cells in batch, fed-batch and continuous cultures. ***Biotechnol. Prog.*** **6:** 144-120.

Peterson, G.L. 1979. Review of the Folin phenol protein quantitation method of Lowry, Roseborough, Farr and Randall. ***Anal. Biochem.*** **100:** 201-220.

Phaff, H.J. 1971. Structure and biosynthesis of the yeast cell envelope, Chapter 5. In: A.H. Rose and J.S. Harrison (eds.). ***The Yeasts: Physiology and Biochemistry of Yeasts.*** Vol 2. Academic Press, London.

Phaff, H.J., Miller, M.W., Mrak, E.M. 1966. ***The Life of Yeasts: Their Nature, Activity, Ecology and Relation to Mankind***. Harvard University Press, USA.

Pinches, A., Huberts, R., van Staden, M., Muhlbauer, R.M. 1991. Process options and parameters in the development and optimisation of bacterial oxidation processes for the preoxidation of refractory sulphide gold ores, pp 1-21. In: ***Proc. South African Inst. Min. Metall. Colloquium on Bacterial Oxidation***. Johannesburg, South Africa.

Poncelet, D., Neufeld, R.J. 1989. Shear breakage of nylon membrane microcapsules in turbine reactor. ***Biotechnol. Bioeng.*** **33:** 95-103.

Prokop, A., Bajpai, R.K. 1992. The sensitivity of biocatalysts to hydrodynamic shear stress. ***Adv. Appl. Microbiol.*** **37:** 165-232.

Providenti, M.A., Lee, H., Trevors, J.T. 1993. Selected factors limiting the microbial degradation of recalcitrant compounds. ***J. Ind. Microbiol.*** **12:** 379-395.

Raghava Rao, K.S.M.S., Rewatkar, V.B., Joshi, J.B. 1988. Critical impeller speed for solid suspension in mechanically agitated solid-liquid contactors. ***AIChE J.*** **34:** 1332. In: V.B. Rewatkar, K.S.M.S. Raghava Rao and J.B. Joshi. 1991. Critical speed for solid suspension in mechanically agitated three-phase reactors. 1. Experimental part. ***Ind. Eng. Chem. Res.*** **30:** 1770-1784.

Ranade, V.V., Joshi, J.B. 1990. Flow generated by a disc turbine: Part I Experimental. ***Trans. Inst. Chem. Eng.*** **68:** (A), 19-33.

Reed, X.B., Princz, M., Hartland, S. 1977. ***Second European Conference on Mixing***. BHRA-Cranfield. Cambridge, B 1.1. In: V.V Ranade and J.B. Joshi. Flow generated by a disc turbine: Part I Experimental. ***Trans. Inst. Chem. Eng.*** **68:** (A), 19-33.

Rehacek, J. 1971. ***Experientia***. **27:** 1103. In: Y. Chisti and M. Moo-Young. 1986. Disruption of microbial cells for intracellular products. ***Enzyme Microb. Technol.*** **8:** 194-204.

Rehacek, J., Schaefer, J. 1977. Disintegration of micro-organisms in an industrial horizontal mill of novel design. ***Biotechnol. Bioeng.*** **19:** 1523-1534.

Reuss, M., Josic, D., Popovic, M., Bronn, W.K. 1979. Viscosity of yeast suspensions. ***Eur. J. Appl. Microbiol. Biotechnol.*** **8:** 167-175.

Reuss, M., Debus, D., Zoll, G. 1982. Rheological properties of fermentation fluids. ***The Chemical Engineer***. June: 233-236.

Reuss, M. 1988. Influence of mechanical stress on the growth of *Rhizopus nigricans* in stirred bioreactors. ***Chem. Eng. Technol.*** **11:** 178-187.

Rewatkar, V.B., Joshi, J.B. 1991. Critical impeller speed for solid suspension in mechanically agitated three-phase reactors. 2. Mathematical model. ***Ind. Eng. Chem. Res.*** **30:** 1784-1791.

Rewatkar, V.B., Raghava Rao, K.S.M.S., Joshi, J.B. 1989. Some aspects of solids suspension in mechanically agitated reactors. ***AIChE J.*** **35:** 1577. In: V.B. Rewatkar, K.S.M.S. Raghava Rao and J.B. Joshi. 1991. Critical speed for solid suspension in mechanically agitated three-phase reactors. 1. Experimental part. ***Ind. Eng. Chem. Res.*** **30:** 1770-1784.

Rewatkar, V.B., Raghava Rao, K.S.M.S., Joshi, J.B. 1991. Critical impeller speed for solid suspension in mechanically agitated three-phase reactors. 1. Experimental part. ***Ind. Eng. Chem. Res.*** **30:** 1770-1784.

Roberts, R.L., Bowers, B., Slater, M.L., Cabib, E. 1983. Chitin synthesis and localisation in cell division cycle mutants of *S. cerevisiae*. ***Mol. Cell. Biol.*** **3**: 922-930.

Roberts, W.L., Campbell, T.J., Rapp, G.R. Jr. 1990. ***Encyclopaedia of Minerals***. 2nd edition. Van Nostrand Reinhold, New York.

Robertson, B., Ulbrecht, J.J. 1986. ***AIChE Annual Meeting***. Miami Beach, Fla. Paper 8c. In: G.B. Tatterson. 1991. ***Fluid Mixing and Gas Dispersion in Agitated Tanks.*** Chapter 4. McGraw-Hill, New York.

Rossi, G. 1990. ***Biohydrometallurgy.*** McGraw-Hill, Hamburg.

Rosvear, A., Kennedy, J.F., Cabral, J.M.S. 1987. ***Immobilised Enzymes and Cells***. Adam Hilge.

Rushton, J.H., Costich, E.W., Everett, H.J. 1950a. Power characteristics of mixing impellers. Part 1. ***Chem. Eng. Prog.*** **46:** (8), 395-404.

Rushton, J.H., Costich, E.W., Everett, H.J. 1950b. Power characteristics of mixing impellers. Part 2. ***Chem. Eng. Prog.*** **46**, (9), 467-476.

Ryan, J.R., Loehr, R.C., Rucker, E. 1991. Bioremediation of organic contaminated soils. ***J. Hazard. Mater.*** **28:** 159-169.

Ryder, D.S., Woods, D.R., Murray, J.P., Masschelein, C.A. 1983. Some practical implications of yeast growth and yeast performances. ***MBAA Technical Quarterly.*** **20:** (1), 9-21.

Sanmugasunderam, V. 1981. ***Kinetic Studies on the Biological Leaching of a Zinc Sulphide Concentrate in Two Stage Continuous Stirred Tank Reactors.*** Ph.D. thesis, Department of Chemical Engineering, University of British Columbia. In: A.D. Bailey. 1993. ***An Assessment of Oxygen Availability, Iron Build-up and the Relative Significance of Free and Attached Bacteria, as Factors Affecting Bio-oxidation of Refractory Gold-bearing Sulphides at High Solids Concentrations.*** Ph.D. thesis, Department of Chemical Engineering, University of Cape Town, South Africa.

Schekman, R., Novick, P. 1982. The secretory process and yeast cell surface assembly, pp 361-393. In: J.N. Strathern, E.W. Jones and J.R. Broach (eds.). ***The Molecular Biology of the Yeast Saccharomyces, Metabolism and Gene Expression***. Cold Spring Harbour Monograph Series, Cold Spring Harbour, NY.

Schlegel, H.G. 1988. ***General Microbiology***. 6th edition. University Press, Cambridge, UK.

Schutte, H., Kraume-Flugel, R., Kula, M.-R. 1986. Scale-up of mechanical cell disintegration - influence of stirrer geometry on residence time distribution and cell disintegration in a 20ℓ high-speed ball mill. ***Ger. Chem. Eng.*** **9:** 149-156.

Schutte, H., Kroner, K.H., Hustedt, H., Kula, M.-R. 1983. Experiences with a 20 litre industrial bead mill for the disruption of microorganisms. ***Enzyme Microb. Technol.*** **5:** 143-148.

Schutte, H., Kula, M.-R. 1988. Analytical disruption of micro-organisms in a mixer mill. ***Enzyme Microb. Technol.*** **10:** 552-558.

Shu, C.-H., Yang, S.-T. 1996. Effect of particle loading on GM-CSF production by *Saccharomyces cerevisiae* in a three-phase fluidised bed reactor. ***Biotechnol. Bioeng.*** **51:** (2), 229-236.

Shuen, J.-S., Solomon, A.S.P., Zhang, □.-F., Faeth, G.M. 1985. Structure of particle-laden jets: measurements and predictions. ***AIAA J.*** **23:** 396-404.

Sinskey, A.J., Fleischaker, M., Tyo, M.A., Giard, D.J., Wang, D.I.C. 1981. ***Ann. N.Y. Acad. Sci.*** **369:** 47-59. In: M.S. Croughan, J.F.P. Hamel and D.I.C. Wang. 1987. Hydrodynamic effects on animal cells grown in microcarrier cultures. ***Biotechnol. Bioeng.*** **29:** 130-141.

Smith, J.J., Lilly, M.D., Fox, R.I. 1990. The effect of agitation on the morphology and penicillin production of *Penicillium chrysogenum.* ***Biotechnol. Bioeng.*** **35:** 1011-1023.

Stanier, R.Y., Doudoroff, M., Adelberg, E.A. 1970. ***The Microbial World.*** 3rd edition. Prentice-Hall, Inc., Englewood Cliffs, New Jersey. In: J.E. Bailey and D.F. Ollis. 1986. ***Biochemical Engineering Fundamentals.*** 2nd edition. McGraw-Hill, Singapore.

Steere, R.L., Erbe, E.F., Moseley, J.M. 1980. Prefracture and cold-fracture images of yeast plasma membranes. ***J. Cell. Biol.*** **86:** 113-122, (1980).

Stegmann, P., Goede, J.F., Ginster, M. March/April 1994. Implementing bioremediation - ongoing improvements in an effective solution to coping with hydrocarbon wastes. ***Chem. Technol.*** 22-27.

Stewart, T.S., Ballou, C.E. 1968. ***Biochemistry***. N.Y. **7:** 1855-1863. In: A.H. Rose and J.S. Harrison (eds.). 1971. ***The Yeasts: Physiology and Biochemistry of Yeasts***. Vol 2. Academic Press, London.

Takahashi, K., Fujita, H., Yokota, T. 1993. Effect of size of spherical particle on complete suspension speed in agitated vessels of different scale. ***J. Chem. Eng. Jpn***. **26:** (1), 98-100.

Tatterson, G.B., Yuan, H.-H., Brodkey, R.S. 1980. ***Chem. Eng. Sci***. **35:** 1369. In: G.B.Tatterson. 1991. ***Fluid Mixing and Gas Dispersion in Agitated Tanks***. McGraw-Hill, New York.

Tatterson, G.B. 1991. ***Fluid Mixing and Gas Dispersion in Agitated Tanks.*** McGraw-Hill, New York. pp 208-214.

Tennekes, H., Lumley, J.L. 1972. ***A First Course in Turbulence.*** MIT Press, Cambridge, MA. In: H. Wu and G.K. Patterson. 1989. Laser-Doppler measurements of turbulent-flow parameters in a stirred mixer. ***Chemical Engineering.*** **44:** (10), 2207-2221.

Toma, M.K., Ruklisha, M.P., Vanags, J.J., Zeltina, M.O., Leite, M.P., Galinina, N.I., Viesturs, U.E., Tengerdy, R.P. 1991. Inhibition of microbial growth and metabolism by excess turbulence. ***Biotechnol. Bioeng.*** **38:** 552-556.

Torma, A.E. 1977. The role of *Thiobacillus ferrooxidans* in hydrometallurgical processes. ***Adv. Biochem. Eng.*** **6:** 1-37.

Torma, A.E., Walden, C.C., Duncan, D.W., Branion, R.M.R. 1970. Microbiological leaching of a zinc sulphide concentrate. ***Biotechnol. Bioeng.*** **12:** 501-517.

Trinh, K., Garcia-Briones, M., Hink, F., Chalmers, J.J. 1994. Quantification of damage to suspended insect cells as a result of bubble rupture. ***Biotechnol. Bioeng.*** **43:** 37-45.

Tuite, M.F., Oliver, S.G. (eds.). 1991. ***Saccharomyces cerevisiae.*** Plenum Press, New York.

Tyagi, R.D., Gupta, S.K., Chand, S. 1992. Process engineering studies on continuous ethanol production by immobilised *S. cerevisiae*. ***Process Biochem.*** **27:** 23-32.

Uhl, V.W., Gray, J.B. (eds.). 1966. ***Mixing: Theory and Practice.*** Vol. 1. Academic Press, New York.

Van Aswegen, P.C. 1993. Bio-oxidation of refractory gold ores. The Genmin experience, Chapter 15. In: ***Biomine '93.*** Australian Mineral Foundation, Inc., Glenside, Australia.

Van Haecht, J.L., Bolipombo, M., Rouxhet, P.G. 1985. Immobilisation of *Saccharomyces cerevisiae* by adhesion: treatment of the cells by Al ions. ***Biotechnol. Bioeng.*** **27:** 217-224.

Van Suijdam, J.C., Metz, B. 1981. Influence of engineering variables upon the morphology of filamentous molds. ***Biotechnol. Bioeng.*** **23:** 111-148.

Vanags, J.J., Rikmanis, M.A., Ushkans, E.J. 1990. Stirring characteristics in bioreactors. ***AIChE J.*** **36:** (9), 1361-1369.

Vand, V. 1948. ***J. Phys. Colloid Chem.*** **52:** 277-299. In: M. Reuss, D. Josic, M. Popovic and W.K. Bronn. 1979. Viscosity of yeast suspensions. ***Eur. J. Appl. Microbiol. Biotechnol.*** **8:** 167-175.

Van't Riet, K. 1983. Mass transfer in fermentation. ***Trends Biotechnol.*** **1:** (4), 113.

Walker, I., Austin, E.P. 1981. p 272. In: P.F. Cooper and B. Atkinson (eds.). ***Biological Fluidised Bed Treatment of Water and Wastewater.*** Ellis Horwood, Chichester. In: G.M. Black, C. Webb, T.M. Matthews and B. Atkinson. 1984. Practical reactor systems for yeast cell immobilisation using biomass support particles. ***Biotechnol. Bioeng.*** **26:** 134-141.

Weast, R.C. 1981. ***CRC Handbook of Chemistry and Physics***. 62nd edition. CRC Press Inc.

Webb, C., Dervakos, G. 1996. ***Studies in Viable Cell Immobilisation.*** Academic Press.

Weisman, J., Efferding, L.E. 1960. Suspension of slurries by mechanical mixers. ***AIChE J.*** **6:** (3), 419-426.

Wichterle, K., Kadlec, M., Zak, L., Mitschka, P. 1984. Shear rates on turbine impeller blades. ***Chem. Eng. Commun.*** **26:** 25-32.

Wichterle, K., Mitschka, P., Hajek, J., Zak, L. 1988. Shear stresses on the walls of vessels with axial impellers. ***Chem. Eng. Res. Des.*** **66:** 102-106.

Wichterle, K., Zak, L., Mitschka, P. 1985. Shear stresses on the walls of agitated vessels. ***Chem. Eng. Commun.*** **32:** 289-305.

Wiedmann, J.A., Steiff, A., Weinspach, P.M. 1980. Investigation of power-consumption, suspension and flooding characteristics of stirred, aerated slurry reactors. ***Ger. Chem. Eng.*** **3:** 303-312.

Yang, J.D., Wang, N.S. 1992. Cell inactivation in the presence of sparging and mechanical action. ***Biotechnol. Bioeng.*** **40:** 806-816.

Yang, J.D., Wang, N.S., Chang, K.C., Calabrese, R.V. 1990. Hybridoma cell inactivation by air sparging in a mechanically agitated bioreactor. Submitted for publication. In: J.M. Boulton-Stone and J.R. Blake. 1993. Bursting bubbles at a free-surface, pp 63-173. In: ***Third International Conference on Bioreactor and Bioprocess Fluid Dynamics***. BHR Group Ltd. Cambridge, UK.

Zhang, Z., Thomas, C.R. 1993. Modelling of animal cell damage in turbulent flows, pp 475-481. In: ***Third International Conference on Bioreactor and Bioprocess Fluid Dynamics***. BHR Group Ltd. Cambridge, UK.

Zlotnik, H., Fernandez, M.P., Bowers, B., Cabib, E. 1984. *Saccharomyces cerevisiae* mannoproteins form in external cell wall layer that determines wall porosity. ***J. Bacteriol.*** **159:** 1018-1026.

Zwietering, T.N. 1958. Suspending of solid particles in liquid by agitators. ***Chem. Eng. Sci.*** **8:** 244-253.

Appendix A: Determination of Protein Concentration by the Lowry Method

The spectrophotometric assay of Lowry *et al.* (1951) was used to determine the soluble protein concentrations in this study. The assay involves the reduction of phosphomolybdic-tungstic mixed acid by proteins to produce one or more of several reduced species which are characteristically blue in colour and which can be determined spectrophotometrically at 660 nm. Measurement of the absorbance of the blue complexes formed by samples of standard protein concentration, allows the protein concentration to be related to the absorbance in the form of a standard curve. From this standard curve, the absorbance of the blue complex formed by any protein sample can be converted to a protein concentration.

Phosphomolybdic-tungstic mixed acid is the active constituent of the Folin-Phenol reagent of Folin and Ciocalteu (Sigma F9252). It contains the chemical species $3H_2O.P_2O_5.13WO_3.5MoO_3.10H_2O$ and $3H_2O.P_2O_5.14WO_3.4MoO_3.10H_2O$. In the Lowry assay, the sensitivity of the mixed acid chromagen to the protein is increased by the prior reaction of the protein with cuprous ions. The cuprous ions chelate in the peptide structure and facilitate electron transfer to the phosphomolybdate-phosphotungstate. The Folin-Ciocalteu reagent is only stable in acid solution. However, the reduction occurs at alkaline pH. Mixing of the copper-protein solution and the Folin-Ciocalteu reagent must therefore be rapid so that reduction of the Folin-Ciocalteu reagent occurs before it is broken down (Lowry *et al.* 1951, Peterson 1979).

The quantities of the reagents used in the Lowry assay and the protocol followed in the assay are detailed below. A typical standard curve, relating the protein concentration to the absorbance of the blue complex at 660 nm, is presented. Calculation of the specific soluble protein release using the absorbance data is detailed, and typical results and the reproducibility of the measurements are discussed.

Reagents:

Reagent A: Dissolve 50 g Na_2CO_3 in 500 ml (final volume) 0.5N NaOH.

Reagent B: Dissolve 1 g $CuSO_4.5H_2O$ in 100 ml (final volume) distilled water.

Reagent C: Dissolve 2 g potassium tartrate in 100 ml (final volume) distilled water.

Reagent D: Dissolve 0.03 g bovine serum albumin (Sigma A4378) in 100 ml (final volume) distilled water.

Reagent E: Add 5 ml of 2 N Folin-Phenol reagent (Sigma F9252) to 50 ml distilled water and mix thoroughly.

Method:

All standards and samples performed in duplicate.

1. Pipette 0, 0.5 and 1 ml bovine serum albumin (BSA) solution (Reagent D) into test tubes for the standard protein curve. Bring the total volume of all test tubes to 1 ml with distilled water.
2. Pipette 1 ml of appropriately diluted supernatants of cell samples into test tubes. The samples in this study were diluted 1:9 or 1:99 so that the absorbance reading at 660 nm was less than 1.10. The standard protein curve (Figure A.1) is no longer linear above this value.
3. Mix together 15 ml Reagent A, 0.75 ml Reagent B and 0.75 ml Reagent C.
4. Add 1 ml of the above mixture to each test tube and mix thoroughly.
5. Incubate tubes for 15 minutes at room temperature.
6. Rapidly add 3 ml of Reagent E to each tube and mix immediately. Addition and mixing of each tube should be completed before proceeding.
7. Incubate the samples in a dark place at room temperature for 45 minutes.
8. Determine the absorbance of each sample at 660 nm. Absorbances should be determined as soon as possible after incubation. The colour complex remains constant for about 45 minutes to 1 hour after incubation.

Calculation of the Specific Soluble Protein Release using the Absorbance Measurements

Each step of this calculation is illustrated below using the results from Run #10.39. For this purpose, the spreadsheet of Run#10.39 is shown in Table A.1. The columns in Table A.1 are numbered for ease of reference in the following discussion.

To calculate the specific soluble protein release using the absorbance measurements:

1. Calculate the 'corrected absorbance' (Table A.1, Column 6) by subtraction of the absorbance of the zero standard protein sample (0 g/l BSA), E, from the average absorbance reading of each sample (Table A.1, Column 5).

2. Determine the standard curve of the protein concentrations (w/v) of the BSA samples as a function of their corrected absorbance readings. A typical standard curve is shown in Figure A.1. Linear regression of this relationship typically yields a correlation coefficient (R^2) above 0.990. In Figure A.1, this relationship is described by Equation A.1 with a correlation coefficient of 0.994.

Soluble protein concentration (g/l) = 0.269 (Corrected absorbance) - 0.005 **Equation A.1**

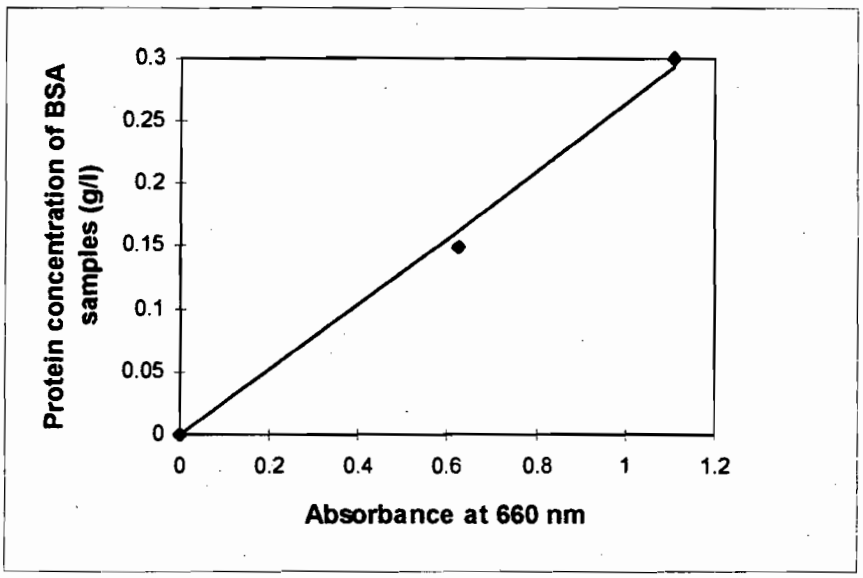

Figure A.1. **A typical standard curve of protein concentration as a function of the absorbance measurement in the Lowry assay.**
Bovine serum albumin (BSA) was used as the protein standard.

3. Calculate the soluble protein concentration of each sample (Table A.1, Column 7) by substituting the corrected absorbance of the sample into the linear expression (eg. Equation A.1). Multiply this concentration by the inverse of the dilution factor used.
4. Subtract the extracellular protein concentration at time zero from the soluble protein concentration of each sample. This corrected protein concentration (Table A.1, Column 8) is the soluble protein released on cell breakage.
5. Divide the corrected soluble protein concentration by the cell dry weight (g cell / l) to obtain the specific release of soluble protein (mg protein / g cell) (Table A.1, Column 9).

Reproducibility of the Lowry Assay

A coefficient of variance (Table A.1, Column 10), defined as the standard deviation of the two absorbance readings divided by their mean, was used to quantify the reproducibility of the Lowry assay. In this study, a coefficient of variance of less than 3% was ensured by repeating the Lowry assay when the coefficient of variance exceeded this value.

Table A.1. **Spreadsheet of the calculation of the specific soluble protein release of Run #10.39 as a function of time.**

Sample	Dilution	Absorbance Reading 1	Absorbance Reading 2	Ave. Absorbance	Corrected, (A - E)	Protein Release (g/l) Calculated	Protein Release (g/l) Corrected	Specific Soluble Protein Release (mg protein/g cell)	Coefficient of Variance in Absorbance Measurements (%)
Column 1	Column 2	Column 3	Column 4	Column 5	Column 6	Column 7	Column 8	Column 9	Column 10
0 min	1:9	0.2067	0.2039	0.2053	0.1787	0.41	0.00	0.0	1.0
4 min	1:9	0.3266	0.3322	0.3294	0.3027	0.74	0.33	6.0	1.2
10 min	1:9	0.5227	0.5364	0.5295	0.5029	1.28	0.87	15.6	1.8
35 min	1:9	1.1688	1.1693	1.1690	1.1424	2.98	2.57	46.3	0.0
35 min	1:99	0.1634	0.1698	0.1666	0.1399	3.23	2.82	50.8	2.7
60 min	1:99	0.2383	0.2451	0.2417	0.2150	5.25	4.84	87.2	2.0
120 min	1:99	0.3674	0.3661	0.3667	0.3401	8.61	8.20	147.8	0.3
210 min	1:99	0.5208	0.5190	0.5199	0.4932	12.74	12.32	222.1	0.3
360 min	1:99	0.6265	0.6260	0.6262	0.5996	15.60	15.19	273.6	0.1
645 min	1:99	0.6840	0.6955	0.6897	0.6631	17.31	16.90	304.4	1.2
900 min	1:99	0.6968	0.6983	0.6975	0.6709	17.52	17.11	308.2	0.1
1200 min	1:99	0.6915	0.6992	0.6953	0.6687	17.46	17.05	307.1	0.8
1440 min	1:99	0.7099	0.6989	0.7044	0.6778	17.70	17.29	311.5	1.1

Appendix B: Phosphate Buffered Saline (PBS)

PBS was used to wash and resuspend the yeast cells prior to the disruption experiments to ensure an isotonic environment and minimise pH fluctuation. The PBS was made up as follows (Pearce 1993):

NaCl	8.0 kg m^{-3}
KCl	0.2 kg m^{-3}
KH_2PO_4	0.2 kg m^{-3}
Na_2HPO_4	2.3 kg m^{-3}
pH	7.5

Appendix C: Calibration of Power Measurements

The validity of the power measurements from the load cell readings was determined by measuring the power input over the impeller speed range of 100 to 550 rpm for the following liquids:

- tap water
- 10%, 30%, 44.3% and 49.5% sucrose solutions
- 56% and 84% glycerol solutions

The Rushton turbine was used in these experiments. The power number (N_p) (Equation 3.3) was plotted as a function of the impeller Reynolds number (N_{RE}) (Equation 3.4) for these liquids. This relationship is shown in Figure C.1. The physical properties of the liquids, required for the calculation of N_P and N_{RE}, were determined from Weast (1981). Figure C.1 also shows the curve of the power number as a function of the impeller Reynolds number that Bates *et al.* (1966) obtained for a 6-bladed Rushton turbine and the same vessel geometry. The excellent agreement between the data in this work and the curve of Bates *et al.* (1966) shows that the power measurements, using the load cell, are accurate.

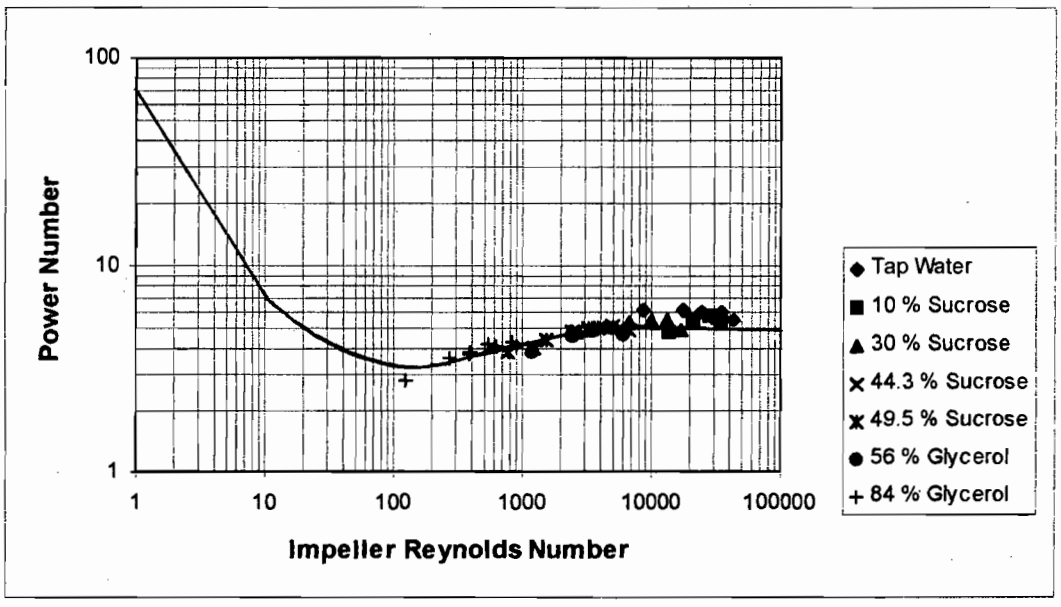

Figure C.1. **Comparison of measured and literature (Bates *et al.* 1966) N_P as a function of N_{RE} for a 6-bladed Rushton turbine and the vessel geometry used in this study.**
The symbols represent the data points obtained in this work. The solid curve represents the relationship obtained by Bates *et al.* (1966).

Appendix D: Error Analysis of the Soluble Protein (R) Calculation of Hetherington *et al.* (1971)

In this appendix, an error analysis is performed on the relationship proposed by Hetherington *et al.* (1971) for the calculation of the soluble protein release from disrupted micro-organisms. The error incurred in this calculation is compared to the error in not considering the volume fraction of the micro-organisms in the calculation of the soluble protein release. Hetherington *et al.* (1971) used a factor, F, to account for the volume fraction of the aqueous phase in the disrupted sample (ml aqueous phase/ml suspension). The soluble protein release per unit cell mass in the disrupted suspension (R) was then calculated as:

$$R = \frac{Fc_U}{c} \qquad \textbf{Equation D.1}$$

where c_U is the protein concentration in the aqueous phase of an undiluted sample (mg protein/ml aqueous phase) and c is the cell concentration (g cell/ml suspension). Values of F were calculated from a series of dilution experiments in which known volumes of suspensions of different cell concentrations and different degrees of disruption were diluted with saline buffer before centrifugation. Both the diluted and undiluted samples were centrifuged and assayed for total protein. The factor, F, was mathematically related to these parameters by the following relationship:

$$F = \frac{V_D}{V_S}\frac{c_D}{c_U - c_D} \qquad \textbf{Equation D.2}$$

where V_D is the volume of saline buffer added as the diluent (ml), V_S is the volume of the disrupted cell suspension (ml) and c_D is the protein concentration in the aqueous phase of the diluted sample (mg protein/ml aqueous phase). Substitution of Equation D.2 into Equation D.1 gives the following relationship:

$$R = \frac{V_D}{V_S}\frac{c_D}{c_U - c_D}\frac{c_U}{c} \qquad \textbf{Equation D.3}$$

Now

$$(dR)^2 = \left(\frac{\delta R}{\delta V_D} dV_D\right)^2 + \left(\frac{\delta R}{\delta V_S} dV_S\right)^2 + \left(\frac{\delta R}{\delta c_D} dc_D\right)^2 + \left(\frac{\delta R}{\delta c_U} dc_U\right)^2 + \left(\frac{\delta R}{\delta c} dc\right)^2$$

Equation D.4

Calculation of the partial derivatives of R with respect to V_D, V_S, c_D, c_U and c, and substitution of these quantities into Equation D.4, yields Equation D.5.

$$\left(\frac{dR}{R}\right)^2 = \left(\frac{dV_D}{V_D}\right)^2 + \left(\frac{dV_S}{V_S}\right)^2 + \left(\frac{c_U dc_D}{c_D(c_U - c_D)}\right)^2 + \left(\frac{c_D dc_U}{c_U(c_U - c_D)}\right)^2 + \left(\frac{dc}{c}\right)^2$$

Equation D.5

Calculation of the relative error in the soluble protein release per unit cell mass, dR/R, requires an estimation of the relative errors in the measurements of V_D, V_S, c_U, c_D and c. The relative errors in the measurements of the volumes, V_D and V_S, were assumed to be 0.8% since this was the error tolerated in this work in the calibration of the pipettes. The average undiluted protein concentration of the disrupted yeast suspensions in this study (c_U) was 9 mg/ml. Using a relative error of 3% in the measurements of the soluble protein concentration for this work (Appendix A), the value of dc_U was estimated as 0.27 mg/ml. Hetherington *et al.* (1971) showed that the values of F were independent of the degree of dilution. Assuming values of 5 ml and 3 ml for V_S and V_D, respectively, the average value of c_D was calculated as 5.6 mg/ml. The relative error of 3% in the soluble protein concentration, used for c_U, was also assumed for c_D, giving a value of 0.17 mg/ml for dc_D. A 2% relative error was assumed for the cell concentration measurements (Section 3.3.2). Substitution of these estimates of dV_D/V_D, dV_S/V_S, c_U, dc_U, c_D, dc_D and dc/c into Equation D.5 yields:

$$\left(\frac{dR}{R}\right)^2 = (0.008)^2 + (0.008)^2 + \left(\frac{(0.17)(9)}{(5.6)(9-5.6)}\right)^2 + \left(\frac{(0.27)(5.6)}{(9)(9-5.6)}\right)^2 + (0.02)^2$$

Hence:

$$\left(\frac{dR}{R}\right)^2 = 9.43x10^{-3}$$

$$\left(\frac{dR}{R}\right) = 9.7\%$$

The relative error associated with using Equation D.3 for the calculation of R, at the conditions in this work, is thus 9.7%. To calculate the relative error incurred in omitting the F-values from the calculation of R, correlations of F as a function of c and c_U, provided by Hetherington *et al.* (1971) (Figure 6), were used. The average cell wet weight concentration used in this study is 0.18 g yeast / ml suspension. Extrapolation of the F-values obtained by Hetherington *et al.* (1971) to the conditions in this study yields values of 0.90-1.00 for F. The average relative error of 5% in omitting the F-values from the calculation of R is less than the relative error incurred in using the F-values to calculate R. It can thus be concluded that at the relatively low yeast concentrations used in this study, it is not necessary to use F-factors in the calculation of the soluble protein release.

Appendix E: Determining R_M from the French Press

This appendix includes the method used to disrupt the yeast cells with the French Press (Manual-fill 20K cell, SLM Intruments). The calculation of the maximum soluble protein available for disruption (R_M), from the French Press data, is also described.

E.1 French Press Method

1. Perform a dry weight analysis of the washed and resuspended yeast suspension (Section 3.3.2).
2. Lubricate the rubber seals on the disruption chamber with water.
3. Press down the plunger to the midpoint of the chamber, turn the chamber upside-down and pour in the yeast suspension.
4. Add the stopper to the disruption chamber and tighten the screw on the side of the chamber to reduce the size of the orifice in the cylinder. The yeast cells are disrupted on rapid decompression and extrusion through this small orifice as the plunger is forced down the disruption chamber by the French Press. Attach the rubber tubing to the outlet pipe from the orifice.
5. Center the disruption chamber under the arm of the French Press.
6. Place a sample bottle in a beaker of ice. This ensures that any denaturation of the protein released, as a consequence of a temperature rise during disruption, will be minimised. Place the rubber tubing from the outlet pipe of the French Press into the sample bottle.
7. Increase the pressure in the French Press till the pressure gauge reads 30 MPa. Release the screw on the disruption chamber slowly until the gauge reading drops to 28MPa. Tighten the screw on the disruption chamber and repeat this procedure until all the sample in the chamber has passed through the orifice.
8. Store the samples of disrupted yeast cells in ice.
9. Clean out the chamber with paper towel and ethanol.

E.2 Calculation of R_M Values

To establish the maximum soluble protein available for disruption (R_M), the yeast suspension was passed five times through the French Press. The samples, from each of the French Press passes, were centrifuged at 4650g for 5 minutes. The supernatants were then diluted by a factor of 1:99 with distilled water for the Lowry assay (Appendix A) which was used to determine the specific soluble protein concentration of each pass. Figure E.1 shows the soluble protein release as a function of the number of passes through the French

Press. It can be seen that the same soluble protein release is obtained for 2 to 5 passes. Two passes through the French Press are thus sufficient to disrupt completely the *Saccharomyces cerevisiae*, used in this study.

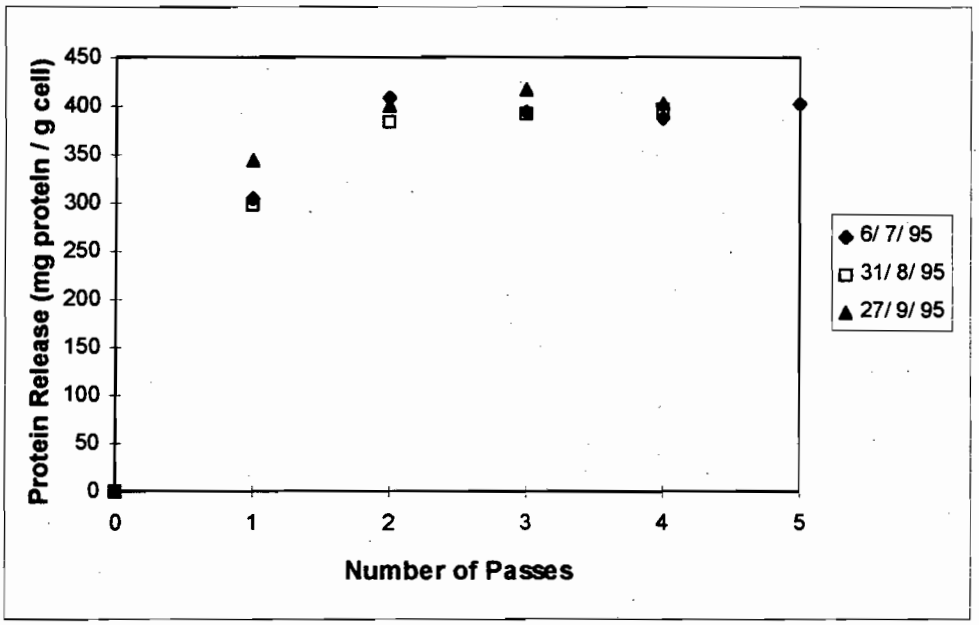

Figure E.1. **Soluble protein release of *Saccharomyces cerevisiae* as a function of the number of passes through the French Press.**
Legends indicate the dates on which the disruption experiments were performed with the French Press. Each date corresponds to a different batch of yeast.

The maximum soluble protein available for disruption (R_M) was determined for each batch of yeast cells used in this study. In these French Press experiments, the yeast cells were passed 4 times through the French Press. R_M was then calculated as the average of the soluble protein release from the second, third and fourth passes. The R_M values, obtained for each of the disruption experiments, are included in Appendix G.

Appendix F: Growth of the *Saccharomyces cerevisiae* during Disruption Experiments run for less than 10 hours

In this appendix, it is verified that the growth of the yeast cells was negligible in the disruption experiments that were run for less than 10 hours. Two disruption experiments were performed at 10% solids (v/v) and 360 rpm to test this hypothesis. 10 mg/l of cycloheximide was added to the one disruption experiment (Run #10.37) and no cycloheximide was added to the other (Run #10.32). Figure F.1 compares the protein release in the two disruption experiments. The raw data for these two experiments is tabulated in Appendix G. Figure F.1 shows that the protein release as a function of time for the two experiments compares very well over the initial ten hours (coefficient of variance of 7.6%). It is thus valid to assume that no growth of the yeast cells occurs in the experiments run for less than 10 hours. The addition of cycloheximide to these disruption experiments was thus not required (see Section 3.4.2).

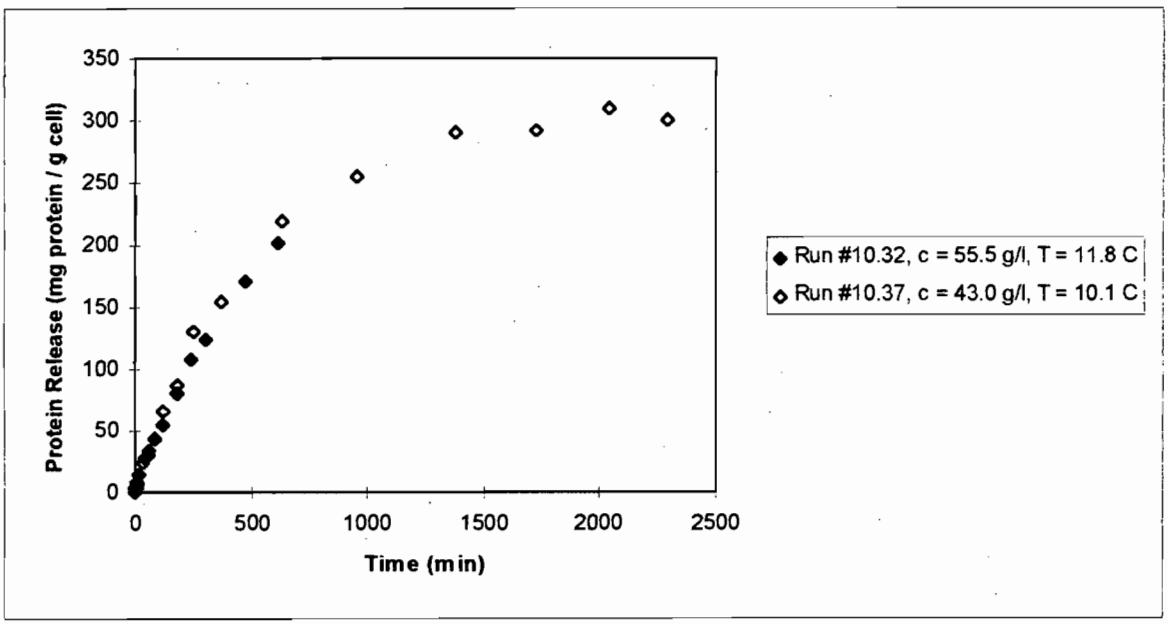

Figure F.1. Comparison of the protein release as a function of time for Run #10.32 (no cycloheximide added) and Run #10.37 (10 mg/l of cycloheximide added) to establish the validity of the assumption that no cell growth occurs in experiments run for less than 10 hours.

Both Run #10.32 and Run #10.37 were performed at 10% solids (v/v) and 360 rpm.

Appendix G: Results of Disruption Experiments for Rushton and Pitched-Blade Turbines

Here, it is shown how the kinetic constants, R_i and k, were calculated from fitting the first order expression to data of the specific soluble protein release as a function of time. These kinetic constants, the data of the soluble protein release as a function of time and the conditions, under which the disruption experiments were performed, are detailed in this appendix.

G.1 Calculation of R_i and k

The calculation of R_i and k is illustrated in this appendix using the data of Run #10.39. Table G.1 shows the specific soluble protein release of Run #10.39 as a function of time. The columns in this table are numbered for ease of reference in the following discussion.

The first order kinetic constants, R_i and k, were calculated using the following algorithm:

1. Estimate values of the kinetic constants, R_i and k.
2. Calculate the deviation term for each sample (Table G.1, Column 3). The deviation term was defined as:

$$\left[Measured\ protein\ release - \Pr edicted\ protein\ release\right]^2$$

$$= \left[R_{measured} - R_i\left(1 - \exp(-k\,t)\right)\right]^2$$

   where the measured protein release ($R_{measured}$) refers to the values in Column 2 of Table G.1, and the sample time (t) refers to the values in Column 1 of Table G.1. Values of R_i and k are the estimates of the kinetic constants made in Step 1 of this algorithm.
3. Calculate the objective function, defined as the sum of the deviation terms in Column 3 of Table G.1.
4. Minimise the objective function, by altering R_i and k, using the Optimiser command in Quattro Pro. The kinetic constants are thus calculated by minimising the sum of the squares of the difference between the measured and predicted soluble protein concentrations.

Table G.1. **Values used in the calculation of the kinetic parameters of Run #10.39.**

Time (min)	Specific Soluble Protein Release (mg protein / g cell)	Deviation Term (mg protein / g cell)^2
Column 1	Column 2	Column 3
0	0.0	0
4	6.0	1
10	15.6	2
35	46.3	77
35	50.8	19
60	87.2	2
120	147.8	16
210	222.1	54
360	273.6	17
645	304.4	2
900	308.2	2
1200	307.1	17
1440	311.5	0

G.2 Disruption Data

In this section, the conditions under which each of the disruption experiments of this study were performed are detailed. Listed are the solids concentration and impeller speed used, the power input, the temperature, the cell dry weight, the experimental duration, and the values of the kinetic constants, R_i, k and R_M. Also listed is the objective function, defined in Section G.1 as the sum of the squares of the difference between the measured specific soluble protein release and that predicted by the first order disruption expression. A coefficient of variance, defined as the standard deviation of the predicted soluble protein release from the measured soluble protein release, divided by the mean measured soluble protein release (Equation G.1), is shown for each disruption experiment as a bracketed quantity after the objective function. The coefficient of variance is used as a relative measure of the accuracy of the first order disruption expression in predicting the specific soluble protein release.

$$CV = \frac{\sqrt{\frac{\sum_{i=1}^{n}(R_{measured,i} - R_{predicted,i})^2}{n-1}}}{\frac{\sum_{i=1}^{n} R_{measured,i}}{n}}$$

Equation G.1

where n is the number of samples taken. A number of the original experiments that were performed in this study were not run sufficiently long for R_i to be reached. The R_i value of these experiments was thus assumed to be that of experiments, in the same yeast batch, that were run at higher agitation intensities. The k values of these experiments were then found using the algorithm presented in Section G.1, but with R_i fixed at the predetermined value. These experiments are denoted by * after the experimental duration in the list of experimental conditions. The assumption made for these experiments was validated by running the same experiments until R_i was reached and comparing the R_i values obtained to those obtained at higher agitation intensities, in the same yeast batch.

Also presented in this section is the data of the specific soluble protein release as a function of time for each of the disruption experiments. The disruption data of each experiment is presented after the list of experimental conditions of the respective experiment. The data is presented first for the disruption experiments performed with the Rushton turbine at 0%, 5%, 10%, 20% and 40% solids (v/v) and over the agitation intensity range of 200 to 900 rpm, and thereafter for the disruption experiments performed with the pitched-blade turbine at 20% solids (v/v) and over the agitation intensity range of 440 to 900 rpm.

G.2.1 Rushton Turbine

0 % Solids

Run # 10.15
N = 754.2 rpm
P = 12.4 W
T = 16.0 °C
Dry Weight = 54.5 g/l
Experimental Duration = 10 hr
Objective Function = 15 (0.7 %)

R_i = -
R_M = 406 mg/g
k = -

Time (min)	Protein Release (mg/g)
0	0.0
4	1.0
8	0.5
10	0.5
20	1.3
40	1.3
60	1.7
90	2.2
120	2.3
180	2.5
360	2.6
600	2.8

5 % Solids

Run # 10.14
N = 749.1 rpm
P = 15.2 W
T = 17.0 °C
Dry Weight = 54.3 g/l
Experimental Duration = 10 hr*
Objective Function = 1017 (5.7 %)

R_i = 321 mg/g
R_M = 406 mg/g
$k = 7.08 \times 10^{-5}\ s^{-1}$

Time (min)	Protein Release (mg/g)
0	0
2	2.5
4	4.4
6	7.5
8	9.2
10	10.9
20	21.3
40	38.1
60	59.3
90	94.5
120	130.7
180	193.1
600	298.2

10 % Solids

Run # 10.34 **R_i = 317 mg/g**
N = 201 rpm **R_M = 401 mg/g**
P = 0.4 W **k = 4.21×10^{-7} s^{-1}**
T = 10.6 °C
Dry Weight = 54.3 g/l
Experimental Duration = 11 hr*
Objective Function = 1 (0.2 %)

Run # 10.11 **R_i = 357 mg/g**
N = 360.0 rpm **R_M = 452 mg/g**
P = 2.4 W **k = 1.9×10^{-5} s^{-1}**
T = 14.0 °C
Dry Weight = 48.0 g/l
Experimental Duration = 4.5 hr*
Objective Function = 426 (3.3 %)

Time (min)	Protein Release (mg/g)	Time (min)	Protein Release (mg/g)
0	0	0	0
2	0.5	2	0.9
4	0.4	4	2.4
6	0.5	6	4.6
8	0.7	8	6.3
10	0.1	10	7.2
20	0.5	20	15.1
40	0.3	40	26.4
60	0.6	60	32.0
90	0.4	90	40.9
120	1.0	120	50.7
180	1.6	270	84.2
240	1.9		
300	2.7		
458	3.6		
660	5.1		

Run # 10.7 **R_i = 357 mg/g**
N = 360.3 rpm **R_M = 452 mg/g**
P = 2.5 W **k = 2.39×10^{-5} s^{-1}**
T = 16.5 °C
Dry Weight = 51.5 g/l
Experimental Duration = 2 hr*
Objective Function = 23 (0.8 %)

Run # 10.37 **R_i = 310 mg/g**
N = 360.3 rpm **R_M = 401 mg/g**
P = 2.7 W **k = 3.21×10^{-5} s^{-1}**
T = 10.1 °C
Dry Weight = 43.0 g/l
Experimental Duration = 38.2 hr
Objective Function = 385 (3.3 %)

Time (min)	Protein Release (mg/g)	Time (min)	Protein Release (mg/g)
0	0	0	0
2	0.4	4	3.4
4	1.2	10	8.0
6	2.5	35	24.3
8	4.1	60	33.3
10	5.2	120	66.7
20	12.0	180	87.6
40	22.4	255	130.5
60	31.7	370	154.4
90	42.9	636	219.5
120	54.0	956	255.1
		1380	291.0
		1725	291.4
		2040	309.4
		2291	299.6

Run # 10.32 **R_i = 317 mg/g**
N = 360.6 rpm **R_M = 401 mg/g**
P = 2.0 W **k = 2.76x10^{-5} s^{-1}**
T = 11.8 °C
Dry Weight = 55.5 g/l
Experimental Duration = 10.3 hr*
Objective Function = 113 (1.7 %)

Time (min)	Protein Release (mg/g)
0	0
2	0.7
4	2.8
6	3.9
8	6.2
20	15.1
40	26.8
60	31.3
90	44.3
120	54.9
180	80.7
240	107.8
300	123.5
480	170.7
618	202.4

Run # 10.18 **R_i = 357 mg/g**
N = 362.7 rpm **R_M = 452 mg/g**
P = 2.5 W **k = 2.79x10^{-5} s^{-1}**
T = 13.7 °C
Dry Weight = 51.8 g/l
Experimental Duration = 3 hr*
Objective Function = 14 (0.6 %)

Time (min)	Protein Release (mg/g)
0	0
2	1.7
4	3.1
6	3.8
8	5.5
10	6.5
20	13.5
40	25.4
60	34.7
90	52.9
120	76.4
180	107.1

Run # 10.21 **R_i = 357 mg/g**
N = 427.1 rpm **R_M = 452 mg/g**
P = 4.2 W **k = 7.74x10^{-5} s^{-1}**
T = 13.0 °C
Dry Weight = 52.0 g/l
Experimental Duration = 13.3 hr
Objective Function = 145 (1.9 %)

Time (min)	Protein Release (mg/g)
0	0
2	3.7
4	7.4
6	9.8
8	13.4
10	15.5
20	28.2
40	55.7
60	81.0
90	126.9
120	158.2
180	196.3
800	349.6

Run # 10.40 **R_i = 309 mg/g**
N = 445.8 rpm **R_M = 382 mg/g**
P = 3.8 W **k = 1.13x10^{-4} s^{-1}**
T = 11.5 °C
Dry Weight = 54.9 g/l
Experimental Duration = 12 hr
Objective Function = 226 (2.8 %)

Time (min)	Protein Release (mg/g)
0	0
4	9.5
10	16.7
20	37.9
40	79.6
60	103.4
120	163.7
180	219.3
240	253.8
360	284.9
540	293.8
720	308.9

Run # 10.19 **R_i = 357 mg/g**
N = 494.5 rpm **R_M = 452 mg/g**
P = 6.1 W **k = 1.2x10^{-4} s^{-1}**
T = 15.0 °C
Dry Weight = 52.1 g/l
Experimental Duration = 3 hr*
Objective Function = 177 (2.2 %)

Run # 10.20 **R_i = 357 mg/g**
N = 532.2 rpm **R_M = 452 mg/g**
P = 7.6 W **k = 1.42x10^{-4} s^{-1}**
T = 14.2 °C
Dry Weight = 49.8 g/l
Experimental Duration = 3 hr*
Objective Function = 195 (2.3 %)

Time (min)	Protein Release (mg/g)	Time (min)	Protein Release (mg/g)
0	0	0	0
2	5.9	2	5.5
4	10.8	4	10.7
6	14.4	6	16.1
8	19.1	8	20.6
10	22.6	10	25.0
20	41.6	20	51.8
40	88.3	40	110.2
60	128.6	60	143.8
90	164.4	90	189.1
120	212.4	120	229.4
180	262.0	180	301.0

Run # 10.9 **R_i = 357 mg/g**
N = 562.1 rpm **R_M = 452 mg/g**
P = 8.3 W **k = 1.44x10^{-4} s^{-1}**
T = 17.5 °C
Dry Weight = 48.0 g/l
Experimental Duration = 5 hr*
Objective Function = 475 (3.5 %)

Run # 10.16 **R_i = 321 mg/g**
N = 745.8 rpm **R_M = 406 mg/g**
P = 15.5 W **k = 2.35x10^{-4} s^{-1}**
T = 17.0 °C
Dry Weight = 54.2 g/l
Experimental Duration = 4 hr
Objective Function = 1158 (6.1 %)

Time (min)	Protein Release (mg/g)	Time (min)	Protein Release (mg/g)
0	0	0	0
2	7.2	2	7.8
4	13.6	4	15.2
6	19.7	6	22.6
8	25.2	8	28.1
10	29.8	10	34.5
20	49.3	20	65.0
40	98.4	40	134.9
60	144.1	60	185.8
90	191.9	90	229.7
120	232.1	120	279.3
300	347.9	180	310.9
		240	308.5

Run # 10.49 **R_i = 347 mg/g**
N = 776.5 rpm **R_M = 399 mg/g**
P = 19.8 W **k = 2.25x10^{-4} s^{-1}**
T = 14.8 °C
Dry Weight = 53.2 g/l
Experimental Duration = 7 hr
Objective Function = 242 (2.7 %)

Run # 10.42 **R_i = 315 mg/g**
N = 905.7 rpm **R_M = 410 mg/g**
P = 24.2 W **k = 2.94x10^{-4} s^{-1}**
T = 17.5 °C
Dry Weight = 53.1 g/l
Experimental Duration = 5.08 hr
Objective Function = 438 (4.4 %)

Time (min)	Protein Release (mg/g)	Time (min)	Protein Release (mg/g)
0	0	0	0
4	16.7	4	19.4
10	41.5	10	41.9
20	95.0	35	148.1
40	144.9	60	213.7
60	189.8	90	250.0
90	242.7	120	271.3
120	273.0	210	317.5
180	320.2	305	305.9
270	338.2		
420	366.7		

20 % Solids

Run # 10.35 **R_i = 317 mg/g**
N = 200.0 rpm **R_M = 401 mg/g**
P = 0.4 W **k = 2.61x10^{-5} s^{-1}**
T = 11.1 °C
Dry Weight = 54.7 g/l
Experimental Duration = 11.2 hr*
Objective Function = 154 (2.1 %)

Run # 10.39 **R_i = 312 mg/g**
N = 273.0 rpm **R_M = 382 mg/g**
P = 1.0 W **k = 9.27x10^{-5} s^{-1}**
T = 9.6 °C
Dry Weight = 55.5 g/l
Experimental Duration = 24 hr
Objective Function = 207 (2.7 %)

Time (min)	Protein Release (mg/g)	Time (min)	Protein Release (mg/g)
0	0	0	0
2	0.9	4	6.0
6	2.3	10	15.6
10	4.2	35	48.9
20	8.6	60	87.2
40	16.7	120	147.8
60	23.8	210	222.1
90	36.0	360	273.6
120	50.5	645	304.4
180	77.1	900	308.2
240	99.0	1200	307.1
340	136.0	1440	311.5
480	170.0		
671	206.7		

Run # 10.30 **R_i = 320 mg/g**
N = 273.2 rpm **R_M = 406 mg/g**
P = 1.0 W **k = 8.89×10^{-5} s^{-1}**
T = 13.4 °C
Dry Weight = 49.2 g/l
Experimental Duration = 5 hr*
Objective Function = 823 (4.8 %)

Run # 10.29 **R_i = 320 mg/g**
N = 360.3 rpm **R_M = 406 mg/g**
P = 2.4 W **k = 1.58×10^{-4} s^{-1}**
T = 11.7 °C
Dry Weight = 51.6 g/l
Experimental Duration = 10 hr*
Objective Function = 565 (3.8 %)

Time (min)	Protein Release (mg/g)	Time (min)	Protein Release (mg/g)
0	0	0	0
2	1.5	2	6.9
4	3.6	4	11.8
6	7.2	6	18.8
8	9.4	8	24.0
10	11.6	10	31.4
20	26.3	20	54.5
40	50.4	40	106.1
60	79.5	60	149.3
90	117.3	90	190.4
120	149.3	120	217.6
180	197.6	180	250.0
240	244.2	240	272.5
300	270.0	300	306.7
		600	328.7

Run # 10.54** **R_i = 315 mg/g**
N = 381.8 rpm **R_M = 400 mg/g**
P = 3.4 W **k = 1.76×10^{-4} s^{-1}**
T = 8.3 °C
Dry Weight = 54.9 g/l
Experimental Duration = 7 hr
Objective Function = 726 (4.9 %)

Run # 10.51** **R_i = 331 mg/g**
N = 407.7 rpm **R_M = 394 mg/g**
P = 4.6 W **k = 2.4×10^{-4} s^{-1}**
T = 11.6 °C
Dry Weight = 57.2 g/l
Experimental Duration = 7.3 hr
Objective Function = 513 (1.9 %)

Time (min)	Protein Release (mg/g)	Time (min)	Protein Release (mg/g)
0	0	0	0
4	19.6	4	30.0
10	61.1	10	77.1
20	114.2	20	138.9
41	200.9	40	222.1
60	234.7	60	264.0
90	267.1	90	292.9
120	289.4	120	300.4
180	308.9	180	326.0
235	307.3	240	332.9
300	308.5	300	338.7
420	333.1	360	330.6
		437	337.0

**These experiments were performed with the physiologically changed yeast, which differed from the yeast used in the remainder of the disruption experiments performed with the Rushton turbine (Section 6.2.3). The k values from Run #10.54 and Run #10.51 were normalised with respect to the other disruption experiments performed with the Rushton turbine.

Run # 10.47 **R_i = 333 mg/g**
N = 425.6 rpm **R_M = 399 mg/g**
P = 4.7 W **k = 3.95×10^{-4} s^{-1}**
T = 12.0 °C
Dry Weight = 54.0 g/l
Experimental Duration = 6 hr
Objective Function = 453 (3.9 %)

Run # 10.48 **R_i = 339 mg/g**
N = 474.8 rpm **R_M = 399 mg/g**
P = 6.8 W **k = 4.11×10^{-4} s^{-1}**
T = 11.0 °C
Dry Weight = 53.9 g/l
Experimental Duration = 7.5 hr
Objective Function = 821 (4.9 %)

Time (min)	Protein Release (mg/g)	Time (min)	Protein Release (mg/g)
0	0	0	0
4	28.1	4	33.2
10	71.7	10	80.7
20	131.8	20	143.3
40	208.3	40	216.1
60	254.1	60	260.3
90	288.3	90	291.4
120	297.5	120	303.1
180	326.4	180	335.5
270	339.3	270	342.6
360	340.4	330	347.4
		450	348.4

Run # 10.27 **R_i = 314 mg/g**
N = 476.8 rpm **R_M = 406 mg/g**
P = 6.1 W **k = 4.12×10^{-4} s^{-1}**
T = 13.1 °C
Dry Weight = 52.8 g/l
Experimental Duration = 13 hr
Objective Function = 1496 (6.8 %)

Run # 10.43 **R_i = 321 mg/g**
N = 661.7 rpm **R_M = 410 mg/g**
P = 14.4 W **k = 6.54×10^{-4} s^{-1}**
T = 14.3 °C
Dry Weight = 53.0 g/l
Experimental Duration = 4.5 hr
Objective Function = 490 (4.6 %)

Time (min)	Protein Release (mg/g)	Time (min)	Protein Release (mg/g)
0	0	0	0
2	14.6	4	44.0
4	27.5	10	109.2
6	47.3	35	247.5
8	62.4	60	277.9
10	78.1	90	302.1
20	131.5	120	322.8
40	205.8	180	317.5
60	238.2	270	331.3
90	256.6		
120	284.0		
240	323.1		
780	330.4		

Run # 10.53** R_i = **317 mg/g**
N = 662.2 rpm R_M = **400 mg/g**
P = 13.6 W **k = 8.18x10^{-4} s^{-1}**
T = 13.2 °C
Dry Weight = 55.6 g/l
Experimental Duration = 4 hr
Objective Function = 775 (5.6 %)

Run # 10.65** R_i = **331 mg/g**
N = 663.2 rpm R_M = **405 mg/g**
P = 15.0 W **k = 7.62x10^{-4} s^{-1}**
T = 11.6 °C
Dry Weight = 52.8 g/l
Experimental Duration = 4 hr
Objective Function = 325 (3.4 %)

Time (min)	Protein Release (mg/g)	Time (min)	Protein Release (mg/g)
0	0	0	0
4	66.3	4	51.7
10	129.4	10	128.0
20	205.9	20	201.1
40	257.3	40	270.9
60	288.6	60	307.0
90	314.7	90	325.5
120	314.3	120	322.9
180	321.4	180	335.8
240	330.6	240	334.0

**These experiments were performed with the physiologically changed yeast to verify that there was a physiological change in the yeast compared to the yeast used in the remainder of the disruption experiments performed with the Rushton turbine (Section 6.2.3).

Run # 10.50** R_i = **306 mg/g**
N = 663.6 rpm R_M = **394 mg/g**
P = 14.7 W **k = 8.86x10^{-4} s^{-1}**
T = 14.9 °C
Dry Weight = 59.1 g/l
Experimental Duration = 4 hr
Objective Function = 319 (3.7%)

Run # 10.13 R_i = **322 mg/g**
N = 744.0 rpm R_M = **406 mg/g**
P = 18.3 W **k = 7.5x10^{-4} s^{-1}**
T = 18.0 °C
Dry Weight = 54.6 g/l
Experimental Duration = 3 hr
Objective Function = 220 (2.7 %)

Time (min)	Protein Release (mg/g)	Time (min)	Protein Release (mg/g)
0	0	0	0
4	66.9	2	25.0
10	129.2	4	47.1
20	199.9	6	73.8
40	260.3	8	98.2
60	295.4	10	123.5
90	302.2	20	190.6
120	304.4	40	270.6
180	301.0	60	304.1
240	317.1	90	309.8
		120	321.9
		177	323.6

**This experiment was performed with the physiologically changed yeast to verify that there was a physiological change in the yeast compared to the yeast used in the remainder of the disruption experiments performed with the Rushton turbine (Section 6.2.3).

Run # 10.41 **R_i = 312 mg/g**
N = 746.8 rpm **R_M = 410 mg/g**
P = 18.3 W **k = 7.38×10^{-4} s^{-1}**
T = 18.5 °C
Dry Weight = 52.8 g/l
Experimental Duration = 3 hr
Objective Function = 462 (4.6 %)

Run # 10.44 **R_i = 327 mg/g**
N = 904.2 rpm **R_M = 410 mg/g**
P = 26.8 W **k = 9.76×10^{-4} s^{-1}**
T = 18.1 °C
Dry Weight = 52.1g/l
Experimental Duration = 3 hr
Objective Function = 454 (4.6 %)

Time (min)	Protein Release (mg/g)	Time (min)	Protein Release (mg/g)
0	0	0	0
4	50.3	2	30.4
10	114.5	6	99.2
20	187.7	10	151.7
40	259.4	35	283.6
60	279.2	60	304.3
90	293.9	90	323.4
120	320.0	180	339.2
180	319.7		

40 % Solids

Run # 10.17 **R_i = 320 mg/g**
N = 758.0 rpm **R_M = 406 mg/g**
P = 21.3 W **k = 4.05×10^{-3} s^{-1}**
T = 21.0 C
Dry Weight = 55.4 g/l
Experimental Duration = 3 hr
Objective Function = 356 (3.6 %)

Time (min)	Protein Release (mg/g)
0	0
2	134.3
4	196.6
6	237.3
8	274.5
20	308.6
40	316.7
60	319.8
90	325.3
120	303.6
180	326.6

G.2.2 Pitched-blade Turbine

20 % Solids

Run # 10.63 **R_i = 353 mg/g**
N = 440.2 rpm **R_M = 405 mg/g**
P = 1.2 W **k = 8.6x10^{-5} s^{-1}**
T = 8.3 °C
Dry Weight = 53.5 g/l
Experimental Duration = 24 hr
Objective Function = 513 (3.7 %)

Time (min)	Protein Release (mg/g)
0	0
4	9.5
10	18.7
35	54.0
60	93.4
120	172.0
210	240.4
360	286.2
600	335.5
900	342.4
1200	353.7
1440	364.6

Run # 10.60 **R_i = 387 mg/g**
N = 474.7 rpm **R_M = 406 mg/g**
P = 1.7 W **k = 1.38x10^{-4} s^{-1}**
T = 7.7 °C
Dry Weight = 52.5 g/l
Experimental Duration = 14 hr
Objective Function = 1163 (5.1 %)

Time (min)	Protein Release (mg/g)
0	0
4	11.5
10	28.2
20	50.7
60	156.7
90	212.7
120	248.2
180	305.0
300	339.6
420	359.1
600	388.6
840	404.0

Run # 10.61 **R_i = 371 mg/g**
N = 511.7 rpm **R_M = 406 mg/g**
P = 2.3 W **k = 1.82x10^{-4} s^{-1}**
T = 7.5 °C
Dry Weight = 51.8 g/l
Experimental Duration = 14.2 hr
Objective Function = 1237 (5.1 %)

Time (min)	Protein Release (mg/g)
0	0
4	15.0
10	40.7
20	72.0
40	128.8
60	182.4
90	234.9
120	280.5
180	303.2
300	343.1
420	368.1
600	377.2
853	377.7

Run # 10.57 **R_i = 307 mg/g**
N = 672.8 rpm **R_M = 403 mg/g**
P = 5.2 W **k = 4.49x10^{-4} s^{-1}**
T = 7.5 °C
Dry Weight = 48.8 g/l
Experimental Duration = 7 hr
Objective Function = 746 (5.4 %)

Time (min)	Protein Release (mg/g)
0	0
4	23.5
10	66.3
20	126.8
40	212.4
60	251.5
90	271.5
120	291.0
180	294.2
300	319.1
420	509.0

Run # 10.56 **R_i = 361 mg/g**
N = 673.1 rpm **R_M = 403 mg/g**
P = 5.4 W **k = 4.98x10^{-4} s^{-1}**
T = 9.5 °C
Dry Weight = 51.7 g/l
Experimental Duration = 10 hr
Objective Function = 1306 (5.8%)

Run # 10.64 **R_i = 353 mg/g**
N = 673.6 rpm **R_M = 405 mg/g**
P = 5.3 W **k = 4.08x10^{-4} s^{-1}**
T = 9.2 °C
Dry Weight = 53.2 g/l
Experimental Duration = 7 hr
Objective Function = 1437 (6.5 %)

Time (min)	Protein Release (mg/g)	Time (min)	Protein Release (mg/g)
0	0	0	0
4	39.3	4	25.9
10	103.2	10	79.1
20	171.3	20	151.7
40	247.4	40	227.1
60	297.8	60	274.7
90	329.8	90	299.9
120	337.1	120	310.4
180	352.5	180	352.3
300	370.0	300	360.7
420	359.1	420	367.1
600	393.0		

Run # 10.62 **R_i = 337 mg/g**
N = 675.5 rpm **R_M = 406 mg/g**
P = 5.3 W **k = 4.48x10^{-4} s^{-1}**
T = 8.5 °C
Dry Weight = 53.0 g/l
Experimental Duration = 7 hr
Objective Function = 1771 (7.9%)

Run # 10.67 **R_i = 330 mg/g**
N = 750.8 rpm **R_M = 372 mg/g**
P = 7.3 W **k = 6.63x10^{-4} s^{-1}**
T = 11.2 °C
Dry Weight = 58.8 g/l
Experimental Duration = 7 hr
Objective Function = 814 (5.2 %)

Time (min)	Protein Release (mg/g)	Time (min)	Protein Release (mg/g)
0	0	0	0
4	25.2	4	41.4
10	59.1	10	112.3
20	149.7	20	178.3
40	241.7	40	270.5
60	265.0	60	296.2
90	298.1	120	317.6
180	322.9	180	313.7
300	333.0	300	341.2
420	356.1	420	337.5

Run # 10.68
N = 904.4 rpm
P = 12.3 W
T = 14.0 °C
Dry Weight = 57.9 g/l
Experimental Duration = 4 hr
Objective Function = 258 (3.1 %)

R_i = 323 mg/g
R_M = 372 mg/g
k = 7.48x10^{-4} s^{-1}

Time (min)	**Protein Release (mg/g)**
0	0
4	48.1
10	118.4
20	196.4
40	271.0
60	295.5
90	315.8
120	328.8
180	318.3
240	326.2

Appendix H: Least Squares Algorithm

Consider an expression of the following form:

$$k = A\,\Phi + B\,N$$

where: k, Φ, N = Measurements

A, B = Constants

For p measurements:

$$k_1 = A\,\Phi_1 + B\,N_1$$

$$k_2 = A\,\Phi_2 + B\,N_2$$

•

•

•

$$k_p = A\,\Phi_p + B\,N_p$$

Let [k] be the vector of the p k measurements and let E be the matrix of the p Φ and p N measurements. Let [d] be the vector of the constants, A and B.

Then: $[k] = E\,[d]$

Let E^T be the transpose matrix of E.

Then: $E^T\,[k] = E^T\,E\,[d]$

$$\therefore\ [d] = (E^T\,E)^{-1}\,E^T\,[k] \qquad \textbf{Equation H.1}$$

Equation H.1 is the Least Squares solution for finding the constants A and B (Fraleigh and Beauregard 1990). This method was used in fitting the models in Chapter 7 and 8 to the cell disruption data. All calculations were done using Quattro Pro.

Appendix I: Cell Death Rate Data of Croughan *et al.* (1988, 1989) and Croughan and Wang (1989)

In this appendix, the death rate (q) data of FS-4 cells immobilised on Cytodex 1 microcarriers is presented as a function of the microcarrier volume fraction (Φ_M), the inert solid particle volume fraction (Φ_i), the total solids volume fraction (Φ_T), the attached cell concentration (c), and the power input per unit volume (P/V). The data was obtained by Croughan *et al.* (1988, 1989) and Croughan and Wang (1989) on agitation of the cells in 125 ml spinner vessels. This data was used in Section 7.5.2 to validate the mechanistic model, developed in this work to describe the disruption of freely suspended *Saccharomyces cerevisiae* in a slurry reactor on agitation with a 6-bladed Rushton turbine (Section 7.4.3).

Table I.1. **Cell death rates (q) of immobilised FS-4 cells as a function of the operating parameters.**

Researcher	Φ_M	Φ_i	Φ_T**	q (1/s)	c (cells/m^3)	P/V (W/m^3)
Croughan *et al.* (1988) α	0.0015	0.0000	0.0015	6.72×10^{-7}	9.69×10^{10}	3.3×10^{-2}
	0.0015	0.0049	0.0064	1.11×10^{-6}	9.69×10^{10}	3.3×10^{-2}
	0.0015	0.0097	0.0112	1.38×10^{-6}	9.69×10^{10}	3.3×10^{-2}
	0.0015	0.0146	0.0161	1.49×10^{-6}	9.69×10^{10}	3.3×10^{-2}
	0.0015	0.0194	0.0209	1.78×10^{-6}	9.69×10^{10}	3.3×10^{-2}
	0.0015	0.0243	0.0258	2.02×10^{-6}	9.69×10^{10}	3.3×10^{-2}
	0.0015	0.0291	0.0306	2.28×10^{-6}	9.69×10^{10}	3.3×10^{-2}
Croughan *et al.* (1988) β	0.0015	0.0000	0.0015	1.00×10^{-11}*	9.69×10^{10}	4.19×10^{-4}
	0.0015	0.0083	0.0098	1.00×10^{-11}*	9.69×10^{10}	4.19×10^{-4}
	0.0015	0.018	0.0195	1.00×10^{-11}*	9.69×10^{10}	4.19×10^{-4}
	0.0015	0.0277	0.0292	1.00×10^{-11}*	9.69×10^{10}	4.19×10^{-4}
Croughan and Wang (1989) γ	0.0049	0.0000	0.0049	1.00×10^{-11}*	2.69×10^{11}	4.19×10^{-4}
	0.0049	0.0000	0.0049	2.9×10^{-7}	2.69×10^{11}	2.11×10^{-3}
	0.0049	0.0000	0.0049	4.36×10^{-6}	2.69×10^{11}	3.3×10^{-2}
Croughan *et al.* (1989) δ	0.00019	0.0000	0.00019	1.00×10^{-11}*	1.29×10^{10}	4.19×10^{-4}
	0.00019	0.0000	0.00019	6.08×10^{-6}	1.29×10^{10}	1.04×10^{-1}

* The cell death rate was estimated as 1.00×10^{-11} where it was reported to be negligible so that the natural logarithm could be taken in the Least Squares analysis (Appendix H).

** Φ_T is the sum of Φ_M and Φ_i

α Data read off Figure 7 in paper of Croughan *et al.* (1988).

β Data read off Figure 5 in paper of Croughan *et al.* (1988).

γ Data read off Figure 4 in paper of Croughan and Wang (1989).

δ Data read off Figure 8 in paper of Croughan *et al.* (1989).

Appendix J: Cell Disruption Data of Mogren *et al.* (1974), Rehacek and Schaefer (1977) and Schutte *et al.* (1986)

The first order disrupton rate constants (k), determined by Schutte *et al.* (1986), and the extents of cell disruption (R/R_i), determined by Mogren *et al.* (1974) and Rehacek and Schaefer (1977), are presented in Table J.1 for the disruption of *Saccharomyces cerevisiae* in bead mills. Table J.1 also includes the volume fraction (Φ_U) of glass beads used by these workers, the glass bead diameter (d_p), the biosuspension flow rate (Q), the agitator speed (N), the power input (P) and the cell dry weight concentration (c). The bead mill models used by each of these workers, and the volumes of the bead mill grinding chambers (V) are also specified in Table J.1. The data in Table J.1 was used to develop the cell disruption models, presented in Section 8.3.2, for the bead mill system.

Table J.1. **First order disruption rate constants (k) and extents of cell disruption (R/R_i) as a function of the operating parameters for the disruption of *Saccharomyces cerevisiae* in a bead mill.**

Researcher	k (s^{-1})	R/R_i (%)	Φ_U	d_p (μm)	Q ($m^3 s^{-1}$)	N (rpm)	P (W)	c ($kg\ m^{-3}$)
Schutte *et al.* (1986)	1.91×10^{-4}	-	0.45	500-850	4.93×10^{-5}	700 (5.1)*	4625	400**
Netzsch Molinex	2.06×10^{-4}	-	0.45	500-850	4.93×10^{-5}	920 (6.7)*	5325	400**
LME20 Bead mill	2.65×10^{-4}	-	0.45	500-850	4.93×10^{-5}	1375 (10.0)*	7625	400**
($V = 0.0227\ m^3$)[α]								
Schutte *et al.* (1986)	2.11×10^{-4}	-	0.45	500-850	4.93×10^{-5}	700 (5.1)*	4375	400**
Netzsch Molinex	2.45×10^{-4}	-	0.45	500-850	4.93×10^{-5}	920 (6.7)*	4875	400**
LME20 "double disc"	3.22×10^{-4}	-	0.45	500-850	4.93×10^{-5}	1375 (10.0)*	6500	400**
Bead mill								
($V = 0.0227\ m^3$)[α]								

Table J.1 Continued

Researcher	k (s^{-1})	R/R_i (%)	Φ_U	d_p (μm)	Q ($m^3 s^{-1}$)	N (rpm)	P (W)	c (kg m^{-3})
Mogren *et al.* (1974)	-	92.7	0.50	500-750	1.64×10^{-5}	2340 (15.0)*	7820	60
Dyno-Muhle KD-5	-	85.5	0.50	500-750	3.51×10^{-5}	2340 (15.0)*	6550	60
Bead mill	-	80.9	0.50	500-750	5.80×10^{-5}	2340 (15.0)*	5650	60
($V = 0.0044\ m^3$)$^{\beta}$	-	78.2	0.50	500-750	7.23×10^{-5}	2340 (15.0)*	5650	60
	-	60.9	0.50	500-750	1.22×10^{-4}	2340 (15.0)*	6000	60
	-	57.3	0.50	500-750	1.36×10^{-4}	2340 (15.0)*	7180	60
	-	97.2	0.50	500-750	2.09×10^{-5}	2340 (15.0)*	6450	110
	-	90.0	0.50	500-750	4.87×10^{-5}	2340 (15.0)*	6180	110
	-	81.8	0.50	500-750	6.24×10^{-5}	2340 (15.0)*	6000	110
	-	75.5	0.50	500-750	8.83×10^{-5}	2340 (15.0)*	6360	110
	-	70.9	0.50	500-750	1.05×10^{-4}	2340 (15.0)*	6640	110
	-	63.6	0.50	500-750	1.33×10^{-4}	2340 (15.0)*	7540	110
	-	96.2	0.50	500-750	3.02×10^{-5}	2340 (15.0)*	6000	160
	-	83.8	0.50	500-750	4.99×10^{-5}	2340 (15.0)*	7270	160
	-	87.3	0.50	500-750	6.51×10^{-5}	2340 (15.0)*	8090	160
	-	78.4	0.50	500-750	8.33×10^{-5}	2340 (15.0)*	9450	160
	-	79.1	0.50	500-750	1.09×10^{-4}	2340 (15.0)*	12730	160
Rehacek and	-	95.5	0.54	318-418	1.39×10^{-5}	1800 (15.0)*	7780	150
Schaefer (1977)	-	93.6	0.54	318-418	2.78×10^{-5}	1800 (15.0)*	7900	150
Prototype I of	-	90.0	0.54	318-418	4.17×10^{-5}	1800 (15.0)*	8160	150
Netzsch LM20 Bead	-	86.3	0.54	318-418	5.56×10^{-5}	1800 (15.0)*	8560	150
mill	-	92.6	0.49	318-418	1.39×10^{-5}	1800 (15.0)*	6810	150
($V = 0.019\ m^3$)$^{\gamma}$	-	90.6	0.49	318-418	2.78×10^{-5}	1800 (15.0)*	6880	150
	-	86.3	0.49	318-418	4.17×10^{-5}	1800 (15.0)*	7310	150
	-	79.1	0.49	318-418	5.56×10^{-5}	1800 (15.0)*	7850	150
	-	85.0	0.46	318-418	1.39×10^{-5}	1800 (15.0)*	5880	150
	-	81.8	0.46	318-418	2.78×10^{-5}	1800 (15.0)*	6000	150
	-	73.1	0.46	318-418	4.17×10^{-5}	1800 (15.0)*	6430	150
	-	58.8	0.46	318-418	5.56×10^{-5}	1800 (15.0)*	6940	150

Notes for Table J.1:

* Bracketed quantity indicates impeller tip speed in m s^{-1}

** Cell wet weight concentration (kg m^{-3})

α Data obtained from Table 5 in paper of Schutte *et al.* (1986)

β Data read off Figures 4-6 in paper of Mogren *et al.* (1974)

γ Data read off Figure 4 in paper of Rehacek and Schaefer (1977)